LOG 63 1989

The Dual Dipmeter (SHDT) tool

The Dual Dipmeter (SHDT) tool, schematically shown in Figure 4, emits a current, called the Emex current, from the entire lower section of the sonde into the formation. A small portion flows from the electrodes (buttons) and is recorded as the dip curves which represent microresistivity changes due to bedding surfaces or fractures cutting across the wellbore.

The rest of the current serves to focus this small electrode current, giving a measurement having very good vertical resolution. Comparing the detail of the microresistivity curves with cores indicates the resolution to be in the order of 1 cm. All current is returned to the metal housing of the tool string above the insulating sleeve. Eight microresistivity curves are thus produced as well as two extra curves from the "speed buttons" on pads 1 and 2.

The inclinometry cartridge fits inside the top of the sonde. Its axis is accurately aligned with that of the sonde and includes a tri-axial accelerometer and three single-axis magnetometers.

The four arms which carry the measure electrodes have a maximum opening of 21 in. A simplified mechanical linkage is used so that the electrodes describe arcs of circles as the caliper arms open out. The opposite arms are linked, making the sonde self-centralizing in the hole. However, in an oval hole each pair of arms will open to a different extent, and the electrodes on them will be noncoplanar. This noncoplanar geometry is accounted for in the computation process when making dip calculations. The HDT dipmeter design used a more complex arm geometry to keep all electrodes coplanar.

The bottom of the sonde, where the dipmeter pads are mounted, is decoupled from the weight of the electronics and communications cartridges by means of a flex joint. Then, using a cross-linked arm arrangement, it can remain centralized in holes where the deviation is up to 70° (with the pad pressure control at its maximum). The centralization assures tangential contact between pads and the borehole wall, ensuring that the electrodes on the pad maintain good formation contact.

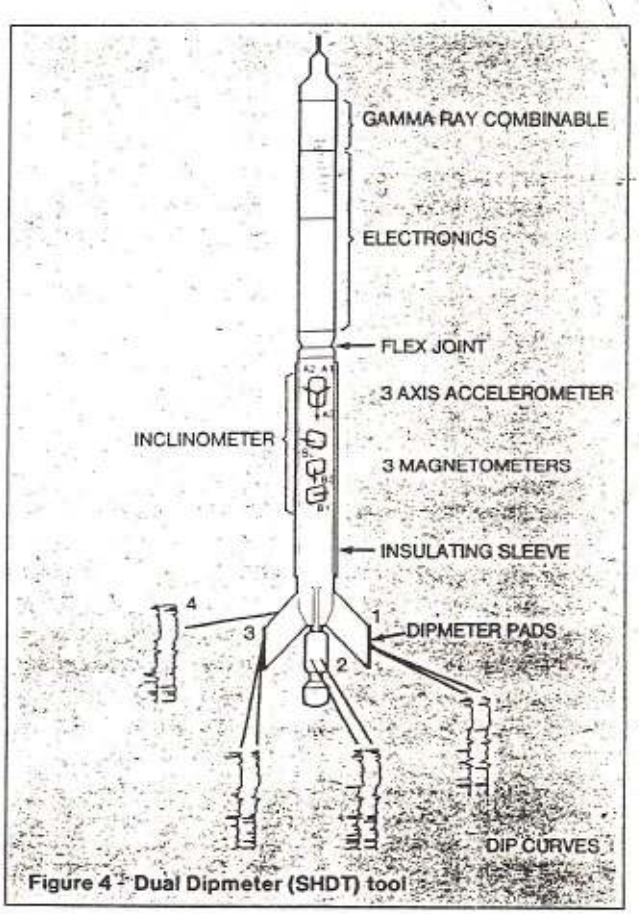

Figure 4 - Dual Dipmeter (SHDT) tool

Major improvements

A number of major improvements have been incorporated in the Dual Dipmeter (SHDT) tool:

- Side-by-side electrode configuration
- Greater inclinometer accuracy
- Greatly improved speed correction
- Reduction of floating-pad problems in deviated wells
- Better pad contact in badly washed out, rugose and ovalized holes
- Higher sampling rate
- Greater dynamic range of electronics

Side-by-side electrode configuration: Figure 5 shows a comparison of the measuring electrodes on the standard HDT and the Dual Dipmeter (SHDT) pads. For the Dual Dipmeter (SHDT) tool there are two measure electrodes on each of the four pads. The short spacing between the side-by-side electrodes (3 cm) results in a better curve likeness than from the pad-to-pad configuration. This enables a larger number of correlations, having high credibility, to be made with the result that shorter correlation intervals can now be used to measure displacements between the side-by-side curves while maintaining a sharp and unambiguous curve match. By using processing methods that exploit the improved data collection capabilities of the Dual Dipmeter (SHDT) tool, a fine vertical resolution of dips is achieved. With previous pad-to-pad configurations the lower limit for meaningful interval correlations was about one dip computation per foot. Using the side-by-side correlation technique, this can be reduced to about 3 in. under favorable conditions, thus enabling more information on sedimentological dips to be derived.

Greater inclinometer accuracy: The mechanical design of the inclinometer used in the HDT tool has been replaced by a tri-axial accelerometer and three magnetometers (Figure 6). The three-axis accelerometer is housed in a single unit. The A1, A2, A3 axes

weight of the electronics and communication cartridges from the lower section of the sonde (Figure 7). This reduces the floating-pad problem as well as sticking and "yo-yo" effects.

Better pad contact in badly washed out, rugose and ovalized holes: The problem becomes even more severe as the hole deviation increases. Figure 8 compares HDT and Dual Dipmeter (SHDT) results obtained over the same interval of hole. Note that the hole is ovalized with large washouts. Caliper 1 (pads 1 – 3) indicates relatively little washout while Caliper 2 (pads 2 – 4) indicates washouts up to to 20 in. The HDT processing was able to determine only a few northly trending dips while the SHDT results accurately delineate the dips of the steeply dipping formation. The improvement results from: the shorter SHDT pads which provide better electrode to formation contact; the opposite pairs of calipers being independently coupled enabling them to open out to a different extent in ovalized holes keeping the tool centralized; the flex joint, and the improved speed correction mentioned previously.

Higher sampling rate: The Dual Dipmeter (SHDT) tool has a sampling rate of 0.1 in. as compared with 0.2 in. for the HDT tool.

Greater dynamic range of electronics: The total (Emex) current that is sent into the formation is automatically controlled by the surface computer to allow for major changes in formation resistivity. In this way the microresistivity curve activity is maintained in both high- and low-resistivity zones so that good correlations can be made. In addition, the microresistivity curves may be played back and rescaled at the wellsite or computing center to remove the visual effect of variation in Emex current. This will ensure that information on grain size or textural changes in the formation is not obscured, as might be the case, on the original raw data curves.

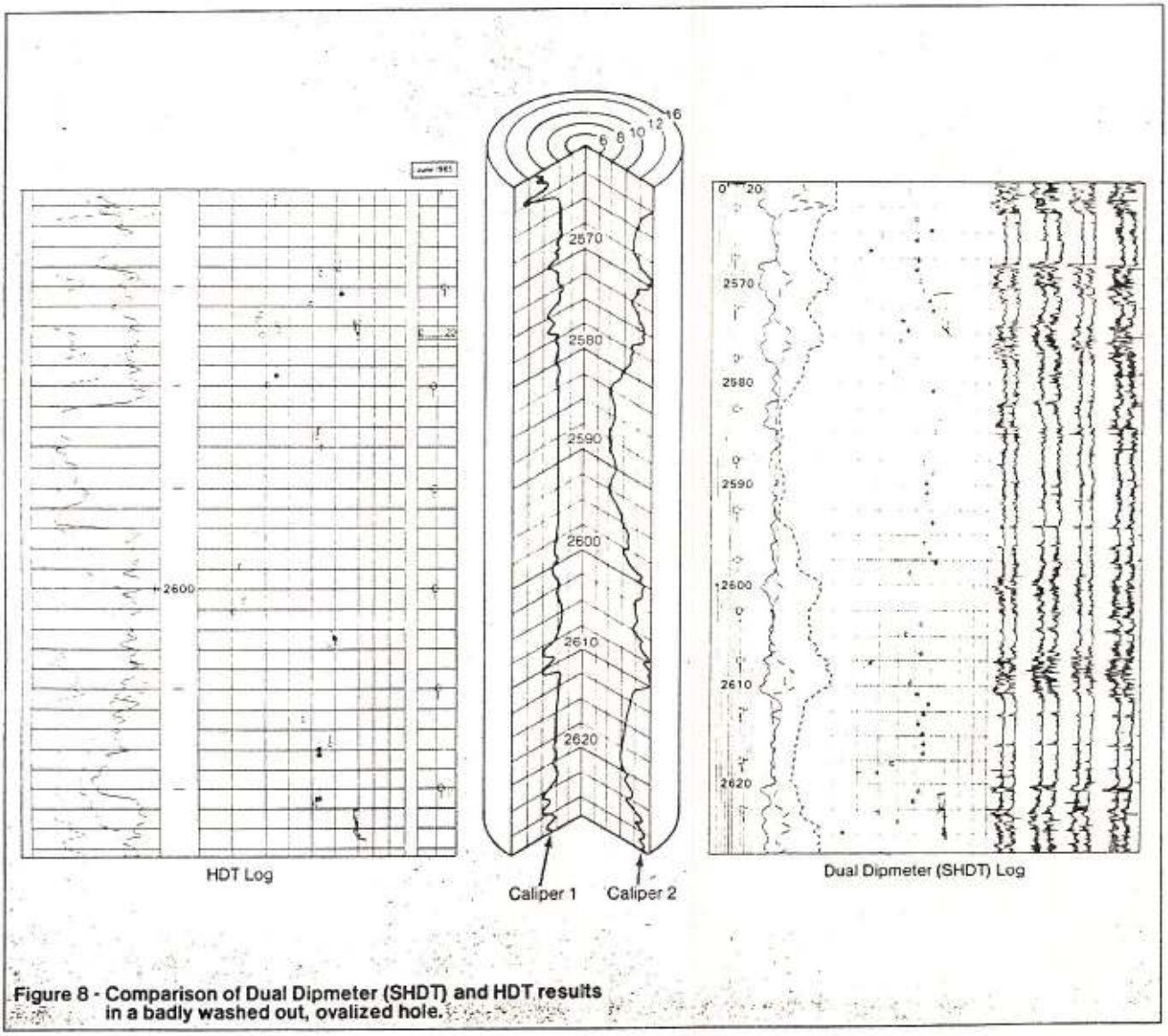

Figure 8 - Comparison of Dual Dipmeter (SHDT) and HDT results in a badly washed out, ovalized hole.

The Dual Dipmeter (SHDT) field log

A real time field log is recorded during the logging runs. The heading of a typical field log, minus cover sheet, is shown in Figure 9, along with a portion of the record.

After listing details concerning the tool and recording system, the log heading also identifies the various curves and scales. The curves presented are:

- Hole deviation — this is computed from sonde deviation using values of sonde length and cartridge stand-off. Either the hole or sonde deviation can be presented (default is the tool deviation calculated with zero stand-off).
- Hole azimuth — displayed on a −40 to 360° scale, this (and the Relative Bearing) curve is suppressed when the displayed deviation is below 0.5°. It reappears when the deviation exceeds 0.7°. This is because azimuth information becomes uncertain at low deviation.
- Pad 1 azimuth — displayed on a −40 to 360° scale, shows the azimuth of Pad Number 1.
- Relative Bearing — displayed on a −40 to 360° scale, this curve is presented as a cross-check between Pad 1 Azimuth (P1AZ) and Hole Azimuth (HAZI). The relationship RB = P1AZ − HAZI should be true at values of deviation up to about 30° (at 30° deviation the maximum error in RB is about 4°, climbing to about 18° at 60° deviation because P1AZ and RB angles are measured in different planes).
- Dip curves — these are the eight raw microresistivity curves before any Emex correction. The speed curves are not presented.
- Emex curves — both Emex current and voltage are displayed. They allow the operation of the Automatic Emex Control to be monitored during logging.
- Calipers — two caliper diameters at 90° to each other are presented on a linear 20-in. scale.

II. Computing Dip

Chapter I introduced the Dual Dipmeter (SHDT), summarized major improvements incorporated in it, and the basis for the conventional correlation techniques presently used for computing the magnitude of dip and the azimuth of its direction. The purpose of this chapter is to discuss the methods developed specifically for processing Dual Dipmeter (SHDT) data using the principles of interval and feature correlation, the presentation of the results, and the products available at the wellsite and at the computing centers.

The determination of formation dip measurements using the HDT dipmeter tool depends on the fundamental principle that to be detected, the bedding plane must be crossed by at least three of the four tool pads. This, in turn, implies that the formation is well bedded or laminated. Unfortunately, this is not always the case, and for many formations pad-to-pad correlations are impossible to establish making sedimentary studies difficult if not impossible. Also, pad-to-pad correlations may be difficult in highly dipping formations or in highly deviated holes.

The Dual Dipmeter (SHDT) tool has been designed specifically to overcome this limitation of the HDT tool and to study sedimentary problems. By providing two microresistivity curves taken 3 cm apart on each of the four tool arm pads, the density of the results is an order of magnitude higher than with conventional HDT hardware and processing. In addition, the improved sonde velocity correction, using the accelerometer data to compute instantaneous sonde speed and length of travel along the borehole, greatly increases the coherence of the results and helps salvage data affected by severe hole conditions. In other words, the quality of the dip data is dependent on the rock, if dips are present the measurement and computation processes will find them. Thus, it now is possible to carry out analysis of Dual Dipmeter (SHDT) results with a vertical resolution in the order of a few inches. This makes it possible to match the results with core data and to predict the configuration of sedimentary features when no core data are available.

The processing methods we will be discussing have been developed to take advantage of the Dual Dipmeter (SHDT) tool improvements. They provide three independent computations of formation dip and allow adapting the interpretation of the results to the specific problem of interest (structural, sedimentary, geometry of the sand body, etc.).

Computation of dip

Programs for computing dip from the Dual Dipmeter (SHDT) measurements: The basic interval correlation program, called Mean Square Dip (MSD), uses all the 28 possible cross correlations to compute 28 displacements (if all are successful). Since only two adjacent displacements are needed to define a plane, a lot of redundancy has been built into the measurement system. The program thus tries to find a "best fit" plane that satisfies most of the displacements.

A second interval correlation method called Continuous Side-By-Side (CSB) is also used. It only considers displacements computed from the side-by-side buttons on the pad. These four computed displacements represent the apparent angle of the set of bedding planes which cut across the borehole.

Finally, feature correlation is provided by the LOCDIP* computation. These pad-to-pad correlations are made over short intervals centered on bed boundaries, as defined by the major inflection points on the microresistivity curves. This method is used to identify and then correlate major individual curve features. The correlation lines are displayed with the actual microresistivity curves in a way similar to the GEODIP computation and presentation.

Before discussing each method in detail, it is useful to look at the sonde velocity correction since it makes possible taking full advantage of the data recorded by the side-by-side buttons on each pad, and the salvaging of data affected by severe hole conditions.

Sonde Velocity Correction: Since the side-by-side

*Mark of Schlumberger

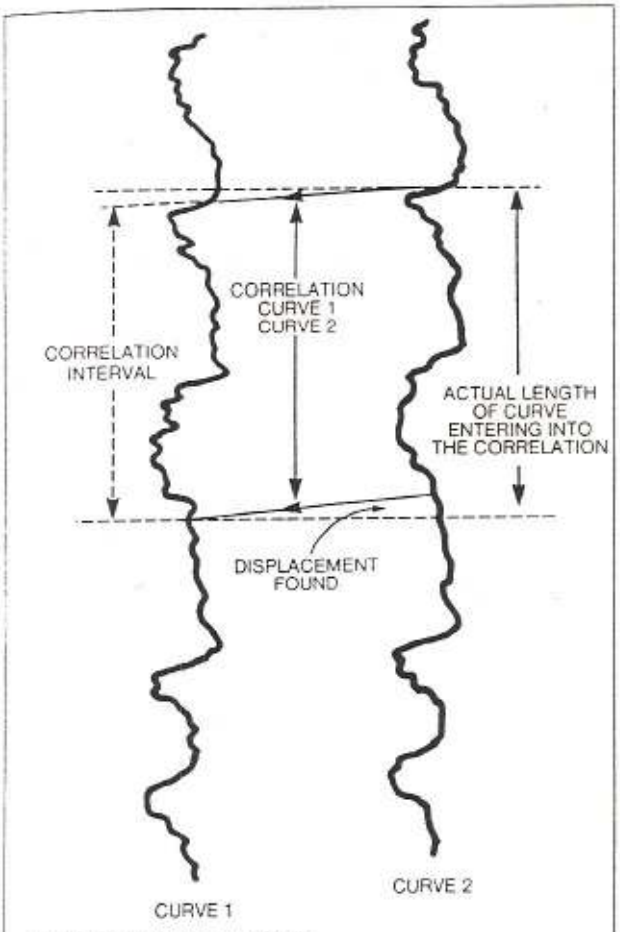

Figure 3 - Low apparent dip

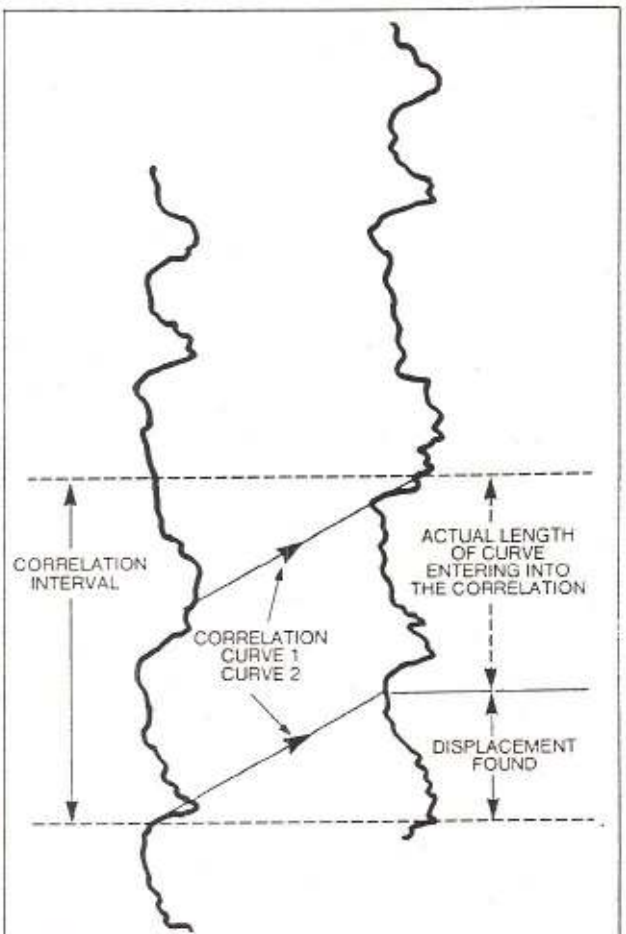

Figure 4 - High apparent dip

for the HDT recording. Like the HDT processing, the correlation method for the Dual Dipmeter (SHDT) curves requires defining an interval length, a step, and a search angle; however, there is a significant difference in the way the cross correlation is made. In the standard interval correlation program, a specific interval of a reference curve is defined and then slid along the interval of the curve it is to correlate with. For the Dual Dipmeter (SHDT) tool, the MSD method considers the same depth interval on each curve and uses only the data within that interval to make correlations. In the case of low apparent dip (Figure 3) it can be seen that nearly all the data points within the interval are considered when the correlation is made. As the apparent dip increases, (Figure 4) less and less points enter into the correlation. A limit is imposed when the search angle is increased until only half the points in the intervals are being used. This corresponds to an apparent dip of about 72 .

In areas where high dips, or high apparent dips because of deviated hole conditions, are expected, this limitation can be overcome by displacing the curves by a known amount before cross correlations are attempted, as shown in Figure 5. The amount of the curve displacement or shift would be that corresponding to the displacement one would expect if the actual dip plane was the same as the assumed or "focussing" plane. Hence, the net displacement used in the dip computation is the interval shift plus the displacement computed between the curves after the shift. The focussing plane can be chosen as:

- A fixed plane defined by the analyst (default is a horizontal plane).
- A plane defined by a previously computed dip.

For most dip computations, experience has shown the following input parameters are usually satisfactory:

- Interval length — typically 4 ft.
- Step distance — expressed as a percent of interval length, usually 50% (e.g., for a 4-ft interval, step distance would be 2 ft) although other values can be used as well.
- Search angle — 30° will usually find most dips relative to a horizontal plane. A double search option (2 x 30°) is available if no credible correlations are found using the 30° search.

The MSD program, then, is primarily used to determine structural dip by finding strong planar events crossing the borehole. The button-button displacements are computed and the best-fit plane

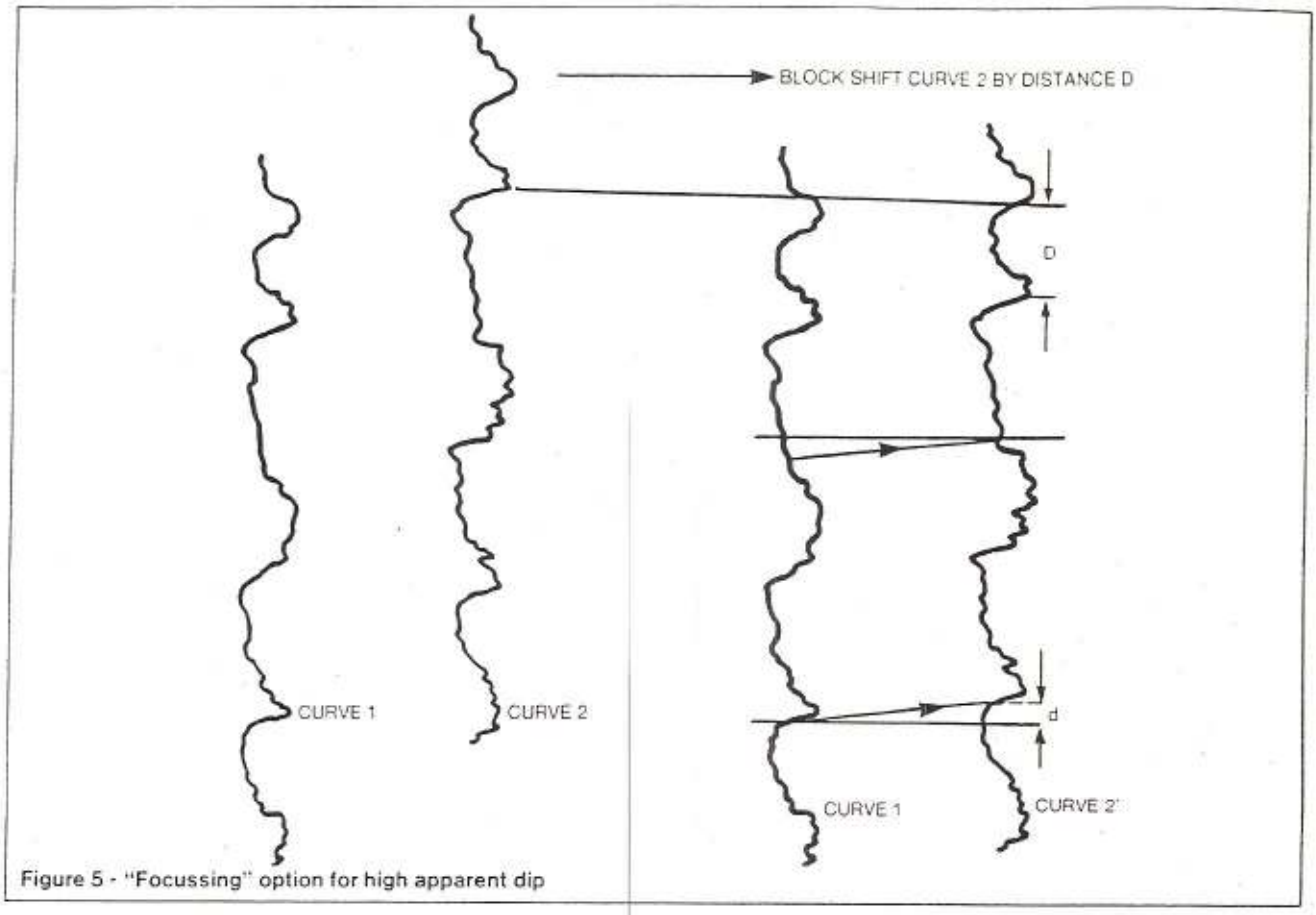

Figure 5 - "Focussing" option for high apparent dip

through them is found, as illustrated in Figure 6.

This initial best-fit can then be refined by an iterative process in which points beyond k standard deviations from this initial best-fit plane (k varying from 2.5 – 1.4) are rejected and a best-fit plane through the remaining points is calculated. An empirical quality factor is assigned to the final best-fit plane. This factor, ranging from 0 to 20, is a function of the number of iterations made and the final number of displacements retained.

There is no vertical continuity logic or clustering routine in the MSD computation: each level is autonomously processed. The redundancy available (28 possible displacements when two are enough to define a dip) reduces the possibility of producing mathematical dips or noise correlations.

Continuous Side-By-Side (CSB): The Continuous Side-By-Side (CSB) processing is a unique feature of the Dual Dipmeter (SHDT) service and takes advantage of the fact that there will be great similarity between the two microresistivity curves recorded by each pad since the two measure buttons are separated by a horizontal spacing of only 3 cm. Thanks to the side-by-side correlations, the CSB processing is able to pick out formation dip even though it may not be apparent on pad-to-pad correlation. Even more important, the CSB program is responsive to the fine bedding structure of the formation making it particularly effective for defining stratigraphic features. This is illustrated in Figure 7 where the curves recorded by pads 2 and 3 are shown for 12 ft of hole. Side-by-side correlations are shown as thin lines, and, for reference, the pad-to-pad correlations found for the same interval are shown as thick lines. From this example, you can see that the number of side-by-side correlations is approximately an order of magnitude greater than the pad-to-pad correlations, and that the

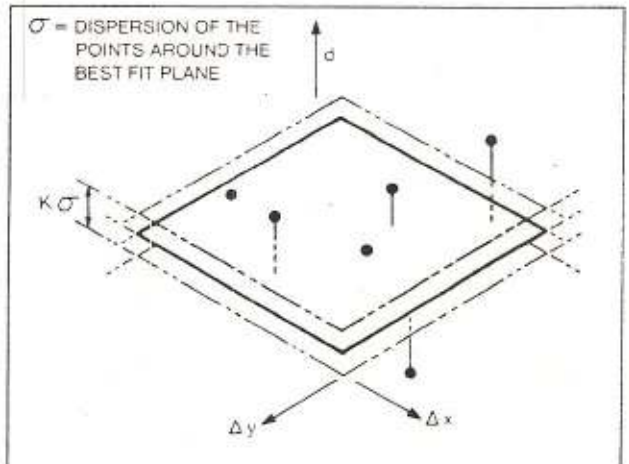

Figure 6 - Best fit plane

resolution is in the order of a few inches.

Another important feature, due to the close proximity of the buttons on the Dual Dipmeter (SHDT) pad, is that the displacements found by side-by-side correlations are much smaller than pad-to-pad displacements. This makes possible the measurement of very high dips which are not detected using pad-to-pad correlation. For such cases, once credible dips are found by CSB processing, they can be used as input to the focussing option for the MSD program.

Figure 8A shows a conventional pad-to-pad MSD correlation for a case of high apparent dip. The well is deviated around 35° to the Southwest, in the same direction as the regional structural trend (30°–40°). Thus, a given bedding surface will cut the borehole high on the Northeast side and low on the Southwest side. Obviously, getting a good correlation is difficult although the quality of the dip curves and the borehole condition is excellent. Figure 8B shows the results obtained with the side-by-side CSB processing. In this case the 3-cm spacing of the buttons allows an unambiguous correlation to be made.

In the standard CSB computation, each pair of microresistivity curves (e.g., 1–1A) is cross correlated using short correlation intervals, 12 in. or less;

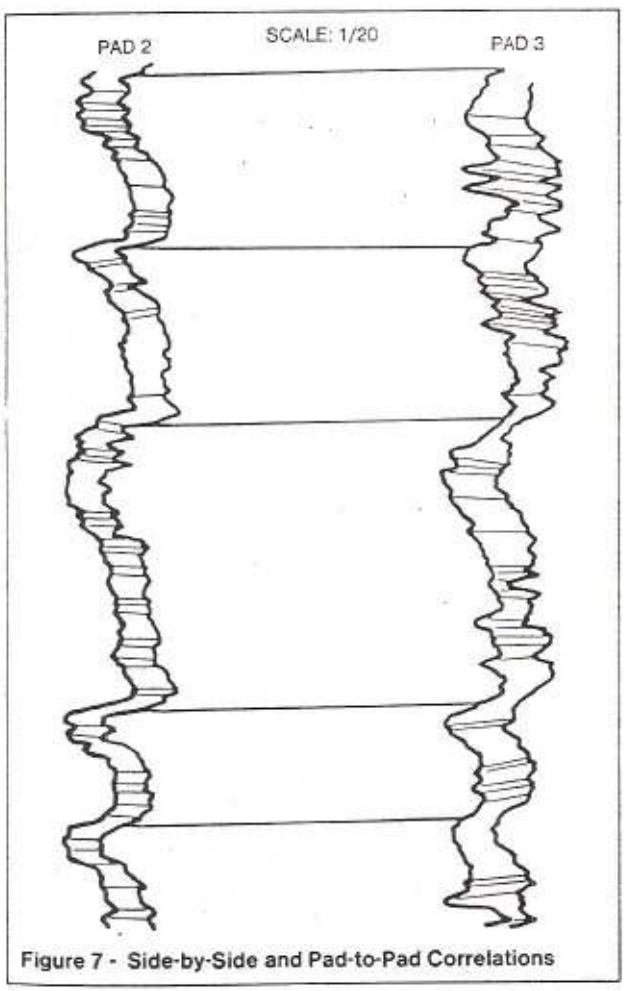

Figure 7 - Side-by-Side and Pad-to-Pad Correlations

under favorable conditions even 4 in. or 3 in. The step distance can be taken equal to half or three quarters of the correlation interval. This gives a vector parallel to the dip plane. Under ideal conditions (planar beds) another vector is found at the same depth by cross correlating the microresistivity curves of an adjacent pad (e.g., 2–2A). These two vectors are then used to define a dip plane.

With only four side-by-side correlations, a cross-check is needed to verify that the bed is indeed planar. If it is, then displacements obtained using microresistivity curves from opposite pads (e.g., 1-1A, 3-3A) should be equal in value but opposite in sign, and the dip can be obtained from any two orthogonal pairs at that depth. However, if this is not the case, a window is opened around the level under examination and the vertical continuity of the displacements a certain number of levels above and below is checked. The pad showing the best vertical continuity is kept. A similar procedure is then followed for pads 2 and 4 and, again, the pad showing the best vertical continuity is kept. The orthogonal pair showing the smoothest continuity within the window is used for dip computation.

In order to evaluate the credibility of the dip, a quality value ranging from 0 to 20 is assigned to each dip according to the vertical continuity and the quality of the correlograms at the various levels or depths.

There are, however, situations (very high real or apparent dips, geological features that do not cross the borehole, fracture, etc.) where it is useful to display all the dips obtained from orthogonal pairs at the same depth. This processing is called 4 SBS and is discussed under Dual Dipmeter (SHDT) results.

LOCDIP: As discussed in Chapter I, inflection points on the microresistivity curves describe geological events in the depositional sequence of the formation. The purpose of the LOCDIP program is to detect the geological events, or boundaries, and where applicable, associate a dip precisely at that boundary independent of dips at other depths. Instead of correlating intervals of curves, it detects features (inflection points) on each curve and attempts to link these around the borehole somewhat similar to GEODIP processing. There are, however, some important differences:

- To be retained as a LOCDIP result, an event must be recognized on at least seven of the eight microresistivity curves; GEODIP logic requires only three out of the four curves. Thus, LOCDIP logic is more demanding than the GEODIP logic.
- LOCDIP results are further refined by cross-correlations made on a 6-in. interval, while GEODIP results are computed directly from the spot events on the curves. This cross-correlation involves the eight curves and includes a repetitive best fit and rejection logic as in the MSD

computation, with a similar criteria for quality coding.

- A measurement of the planarity is derived for each of the possible dip planes at any level. The retained value corresponds to the surface which best approximates the set of these planes. By convention, a perfectly planar surface has a planarity of 100.
- Some events are recognized on only a few of the dip curves. In this case, the available correlations are traced across the applicable curves, with an options notation of "F" (fracture) or "P/L" (pebble or lens) for single pad events or two/three pad events, respectively. These interpretations, however, are not to be considered as certain, but rather as possible.

Dual Dipmeter (SHDT) results and products

Thus far, methods for handling and processing Dual Dipmeter (SHDT) data have been discussed. Obviously, a number of products and presentations are possible, each designed to answer a particular need. Some, utilizing the power of the CSU* system are available at the wellsite, others require capabilities found at the computing center (FLIC). To put all this in perspective, Figure 9 provides a breakdown of the products and where they are available. First, we will consider those available at the wellsite.

- Field log — A real-time monitor film is recorded during the logging run. It presents the eight microresistivity dip curves, the inclinometer data, the caliper diameters with the Emex current and voltage on a 1/200 scale.
- Field edit tape — A customer tape containing all the data required to compute dip results as recorded. All data have been corrected to account for downhole amplifier variations with temperature, and the dip curves are Emex corrected. The Emex current and voltages are recorded.
- Emex-corrected curves — This is a useful playback especially on the 1/40 scale as it

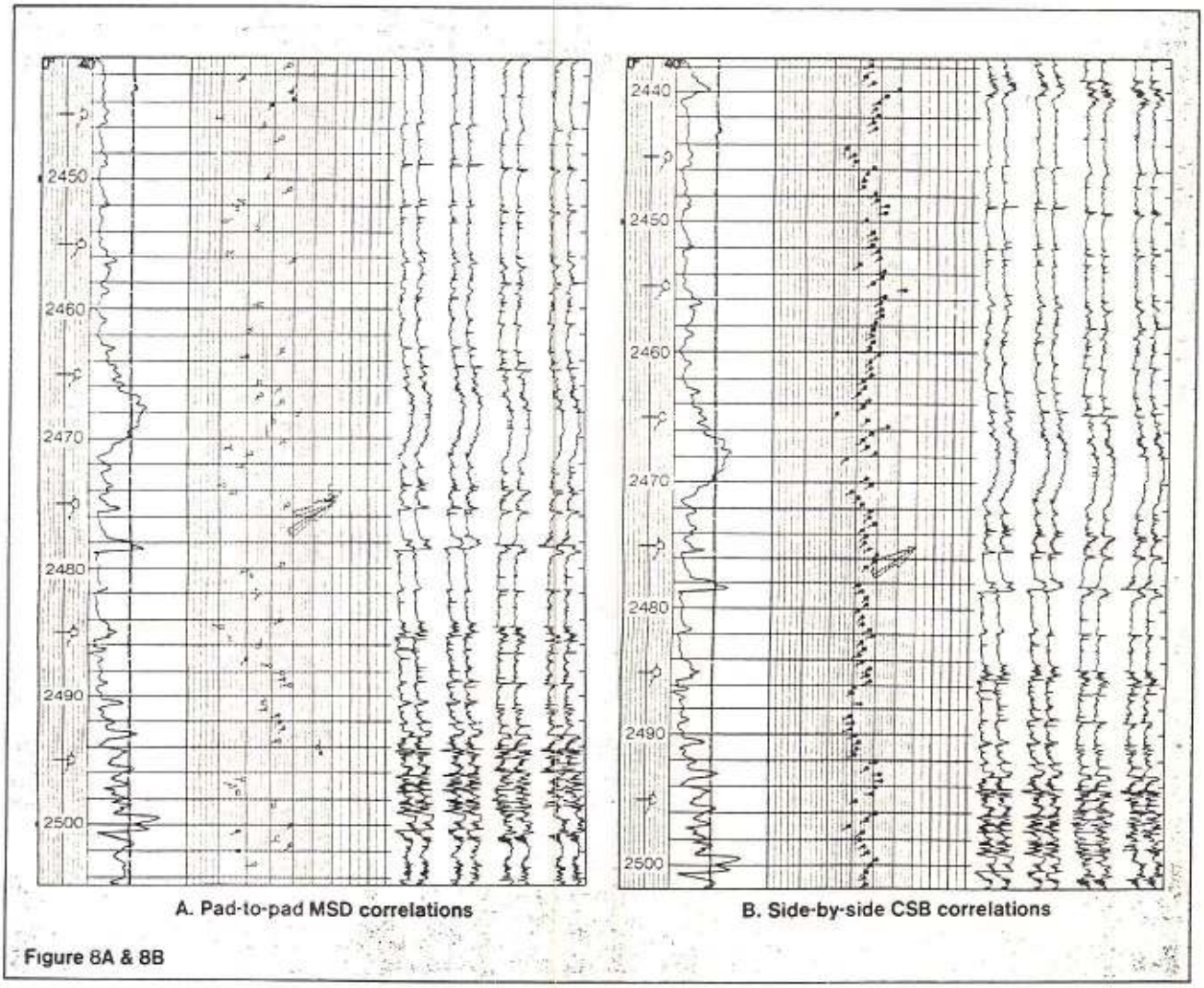

A. Pad-to-pad MSD correlations

B. Side-by-side CSB correlations

Figure 8A & 8B

*Mark of Schlumberger

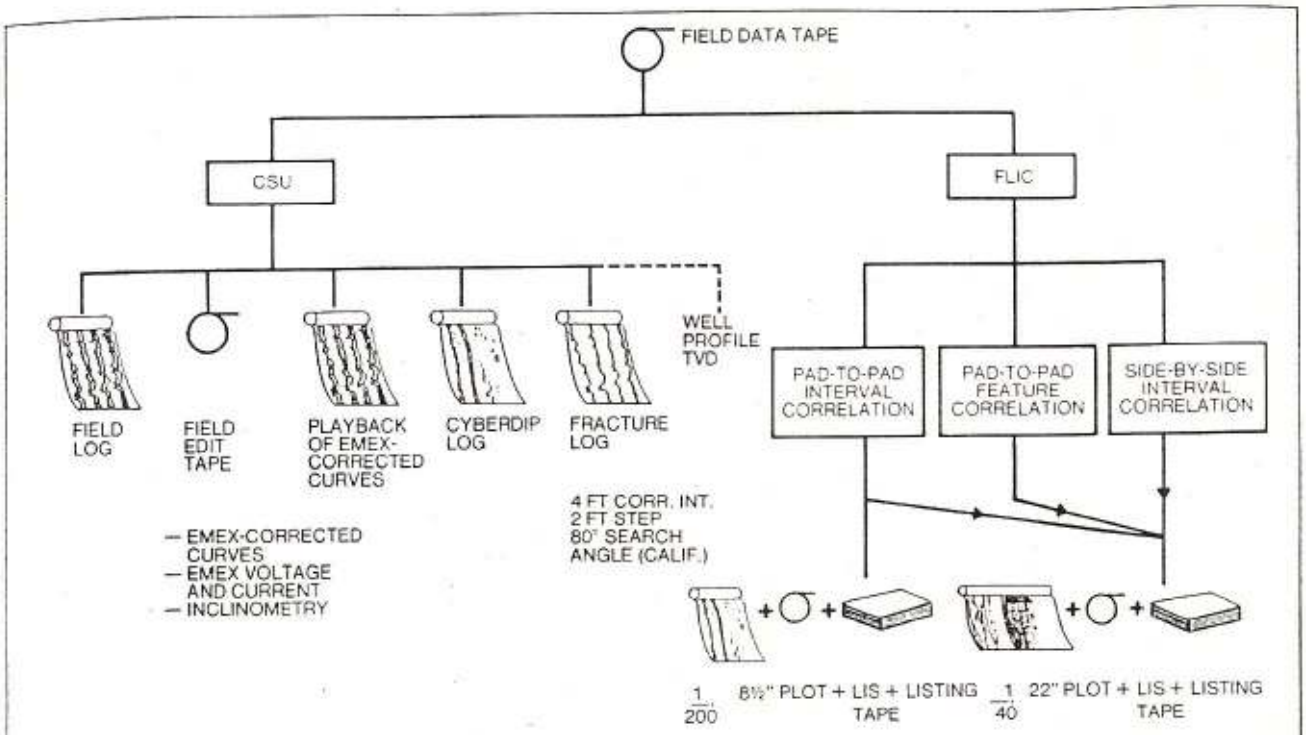

Figure 9 - Dual Dipmeter (SHDT) products

allows detailed examination of the grain-size variation, textural information and thin beds. This large scale playback is normally only made through the potential reservoir sections.

- CYBERDIP Log — The present program uses pad-to-pad interval correlation techniques, with a fixed 4-ft correlation length and 2-ft step distance. The search angle is 80° and the California option is used, which is suitable in most deviated or vertical wells. In the California option the search angle is referred to a plane normal to the borehole rather than to the horizontal.

  The user selects which set of four curves he wishes to use, whether 1-2-3a-4a or 1a-2a-3-4. The speed correction is made using the speed curves.

- FIL* Fracture Identification log — The depth differences between side-by-side pairs are computed, and then the corrected curves are played back over each other. This highlights any conductivity anomalies which may be caused by mud-filled fractures.

- Well profile — Information on hole direction and deviation is presented as a well profile plot. This directional information can be used to recompute logs to their true vertical depths.

Other products require the capabilities found in the computing center (FLIC). Here, full use is made of the inclinometer data to provide accurate directional information and speed corrections for the dip curves. The processing of the Dual Dipmeter (SHDT) data is designed to extract the maximum amount of dip information from the raw curves.

Presentation of the Dual Dipmeter (SHDT) results is produced through the DUALDIP* program. The presentations can be tailored to meet the needs of the user and may include combinations of the following: MSD, CSB, 4 SBS, LOCDIP and STRATIM presentations, the eight dip curves, the synthetic resistivity (SYNRES) and Gamma Ray curves, calipers and hole drift data. The depth scale is usually 1/40. Uses of the information presented will be covered in detail in Chapter V. Here it will suffice to simply point out certain important features concerning the information recorded on the DUALDIP presentation.

- Pad-to-pad interval correlation (MSD) — Correlation intervals in the order of 4 foot x 2 foot are used. The results, recorded as triangular arrows, are suitable for structural interpretation and for recognizing larger scale stratigraphic features. A solid triangle indicates a good quality dip where the number of points beyond k standard deviations is small and few displacements are discarded. A low quality dip is indicated by an open triangle. In this case, the number of points beyond k standard deviation is large and many displacements are discarded.

  In addition to the DUALDIP presentation, the

*Mark of Schlumberger

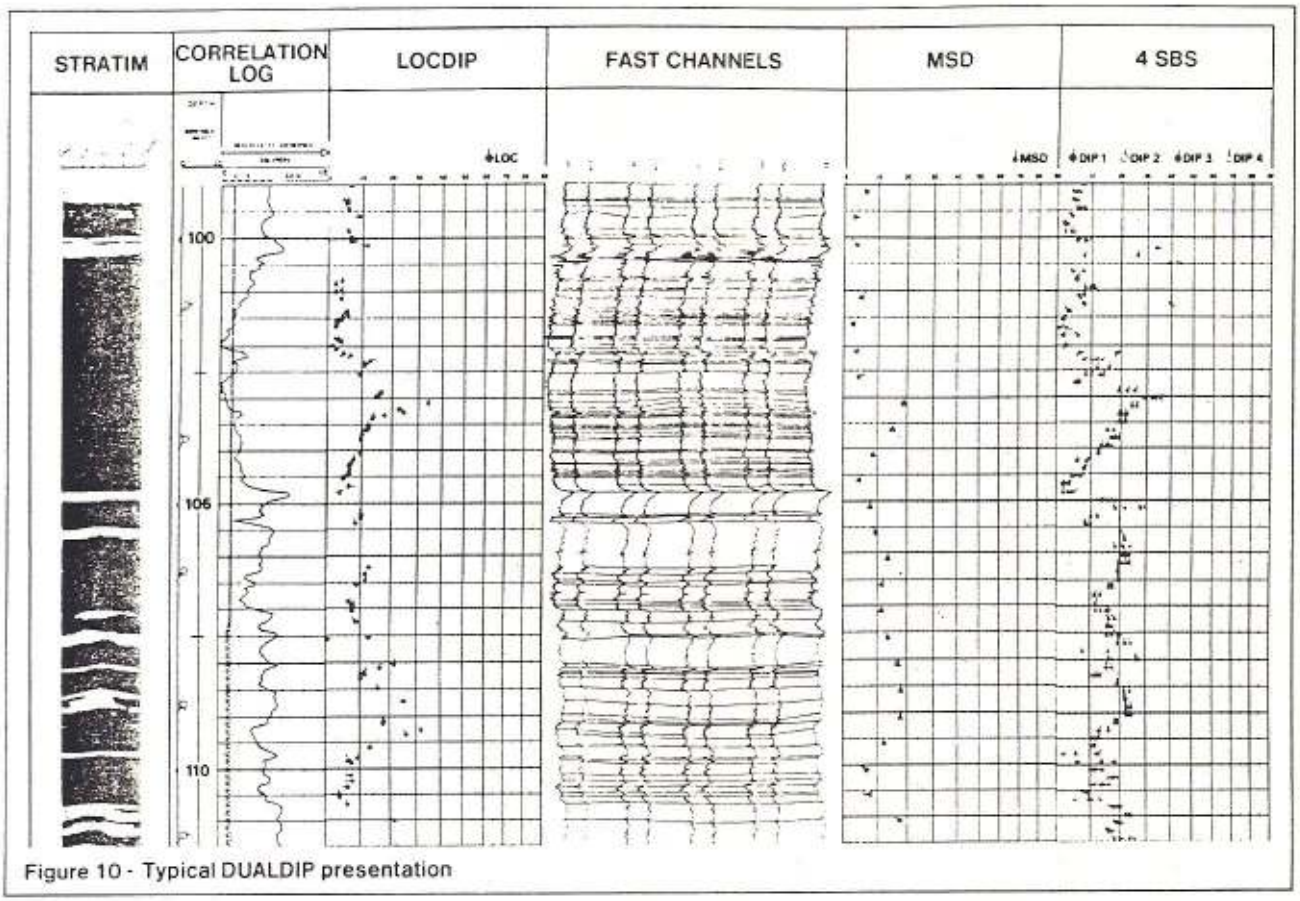

Figure 10 - Typical DUALDIP presentation

results can be displayed on an 8½-in.-wide, 1/200 scale plot.

- Pad-to-pad feature correlation (LOCDIP) —The dips corresponding to the major bed boundaries are shown on the DUALDIP plots as "square headed" tadpole plots.

  The correlation lines corresponding to these dips are shown on the microresistivity curves: the first curve is repeated as curve Number 9. Dashed lines may be shown which represent features recognized on two to six of the curves. Solid correlation lines are recognized on seven or all eight curves. A 1/40 scale highlights the information on grain-size variation and thin beds which is contained in the Emex-corrected raw curves.

- Side-by-side interval correlation (CSB) — Here a short correlation interval (down to 8 in.) is used to provide a high dip density suitable for more detailed stratigraphic work. A step distance of 4 in. gives three correlation tadpoles per foot. The results are plotted on a 1/40 scale as round headed tadpoles on the DUALDIP plot. A good quality dip is shown as a solid tadpole, a poor quality dip as an open tadpole.

- 4 SBS is used to output all four dip values from pad-pairs 1–2, 2–3, 3–4, and 4–1 using different symbols. As 4 SBS takes all possible dip results at any one correlation level, it provides an estimation of the planarity and quality rating of those dip results. Thus, the magnitude and direction of 4 SBS results is not an important consideration, but the spread of data is.

- STRATIM is a graphic representation of the resistivity variations around the wellbore seen by the eight microresistivity curves. Utilizing LOCDIP correlation links and the resistivity variations recorded by each curve in the processing, events that exist across the wellbore, and the dip associated with them, can be distinguished, as well as localized events such as pebbles, nodules, fractures, etc. For presentation a grey scale is created that is a function of the resistivity — black, low resistivity; white, high resistivity.

- SYNRES is a presentation of the reconstructed microresistivity dip curves. The raw dipmeter curves can be rescaled utilizing the Emex voltage and Emex current. Because of the very high sampling rate of the dipmeter and the sharp focusing, the vertical resolution of the rescaled resistivity curves is very good. They can be used to obtain the net sand count in thin interbedded sand/shale sequences and for obtaining a value

of hydrocarbon saturation for reservoir evaluation purposes.

Also presented on the DUALDIP plot are the caliper diameters, the hole deviation, the reconstructed resistivity curve (SYNRES) and, if recorded for additional lithological control, the Gamma Ray and SP curves.

Figure 10 is a typical example of a DUALDIP presentation that includes STRATIM, a correlation log. LOCDIP, the eight Emex-corrected microresistivity dip curves, MSD and 4 SBS results. Figure 10A is an enlargement of the STRATIM and 4 SBS results for the interval 100–170m of Figure 10. The sedimentary unit is an eolian dune sand sequence. The information obtained from these results concerning permeability barriers and the permeability anistropy within the dunes is of particular importance when designing the best completion method for efficient depletion of such a reservoir.

The fine detail contained on these curves allows you to infer much about the formations logged by the Dual Dipmeter (SHDT) tool. For example:

- The type of lithology (shales, sands, conglomerates, etc.) from the shape and likeness of the curves.
- Fining upwards, coarsening upwards sequences. This is done by analyzing the resistivity variations across the interval of interest, either from the microresistivity curves themselves or from the synthetic resistivity curves. Use of the Gamma Ray curve will often prove to be helpful. Care should be exercised, however, to ensure that fluid saturations are taken into account when inferring grain-size variations from resistivity gradients.
- Homogeneous bodies having no apparent bedding as opposed to finely striated, laminated bodies.
- Parallel vs. nonparallel bedding. This is especially important in sandstones, and has found application to the study of turbidites.
- Correlation lines may involve anywhere from eight microresistivity curves down to two. The interpretation made on this basis (pebble, lens, etc.) will depend on whether the anomaly is resistive or conductive, the number of curves involved, etc.
- Open fractures usually will show as an isolated conductive spike which may or may not correlate with similar spikes on other curves.

Selected examples covering such applications of Dual Dipmeter (SHDT) data will be discussed in Chapter V.

Chapters I and II have served to introduce the Dual Dipmeter (SHDT) tool and the computation of dips. Before discussing specific applications of Dual Dipmeter (SHDT) data, we will briefly review, in Chapters III and IV, how dips are interpreted in geologic terms.

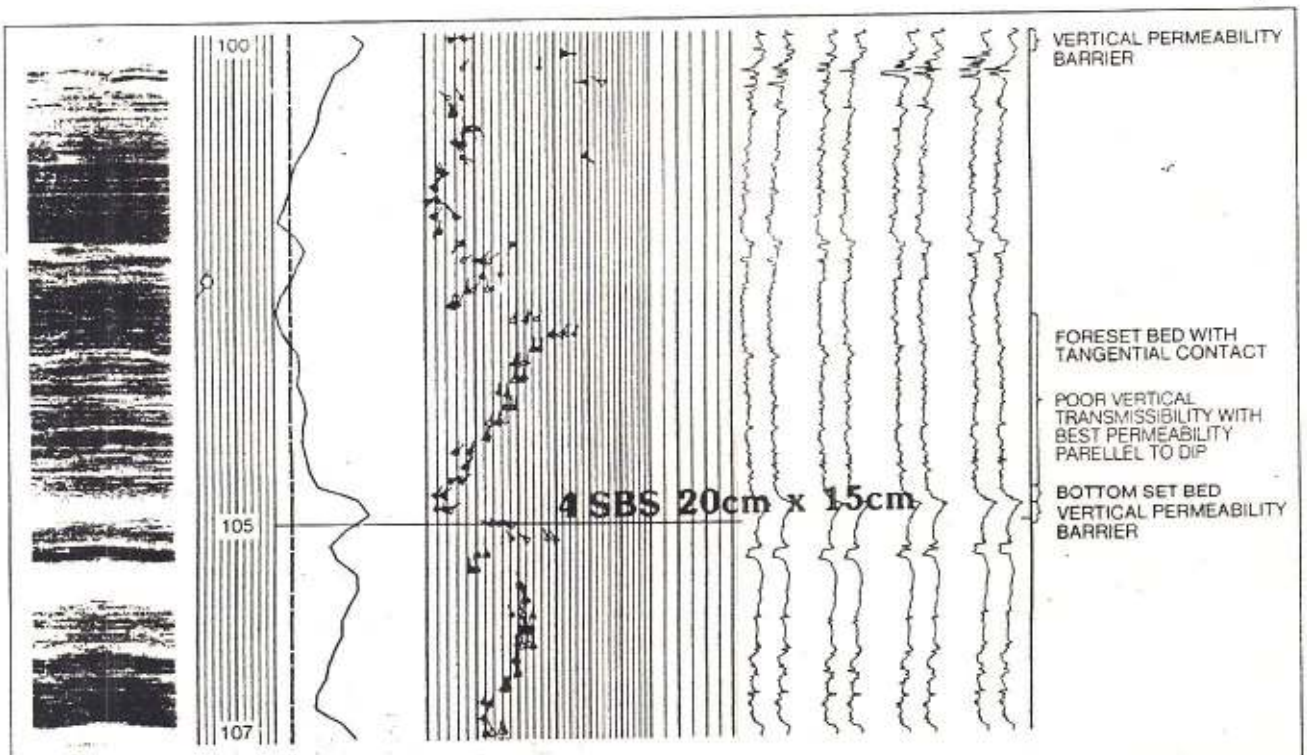

Figure 10A - Enlargement of section 100 ft to 107 ft

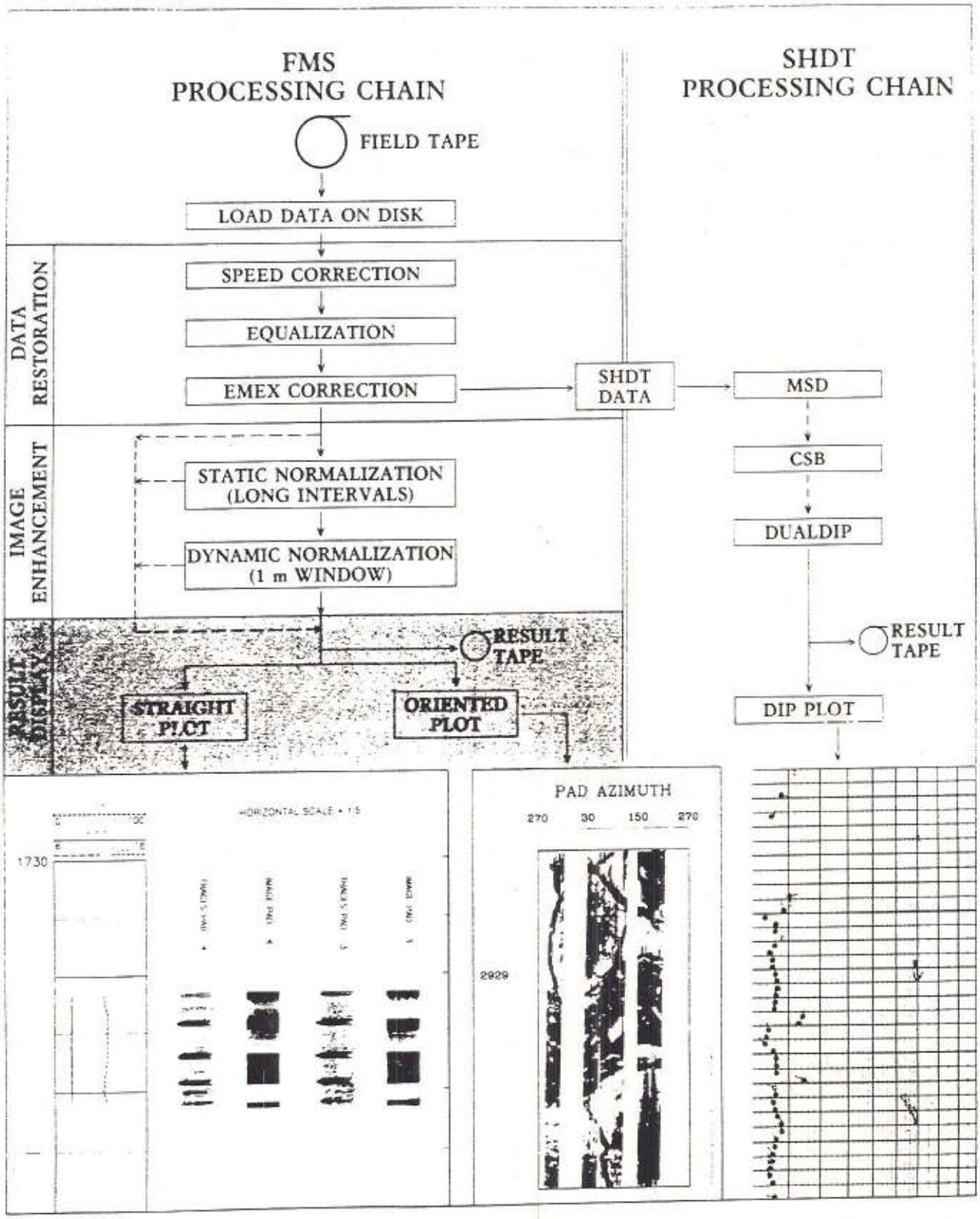
FMS
PROCESSING CHAIN
SHDT
PROCESSING CHAIN
FIELD TAPE
LOAD DATA ON DISK
DATA RESTORATION
SPEED CORRECTION
EQUALIZATION
EMEX CORRECTION
SHDT DATA
MSD
CSB
DUALDIP
IMAGE ENHANCEMENT
STATIC NORMALIZATION (LONG INTERVALS)
DYNAMIC NORMALIZATION (1 m WINDOW)
RESULT TAPE
RESULT TAPE
RESULT DISPLAY
STRAIGHT PLOT
ORIENTED PLOT
DIP PLOT
HORIZONTAL SCALE = 1/5
1730
PAD AZIMUTH
270
30
150
270
2929

FORMATION MICRO-SCANNER

"BOREHOLE IMAGING"

- SCALA 1/10
- NORMALIZZAZIONE SU 1m.
- PRESENTAZIONE ORIENTATA "CORESCAN"

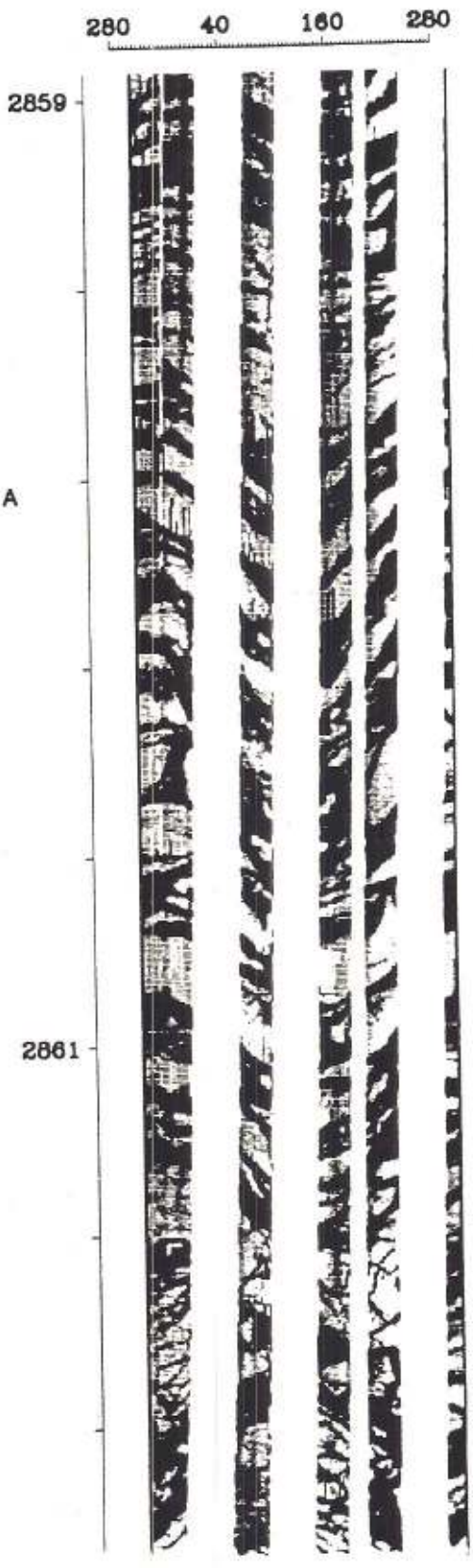

FORMATION MICRO-SCANNER

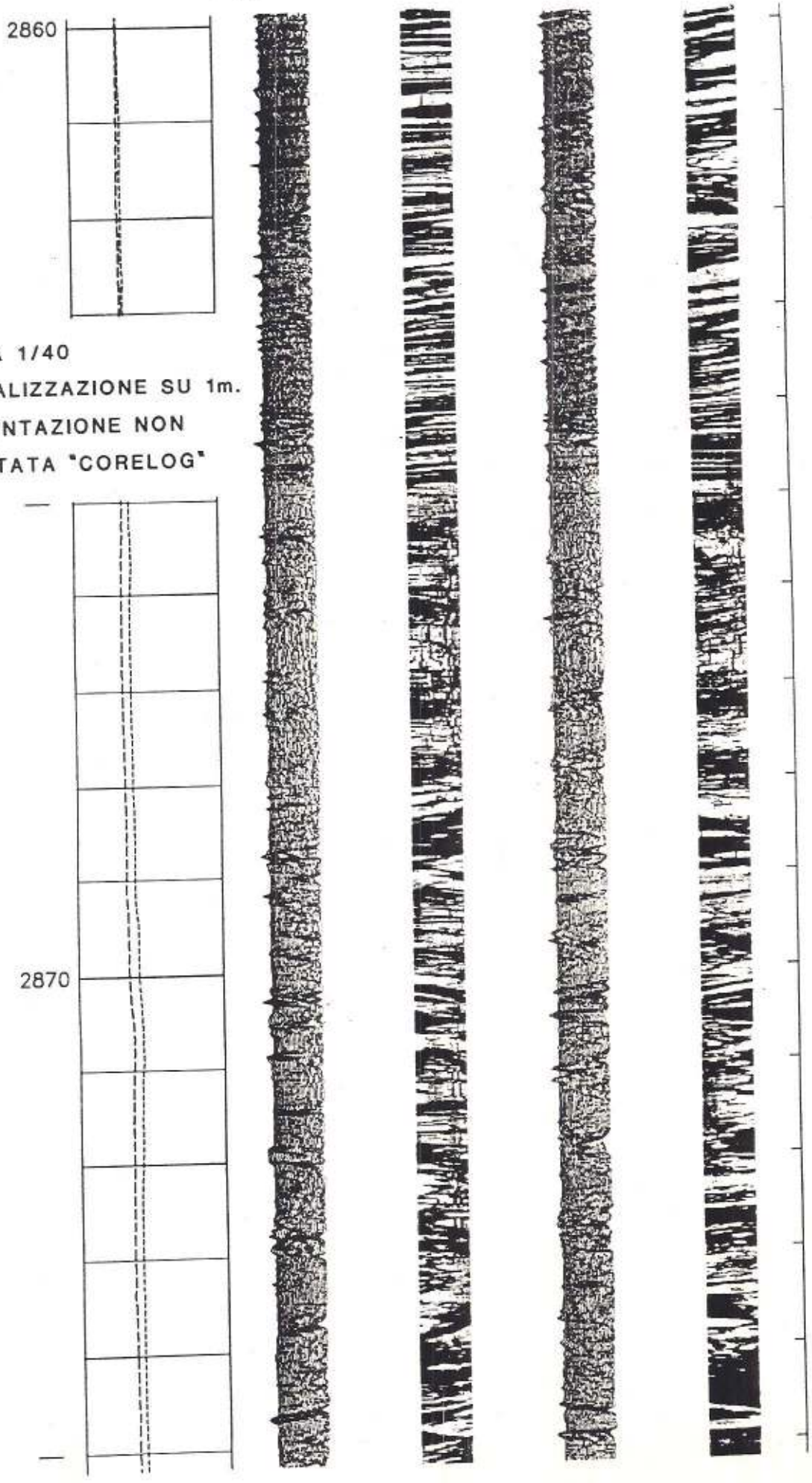

- SCALA 1/40
- NORMALIZZAZIONE SU 1m.
- PRESENTAZIONE NON ORIENTATA "CORELOG"

NORMALIZZAZIONE SU LUNGHI INTERVALLI

NORMALIZZAZIONE SU 1 METRO

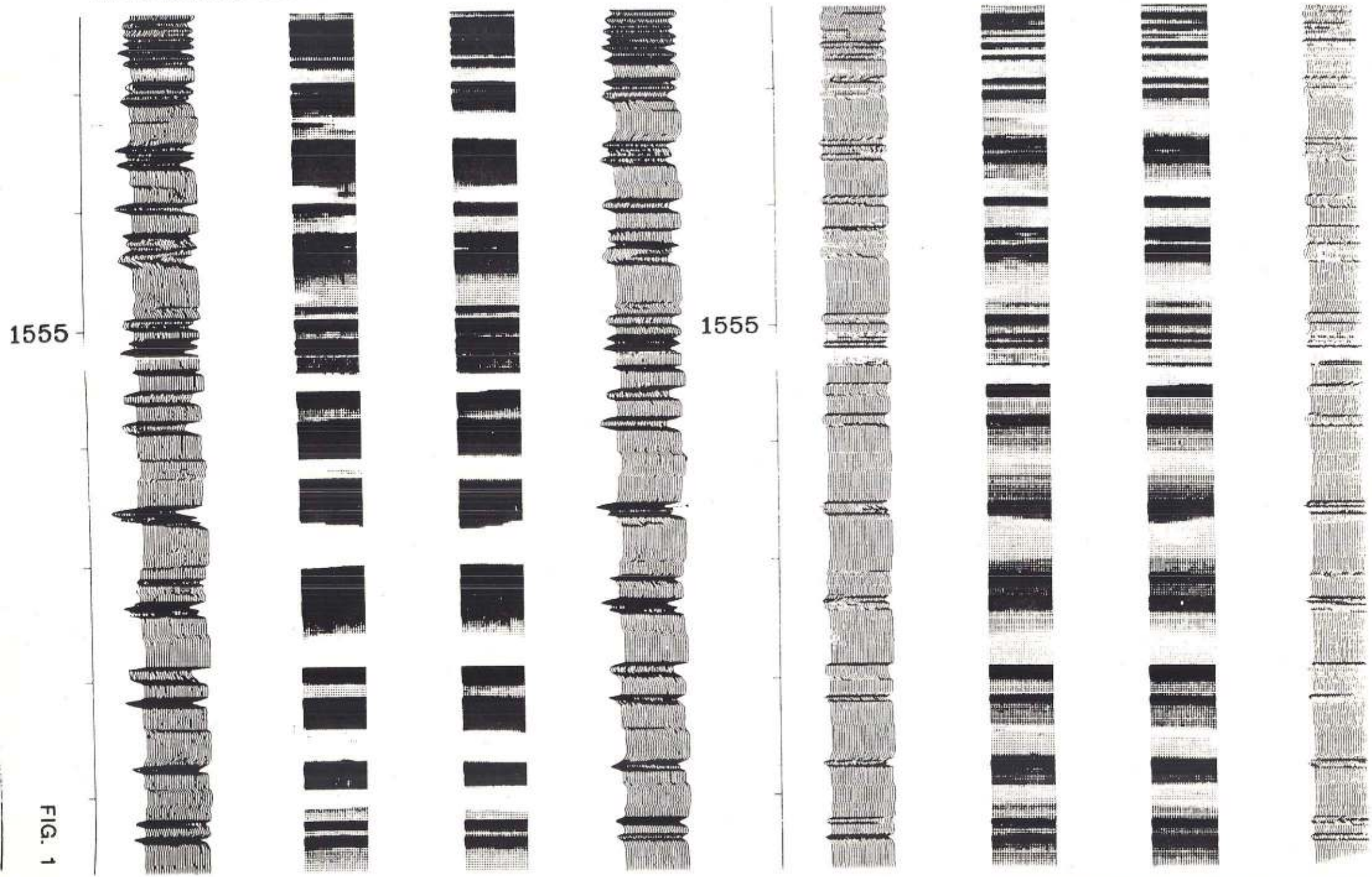

FIG. 1

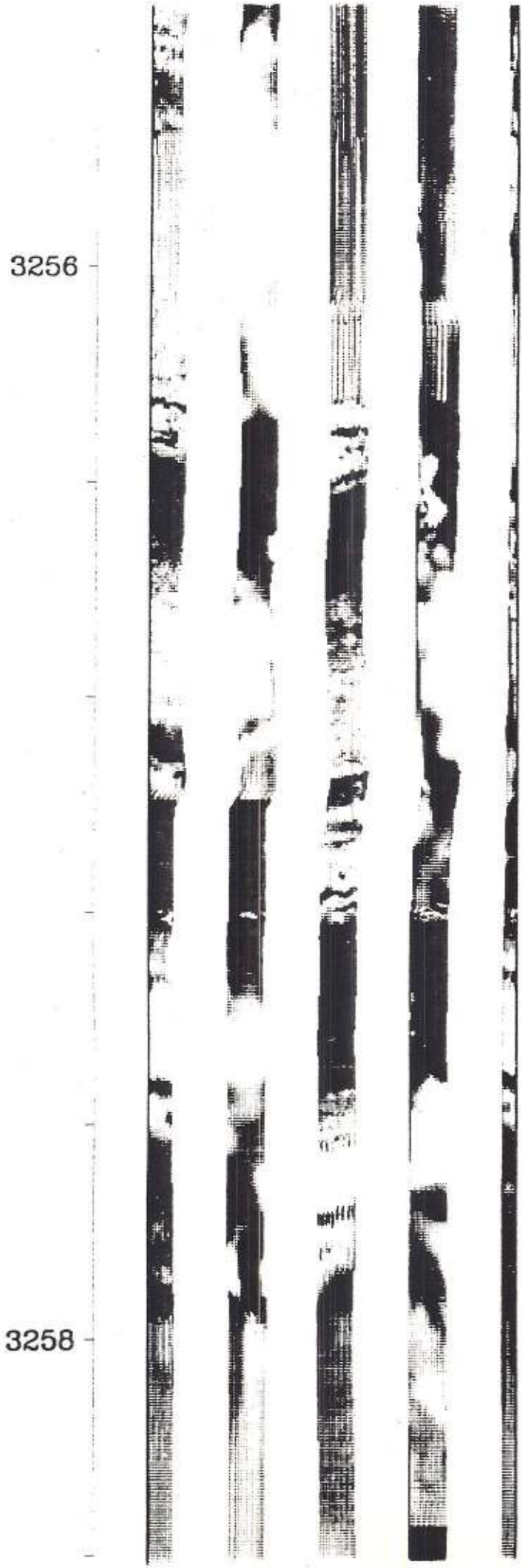
3256
3258

THE OBDT* TOOL

Oil-Base mud Dipmeter Tool (OBDT)*
A new principle applied to dip measurement in oil-base mud wells.

The OBDT* tool is a dipmeter specifically designed for logging in oil-base mud. It uses four micro-induction sensors to measure the variations of formation conductivity. The induction principle avoids the main limitation of tools based on electrode devices, which is the erratic influence of the non-conductive mud on the injection of current into the formation.
The log can be recorded with a single pass of the OBDT tool, and the processing is made with current programs: CYBERDIP* at the wellsite, CLUSTER* or GEODIP* in computing centers.

Operational limitations

- The mud should be less conductive than the formation.
- The tool rotation rate should not exceed 1 turn per 40 ft (12 m).
- Although it is not necessary for the sensor to make contact with the formation, the data quality is affected by borehole damage.
- Resistivity of the formation should be lower than 200 ohm-m.

Features

- A three-axis accelerometer and a three-axis magnetometer provide precise measurements of borehole drift and tool attitude.
- In the dip processing, fluctuations of tool velocity are computed from the acceleration measurement, and eliminated.
- The volumes investigated by the pads are well defined, being controlled by the magnetic field distribution around each sensor. The accuracy with which bed boundaries are thus determined results in regular and repeatable computed dips.

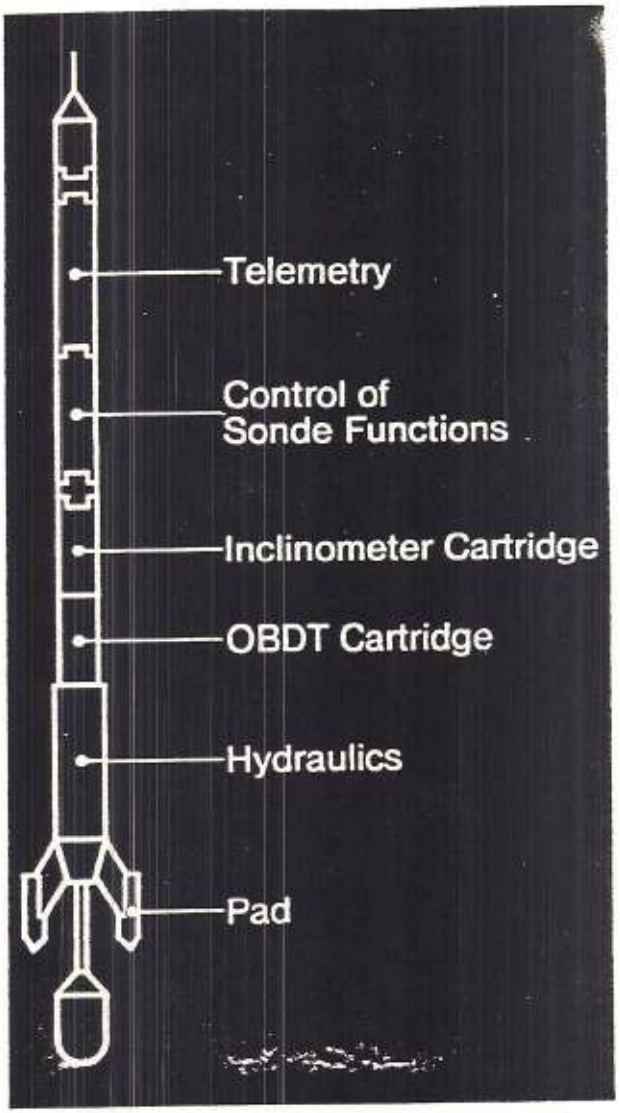

Tool specifications

SPECIFICATIONS	ENGLISH UNITS	S.I. UNITS
Length	32.5 ft	9.9 m
Weight	323 lb	147 kg
Diameter	4.5 inches	114 mm
Minimum hole size	5.5 inches	140 mm
Maximum opening	21.0 inches	533 mm
Pressure rating	20,000 psi	1400 Bars
Temperature rating	350° F	175° C
Logging speed	1800 ft/hr	570 m/hr
Tool Dev. accuracy	± 0.2 deg.	± 0.2 deg.
Tool Azim. accuracy	± 2.0 deg.	± 2.0 deg.

* Mark of Schlumberger

SISTEMA DI FOCALIZZAZIONE E MISURA

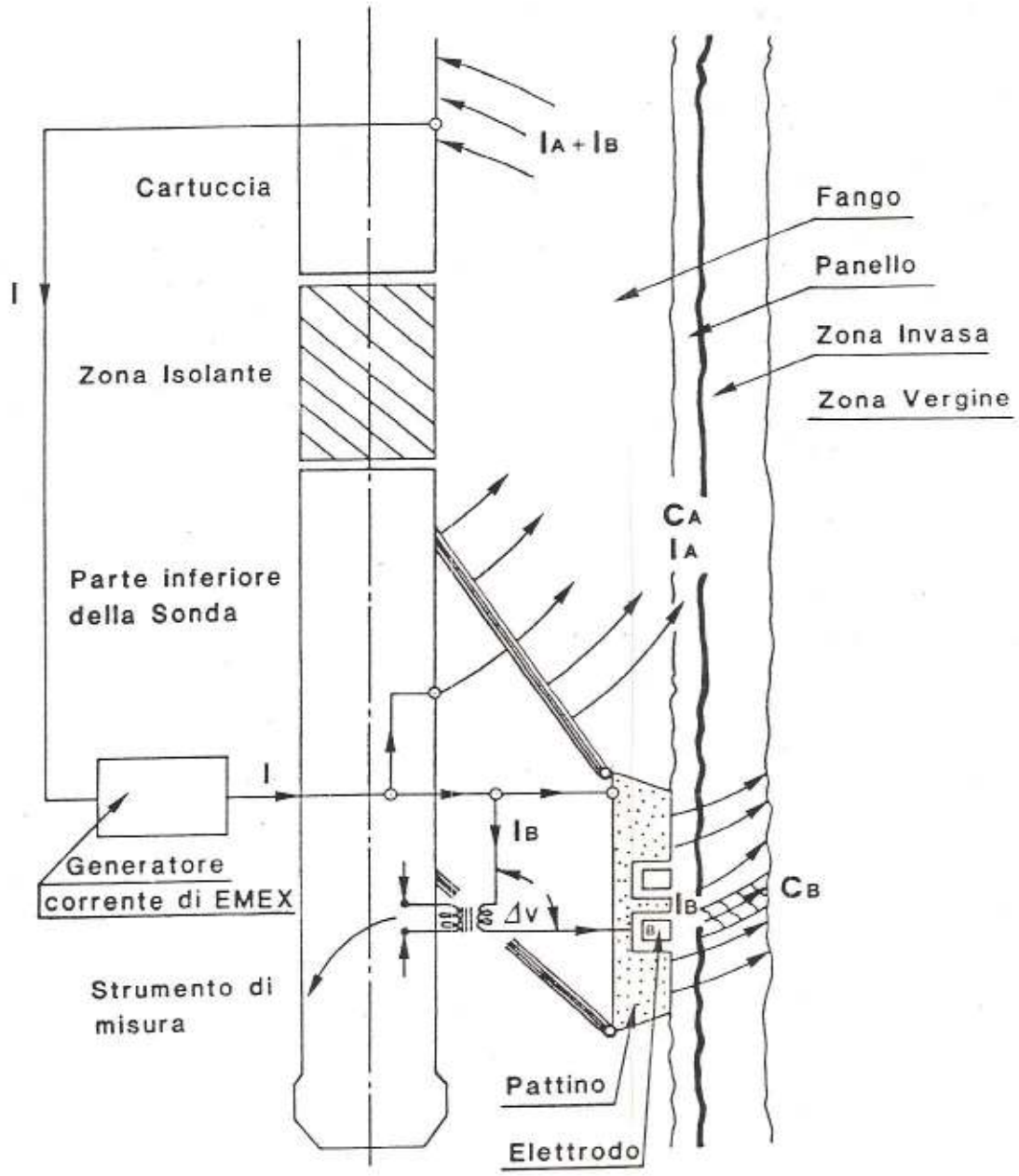

$I_{emex} = I_A + I_B = \text{costante}$

$I_A = K_A \cdot V_A \cdot C_A$ $\qquad$ $I_B = K_B \cdot V_B \cdot C_B$

$I_A >> I_B \rightarrow I_A = I_{emex}$ $\qquad$ $\Delta V \simeq 0 \rightarrow V_A = V_B$

$$I_B = K_B \cdot C_B \cdot \frac{I_A}{K_A \cdot C_A} = K \cdot I_{emex} \cdot \frac{C_B}{C_A}$$

IL DIAMETRO ELETTRICO

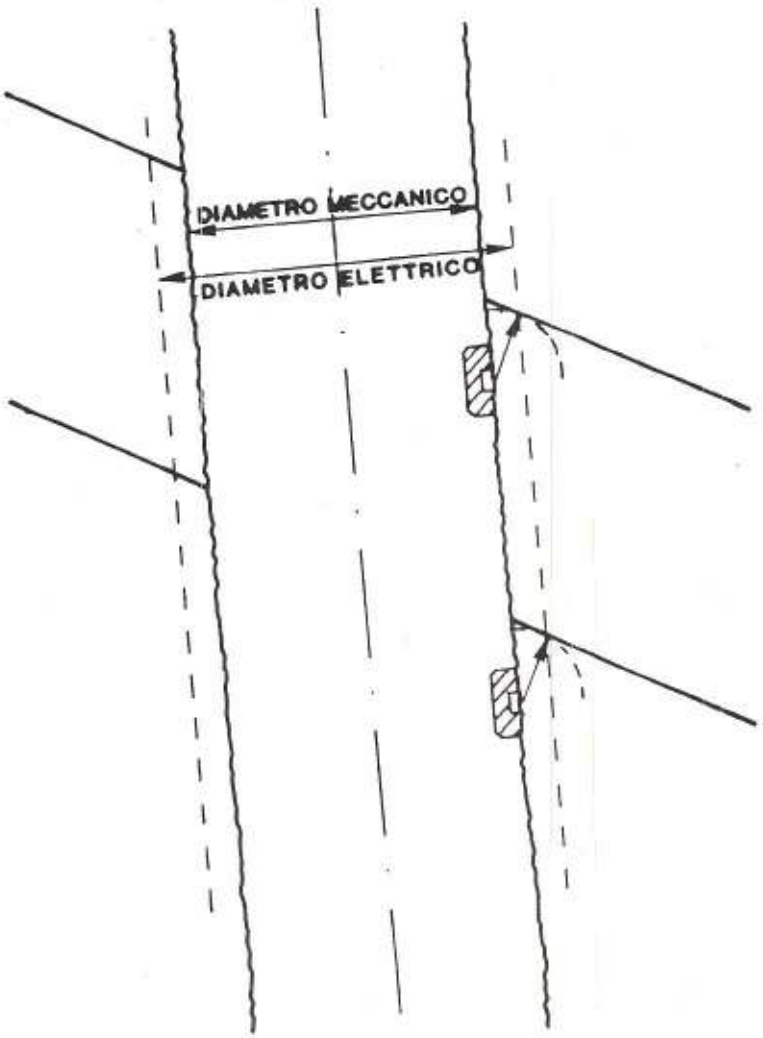

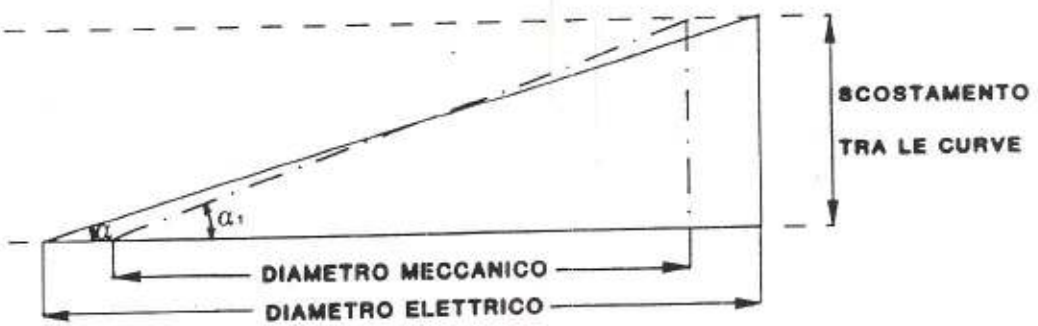

α_1 = PENDENZA APPARENTE

α = PENDENZA VERA

DIAM. ELETT.= DIAM. MECC.+1,6"

SPEED CORRECTION

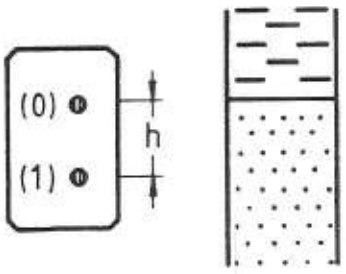

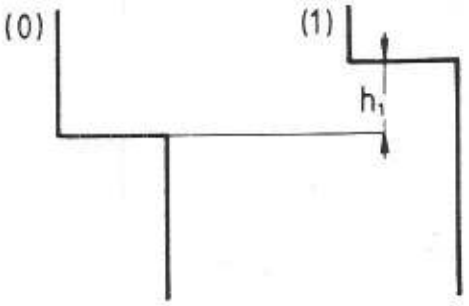

$h = h_1$ NORMAL SPEED

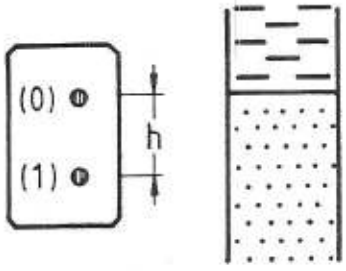

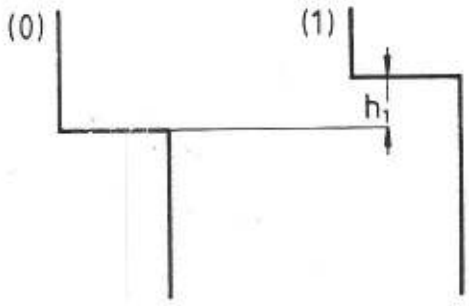

$h_1 < h$ HIGH SPEED

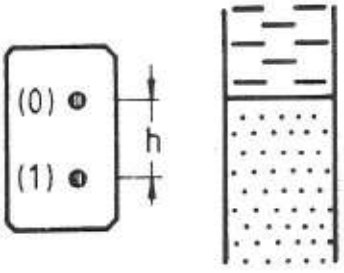

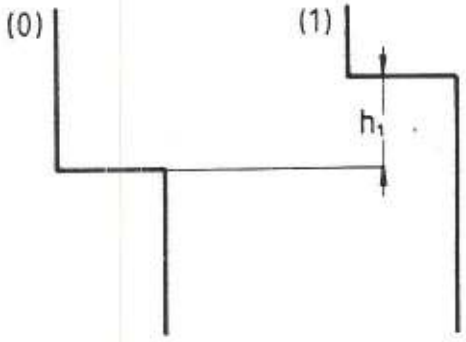

$h_1 > h$ LOW SPEED

$$h_C(1-2) = h(1-2) \cdot \frac{h}{h_1}$$

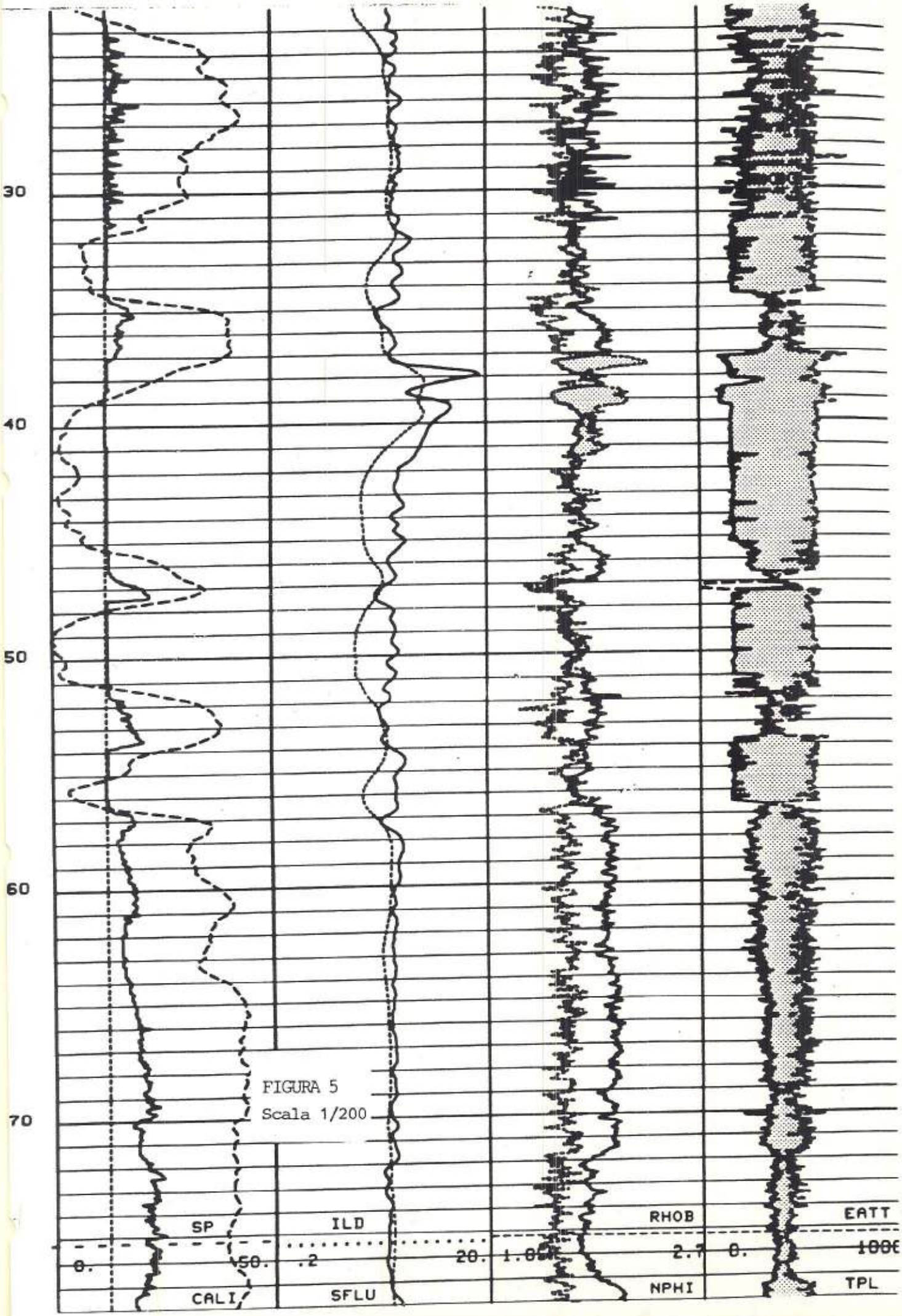

FIGURA 5
Scala 1/200

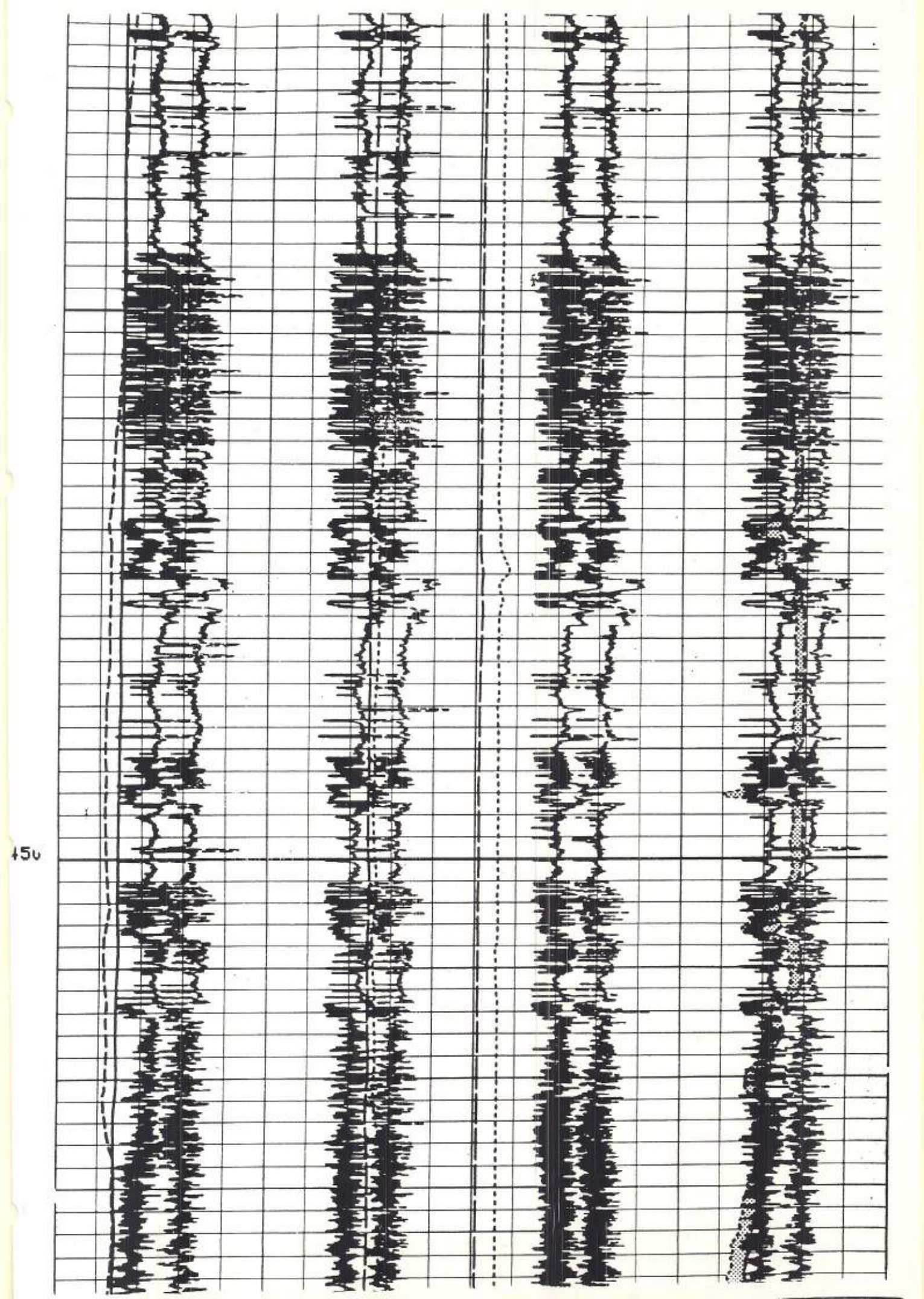

2.1 CALIBRAZIONI ALLA BASE OPERATIVA

2.1.1 **Deviation check**

Il deviation check consente di verificare il corretto funzionamento del pendolo usato per la misurazione della deviazione del pozzo. Il meccanismo viene controllato sia per bassi valori di inclinazione che per alti valori.
Lo strumento viene montato su un apposito sostegno fornito di scala graduata e inclinato, quindi si controlla che il valore che compare sul monitor, che è quello indicato dal pendolo, corrisponda al reale valore di inclinazione indicato sulla scala graduata.

2.1.2 **North check**

Il north check permette di verificare il corretto funzionamento della bussola utilizzata per misurare l'azimut del pattino 1 nel HDT low angle e l'azimut del pozzo nel HDT high angle.
La procedura più semplice consiste nell'orientare il pattino 1 verso il N indicato da una bussola tenuta dall'operatore lontana da materiali che potrebbero influenzarne la lettura, e controllare che la curva del P1AZ sia uguale a 0° o 360°.
Se, invece, viene fatta coincidere con lo 0° la curva del HAZI inclinando lo strumento verso N, il valore del P1AZ sarà uguale a quello del RB e le due curve relative si sovrappongono. (Si ricorda che HAZI = P1AZ - RB da cui per HAZI = 0. P1AZ = RB).

2.1.3 **Caliper check**

La calibrazione del caliper viene eseguita utilizzando 2 anelli di diametro differente dei quali si effettua la misura aprendo i pattini dello strumento.
Per ciascuno dei due caliper, C1 e C2, si ottengono dunque due misure che, con i due valori noti di riferimento, permettono di calcolare i parametri di gain e di offset (vedi figura 4). Tali valori vengono memorizzati e verranno utilizzati come controllo in cantiere al momento della registrazione quando il check viene ripetuto secondo le medesime modalità.

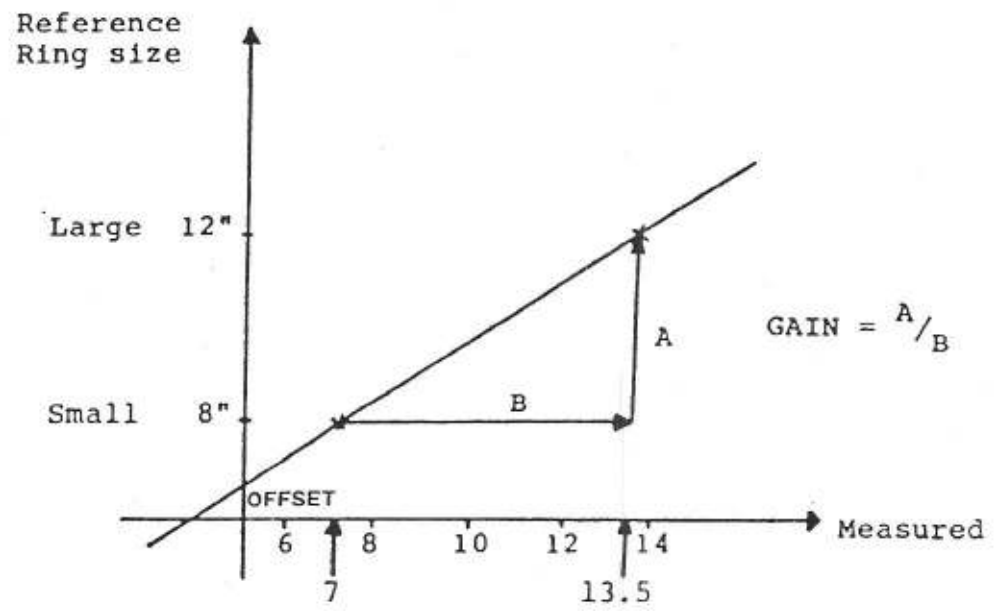

$$\text{Gain} = \frac{\text{large ring size (12")} - \text{small ring size (8")}}{\text{reading in large ring} - \text{reading in small ring}}$$

Offset = large ring size (12") - (reading in large ring) X (gain)

$$\text{gain} = \frac{12 - 8}{13.5 - 7} = 0.615$$

offset = 12 - (13.5 X 0.615) = 3.69

Measured signal 12"

actual hole size = 12 X (gain .615) + (offset 3.69) = 11.07"

Fig. 4 - Calibrazioni alla base operativa: caliper check.

2.2 CALIBRAZIONI DI CANTIERE

Prima di iniziare la discesa dell'attrezzo in pozzo e possibilmente al termine della registrazione è opportuno verificare che tutto funzioni regolarmente. Le operazioni che l'ingegnere esegue non sono delle vere e proprie calibrazioni, se si eccettua quella del caliper, ma dei controlli sulle varie parti dello strumento i cui risultati devono essere presentati in coda al log.

2.2.1 **Deviation check** (fig. 5)

Il controllo viene effettuato con lo strumento appeso al derrick, inizialmente in posizione quasi verticale, quindi via via più inclinata. Quando l'attrezzo è verticale, la curva del relative bearing si muove in maniera casuale perchè non esiste una generatrice superiore di riferimento, e la curva del HAZI risulta ad essa speculare.
Successivamente lo strumento viene inclinato e l'ingegnere controlla che sul monitor la curva della deviazione (linea continua) si muova. In questo modo si verifica esclusivamente che il pendolo non sia bloccato ma non è possibile controllare che il valore misurato corrisponda all'effettiva deviazione dell'attrezzo.

2.2.2 **North check** (fig. 5)

In cantiere il nord segnato dalla bussola non è esattamente il nord magnetico a causa della presenza di numerosi fattori che influenzano la lettura, per cui anche questa operazione è un semplice controllo di funzionamento e non una vera calibrazione.
L'attrezzo, che è appeso al derrick, viene inclinato verso N (HAZI = 0) e fatto ruotare in senso orario in passi successivi di 90°. Tale rotazione è evidenziata dalle curve del RB e del P1AZ che risultano sovrapposte. Nell'esempio in figura, l'HAZI non è esattamente verso N e quindi si nota una leggera separazione tra le due curve.
Questo tipo di operazione, con l'utilizzo dei nuovi tools, viene eseguita assai raramente e generalmente sostituita da una più rapida procedura che consiste nel rivolgere il pattino n. 1 verso N e controllare la relativa lettura dello strumento. Tale operazione viene generalmente eseguita contemporaneamente al deviation check.

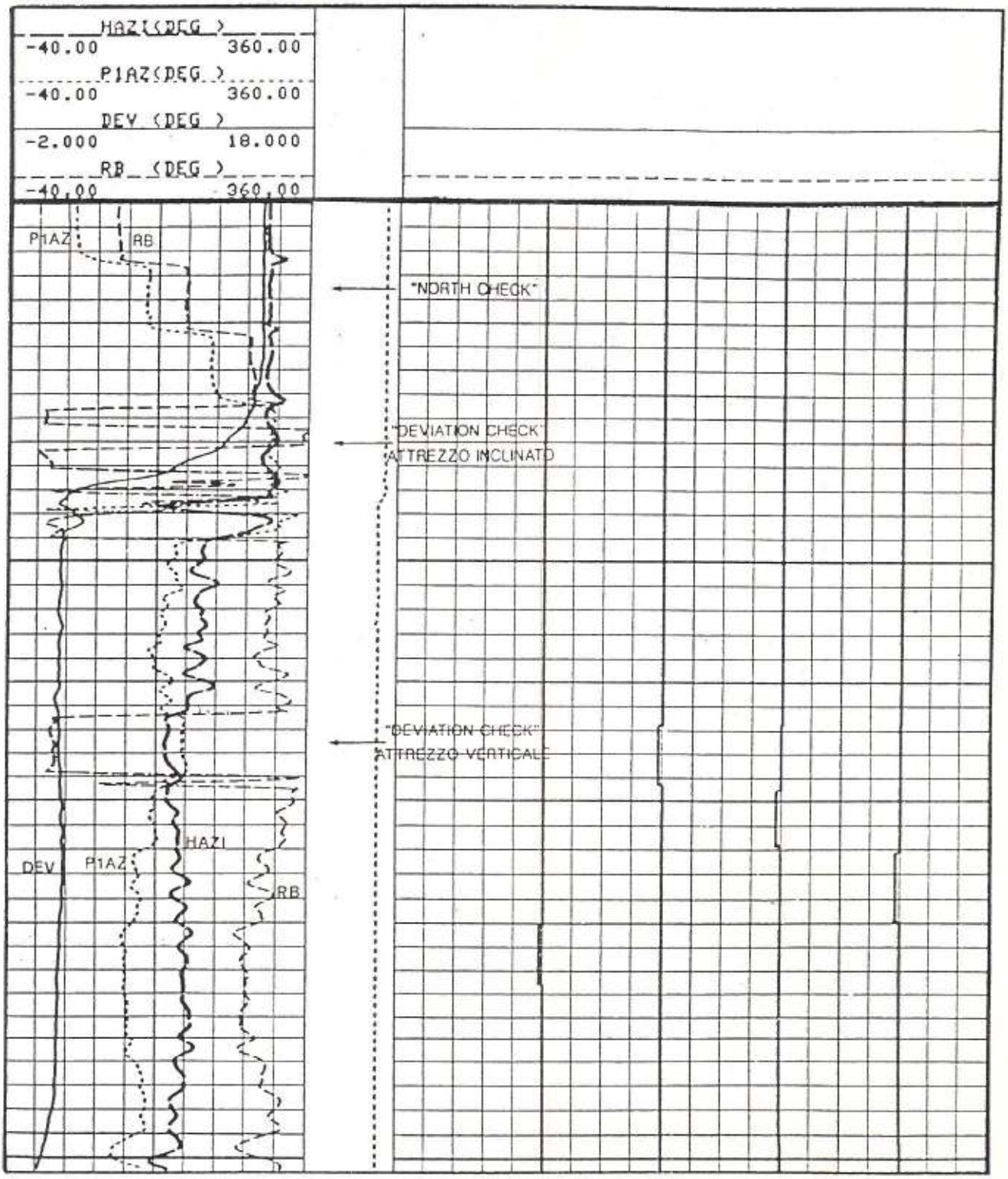

Fig. 5 - Calibrazioni di cantiere: "deviation check" e "north check".

2.2.3 **Relative bearing check o rotation check (fig. 6)**

Il rotation check viene eseguito per verificare che il meccanismo utilizzato per la misura del relative bearing, che negli attrezzi meccanici consiste in un peso eccentrico libero di ruotare attorno ad un asse verticale, sia perfettamente funzionante. In pratica si tratta di verificare che il fenomeno di sticking che si verifica quando lo strumento è verticale, scompaia per inclinazioni di 2° o maggiori.

Il check consiste in una rotazione e mezza dello strumento leggermente inclinato prima in senso orario quindi antiorario o viceversa che viene evidenziata dalla curva del relative bearing con una caratteristica forma a V.

Nel SHDT e nei tools Dresser della serie 1016 che fanno uso di magnetometri e accellerometri tale check risulta ovviamente inutile.

2.2.4 **Button check (fig. 7,8)**

Il check dei bottoni ne verifica il collegamento e il buon funzionamento senza interferenze.

L'operazione consiste nel toccare uno alla volta i vari bottoni procedendo in senso orario verificandone la relativa risposta sul monitor che consiste in una più o meno marcata flessione verso sinistra della curva. Tale flessione deve interessare una sola curva per volta, quella relativa al bottone controllato, dimostrando l'assenza di interferenze (cross talk) che si ripercuoterebbero negativamente sulle correlazioni qualora si verificassero durante la registrazione.

Il controllo viene eseguito anche per lo speed bottom la cui curva viene registrata solo su nastro e utilizzata poi per la correzione di velocità. A questo proposito si ricorda che i vecchi HDT per fango ad olio e tutti gli strumenti Dresser non dispongono di tale bottone supplementare.

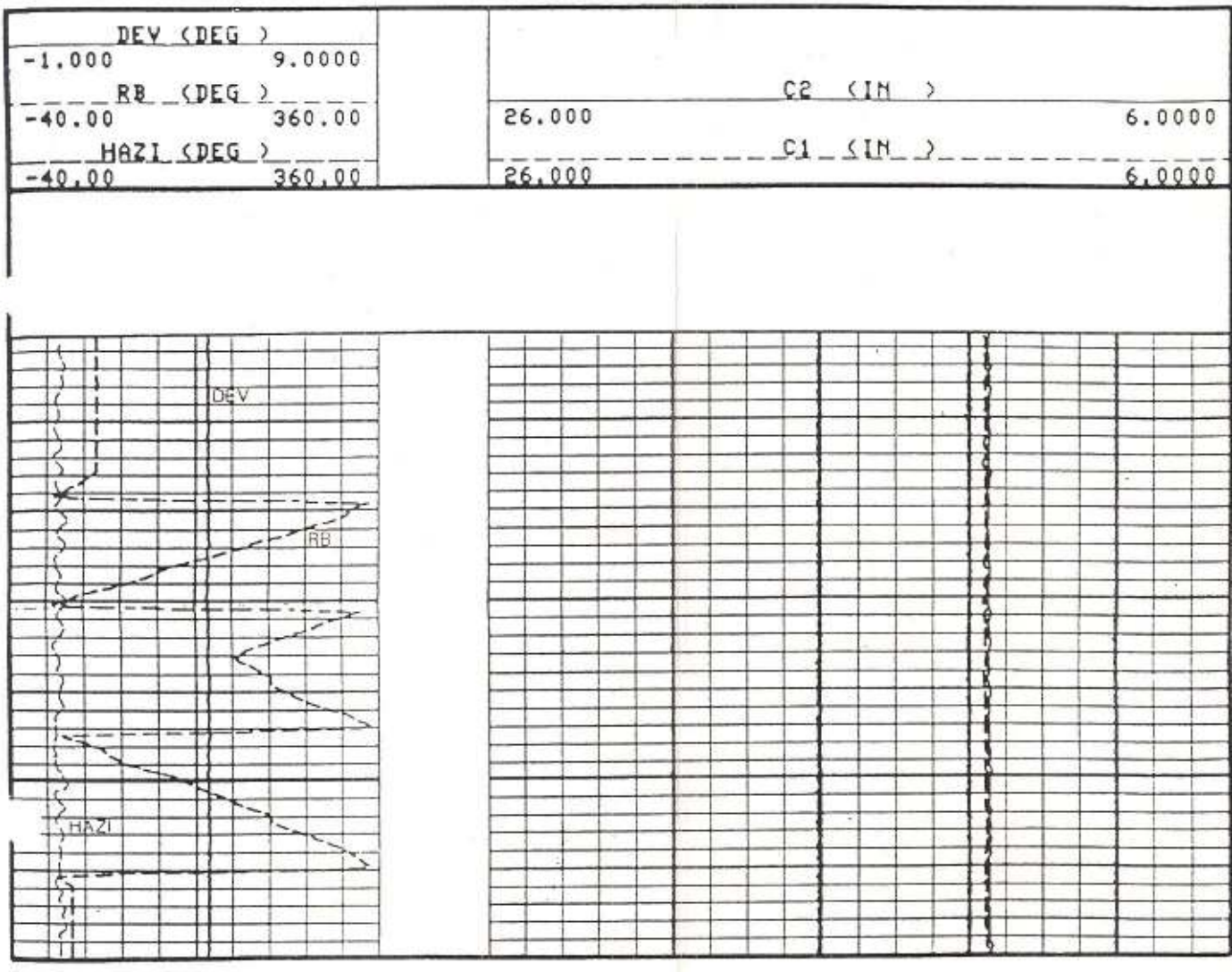

Fig. 6 - Calibrazioni di cantiere: rotation check.

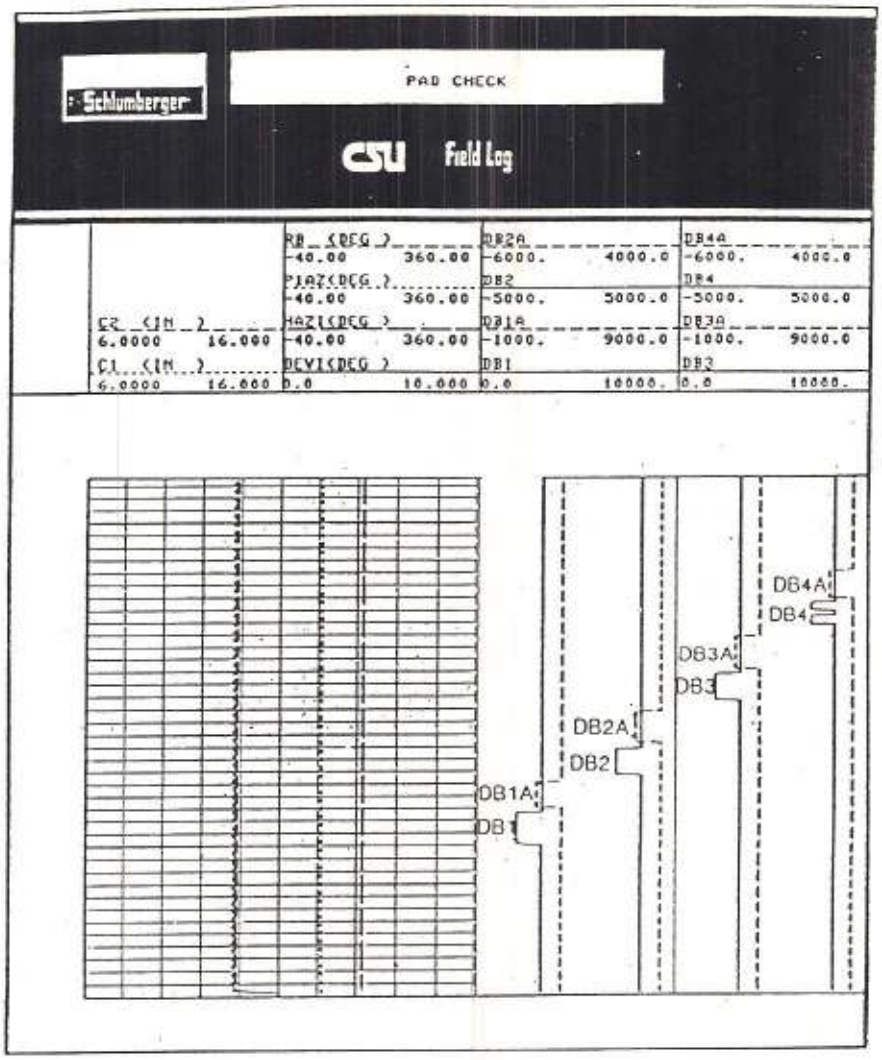

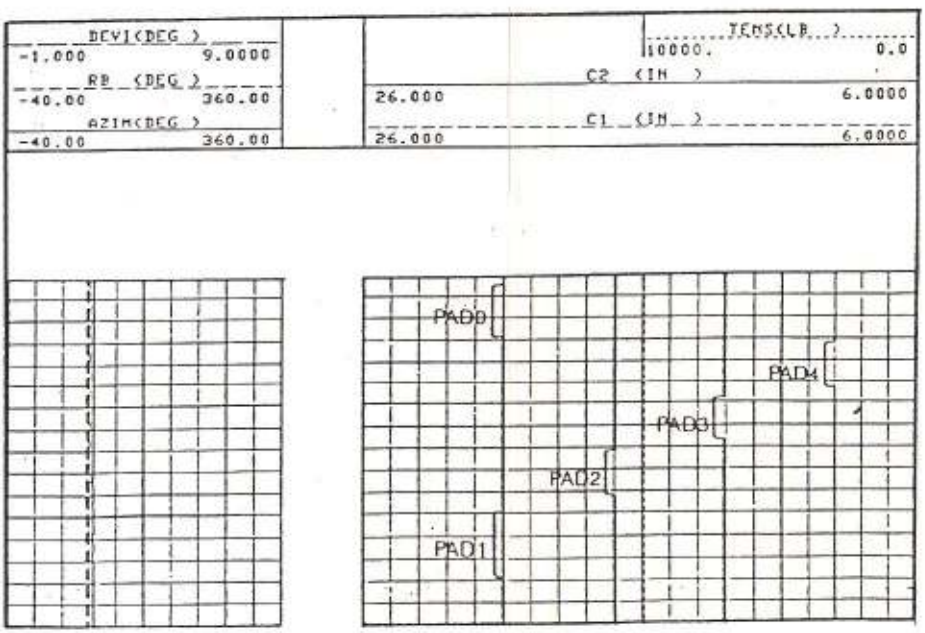

Fig. 7 - Calibrazioni di cantiere: button check SHDT e HDT.

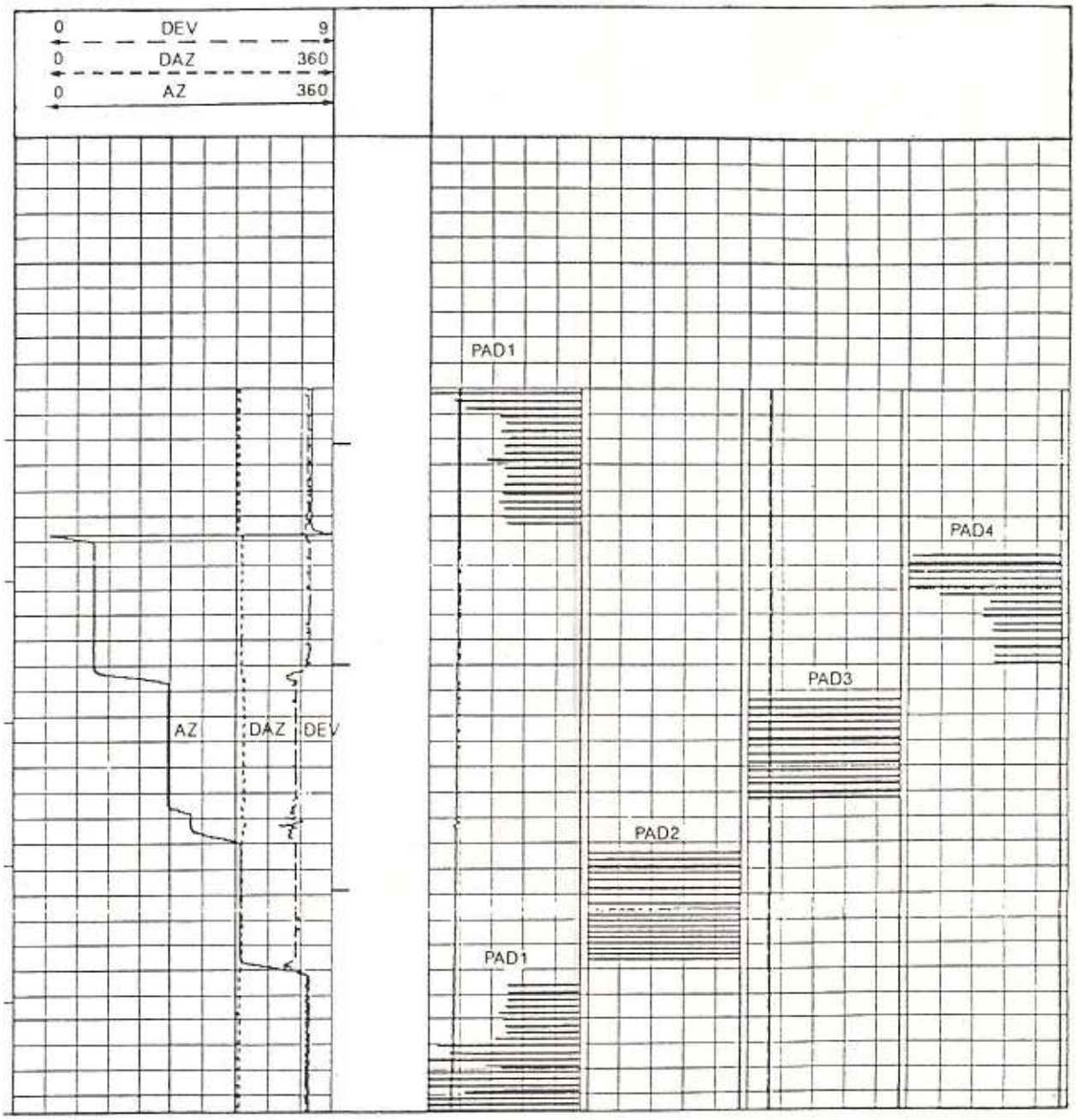

Fig. 8 - Calibrazioni di cantiere: button check diplog.

2.2.5 **Caliper check (fig. 9)**

La calibrazione del caliper viene eseguita come detto, anche in cantiere utilizzando due anelli di diametro differente indicati come small e large sul log.

In generale i valori dei due diametri non devono essere troppo vicini tra loro e ricadere nell'intorno di quelli che si prevedono di misurare in pozzo. Per ciascuno dei due caliper, C1 e C2, vengono ricalcolati un gain e un offset che vengono confrontati con quelli ottenuti alla base operativa e quindi memorizzati. Successivamente, durante la registrazione ciascuna misura di caliper viene moltiplicata per il gain e al risultato viene aggiunto l'offset per ottenere il valore di diametro calibrato. Al termine della registrazione è opportuno ripetere un controllo per verificare che l'inevitabile drift subito dallo strumento sia entro limiti accettabili. Tale controllo viene generalmente eseguito nel casing durante la risalita.

Ai check presentati, validi per tutti gli strumenti, si aggiungono per i tools che hanno sostituito le parti meccaniche con magnetometri e accellerometri, la misura dell'intensità e inclinazione del campo magnetico e una misura dell'accellerazione di gravità.

La prima viene eseguita in discesa, fuori scarpa per controllare il corretto funzionamento del magnetometro; la seconda, che serve per controllare l'accelerometro viene eseguita tarandosi con un valore di 9.8 m/sec^2.

```
                BEFORE SURVEY CALIBRATION SUMMARY

  PERFORMED:    24-MAY-88 03:22
  PROGRAM FILE: HDT    (VERSION    30.22   87/02/10  87/02/09)

HDTE                CALIPER CALIBRATION SUMMARY

              MEASURED                    CALIBRATED
            SMALL   LARGE                SMALL     LARGE        UNITS
    C1       7.73    19.4                 6.00      16.0          IN
    C2      19.88     8.3                16.00       6.0          IN

   CP 30.22           FILE    0       24-MAY-88 03:21
```

Fig. 9 - Calibrazioni di cantiere: caliper check.

CALCOLO MANUALE

DA LOG :

- AZIMUT ELETTRODO # 1 (PIAZ)
- RELATIVE BEARING
- INCLINAZIONE DEL FORO
- AZIMUT DELL'INCLINAZIONE (HAZI)

  (LETTURA DIRETTA O
  HAZI = PIAZ - RB)

- CALIPER (1-3)
- CALIPER (2-4)

CORRELAZIONE TRA LE CURVE
(NE VENGONO USATE GENERALMENTE 3 SU 4)

E MISURA DI 2 SCOSTAMENTI :

- SCOSTAMENTO TRA CURVE ADIACENTI
- SCOSTAMENTO DIAGONALE

CALCOLARE :

$$D = \frac{CAL\,(1-3) + CAL\,(2-4)}{2} + 1.8$$

CORREZIONE PER LA DEVIAZIONE DEL POZZO E CALCOLO DELL'AZIMUT E DELLA PENDENZA VERI

- UTILIZZO DELLO STEREONET - OVERLAY

  RUOTARE L'OVERLAY FINO AL FAR COINCIDERE HAZI CON IL PUNTO E

  SEGNARE IL PUNTO A CON

  AZ = P1AZ + APP AZ

  E PENDENZA = PENDENZA APPARENTE

  SCENDERE LUNGO UN PARALLELO DAL PUNTO A DI TANTI GRADI PARI ALL'INCLINAZIONE DEL POZZO

  LEGGERE NEL PUNTO B <u>L'INCLINAZIONE VERA</u> DELLO STO E L'AZIMUT RIFERITO AL NORD MAGNETICO

  $AZI_{GEOG} = AZI_{MAG} \pm$ DECLINAZIONE MAGNETICA

CALCOLO DELLA PENDENZA E DELL'AZIMUT APPARENTI RIFERITI ALL'ELETTRODO # 1

- PER PICCOLI SCOSTAMENTI

  (MENO DI 3 INCHES PER CURVE ADIACENTI E 4 INCHE PER CURVE DIAGONALI)

  ENTRARE NELL'ABACO 1 CON I 2 SCOSTAMENTI PER RICAVARE ϕ AZIMUT APPARENTE.

  RICAVARE LA PENDENZA APPARENTE θ CON L'ABACO 2

- PER GROSSI SPOSTAMENTI

  MOLTIPLICARE GLI SCOSTAMENTI PER $\frac{1}{2}$ (o $\frac{1}{5}$ o $\frac{1}{10}$)

  RICAVARE ϕ AZIMUT APPARENTE CON L'ABACO 1

  ENTRARE NELL'ABACO 2 PER RICAVARE θ PENDENZA APPARENTE DOPO AVER MOLTIPLICATO I VALORI PRECEDENTEMENTE TROVATI PER 2 (05 o 10)

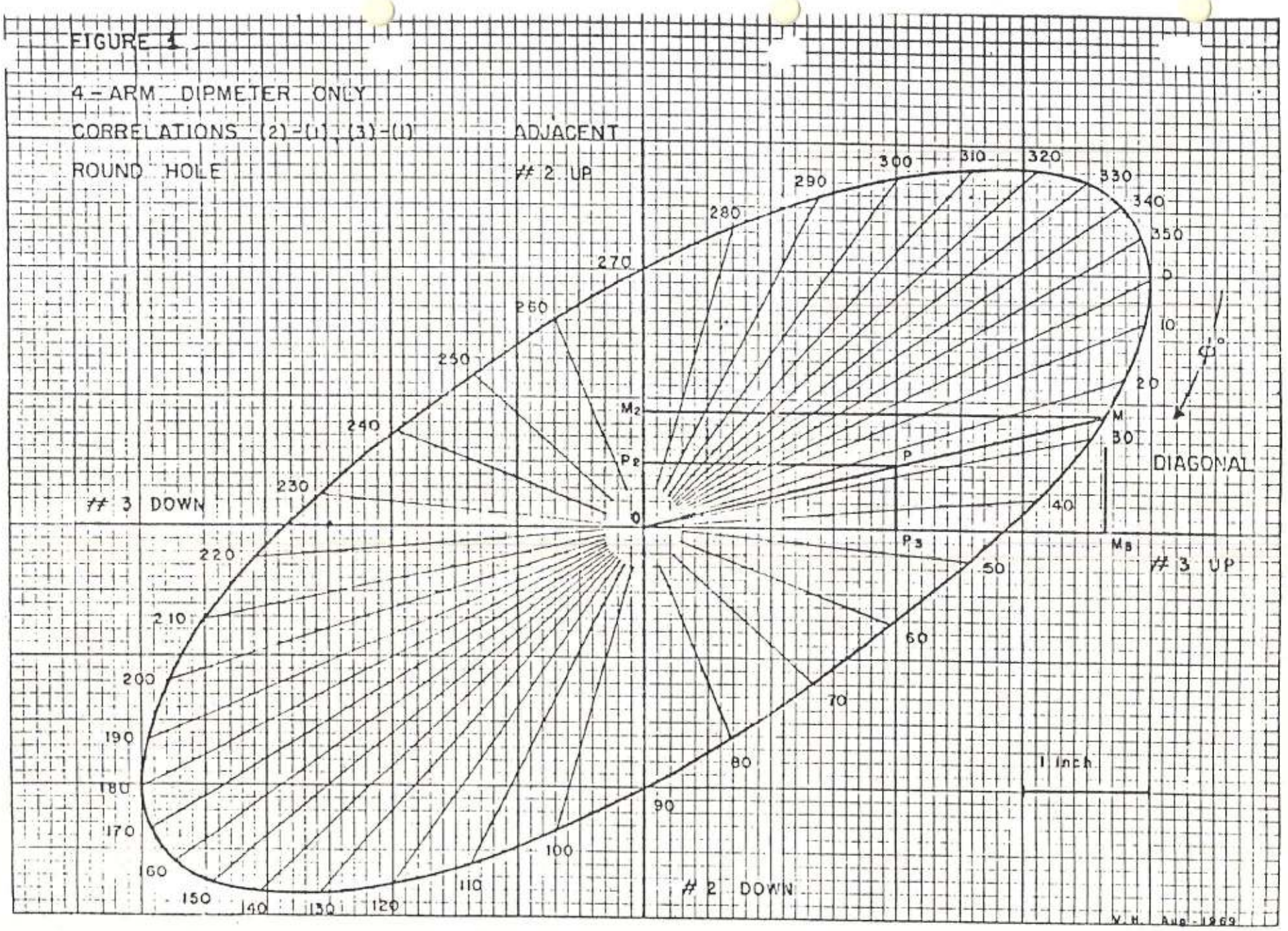
FIGURE 1
4-ARM DIPMETER ONLY
CORRELATIONS (2)-(1), (3)-(1)
ROUND HOLE
ADJACENT
2 UP
DIAGONAL
3 DOWN
3 UP
2 DOWN
1 inch
V.H. Aug-1969

FIGURE 13

4 - ARM DIPMETER ONLY — APPARENT DIP DETERMINATION

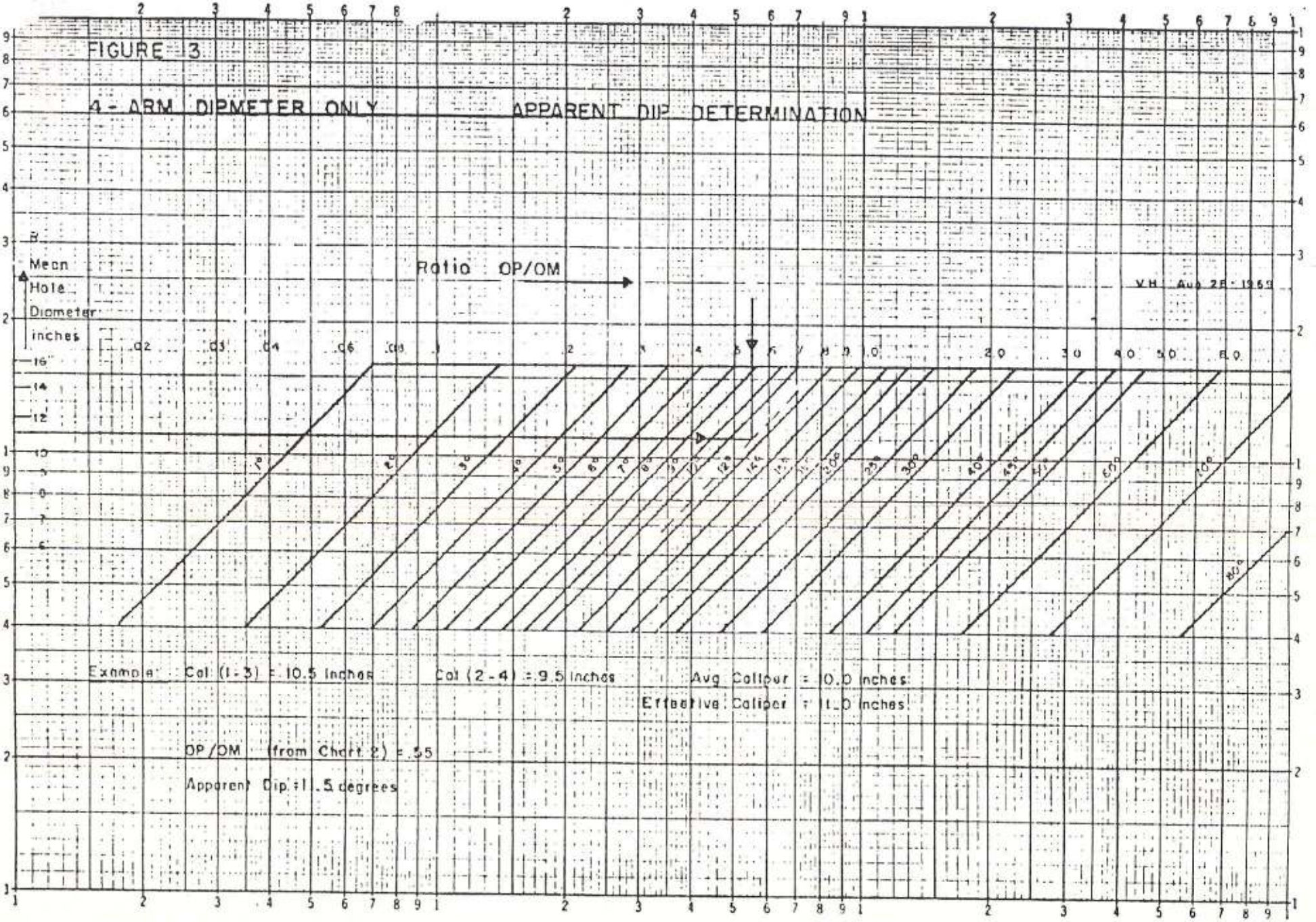

Example: Col (1-3) = 10.5 inches Col (2-4) = 9.5 inches Avg Caliper = 10.0 inches

Effective Caliper = 11.0 inches

OP/OM (from Chart 2) = .55

Apparent Dip = 11.5 degrees

CORREZIONE PER LA DEVIAZIONE DEL POZZO

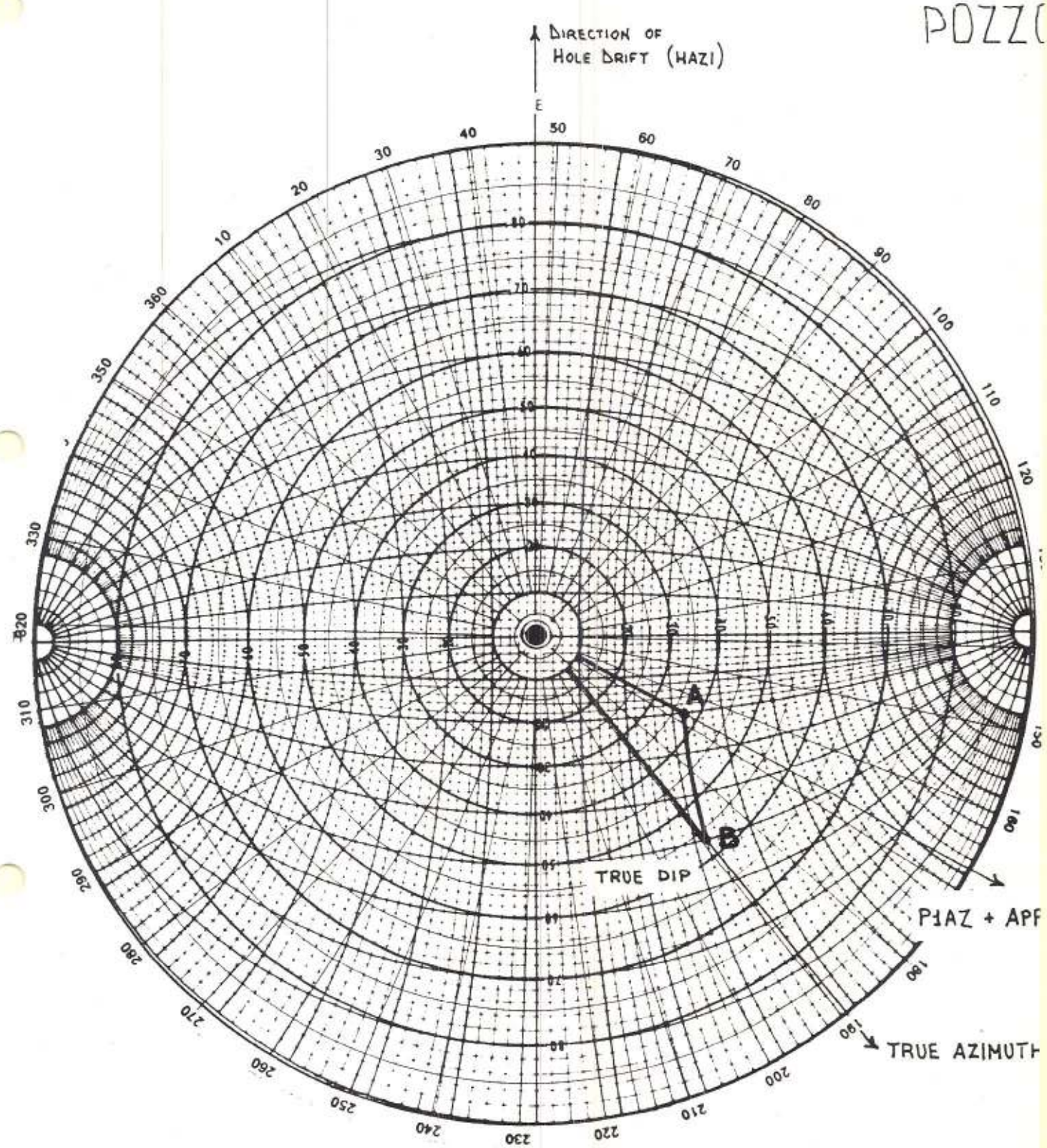

DEPTH (FEET)	CALIPERS D13 (INCHES)	D24	CURVE DISPLACEMENTS H12	H23	H34 (INCHES)	H41	H13	H24	MAX	WELL DEVIATION DEV (DEGREES)	DVAZ	TOOL ORIENTATION PAZ (DEGREES)	RB
3836	8.9	8.4	-0.34	-0.99	0.39	0.79	*	*	57	2.3	7	202	195
3834	8.8	8.4	-0.29	4.20	-0.29	1.26	-1.91		46	2.4	7	203	196
3832	8.8	8.4	3.58	1.46			-0.45		10	2.4	5	203	198
3830	8.8	8.4	-2.97	1.42	-0.06	1.07	-2.22		24	2.4	3	202	199
3828	8.8	8.4	-3.24		1.77	0.74	1.52		31	2.5	2	200	198
3826	8.7	8.4	-3.21	-0.40	1.21	0.49	-3.35		36	2.5	3	201	198
3824	8.6	8.4	-0.90	-0.28	1.10	0.37		0.73	38	2.5	4	204	200
3822	8.5	8.4	-1.04	-0.04	1.12	0.51		0.94	35	2.6	4	202	198
3820	8.6	8.2	-4.45	5.10	1.21	3.22	-3.20		40	2.7	3	196	193
3818	8.5	8.1	0.63	0.11	6.88	-0.07		-0.20	22	2.6	3	191	188
3816	8.5	8.4	0.70	0.04			0.60		27	2.5	5	191	185
3814	8.6	8.5	-0.90	1.04	-0.80		0.11		30	2.4	4	188	183
3812	8.6	8.4	-0.57	0.97			0.62		25	2.3	360	185	184
3810	8.5	8.3	0.16	0.99	0.87	-1.92	*	*	23	2.2	359	182	183
3808	8.5	8.2			0.79	-1.16	-0.17		24	2.1	360	177	177
3806	8.6	8.2	-2.42	1.56	1.27	-0.11			37	2.1	359	172	173
3804	8.6	8.3		0.19	-4.47			-4.16	14	2.1	358	171	172
3802	8.6	8.5		NO CORRELATION						2.0	1	174	172
3802	8.6	8.5		NO CORRELATION						2.0	1	174	172
3800	8.4	8.6	-5.80	-6.00	0.38	-9.13			35	2.0	360	183	182
3798	8.0	8.3		5.49	0.93	-2.31			37	2.0	359	192	192
3796	8.2	8.2	0.81	0.11	-0.78		1.16		14	2.0	2	194	192

Fig 3 — Example of results from an existing Dipmeter program used as input to CLUSTER.

DEPTH (FEET)	ADJACENT-CURVE DISPLACEMENTS (INCHES) H12	H23	H34	H41	PAZ (DEGR.)
OPEN ZONE					
3858	3.71	-0.69	3.43	-3.27	181
3856	0.81	-0.65	-0.90	0.78	192
3854	0.97	-0.43	-1.24	-0.70	189
3852	0.92	-0.46	-1.39		182
3850	0.77	-0.20	-1.45	0.59	178
3848	0.70	-0.12	-4.46		176
3846		-0.31	-4.82		180
STABLE ZONE					
3844	0.32	-0.58	-0.37	0.45	195
3842	0.11	-0.79	-0.34	0.36	205
3840	-0.04	-0.93		0.65	208
3838	-0.25	-1.03	0.44	0.73	205
3836	-0.34	-0.99	0.39	0.79	202
OPEN ZONE					
3834	-0.29	4.20	-0.29	1.26	203
3832	3.58	1.46			203
3830	-2.97	1.42	-0.06	1.07	202
3828	-3.24		1.77	0.74	200
3826	-3.21	-0.40	1.21	0.49	201
3824	-0.90	-0.28	1.10	0.37	204
3822	-1.04	-0.04	1.12	0.51	202
3820	-4.45	5.10	1.21	3.22	196
3818	0.63	0.11	6.88	-0.07	191
3816	0.70	0.04			191
OPEN ZONE					
3814	-0.90	1.04	-0.80		188
3812	-0.57	0.97			185
3810	0.16	0.99	0.87	-1.92	182
3808			0.79	-1.16	177
3806	-2.42	1.56	1.27	-0.11	172
3804		0.19	-4.47		171
3802					174
3800	-5.80	-6.00	0.38	-9.13	183
3798		5.49	0.93	-2.31	192
3796	0.81	0.11	-0.78		194

Fig. 8 — Example of zoning.

MSD

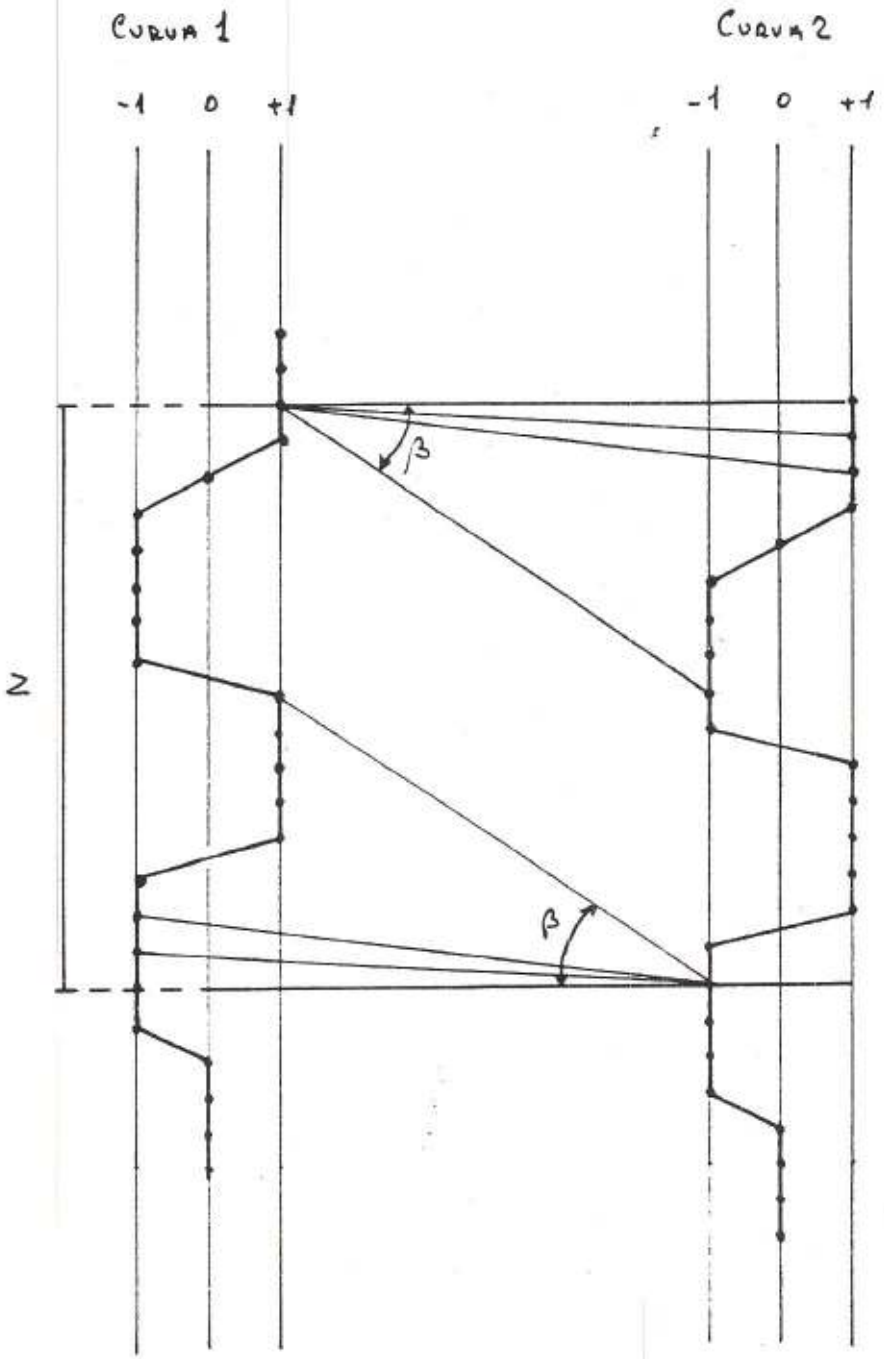

per $\alpha < \beta$ il programma va fino ad α
per $\alpha > \beta$ il programma va fino a β

SCALE: 1/20

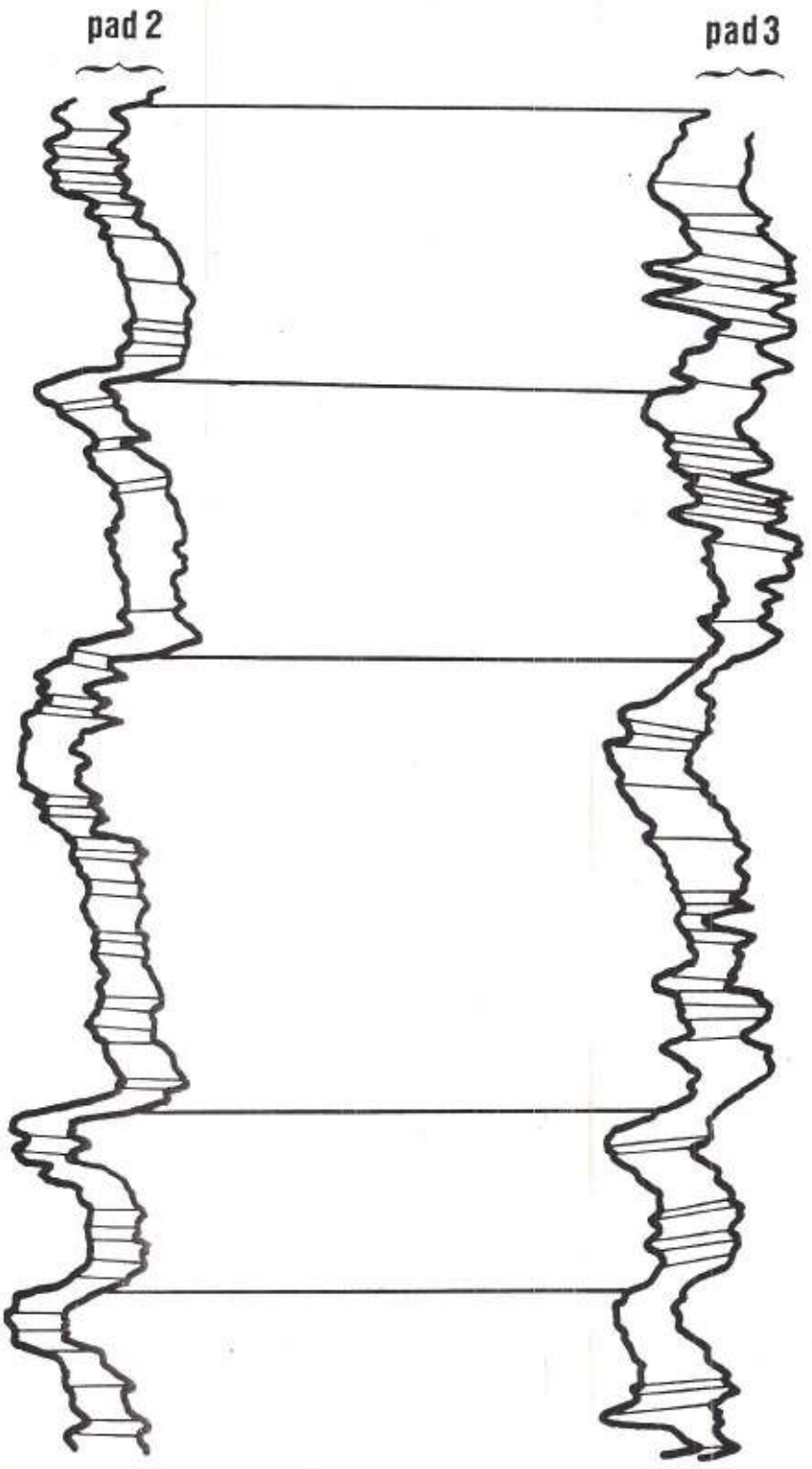

SIDE BY SIDE AND PAD TO PAD CORRELATIONS

Schlumberger

SHOT
9-82 16

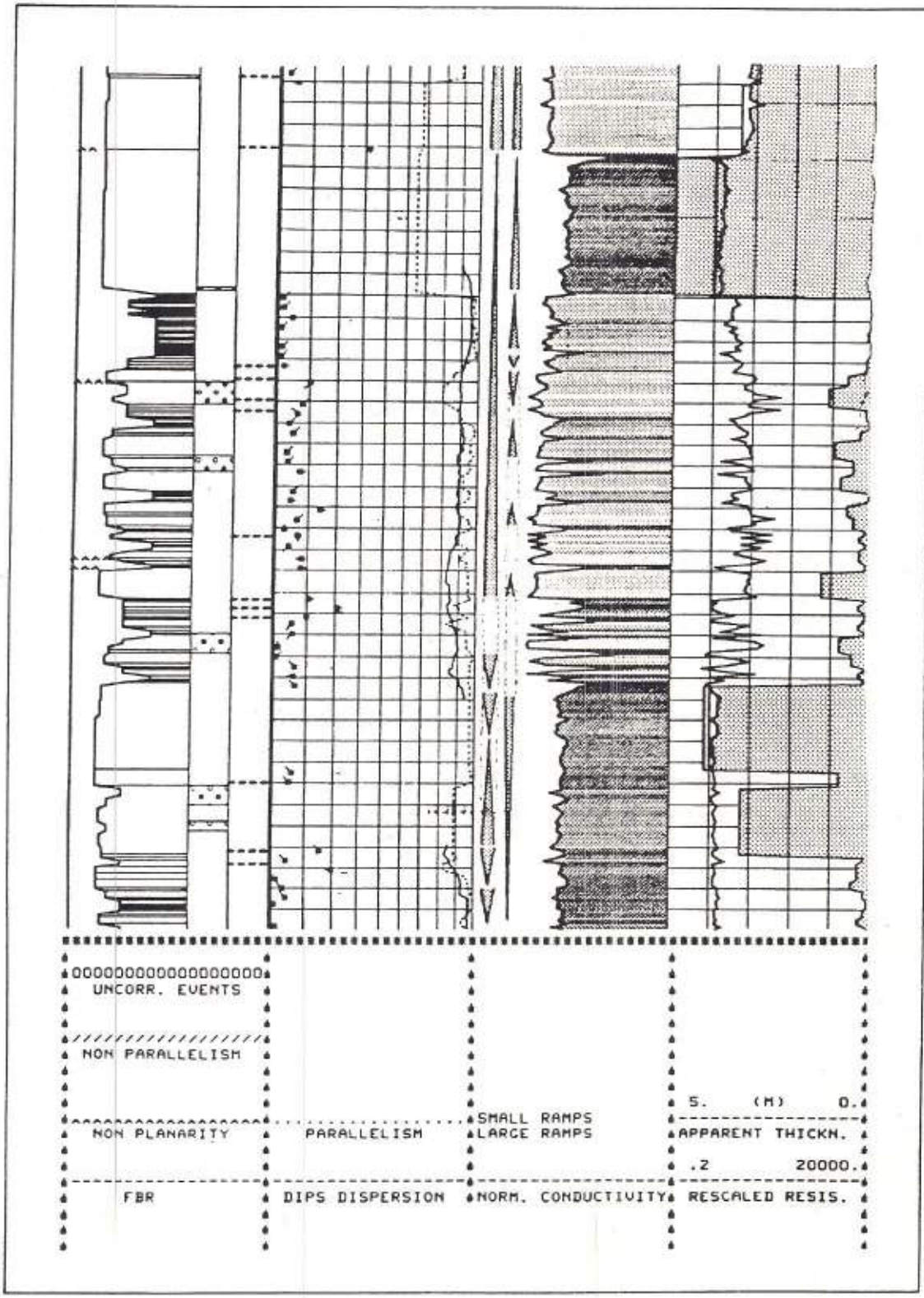

Fig. 101 - Syndip

DEPTH
DIP ANGLE AND DIRECTION
N
W
E
S
CSB
LOC
BOREHOLE DRIFT
G R
0
150
RESISTIVITY INCREASES
CALIPERS
0
6
C1-3
C2-4
16
0
10
20
30
40
50
60
70
80
90
3020
3025
3030
3035
3040
3045
3050
3055
3060
3065
3070
3075
DIP
DIP AZIMUTH
NOT CORRECTED FOR ENEX
NO FILTER
DEFINITION FACTOR 4
LOGARITHMIC PRESENTATION
DATA FROM 0.00 TO 81.70
SCALE FROM 0.00 TO 50.00
CAL
DIP
DIP AZ
GR

DIRECTIONAL SURVEY

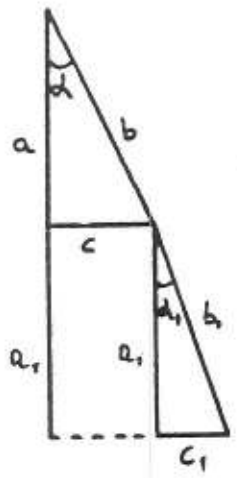

PROFONDITÀ VERTICALE

$a = b \cdot \cos\alpha$

$a_1 = b_1 \cdot \cos\alpha_1$

PROF. VERT. $= a + a_1 + \ldots\ldots\ldots$

SCOSTAMENTO

$c = b \cdot \operatorname{sen}\alpha$

$c_1 = b_1 \cdot \operatorname{sen}\alpha_1$

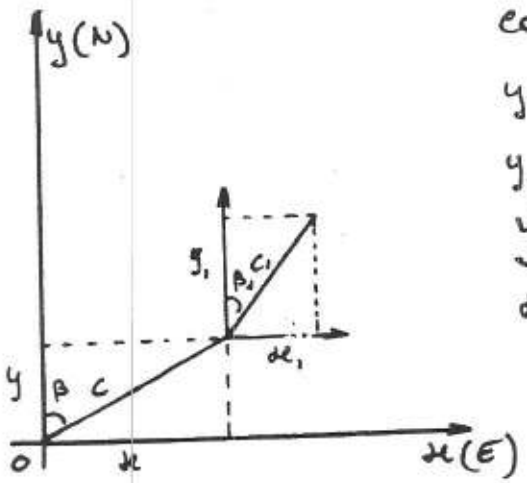

COORDINATE

$y = c \cdot \cos\beta$ $\qquad x = c \cdot \operatorname{sen}\beta$

$y_1 = c_1 \cdot \cos\beta_1$ $\qquad x_1 = c \cdot \operatorname{sen}\beta_1$

$y_{(N)} = y + y_1 + \ldots\ldots$

$x_{(E)} = x + x_1 + \ldots\ldots$

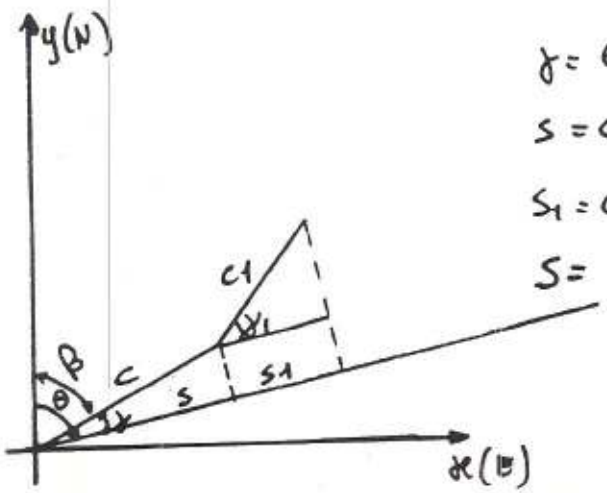

$\gamma = \theta - \beta$

$s = c \cdot \cos\gamma$

$s_1 = c_1 \cdot \cos\gamma_1$

$S = s + s_1 + \ldots\ldots$

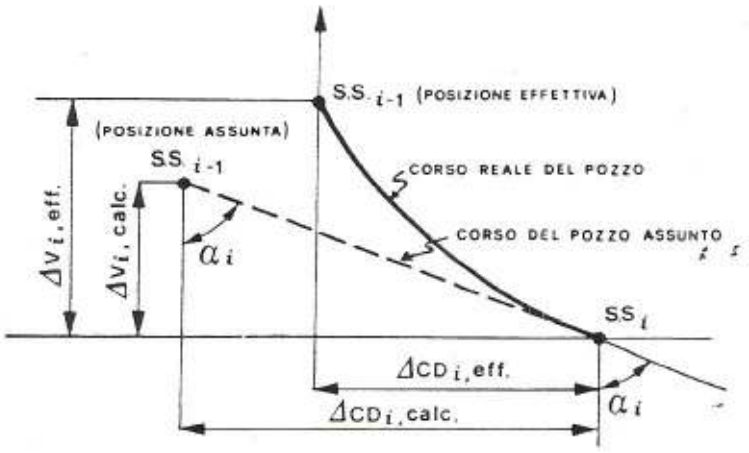

- INCREMENTO DI PROFONDITA' VERTICALE:

$$\Delta V_{i,calc.} = \Delta CL_i \times \cos\alpha_i$$

- AVANZAMENTO ORIZZONTALE:

$$\Delta CD_{i,calc.} = \Delta CL_i \times \text{sen}\,\alpha_i$$

a) CONFRONTO TRA CORSO REALE E CALCOLATO DEL POZZO TRA LE STAZIONI DI PROVA S.S. $i-1$ E S.S. i NEL PIANO VERTICALE

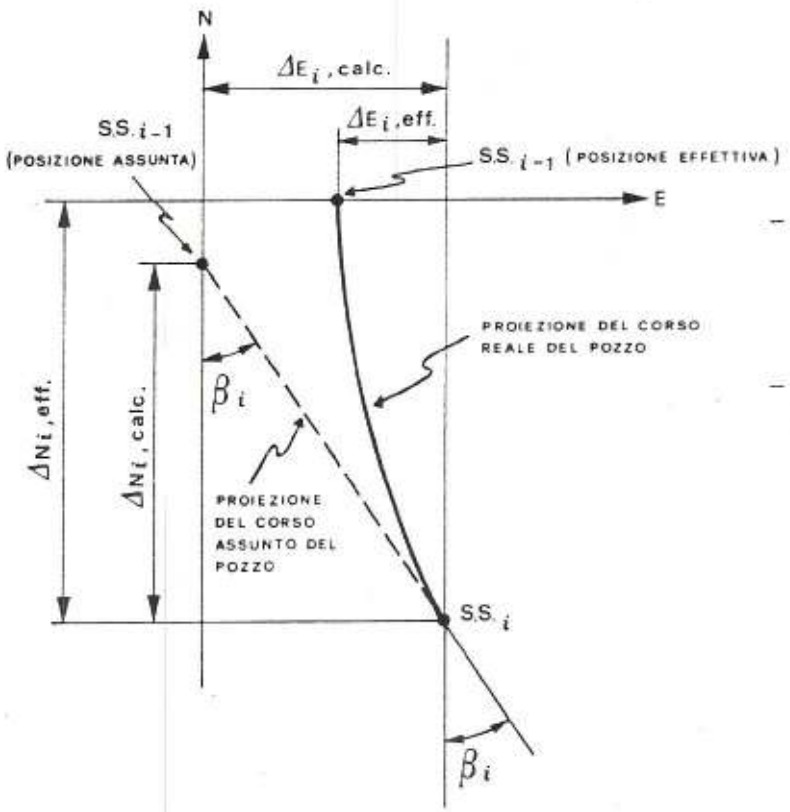

- INCREMENTO DI COORDINATE METRICHE N:

$$\Delta N_{i,calc.} = \Delta CD_{i,calc.} \times \cos\beta_i = \Delta CL_i \times \text{sen}\,\alpha_i \times \cos\beta_i$$

- INCREMENTO DI COORDINATE METRICHE E:

$$\Delta E_{i,calc.} = \Delta CD_{i,calc.} \times \text{sen}\,\beta_i = \Delta CL_i \times \text{sen}\,\alpha_i \times \text{sen}\,\beta_i$$

b) CONFRONTO TRA CORSO REALE E CALCOLATO DEL POZZO TRA LE STAZIONI DI PROVA S.S. $i-1$ E S.S. i NEL PIANO ORIZZONTALE

Fig. IV.5. RAPPRESENTAZIONE DEL CORSO DEL POZZO NEI PIANI VERTICALE ED ORIZZONTALE TRA DUE STAZIONI DI PROVA SUCCESSIVE COL METODO DELLE TANGENTI.

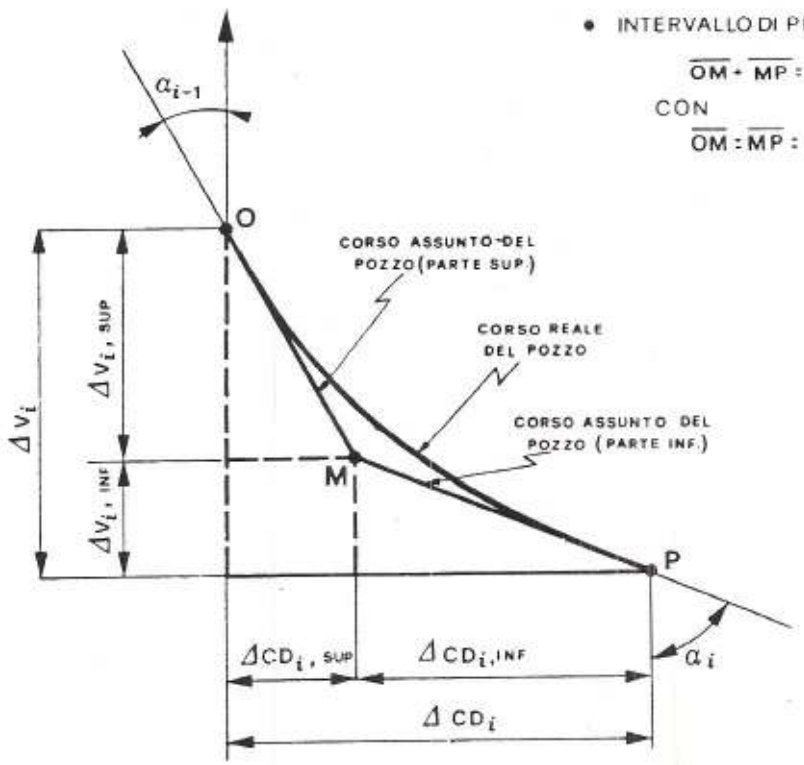

- INTERVALLO DI PROFONDITA' MISURATA

$\overline{OM} + \overline{MP} = \Delta CL_i$

CON

$\overline{OM} = \overline{MP} = \Delta CL_i/2$

- INCREMENTO DI PROFONDITA' VERTICALE

- PARTE SUPERIORE: $\Delta V_{i,SUP} = \frac{\Delta CL_i}{2} \cdot \cos\alpha_{i-1}$
- PARTE INFERIORE: $\Delta V_{i,INF} = \frac{\Delta CL_i}{2} \cdot \cos\alpha_i$
- TOTALE : $\Delta V_i = \frac{\Delta CL_i}{2} \cdot (\cos\alpha_{i-1} + \cos\alpha_i)$

- AVANZAMENTO ORIZZONTALE

- PARTE SUPERIORE : $\Delta CD_{i,SUP} = \frac{\Delta CL_i}{2} \cdot \text{sen}\alpha_{i-1}$
- PARTE INFERIORE : $\Delta CD_{i,INF} = \frac{\Delta CL_i}{2} \cdot \text{sen}\alpha_i$
- TOTALE : $\Delta CD_i = \frac{\Delta CL_i}{2} \cdot (\text{sen}\alpha_{i-1} + \text{sen}\alpha_i)$

FIG. IV.7.- RAPPRESENTAZIONE DEL CORSO DEL POZZO NEL PIANO VERTICALE TRA DUE STAZIONI DI PROVA SUCCESSIVE COL METODO DELLE TANGENTI BILANCIATO

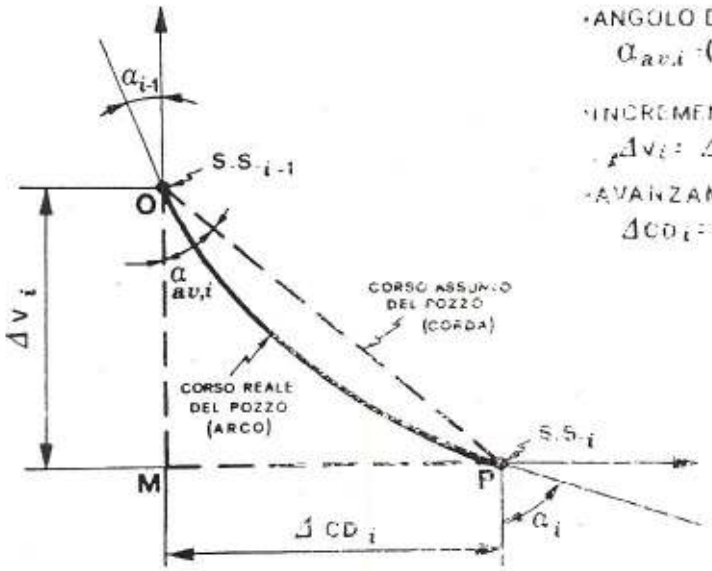

·ANGOLO DI INCLINAZIONE MEDIO

$$\alpha_{av,i} = (\alpha_{i-1} + \alpha_i)/2$$

·INCREMENTO DI PROFONDITÀ VERTICALE

$$\Delta V_i = \Delta CL_i \cdot \cos\alpha_{av,i}$$

·AVANZAMENTO ORIZZONTALE

$$\Delta CD_i = \Delta CL_i \cdot \operatorname{sen}\alpha_{av,i}$$

a) CONFRONTO TRA CORSO REALE ED ASSUNTO DEL POZZO TRA LE STAZIONI DI PROVA S.S.$_{i-1}$ E S.S.$_i$ NEL PIANO VERTICALE

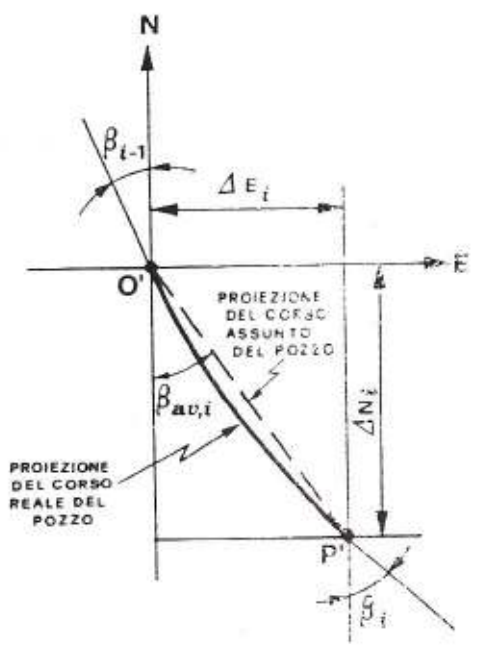

·ANGOLO DI DIREZIONE MEDIO:

$$\beta_{av,i} = (\beta_{i-1} + \beta_i)/2$$

·INCREMENTO DI COORDINATE METRICHE **N**:

$$\Delta N_i = \Delta CD_i \cdot \cos\beta_{av,i} = \Delta CL_i \cdot \operatorname{sen}\alpha_{av,i} \cdot \cos\beta_{av,i}$$

·INCREMENTO DI COORDINATE METRICHE **E**:

$$\Delta E_i = \Delta CD_i \cdot \operatorname{sen}\beta_{av,i} = \Delta CL_i \cdot \operatorname{sen}\alpha_{av,i} \cdot \operatorname{sen}\beta_{av,i}$$

b) CONFRONTO TRA CORSO REALE ED ASSUNTO DEL POZZO TRA LE STAZIONI DI PROVA S.S.$_{i-1}$ E S.S.$_i$ NEL PIANO ORIZZONTALE

FIG. IV.10 - RAPPRESENTAZIONE DEL CORSO DEL POZZO NEI PIANI VERTICALE ED ORIZZONTALE TRA DUE STAZIONI DI PROVA SUCCESSIVE COL METODO DELL'ANGOLO MEDIO

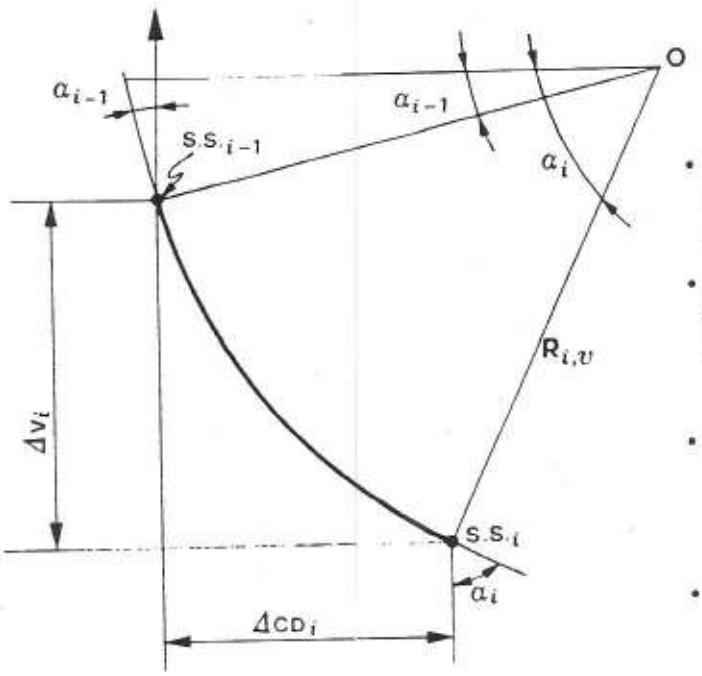

- INCREMENTO DELL'ANGOLO DI INCLINAZIONE:
$$\alpha_{D.A.R.} = (\alpha_i - \alpha_{i-1}) / \Delta CL_i$$
- RAGGIO DI CURVATURA NEL PIANO VERTICALE:
$$R_{i,v} = \frac{180}{\pi} \times \frac{1}{\alpha_{D.A.R}}$$
- INCREMENTO DI PROFONDITA' VERTICALE:
$$\Delta V_i = R_{i,v} \times (\operatorname{sen}\alpha_i - \operatorname{sen}\alpha_{i-1})$$
- AVANZAMENTO ORIZZONTALE:
$$\Delta CD_i = R_{i,v} \times (\cos\alpha_{i-1} - \cos\alpha_i)$$

a) CORSO DEL POZZO NEL PIANO VERTICALE TRA DUE STAZIONI DI PROVA SUCCESSIVE S.S.$_{i-1}$ E S.S.$_i$

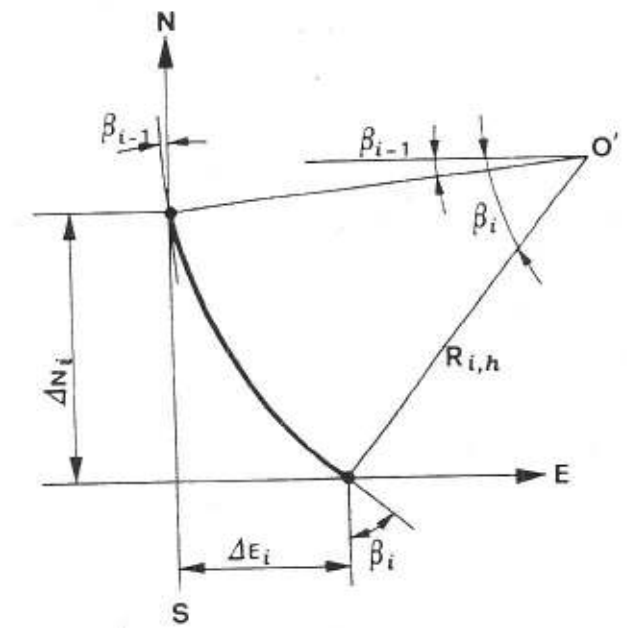

- INCREMENTO DELL'ANGOLO DI DEVIAZIONE:
$$\beta_{d.a.r.} = (\beta_i - \beta_{i-1}) / \Delta CD_i$$
- RAGGIO DI CURVATURA NEL PIANO ORIZZONTALE:
$$R_{i,h} = \frac{180}{\pi} \times \frac{1}{\beta_{d.a.r.}}$$
- INCREMENTO DI COORDINATE METRICHE N:
$$\Delta N_i = R_{i,h} \times (\operatorname{sen}\beta_i - \operatorname{sen}\beta_{i-1})$$
- INCREMENTO DI COORDINATE METRICHE E:
$$\Delta E_i = R_{i,h} \times (\cos\beta_{i-1} - \cos\beta_i)$$

b) CORSO DEL POZZO NEL PIANO ORIZZONTALE TRA DUE STAZIONI DI PROVA SUCCESSIVE S.S.$_{i-1}$ E S.S.$_i$

FIG. IV. 12 – RAPPRESENTAZIONE DEL CORSO DEL POZZO NEI PIANI VERTICALE ED ORIZZONTALE TRA DUE STAZIONI DI PROVA SUCCESSIVE COL METODO DEL RAGGIO DI CURVATURA

CALCOLO DELLO SPESSORE REALE DI UNO STRATO

(STRATI INCLINATI E POZZO DEVIATO)

PROIEZIONE DELLA LINEA DI MASSIMA PENDENZA DELLO STRATO E DEL POZZO SU DI UN PIANO ORIZZONTALE

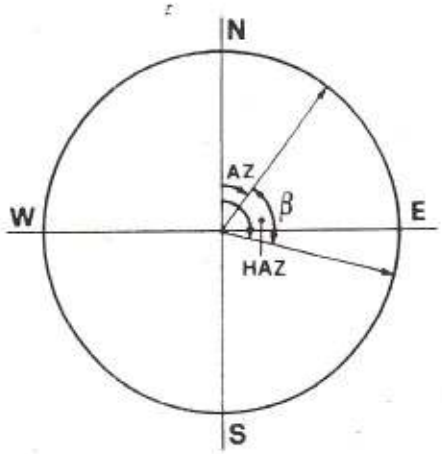

PROIEZIONE DELLO STRATO E DEL POZZO SU DI UN PIANO VERTICALE CHE HA LA STESSA DIREZIONE DEL POZZO

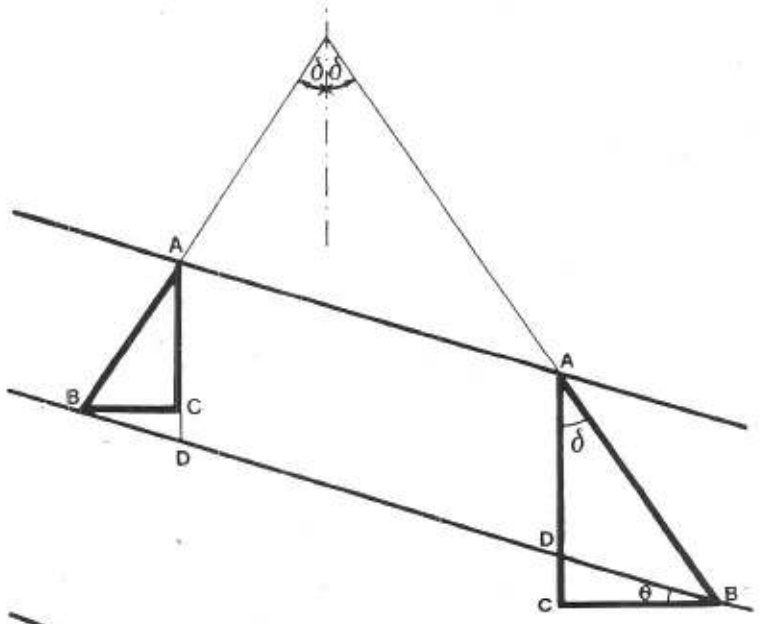

PROIEZIONE DELLO STRATO SU DI UN PIANO VERTICALE CHE HA LA STESSA DIREZIONE DELL'IMMERSIONE

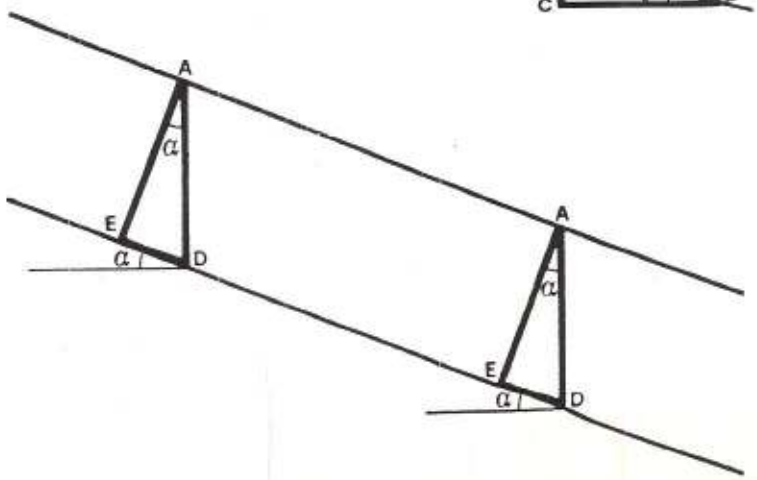

S = SPESSORE MISURATO DELLO STRATO (SPESSORE APPARENTE).

AC = MISURA VERTICALE DELL'INTERVALLO AB.

AB = SPESSORE DELLO STRATO LUNGO LA VERTICALE PASSANTE PER IL PUNTO DI INTERSEZIONE POZZO - STRATO (ISCORA)

BC = SCOSTAMENTO DEL POZZO NELL'ATTRAVERSAMENTO DELLO STRATO.

AE = SPESSORE REALE DELLO STRATO.

α = PENDENZA DELLO STRATO.

AZ = AZIMUT O IMMERSIONE DELLO STRATO.

δ = INCLINAZIONE DEL POZZO.

γ = DIREZIONE DEL POZZO.

β = ANGOLO TRA LA DIREZIONE DEL POZZO E L'IMMERSIONE DELLO STRATO ($\gamma AZ - AZ$)

θ = PENDENZA APPARENTE DELLO STRATO LUNGO LA DIREZIONE DEL POZZO.

$AC = AB \cdot \cos\delta$ $\qquad$ $BC = AB \cdot \operatorname{sen}\delta$

$\alpha : \operatorname{tg}\delta = \operatorname{tg}\alpha \cdot \cos\beta$ $\qquad$ $DC = BC \cdot \operatorname{tg}\theta$

$AD = AC - DC = AB \cdot \cos\delta - BC \operatorname{tg}\theta = AB \cos\delta - AB \operatorname{sen}\delta \cdot \operatorname{tg}\alpha \cdot \cos\beta =$

$= AB(\cos\delta - \operatorname{sen}\delta \cdot \operatorname{tg}\alpha \cdot \cos\beta)$

$AE = AD \cdot \cos\alpha$

Nota: NEL CASO DEL POZZO INCLINATO IN DOWN DIP ($90° > \beta > 270°$) IL VALORE DEL COSENO È POSITIVO E PERTANTO ALLA FINE DEL CALCOLO AD SARÀ UGUALE A $AC - DC$.

NEL CASO DEL POZZO INCLINATO IN UP DIP ($90° < \beta < 270°$) IL VALORE DEL COSENO È NEGATIVO E PERTANTO ALLA FINE DEL CALCOLO AD SARÀ UGUALE A $AC + DC$

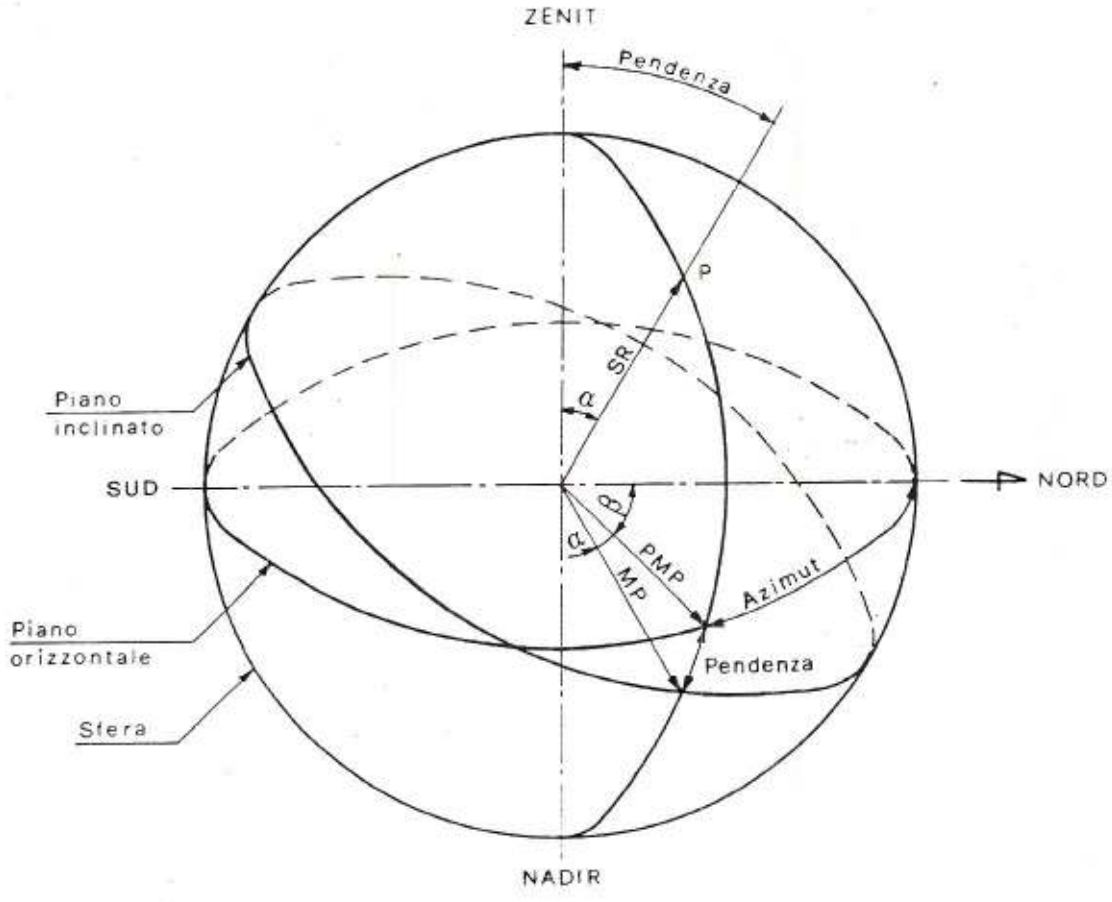

LEGENDA:

α = Angolo di pendenza
β = Azimut
MP = Linea di massima pendenza
PMP = Proiezione della linea di massima pendenza sul piano orizzontale
SR = Semiretta perpendicolare al piano verticale

Fig. 16 - Proiezioni stereografiche: rappresentazione grafica di punti e piani nella sfera

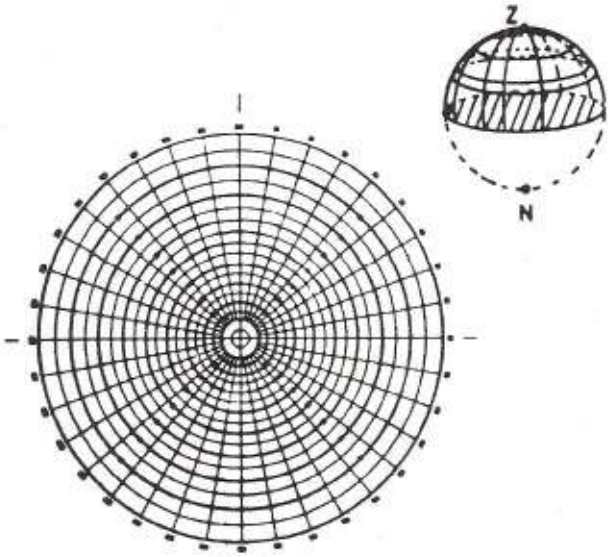

FIG.1

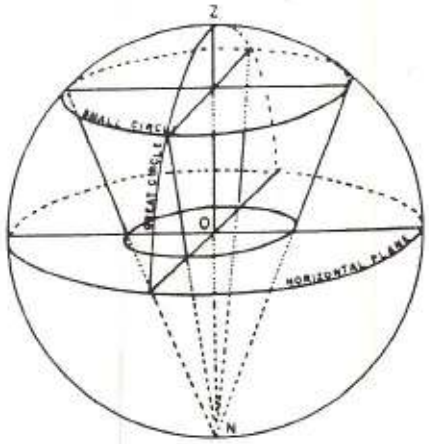

FIG.2

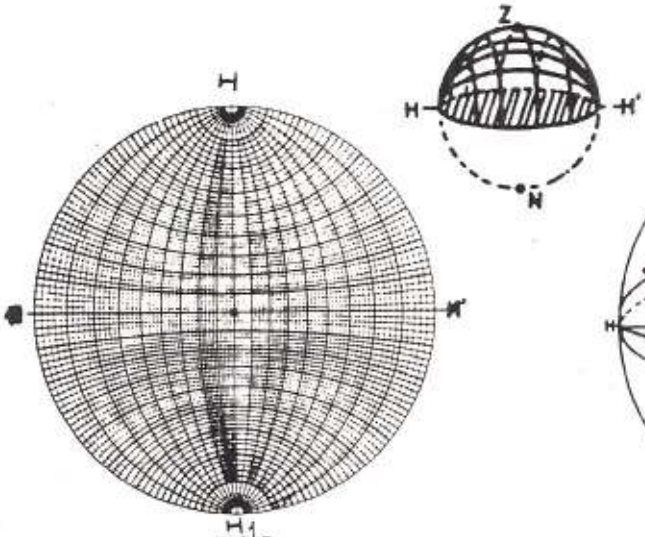

FIG.3

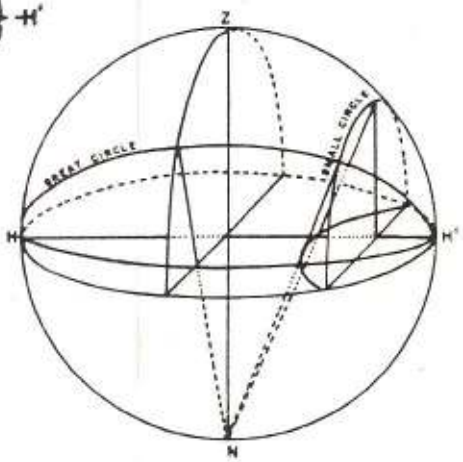

FIG.4

THE OVERLAY (Fig. 1)

This is a circular piece of transparent plastic paper, pinned to the center of the Stereonet in a way that leaves it free to rotate.

Although mobile, we will regard **the Overlay as the fixed reference element**, oriented with respect to North.

On it are printed radial lines and concentric circles.

Fig. 2 shows how those lines are derived: the Overlay is the projection of the Upper Hemisphere, from point N ("Nadir") onto a plane perpendicular to diameter ZN, the Equator. Point Z is the Zenith. The set of planes through axis ZN cut the sphere along **Great circles**, or **Z-Meridians**. If a Z-Meridian is chosen as Origin, we will call **Longitude** the angular distance of any Z-Meridian to this origin, counted positive clockwise from 0° to 360°. In the central projection from N, Z-Meridians project as radial lines on the Overlay, with Longitude represented in true magnitude.

Consider now a set of cones, of common axis, ZN, and regularly increasing summit angle. They cut the hemisphere along circles of increasing radius, called **Small Circles** or **Z-Parallels**. We will call **Latitude** the half-summit angle of each cone, i.e., zero at point Z and 90° at the Equator. This is contrary to geographic practice, yet is no cause for confusion in what follows. Z-Parallels project as concentric circles on the Overlay, forming the Concentric Grid. The projected circles are smaller than the Z-Parallel circles themselves, and their spacing on the Grid is not linear. Each one corresponds to a value of Latitude.

It is customary to refer to the projected Z-Meridian and Z-Parallel directly as Z-Meridians and Z-Parallels.

1 M X 0.5 M 35 DEG.X 2
REFERENCE 124.25405
0 16
ANG
950
1000
1050

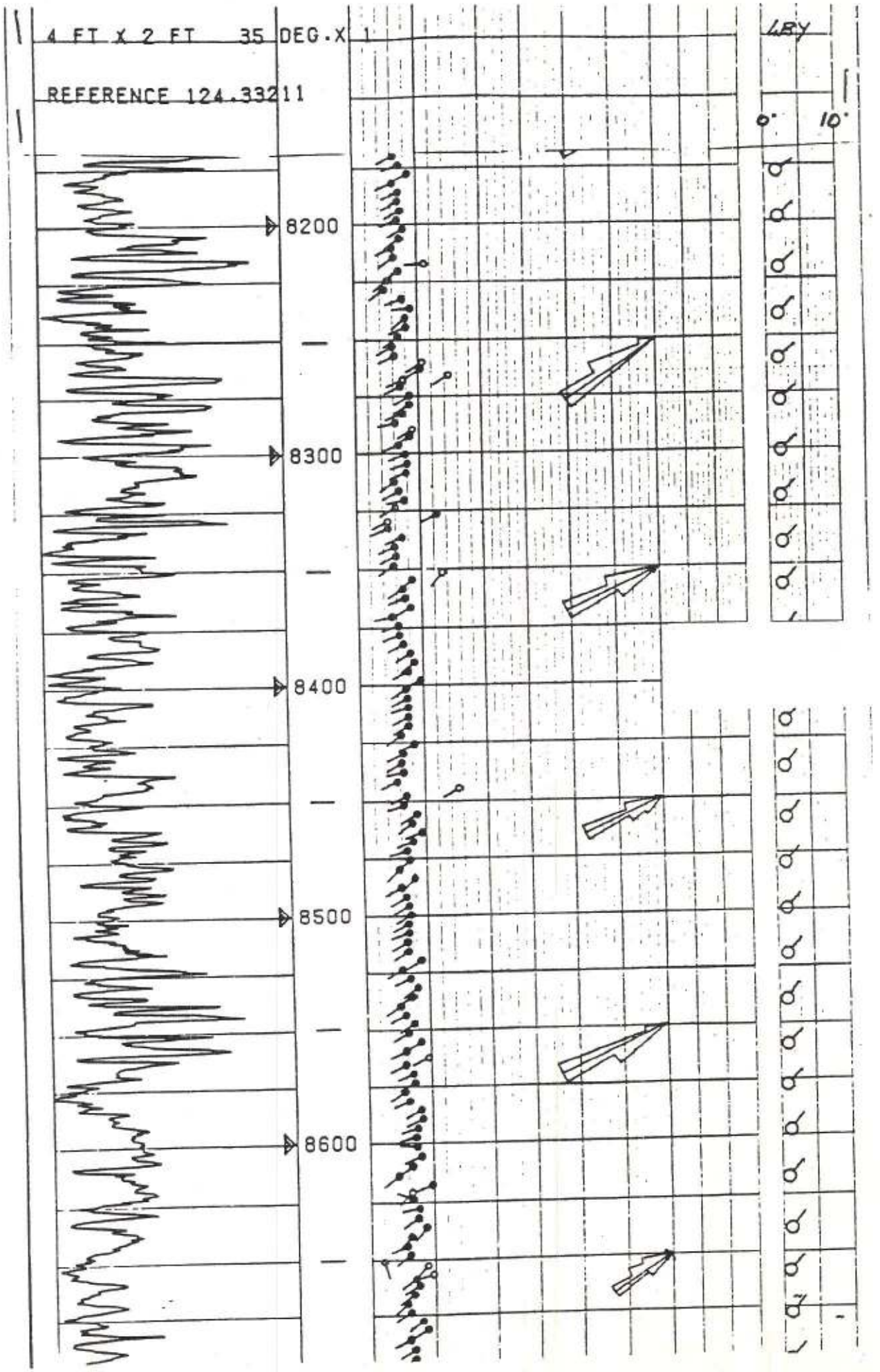
4 FT X 2 FT 35 DEG.X 1
REFERENCE 124.33211
LBY
0°
10°
8200
8300
8400
8500
8600

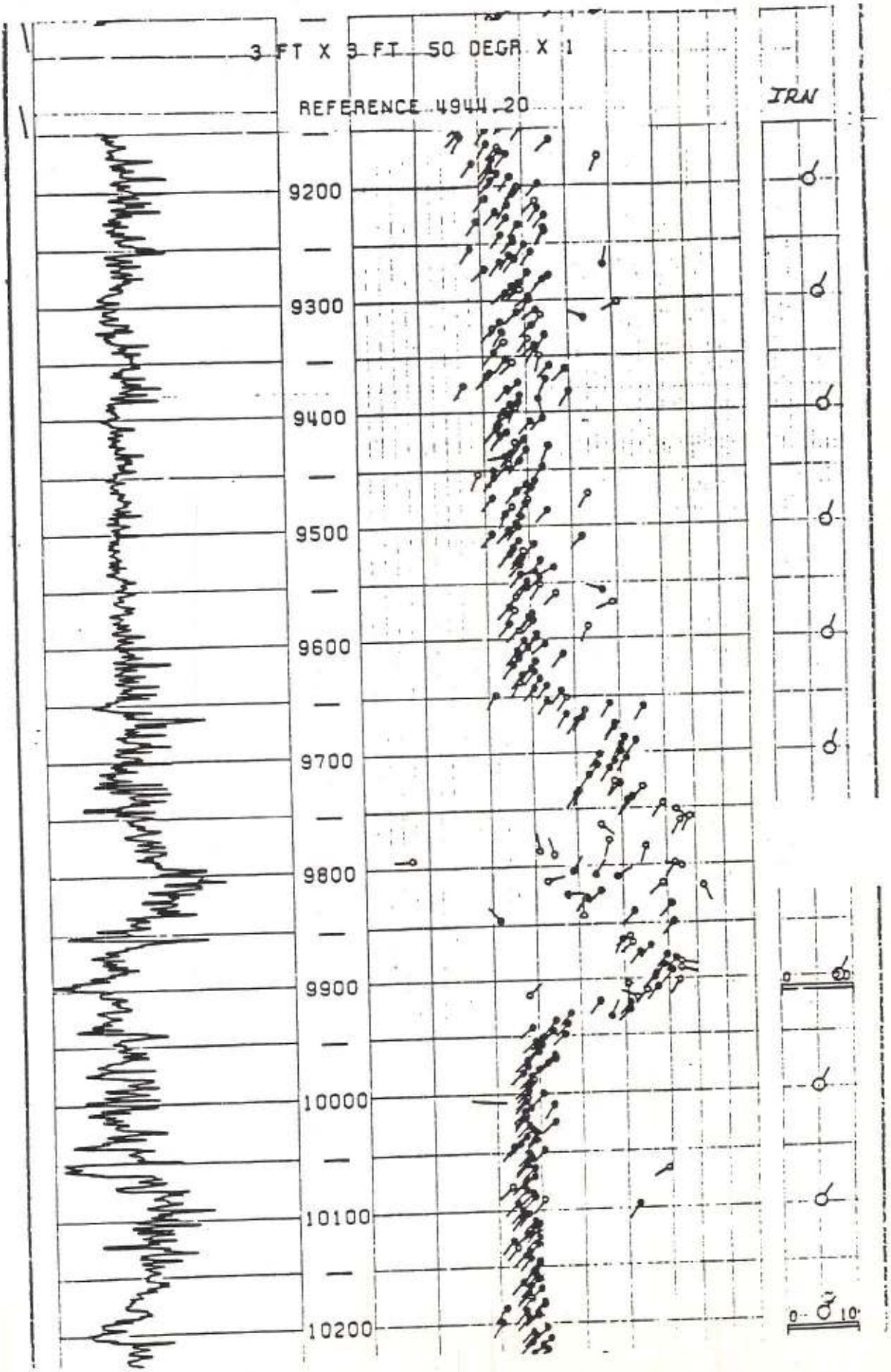
3 FT X 3 FT 50 DEGR X 1
REFERENCE 4944.20
IRN
9200
9300
9400
9500
9600
9700
9800
9900
10000
10100
10200
0
10

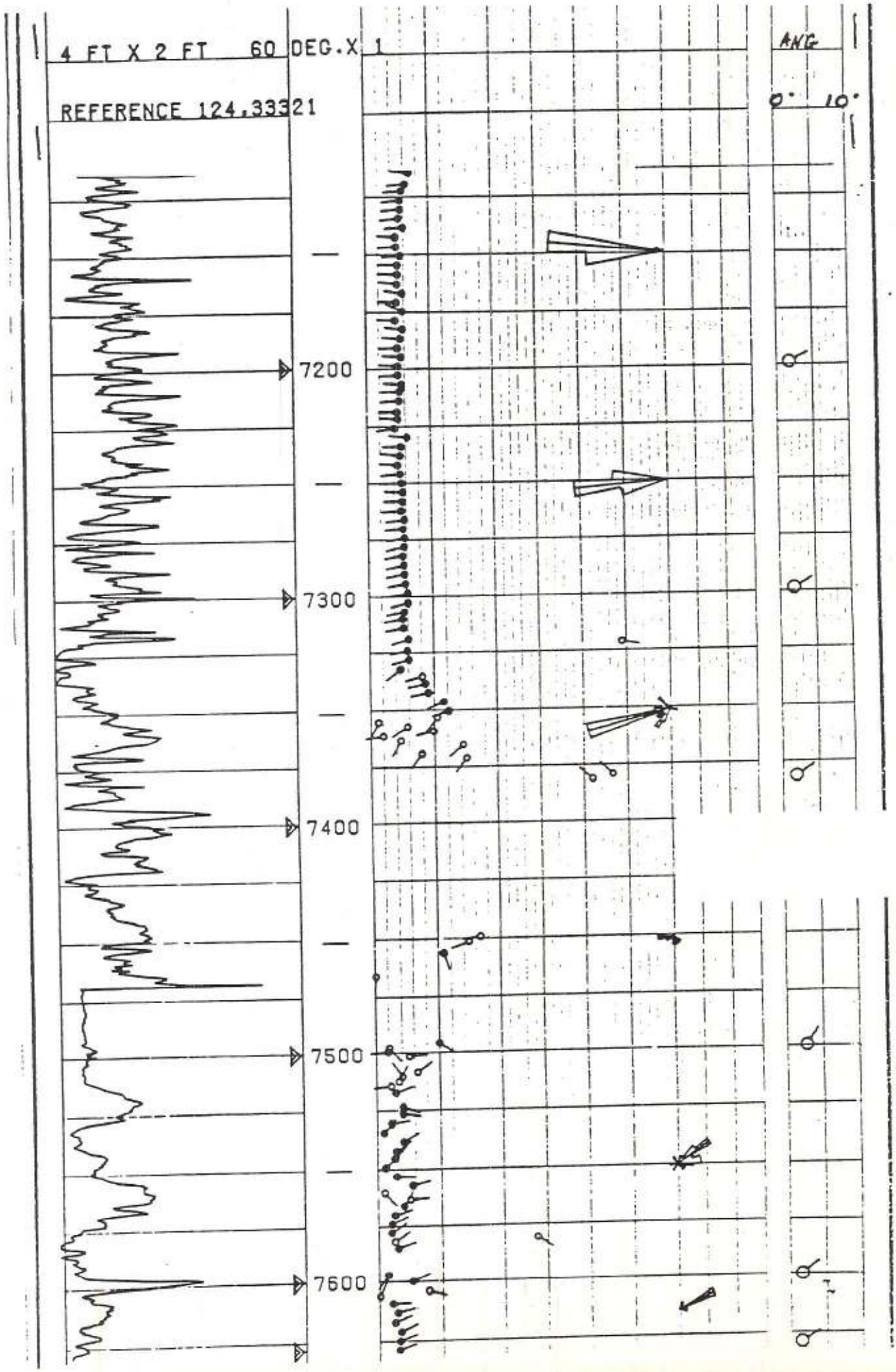
4 FT X 2 FT 60 DEG.X 1
REFERENCE 124,33321
ANG
0° 10°
7200
7300
7400
7500
7600

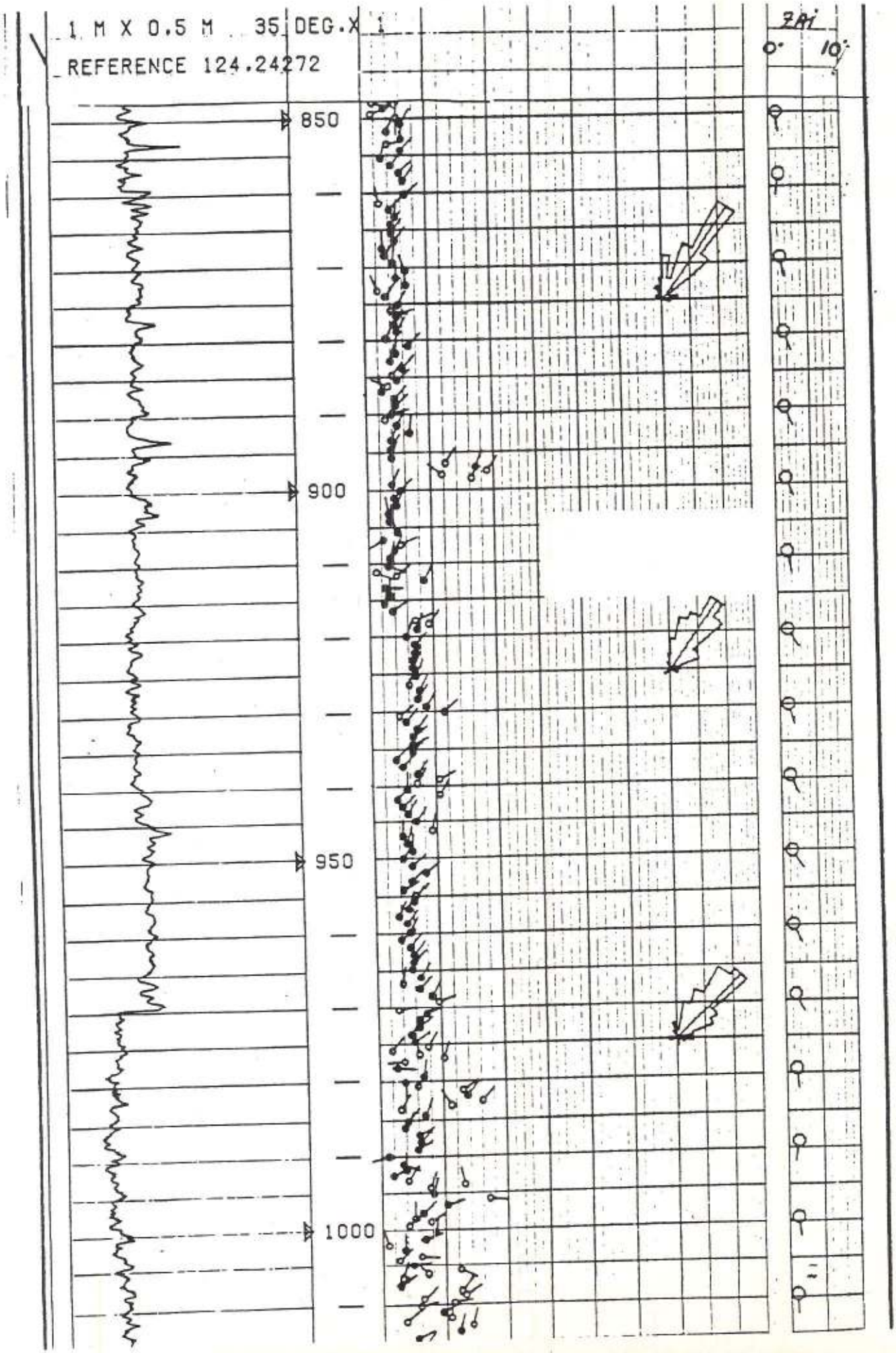
1 M X 0.5 M 35 DEG.X 1
REFERENCE 124.24272
ZAi
0°
10°
850
900
950
1000

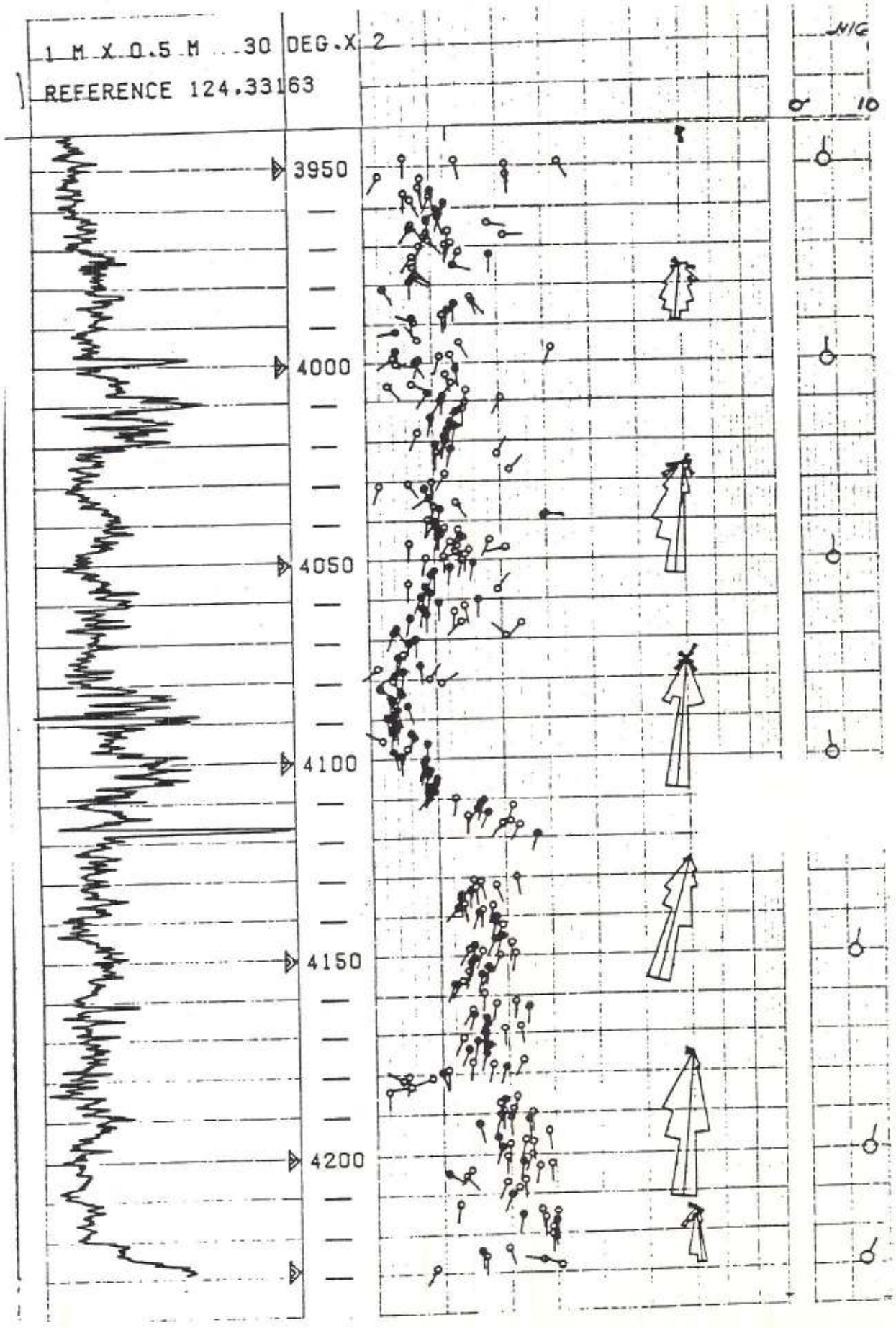
1 M X 0.5 M 30 DEG X 2
REFERENCE 124.33163
NIG
0
10
3950
4000
4050
4100
4150
4200

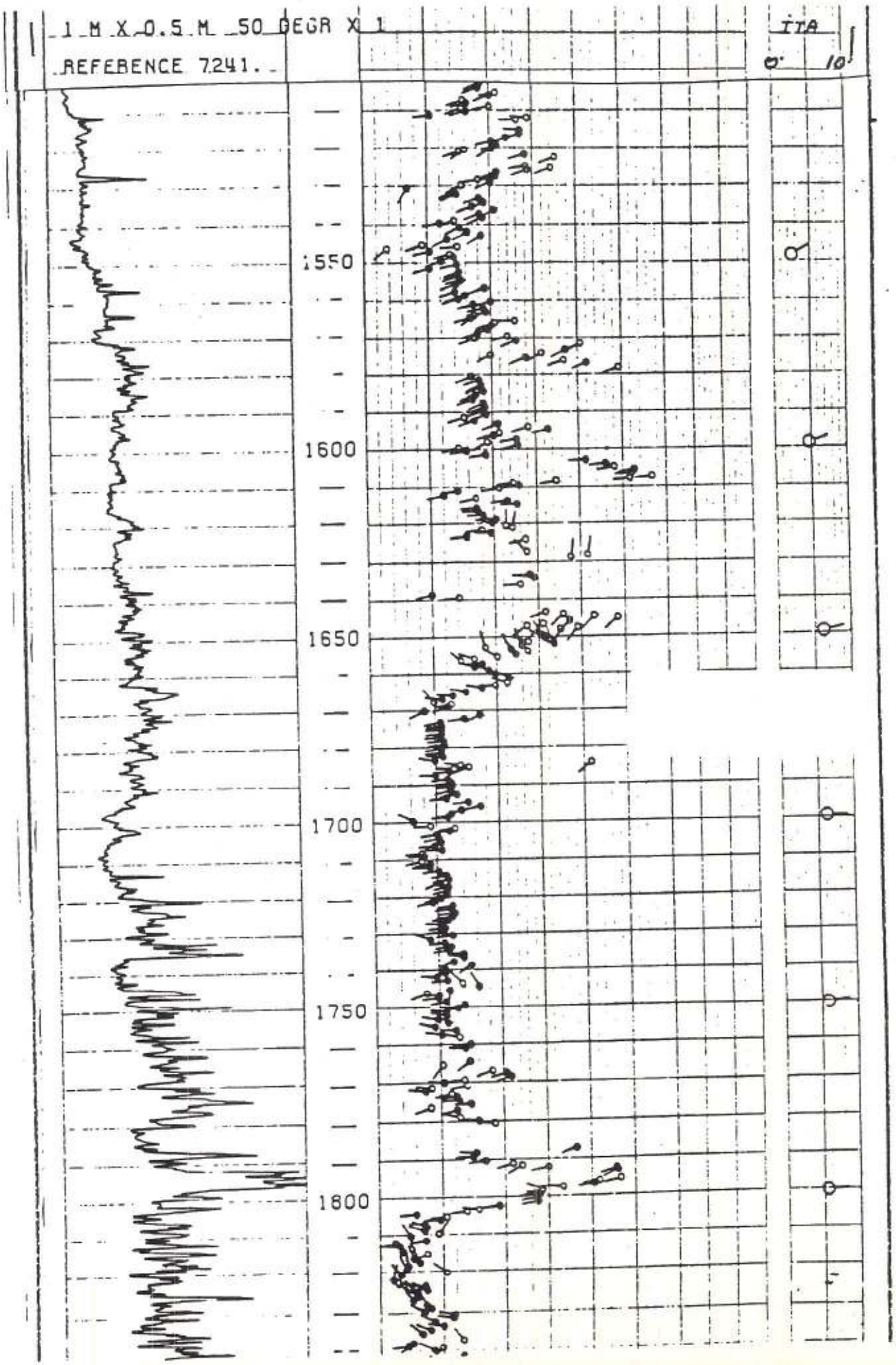
1 M X 0.5 M 50 DEGR X 1
REFERENCE 7241.
ITA
0
10
1550
1600
1650
1700
1750
1800

FOLD CILINDRICAL

(I) FOLD SYMMETRICAL

AXIAL PLANE IS VERTICAL

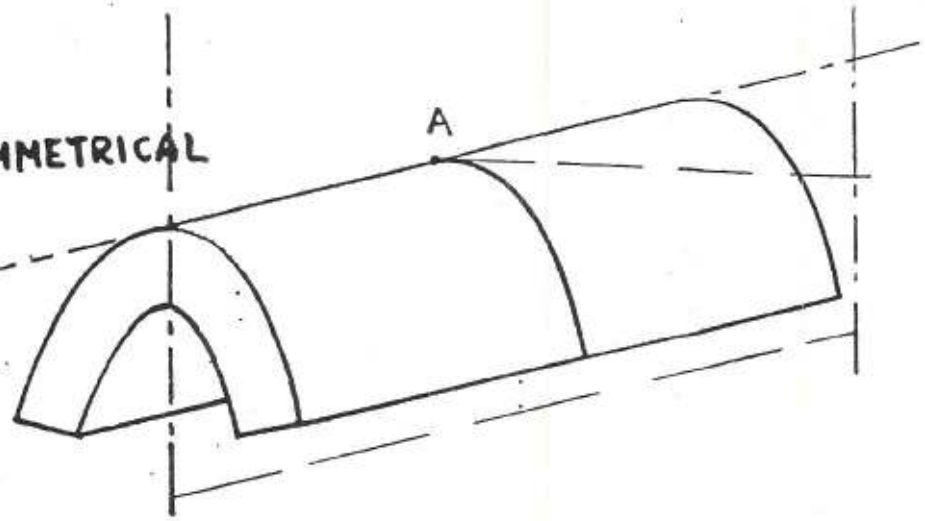

Il piano assiale unisce le cerniere dei singoli strati cioè i punti dove si ha deviazione di direzione e/o immersione.
L'intersezione del piano assiale coi singoli strati rappresenta l'asse.

(II) FOLD ASYMMETRICAL

AXIAL PLANE IS TILTED.

THERE IS TILT

AXIS IS HORIZONTAL : NO PLUNGE

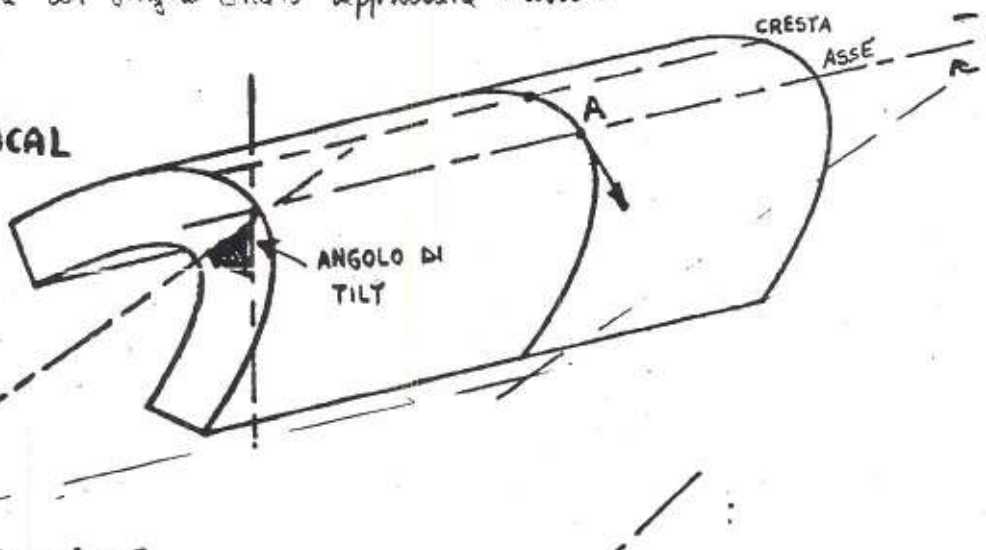

(III)

AXIS IS NOW NOT HORIZONTAL ANYMORE.

THERE ARE: TILT AND PLUNGE.

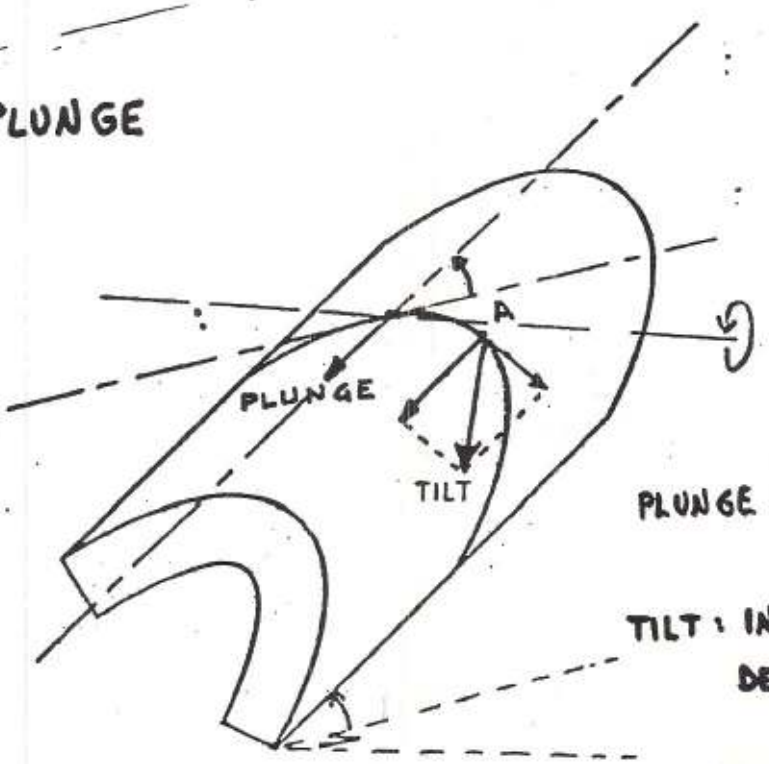

PLUNGE : INCLINAZIONI DELL'ASSE

TILT : INCLINAZIONE DELLA STRUTTURA

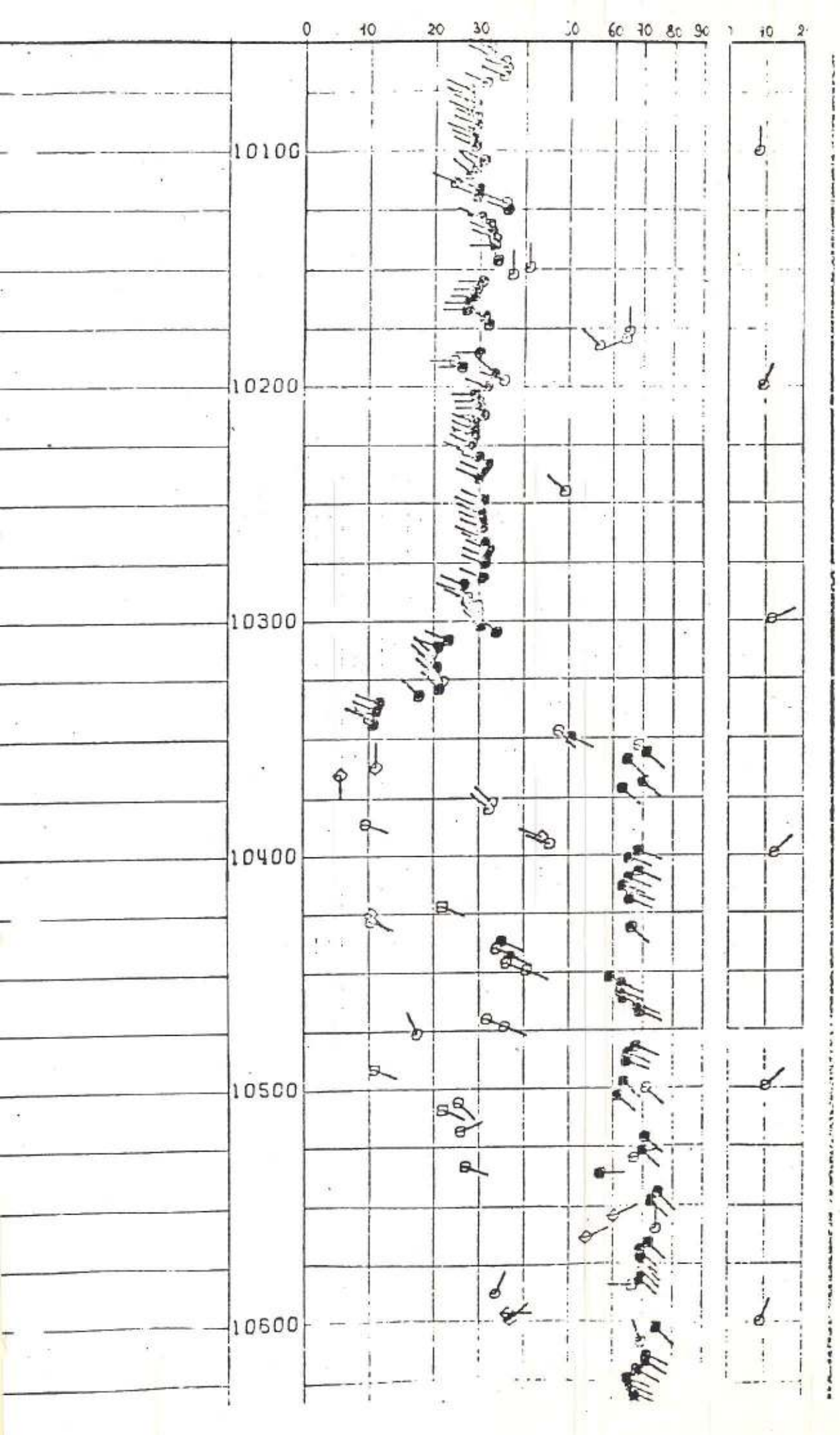
0
10
20
30
60
70
80
90
10
10100
10200
10300
10400
10500
10600

$P_1 = 68° \times 112°$

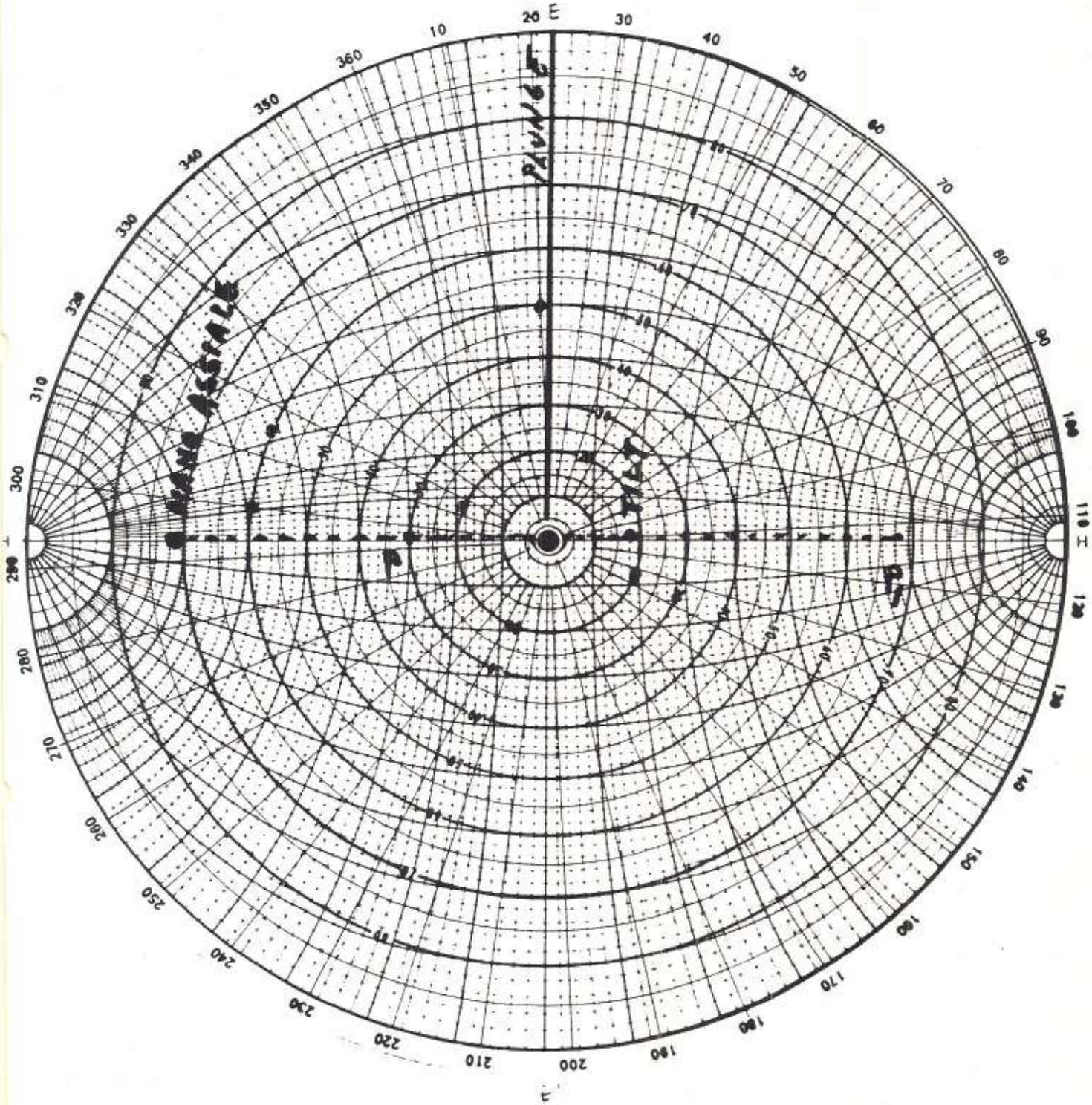

ANGOLO DI PIEGAMENTO : DISTANZA P-P. = 98°

PLUNGE : AZIMUT IN CORRISPONDENZA DI 'E' = 22°
PENDENZA NEL PUNTO D'INCONTRO PIANO E E' CON MERIDIANO P-P' = 1°

• TILT : PUNTO MEDIANO SEGMENTO P-P1 ; AZIMUT = 108° ; PEND = 18°

• PIANO ASSIALE : PUNTO A 90° SUL MERIDIANO P-P1 ; AZIMUT = 296° ; PEND. = 71°

TYPES OF DISTORTION FOUND NEAR FAULT PLANES

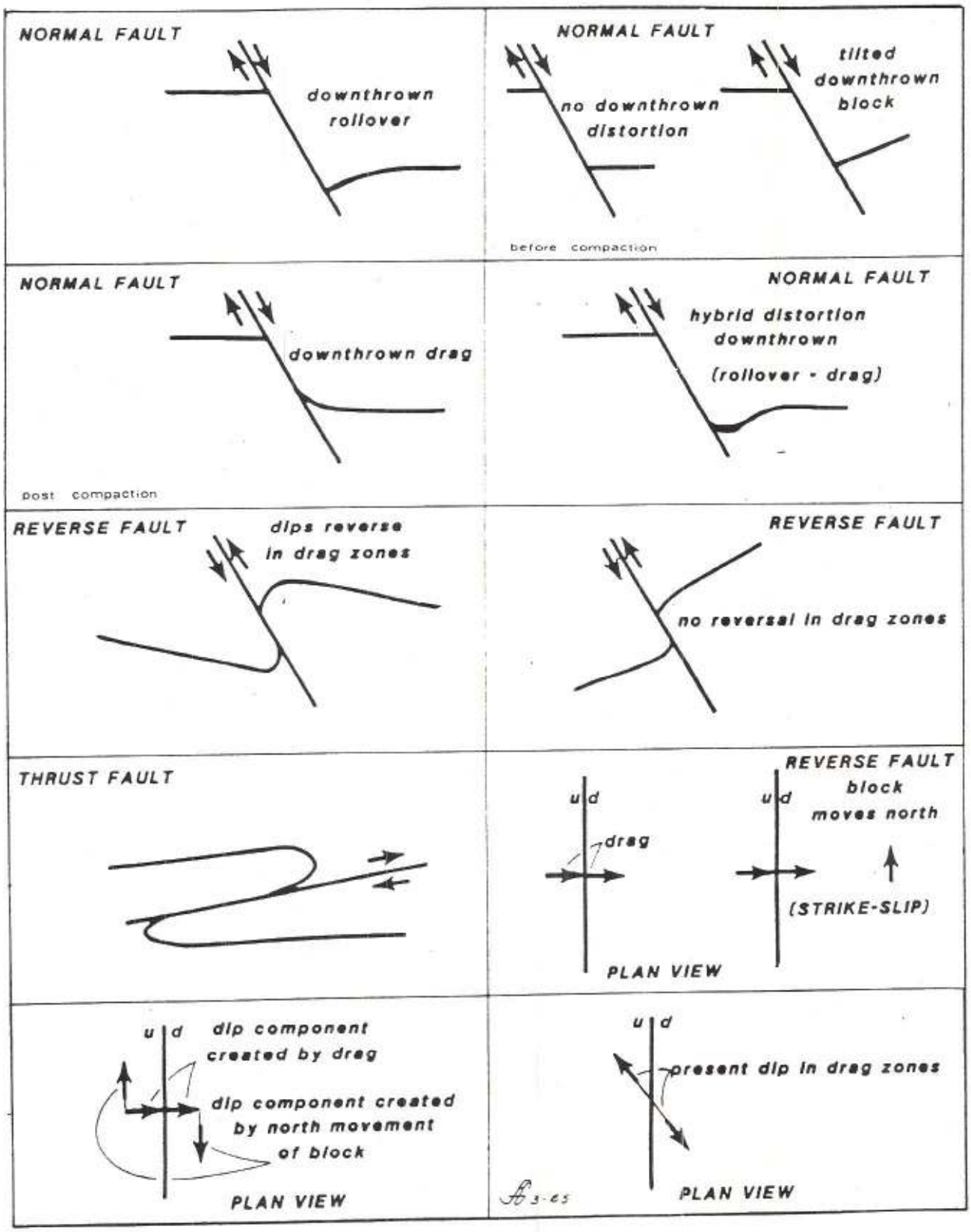

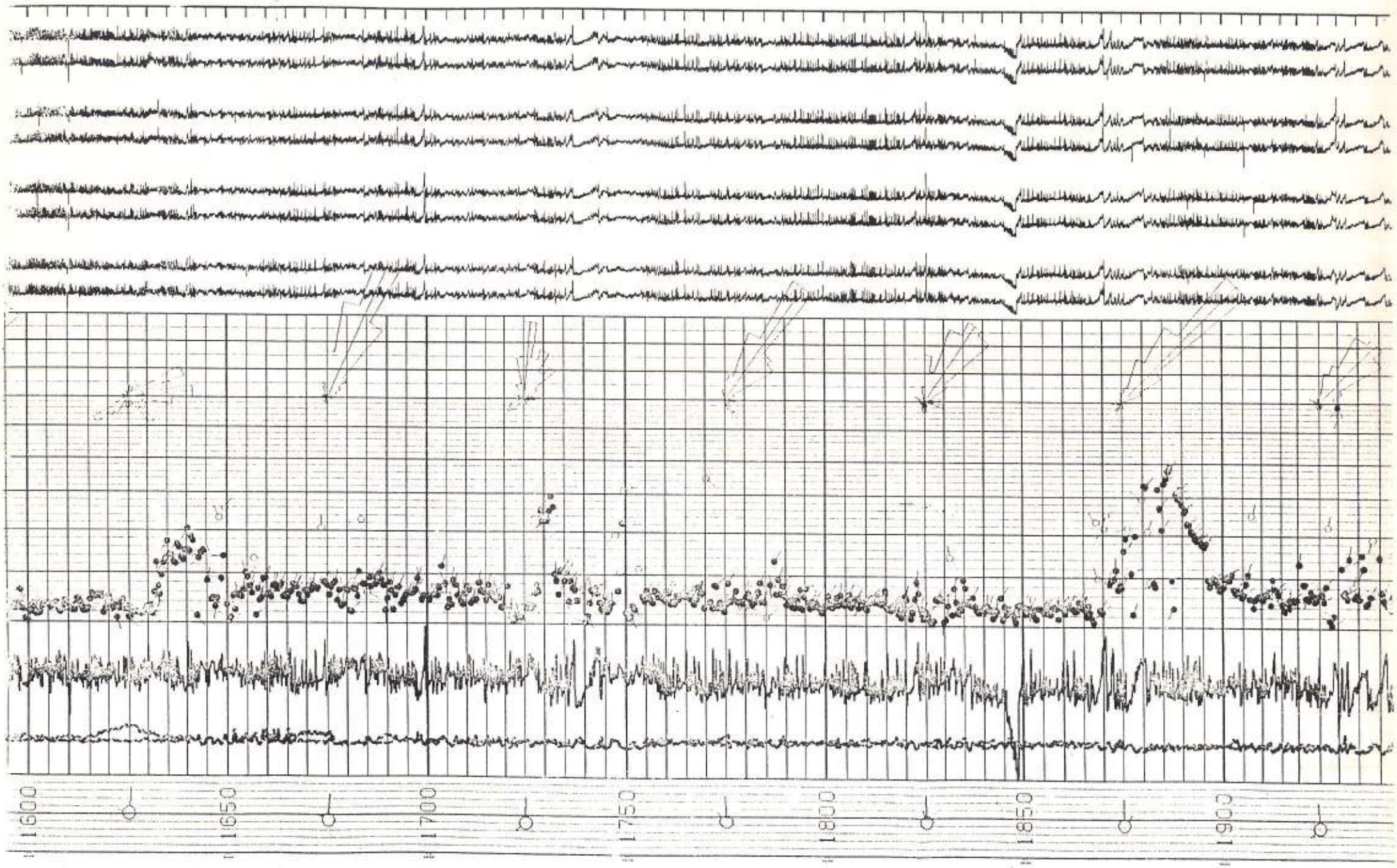
1600
1650
1700
1750
1800
1850
1900

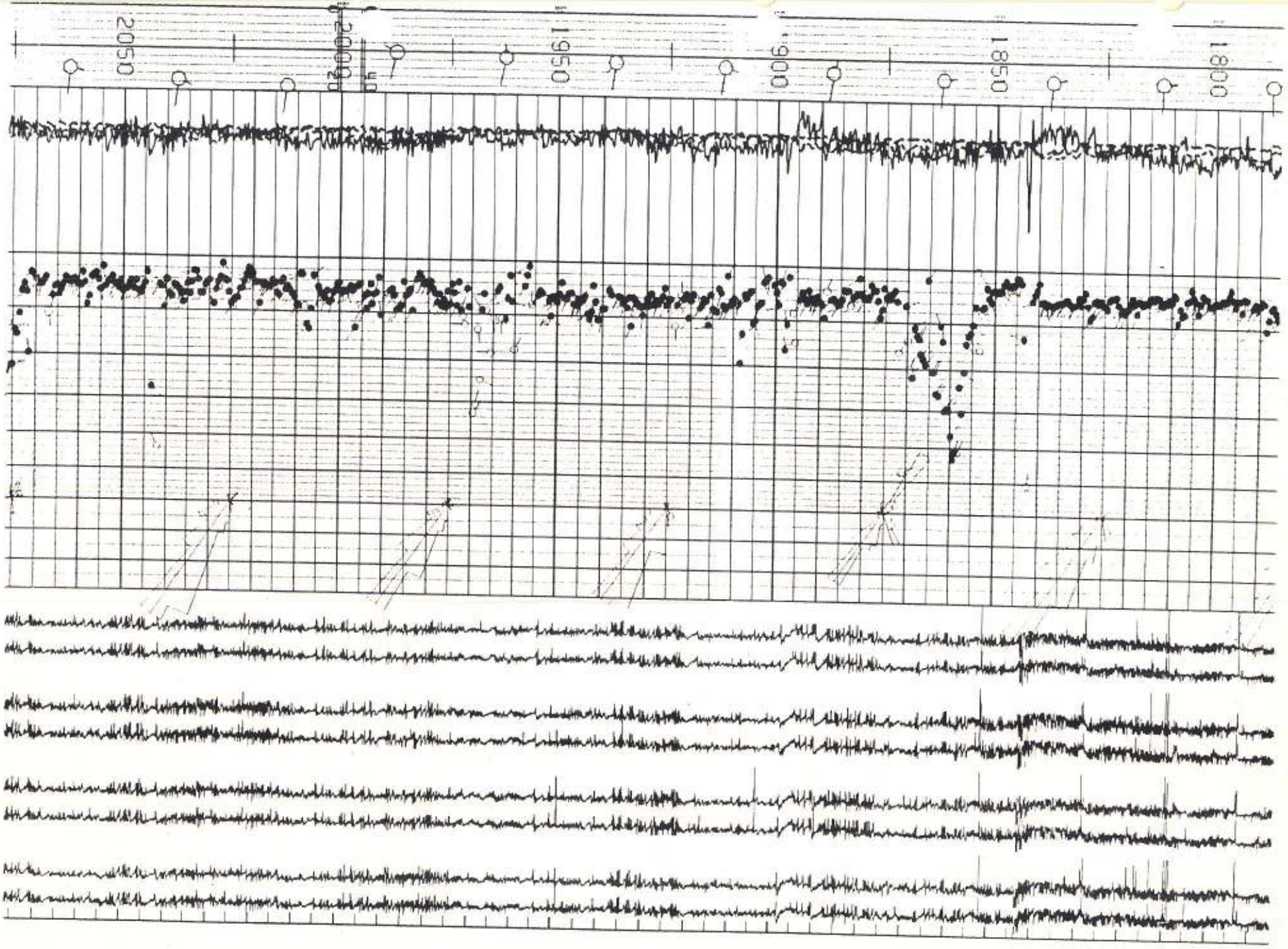
2050
2000
1950
1900
1850
1800

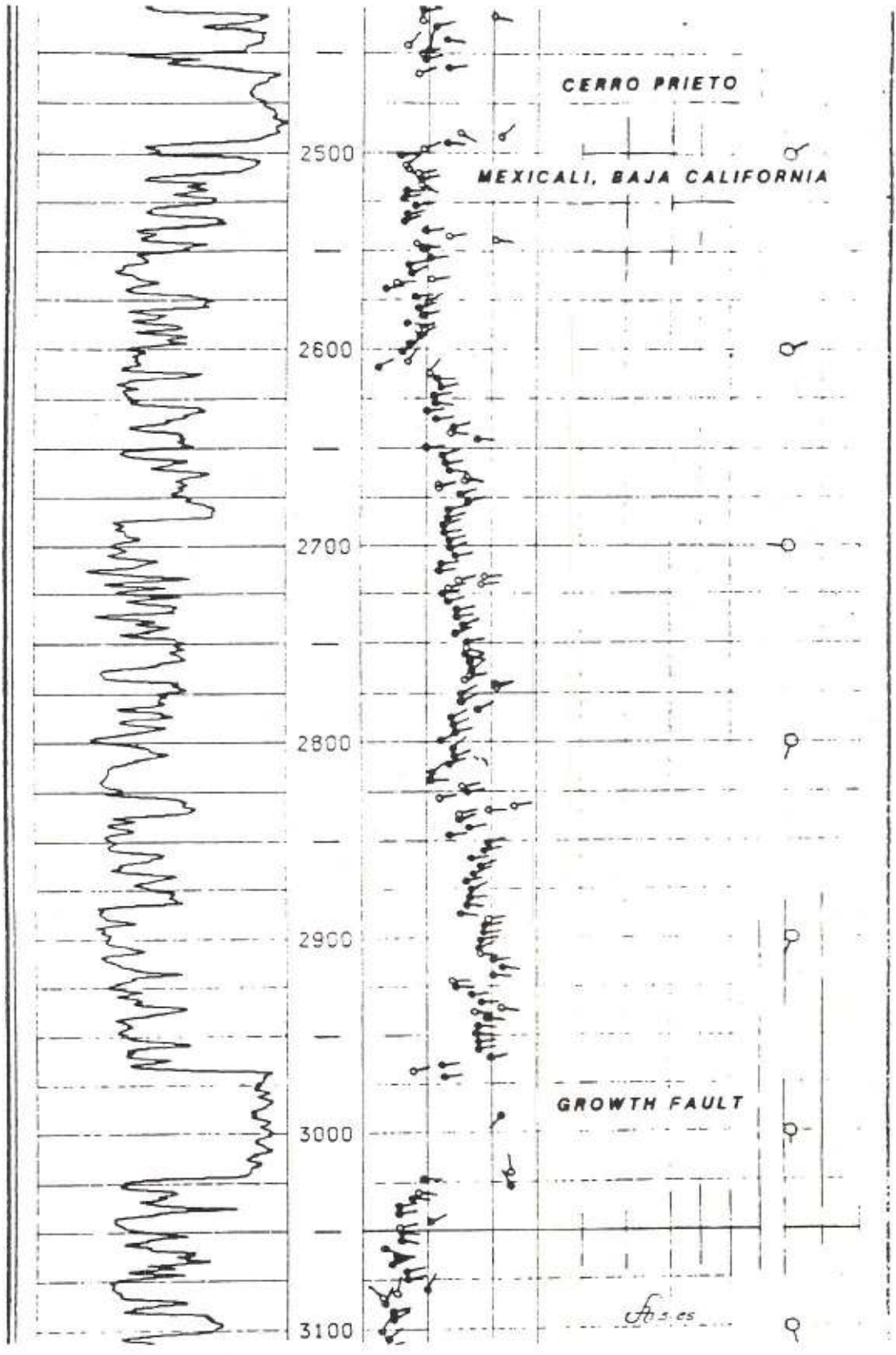
CERRO PRIETO
MEXICALI, BAJA CALIFORNIA
2500
2600
2700
2800
2900
3000
3100
GROWTH FAULT

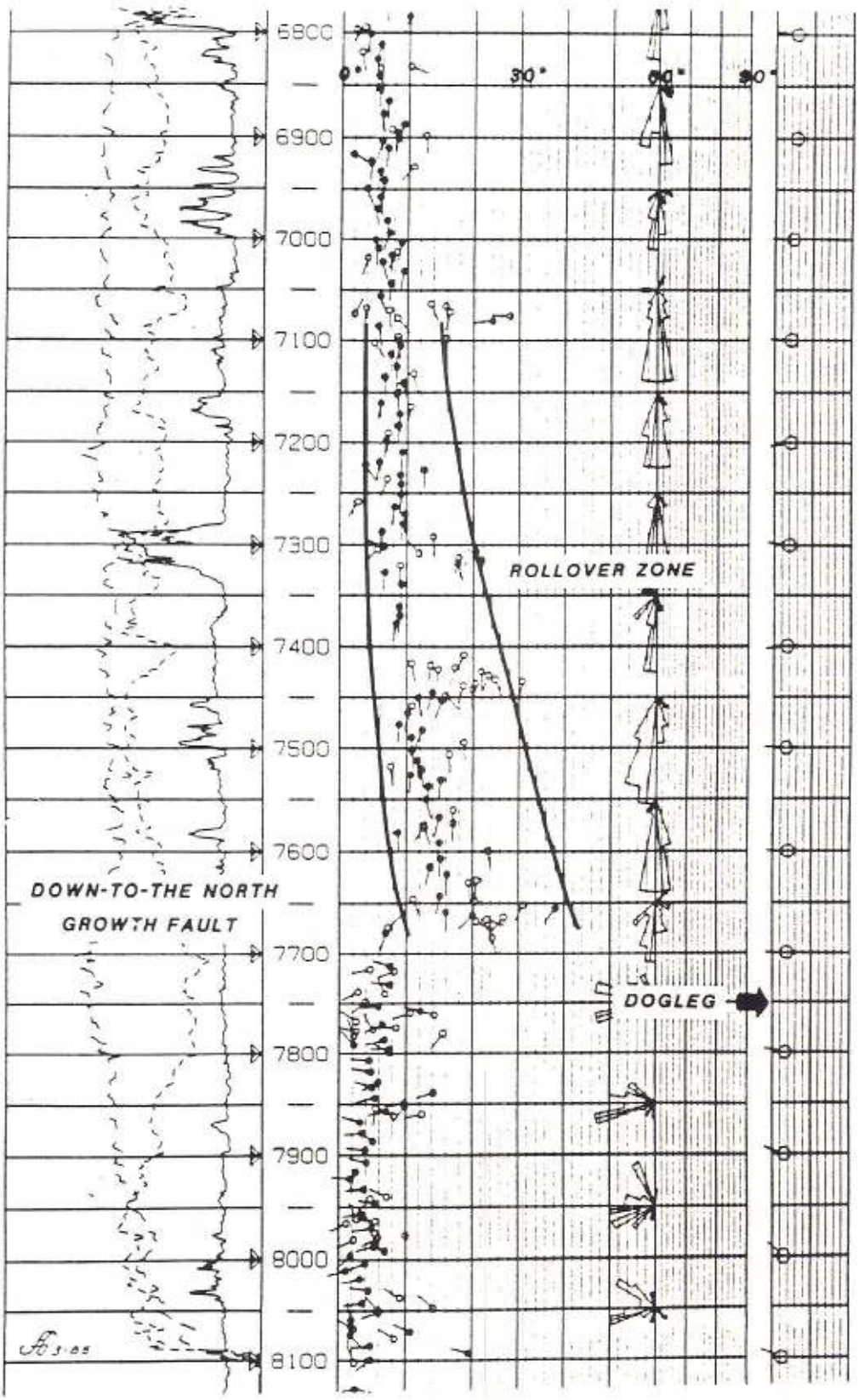
6800
6900
7000
7100
7200
7300
7400
7500
7600
7700
7800
7900
8000
8100
0°
30°
60°
90°
ROLLOVER ZONE
DOWN-TO-THE NORTH
GROWTH FAULT
DOGLEG

ESEMPIO n° 8

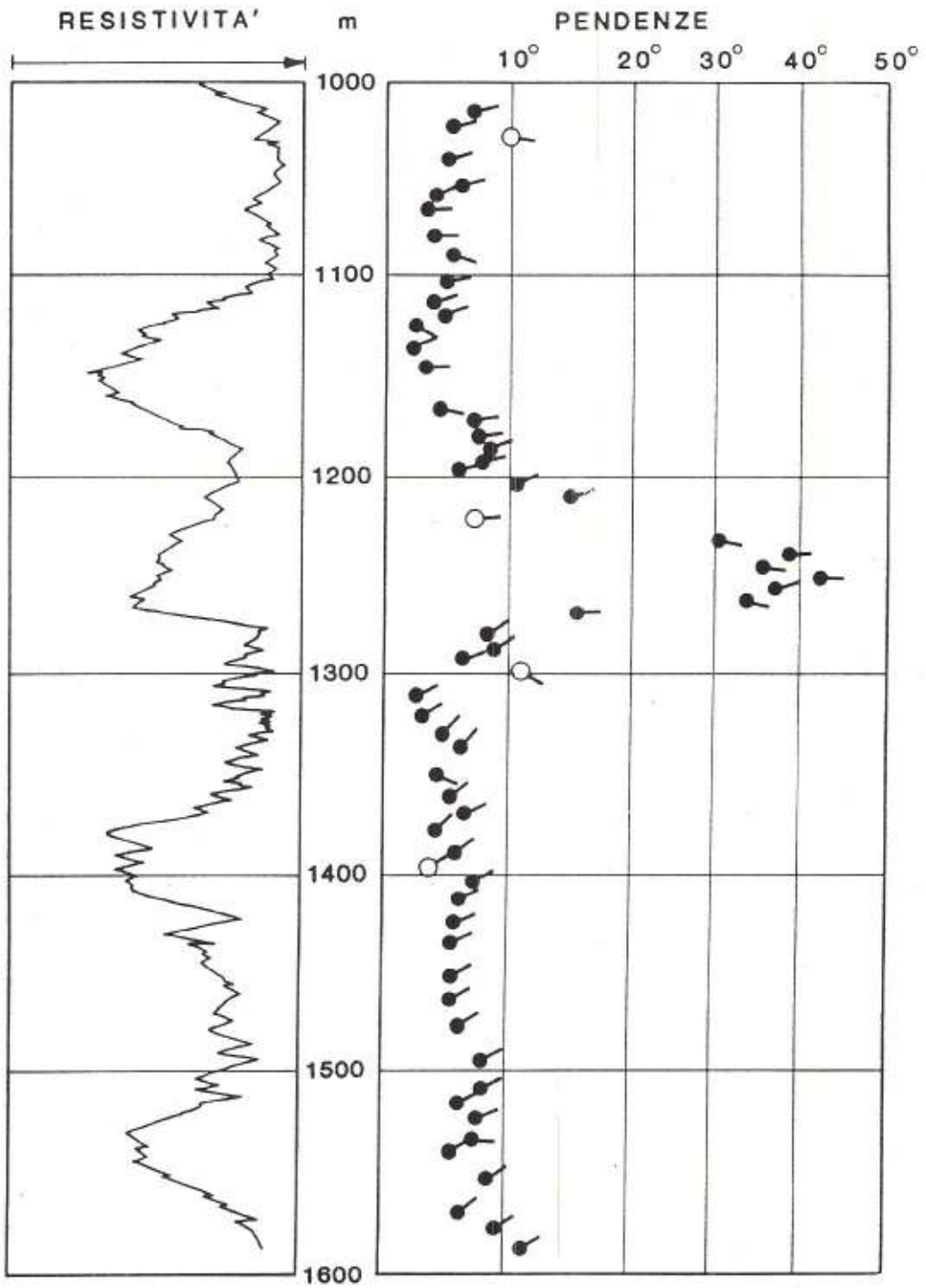
RESISTIVITA'
m
PENDENZE
10°
20°
30°
40°
50°
1000
1100
1200
1300
1400
1500
1600

ESEMPIO n° 9

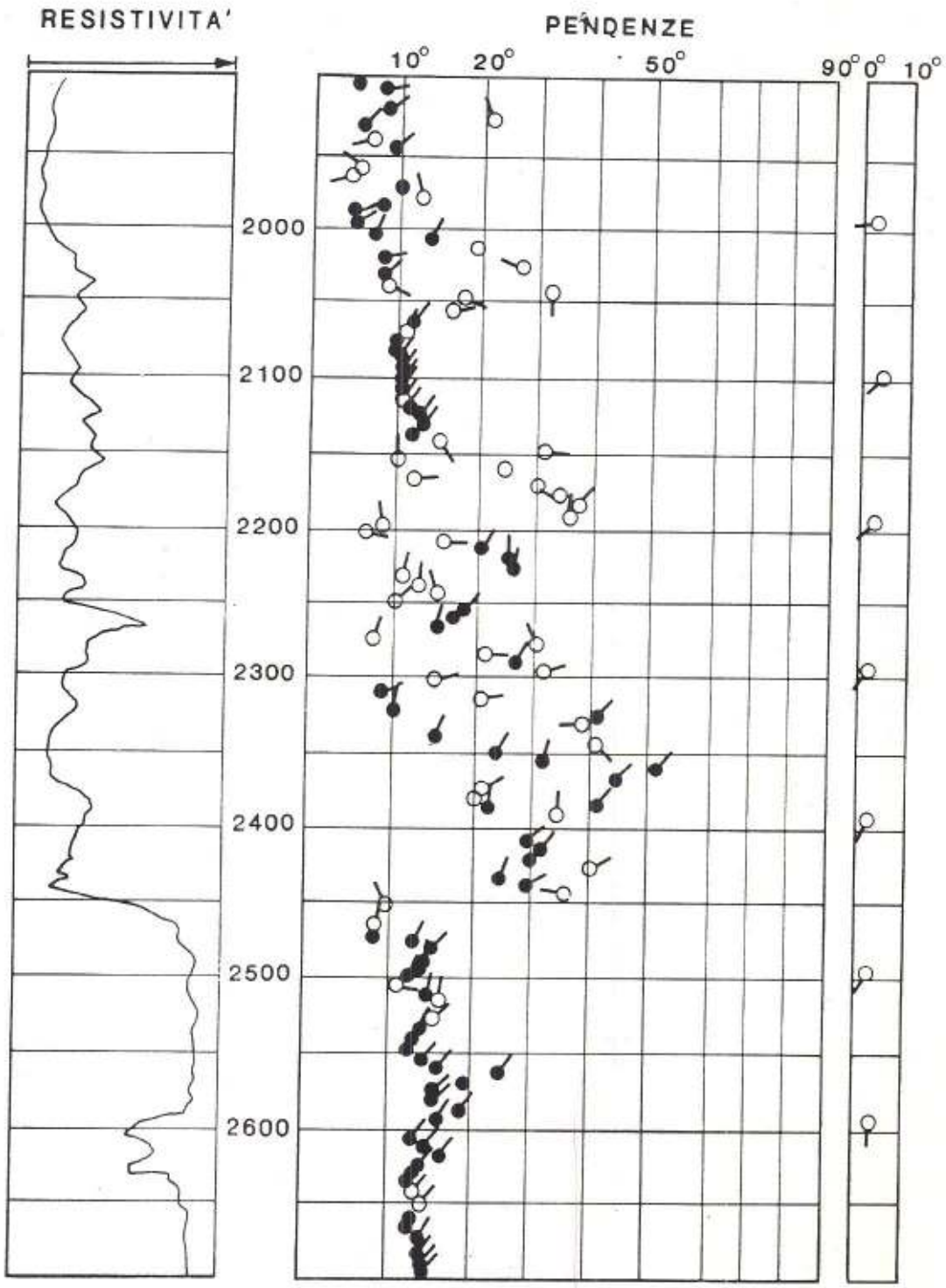
RESISTIVITA'
PENDENZE
10°
20°
50°
90°
0°
10°
2000
2100
2200
2300
2400
2500
2600

ESEMPIO n° *10*

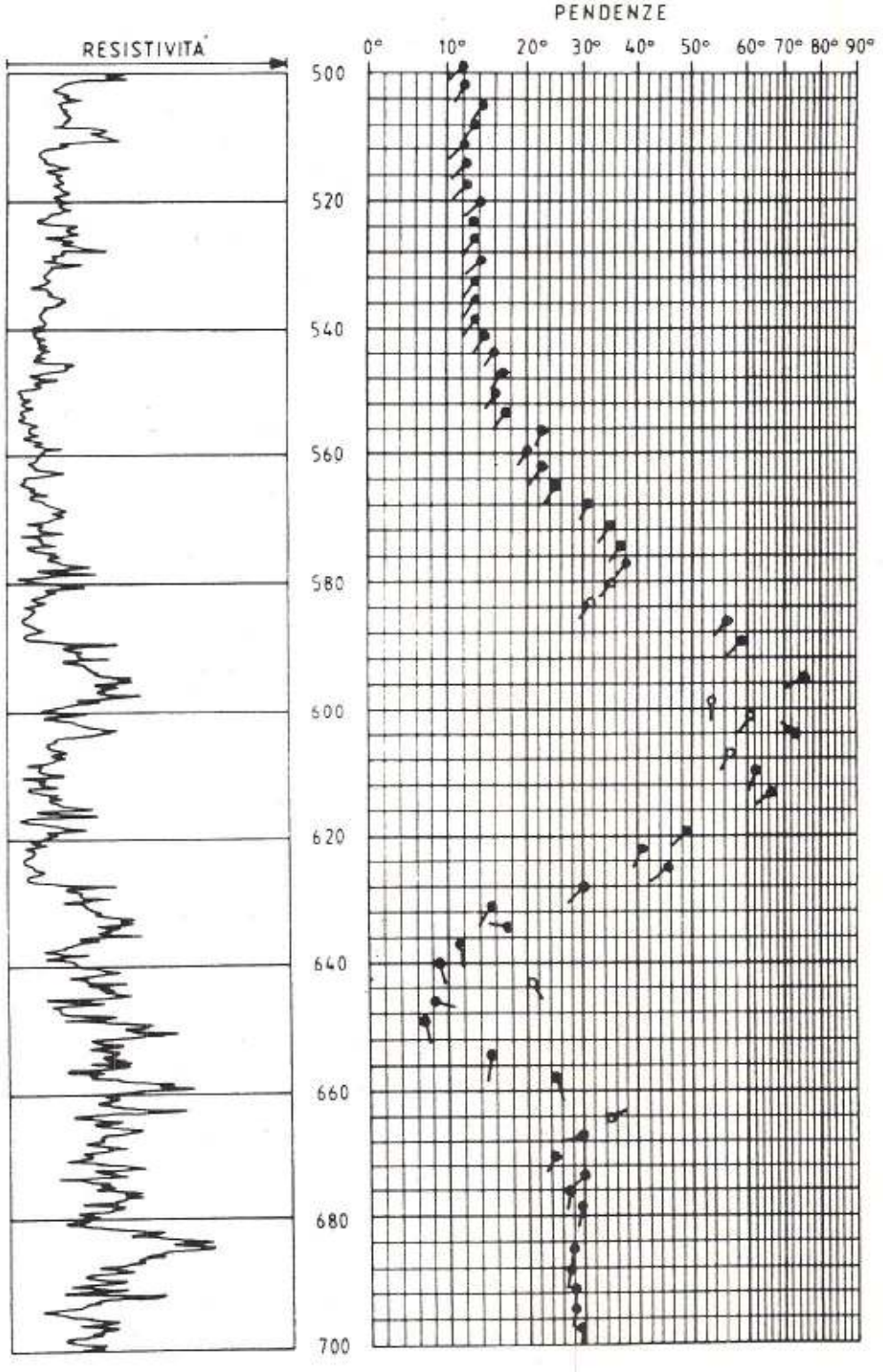
RESISTIVITA
PENDENZE
0°
10°
20°
30°
40°
50°
60°
70°
80°
90°
500
520
540
560
580
600
620
640
660
680
700

ESEMPIO n° *11*

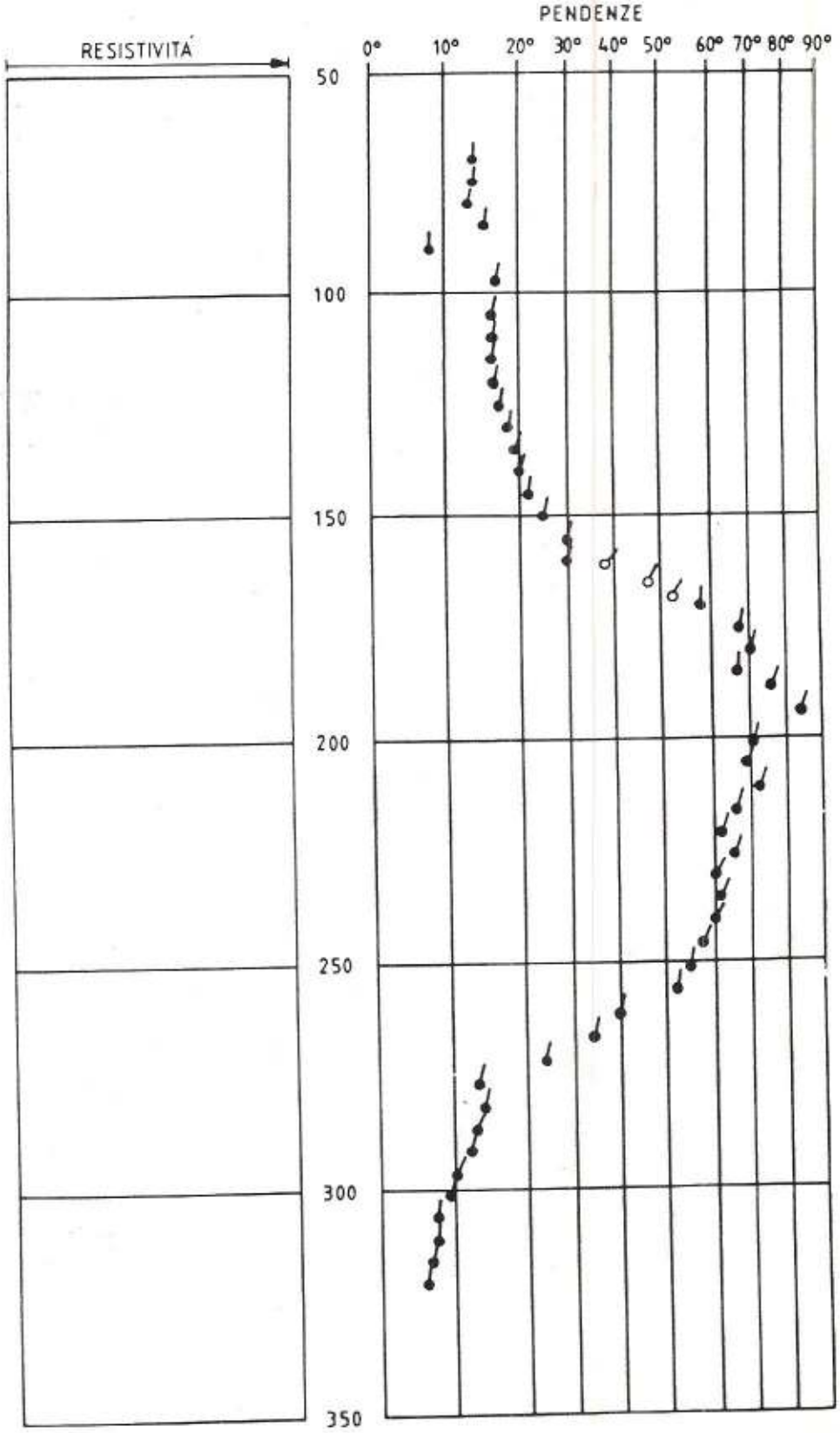
PENDENZE
RESISTIVITÀ
0°
10°
20°
30°
40°
50°
60°
70°
80°
90°
50
100
150
200
250
300
350

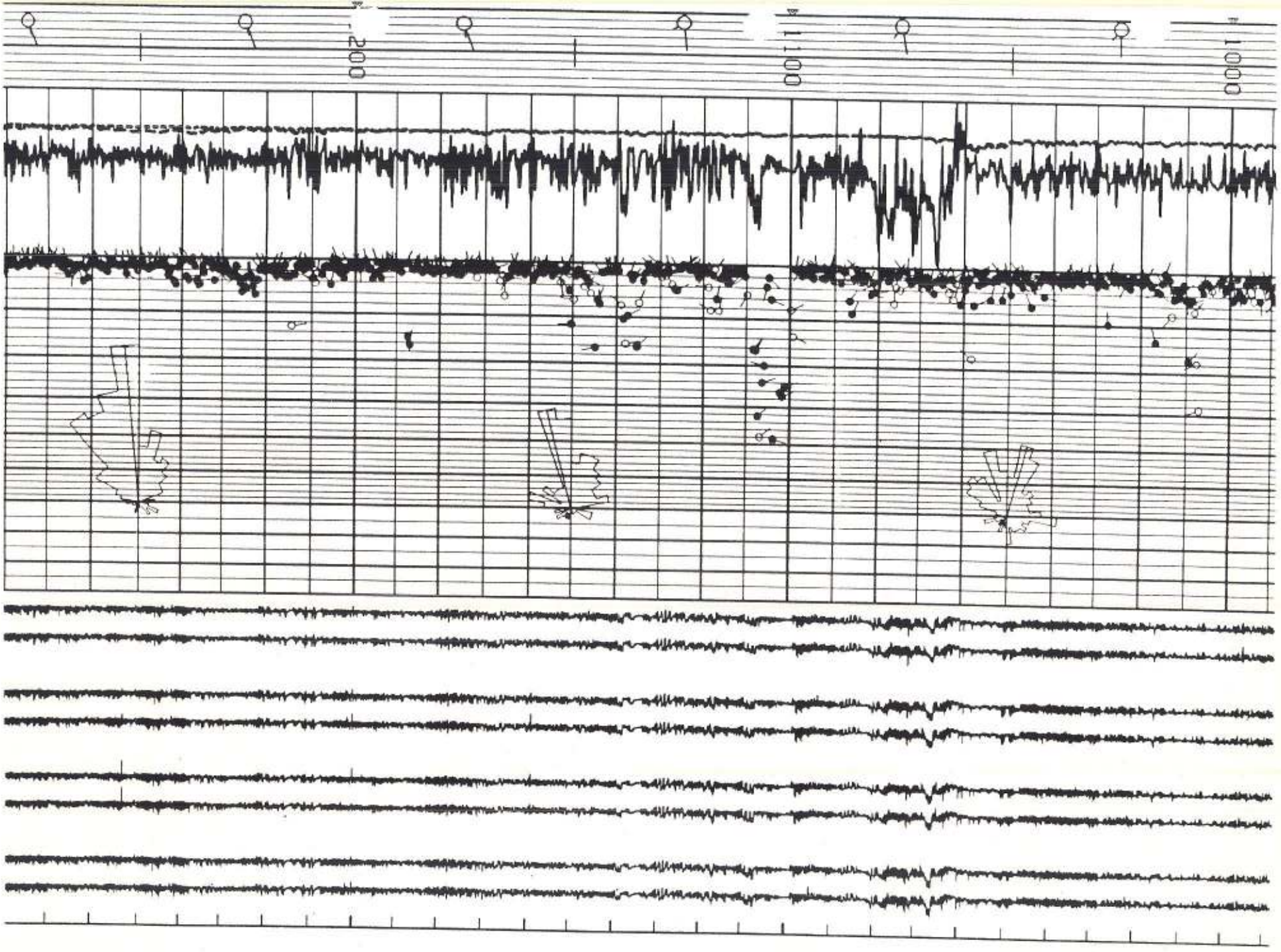
200
1100
1000

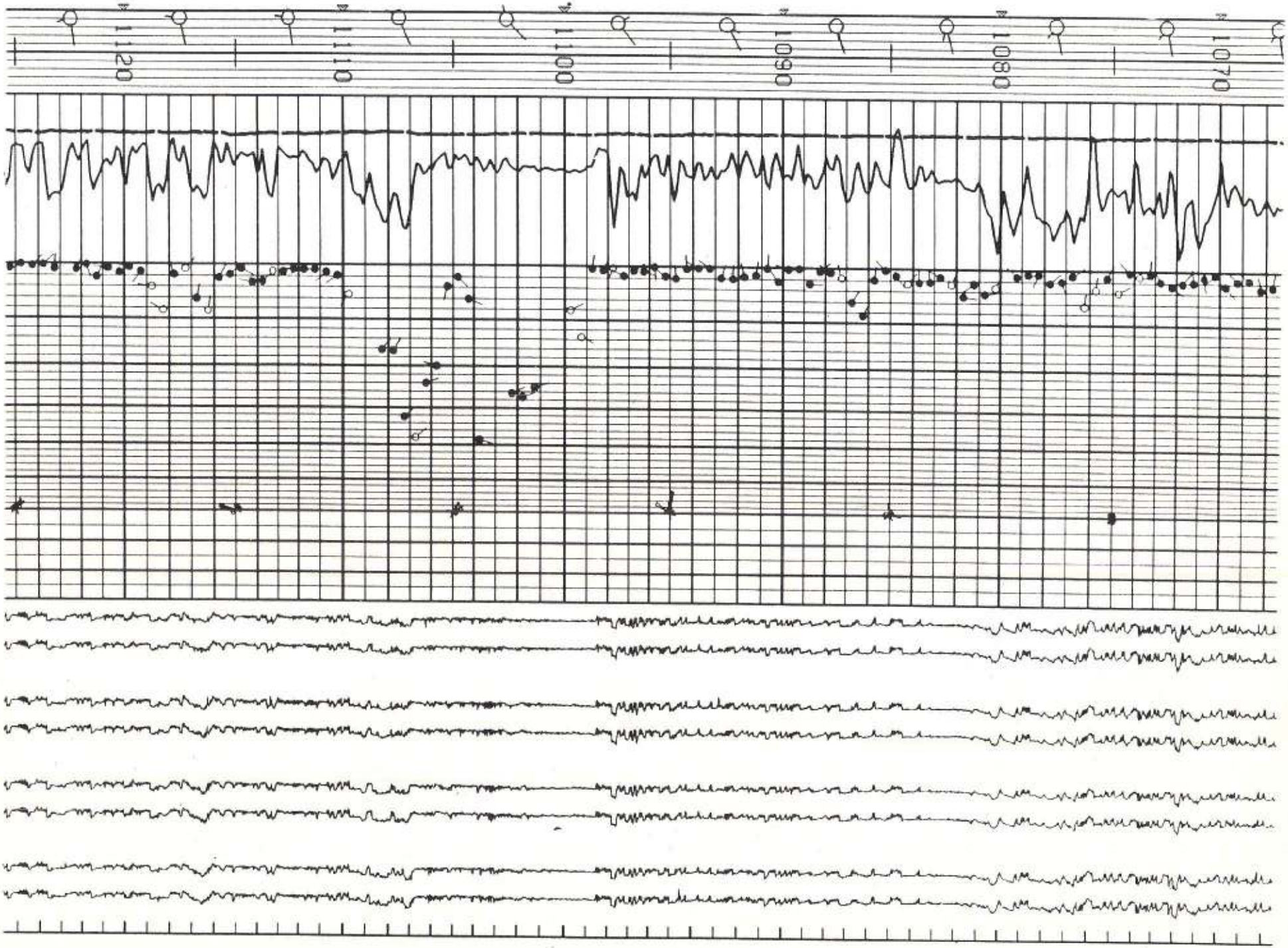
1120
1110
1100
1090
1080
1070

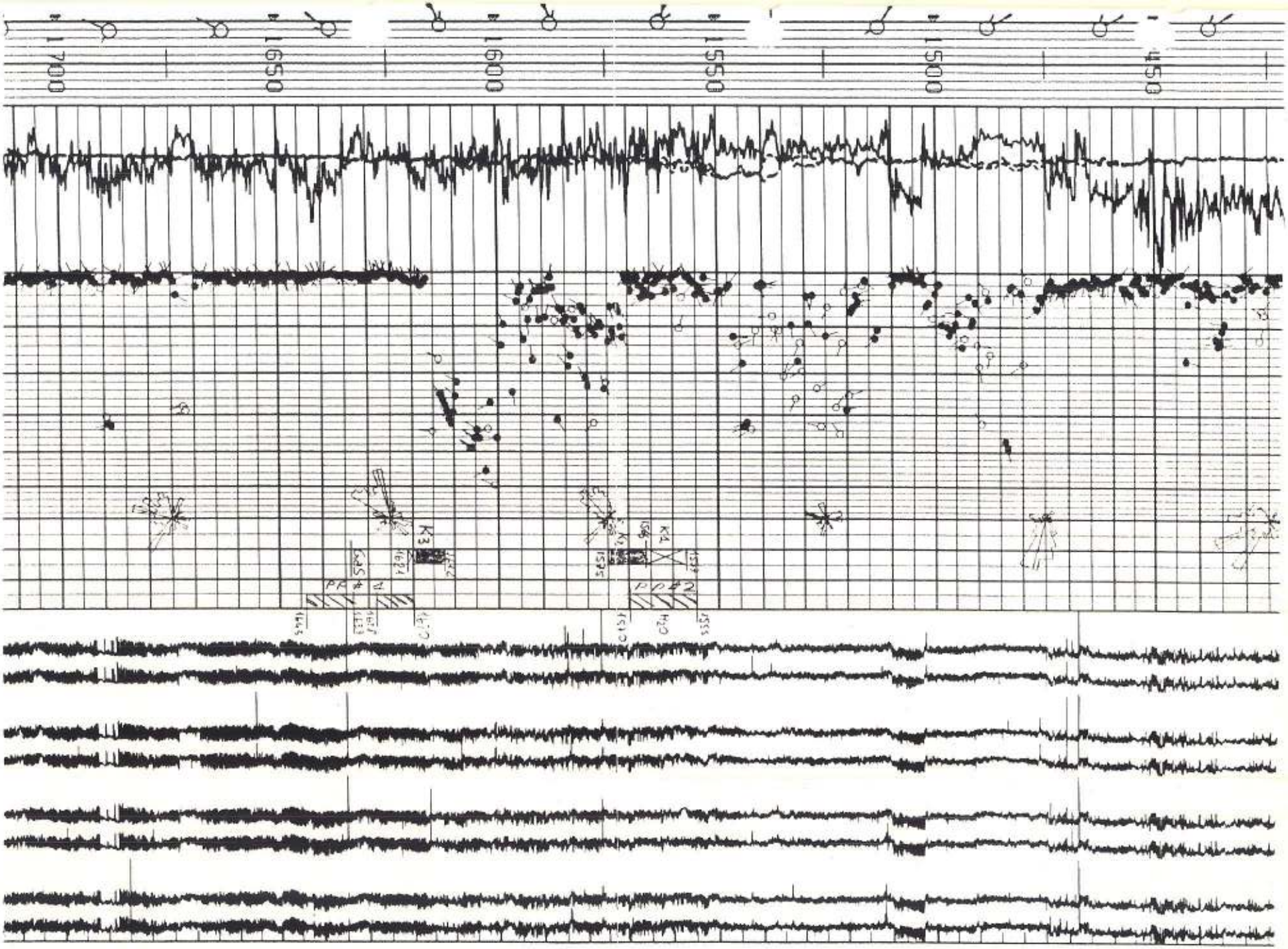
1700
1650
1600
1550
1500
1450

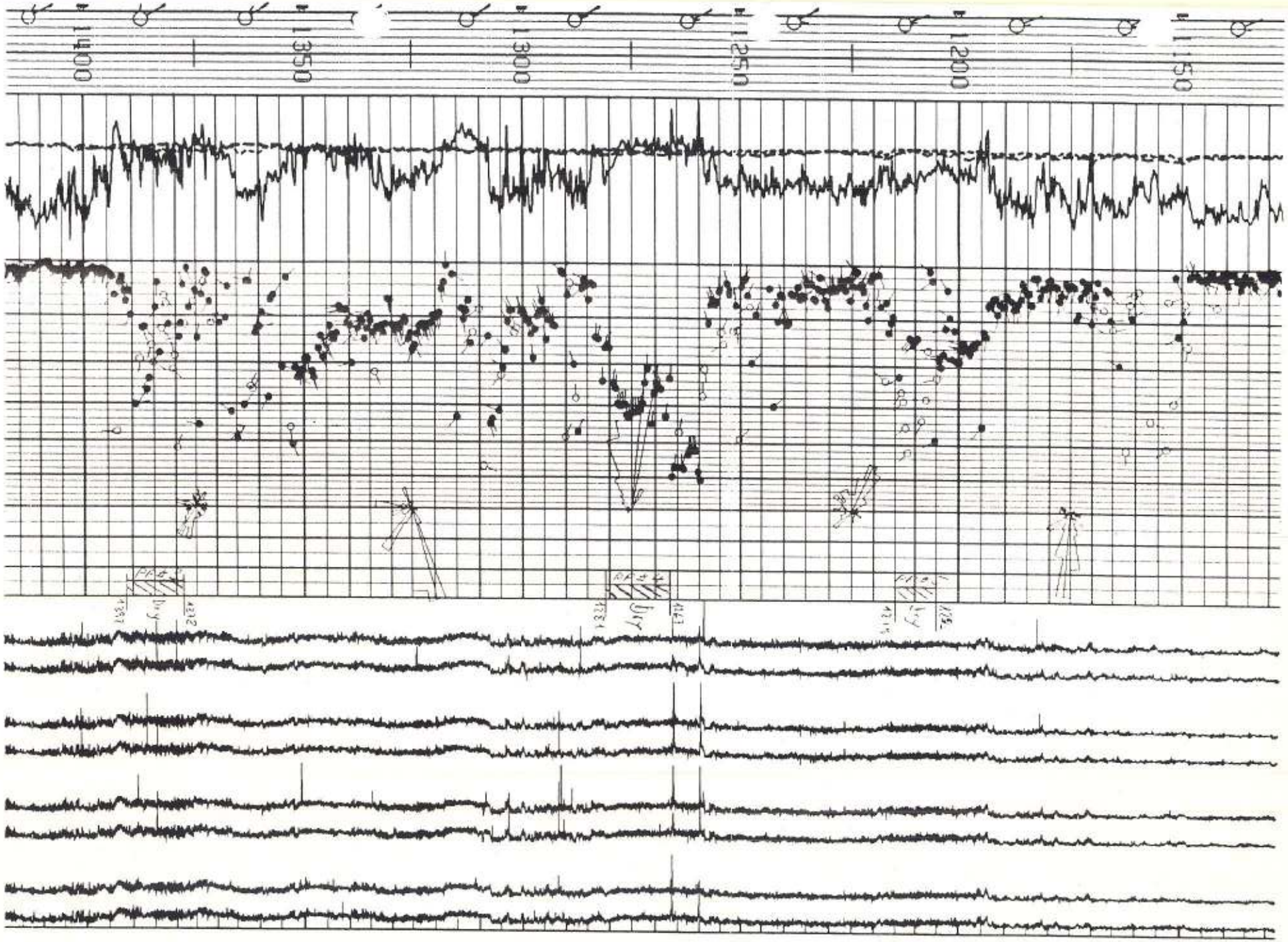
1400
1350
1300
1250
1200
1150

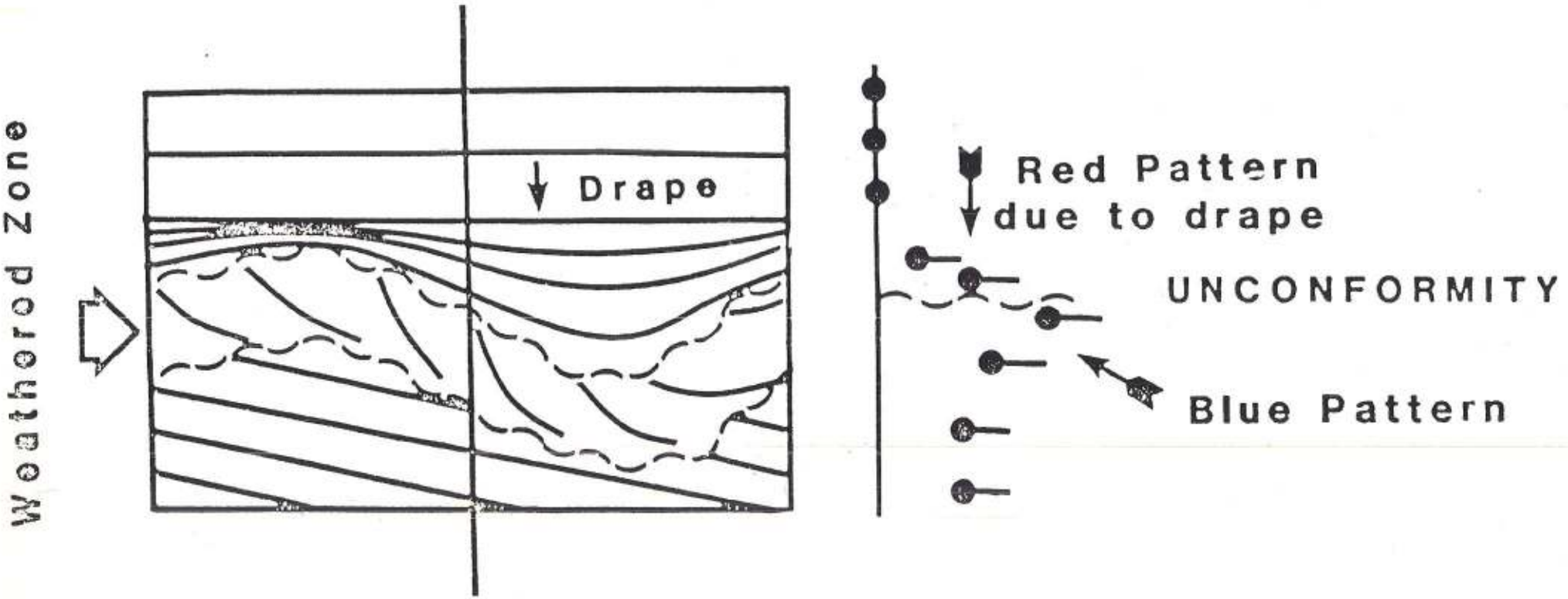
Weathered Zone
Drape
Red Pattern
due to drape
UNCONFORMITY
Blue Pattern

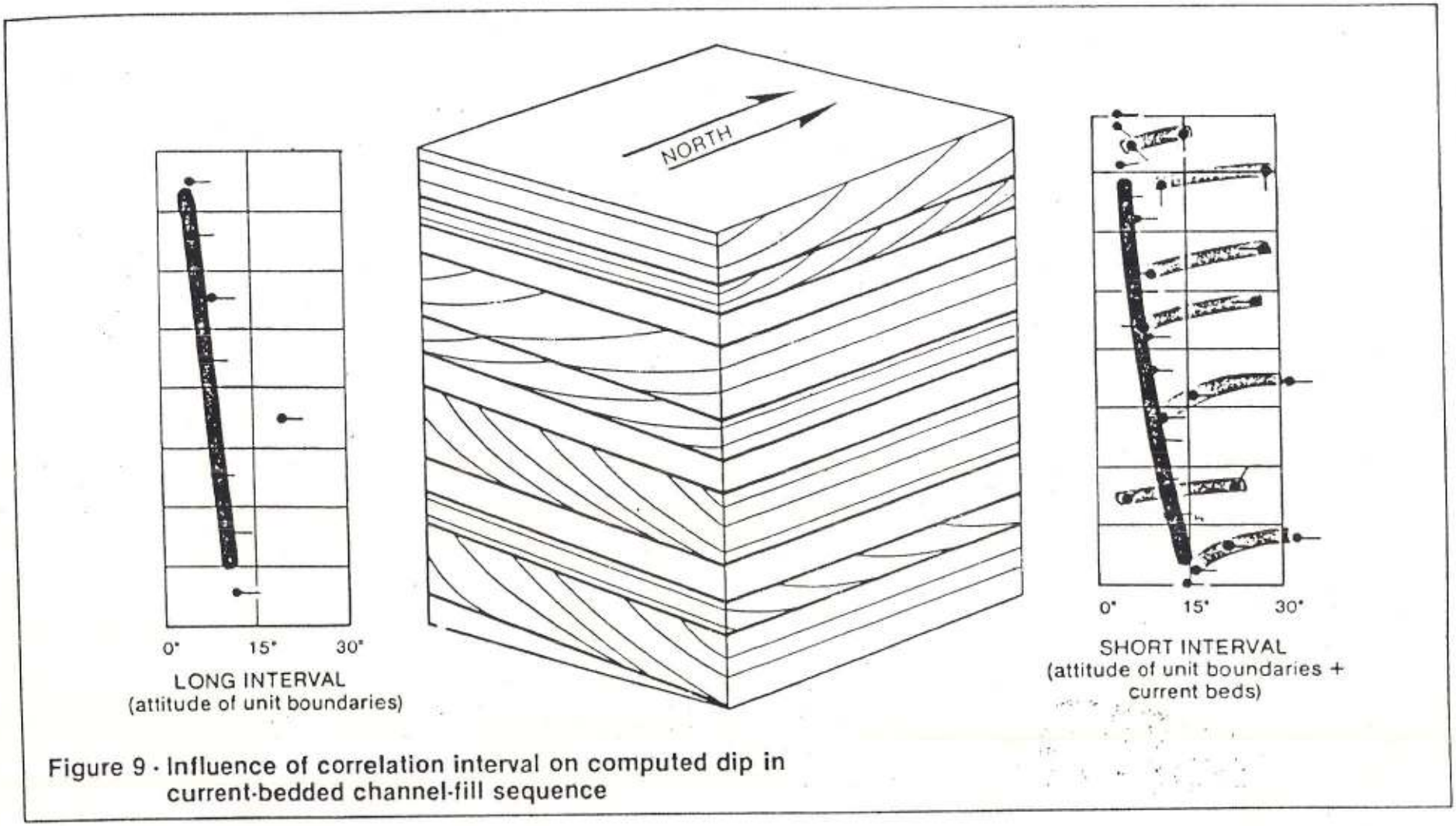

Figure 9 · Influence of correlation interval on computed dip in current-bedded channel-fill sequence

Dipmeter Interpretation Rules

J.A. Gilreath

published by
The Technical Review

Schlumberger Educational Services
1331 Lamar, Suite 1175
Houston, Texas 77010
713-650-8448

Part stratigrapher, part petroleum geologist, and part sedimentologist, the dipmeter interpreter peers down boreholes to figure out, among other things, which way the wind blew at a given time — 2 or 5 or 8 million years ago. Knowing which way the wind blew helps tell which way oil flows and, ultimately, where the drill bit goes. Simple. But not so simple.

To discern details as fine as wind direction, the dipmeter interpreter examines stratigraphic information from a number of wells. The interpreter moves back and forth from the big picture to the small picture, adjusting one then the other to shape the optimum three-dimensional picture of a certain horizon at a certain time. Gilreath starts with the depositional environment constrained to two or three possibilities. He first addresses the big picture: Are we in a delta? A stream bed? A barrier island? A reef? Subsequent questions examine one corner of the big picture: If we're in a delta, what part? If we're in a stream bed, exactly where? If we're in a barrier island, are we on the seaward side or the landward side? Finally, the last questions fine-tune the stratigraphic interpretation: Which way the wind blew, the currents flowed, the tides ebbed and flooded, and what each means to the shape, character, and extent of rock bodies. Addressing these last questions ultimately determines strategies for the exploration, drilling, and production of oil and gas.

Summed up, Gilreath's interpretation scheme has four steps:

- Limit likely depositional environments based on client's knowledge or key logs (e.g., bound water and shale resistivities and dip scatter).
- Determine gross structural dip and delete it if necessary.
- Ascribe missing and repeat sections to unconformities or faults (see page xx).
- Using knowledge of dip, structure, lithology and depositional environment, make a stratigraphic interpretation, which includes an estimate of the shape and extent of reservoir rock. Examples in this supplement summarize this final step.

Method of Plotting

The tadpole plot is the traditional graphic device used on dipmeter logs. It gives three pieces of information: (1) the lateral position of the tadpole head represents dip magnitude, which increases to the right from 0 degrees to 90 degrees; (2) the tail projects from the head in the downdip direction; (3) and the vertical position of the head indicates depth. The top of the plot is north.

Dips are grouped into four color-coded patterns:

Blue indicates dips decreasing downward.

Red indicates dips increasing downward.

Green indicates no change in dip with depth. This is usually taken to indicate structural dip, the tilting imposed on the rock by tectonic forces.

Yellow is assigned to random dips.

Since different stratigraphic features can create the same dip patterns, it is important to limit the depositional environment before keying a dip pattern to a stratigraphic feature. The meanings of various dip patterns in the context of different depositional environments are shown in the following series of theoretical dip versus lithology patterns for common depositional environments. Each log is discussed from the bottom up.

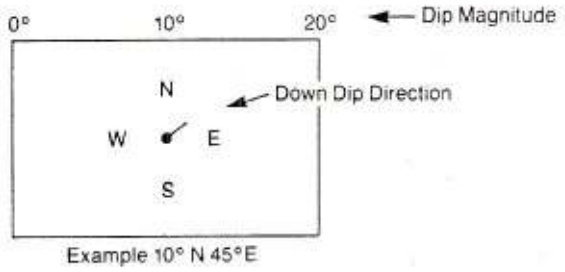

Example 10° N 45°E

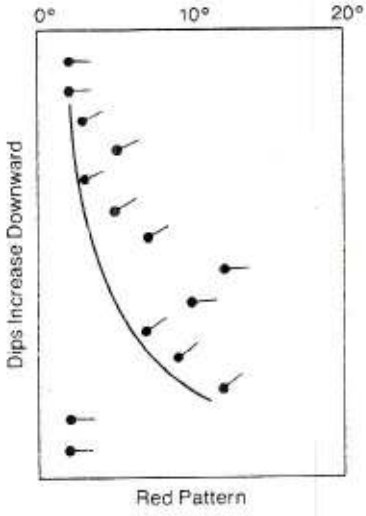

Red Pattern

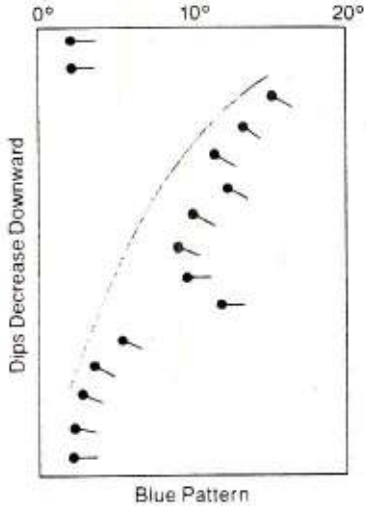

Blue Pattern

Green Pattern — Dips constant with depth

Yellow Pattern — Random dips

Nonmarine/Continental

The four structural (green) dip patterns indicate sediments deposited essentially flat in an upper delta plain. (You can expect sands in such an environment to have secondary porosity from plant-produced acids that have dissolved sand grains.)

The yellow "bag-of-nails" pattern near the bottom results from disturbed bedding from high-energy surges in the flood plain. You'll be able to discern few, if any, structural dips in such environments.

Moving up again, the green over blue patterns are characteristic of eolian dunes, especially transverse and barchan. The wind blew toward the downdip direction (west to east). Dome and parabolic dunes produce mainly red patterns, also with the wind blowing downdip. Longitudinal dunes produce red or blue patterns with dip direction normal to prevailing wind direction.

Blank zones result from destruction of bedding planes from bioturbation and rooting, indicating marsh or swamp deposits.

Red dip patterns within shale zones (indicated on the spontaneous potential or gamma-ray [SP/GR] curve) suggest clay-filled stream channels. The downdip direction is toward the thalweg.

The blue over red pattern, with the blue dipping normal to the red, and the SP/GR curve indicating sand, suggests a stream channel. The red dips are normal to channel strike (northwest-southeast). Flow direction is downdip of the blue pattern (to the southeast).

Several blue patterns at the top of the log are typical of point bar sands, when core and other geological studies indicate a fluvial environment. These dips are in the direction of current flow ± 60 degrees. If the patterns extend more than 3 feet, they probably result from accretion deposits, which dip toward the thalweg, rather than from trough cross-bedding, in which they would dip down current.

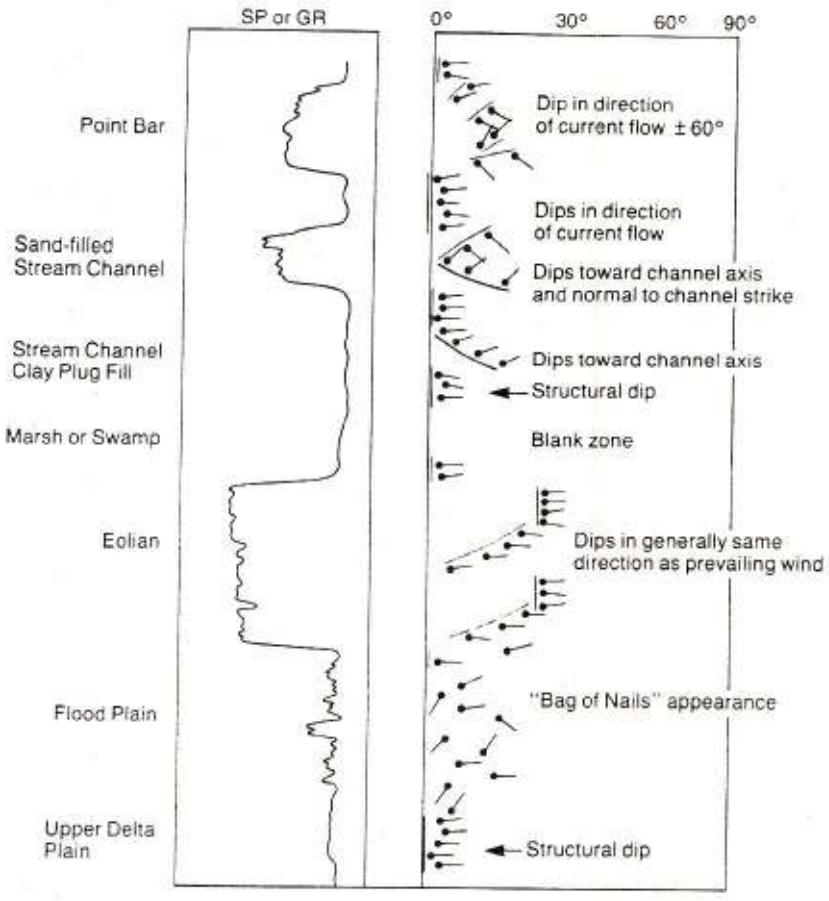

Continental Shelf: Delta Dominated

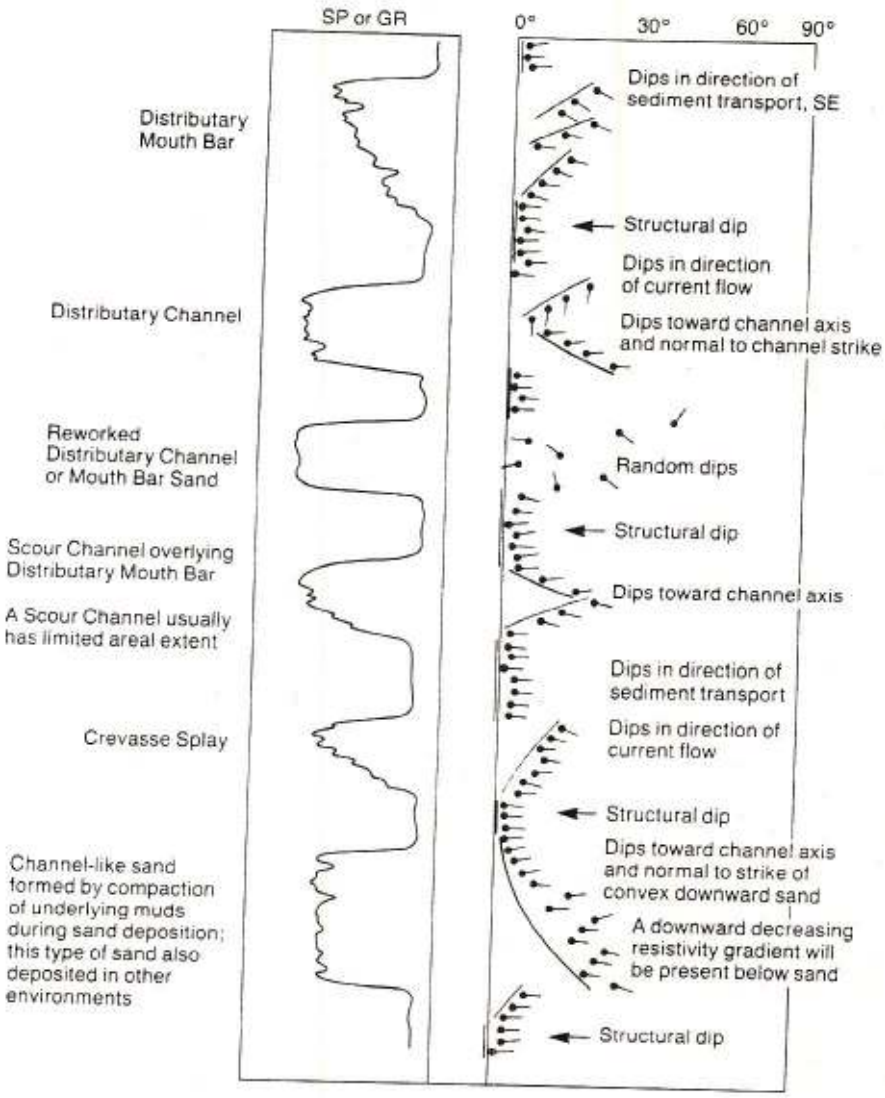

The sudden decrease in the SP/GR log is of limited use here, but coupled with an increase in the resistivity log (not shown) it would indicate compaction of a mud, probably by an overlying sand. The long, sweeping red pattern suggests a channel-like sand. The red dips are normal to the axis of the sand. Such sands can be more than 2,000 feet thick.

Moving up, the blue patterns can indicate either a crevasse splay or a distributary point bar. The saw-tooth SP/GR curve, indicating pulses of deposition, is not much help, since it is associated with many features. Resorting to information from other wells can be helpful and often necessary to distinguish crevasse splays from distributary points bars. Sands limited in areal extent suggest a crevasse splay; extensive sands suggest a distributary mouth bar. In this example, current flow is downdip (southeast). The underlying structural dip (green) probably indicates that the splay or bar formed over a flat-lying delta outwash plain.

Red over blue patterns dipping in parallel are characteristic of a distributary mouth bar sand topped by a scour channel. The blue patterns, which result from foreset bed deposition, dip in the direction of current flow (to the east-southeast) and the red patterns which result from drape over the base of the channel, dip toward the scour channel axis (east-southeast).

The overlying yellow pattern could have a few causes, but is most likely a reworked distributary channel or mouth bar sands, since it is sandwiched between channel deposits. These sands tend to be clean, with good permeabilities and porosities.

The red pattern (from drape) overlain by a blue pattern (from foreset beds) dipping normal to it suggests a distributary channel. The red pattern dips toward the channel axis, and the blue pattern dips downstream (south).

The topmost feature was identified as a distributary mouth bar based on studies in other wells. Based on the dipmeter plot alone, the bar is indistinguishable from a crevasse splay. The multiwell study, however, permitted mapping a channel. It was logical to conclude that the blue patterns at what seemed to be the end of the channel must indicate a distributary mouth bar. In general, blue patterns dipping away from the channel axis indicate crevasse splays; blue patterns dipping parallel to channel strike are due to a distributary mouth bar. Variation in dip magnitude gives some indication about the shape of the distributary mouth bar. When dip varies 10 degrees or more, the bar tends to be elongate downdip. When dip varies less than 10 degrees, the bar tends to be crescent- or fan-shaped.

Continental Shelf: Tide, Wave, and Current Dominated (1)

Stratigraphic features of this environment are often the result of reworking of previously deposited deltaic sediments.

The two green patterns at bottom are interpreted as parallel cross-beds dipping seaward about 20 degrees. Existing knowledge of the area's lithology, based on cores or density and neutron logs, established this as a carbonate zone. The parallel cross-bedding could be from an eolian feature, but it probably indicates beachrock, a carbonate that forms at the saltwater–freshwater interface along the shoreline.

The red pattern, produced by drape, overlying the blue pattern, produced by cross-bedding, indicates a bar identified by the client as oolitic. The pinch-out is downdip (northeast) and the strike of the bar is normal to dip (northwest–southeast). Dips within the bar are irrelevant. The key sign of a bar or reef is a red pattern, which indicates a convex upward feature, above a permeable zone. A blue pattern, indicating a convex downward feature, above a permeable zone would suggest a channel-like feature.

The next zone shows more characteristics of a reef: a blank zone — caused by massive, nonbedded reef material — over a blue pattern, caused by mud compaction, and under a red pattern, caused by drape over the reef flank. The red patterns dip toward the pinch-out (east–northeast) and normal to the strike of the reef (north–northwest by south–southeast). The blue pattern, which results from compaction, dips toward the thickest part of the reef.

The next set of red patterns overlying numerous dips at odd angles suggests a buried beach ridge. Beach ridges typically have dips in many directions, as opposed to bar deposits, which tend to have uniform dips from reworking by waves. The red patterns indicate the top of the ridge and the numerous dips indicate the ridge's interior. The red patterns dip toward the shale-out (northeast) and normal to the strike of the beach (northwest–southeast).

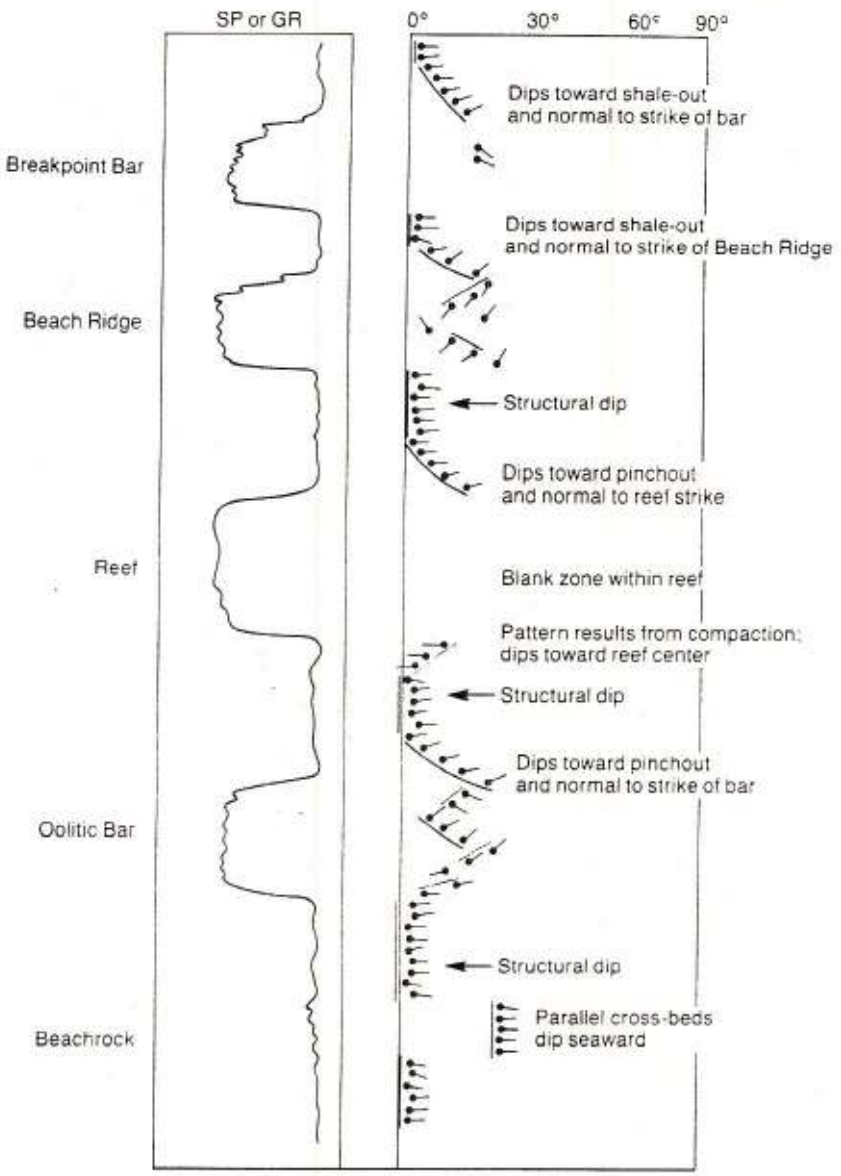

Finally, the uppermost red pattern overlying two dips normal to the general red trend suggests a sand bar that formed at the wave break point. The homogeneity of the dips is strong evidence for reworking, a characteristic of breakpoint bars. The red pattern dips toward shale-out (northeast) and normal to the strike of the bar (northwest–southeast). Breakpoint bars can be distinguished from longshore current sand waves in that the former are usually overlain by a red pattern, and the latter have blue patterns within the sand. Dips in both can be seaward or landward.

Continental Shelf: Tide, Wave, and Current Dominated (2)

Based on knowledge that the well intersects a beach, the bottommost blue pattern, sandwiched between green patterns, indicates a slip face sand on the landward side of the beach. The blue dips point landward (west) and are normal to the beach strike (north–south).

Again, based on knowledge of a beach environment, the collection above of varying blue patterns with dips landward indicates festoon cross-bedding. This type of a bedding is common in primary dunes, the first row behind the beachface, and is caused by variations in wind direction. The overlying green pattern probably indicates a berm.

The few overlying random dips overlain by a blue pattern suggests a runnel: the blue pattern derives from megaripples and the random dips are from small-scale ripples. (Small-scale ripples can also produce blank zones.) The dip of the megaripples parallels the strike of the beach (north–south).

Above the runnel, green patterns of varying dip magnitude suggest parallel cross-bedding in beachface sands. Since the sea was downdip of the cross-bedding, at the time of deposition it lay to the east. The flatter lying sands above suggest the lower energy environment of the upper shoreface sands. The random dips above suggest the high energy and bioturbation of the lower shoreface. This area can also be indicated by a blank zone.

Blue patterns overlying green suggest longshore current sand waves overlying a fossil shoreline, given knowledge of a silicate shore. The blue patterns dip in the direction of longshore transport (from north to south) and parallel the shoreline strike (north–south).

Landward dipping blue patterns indicate landward sediment transport, probably produced by a tidal flood delta or a washover fan. The overlying seaward dipping blue pattern suggests a tidal ebb delta.

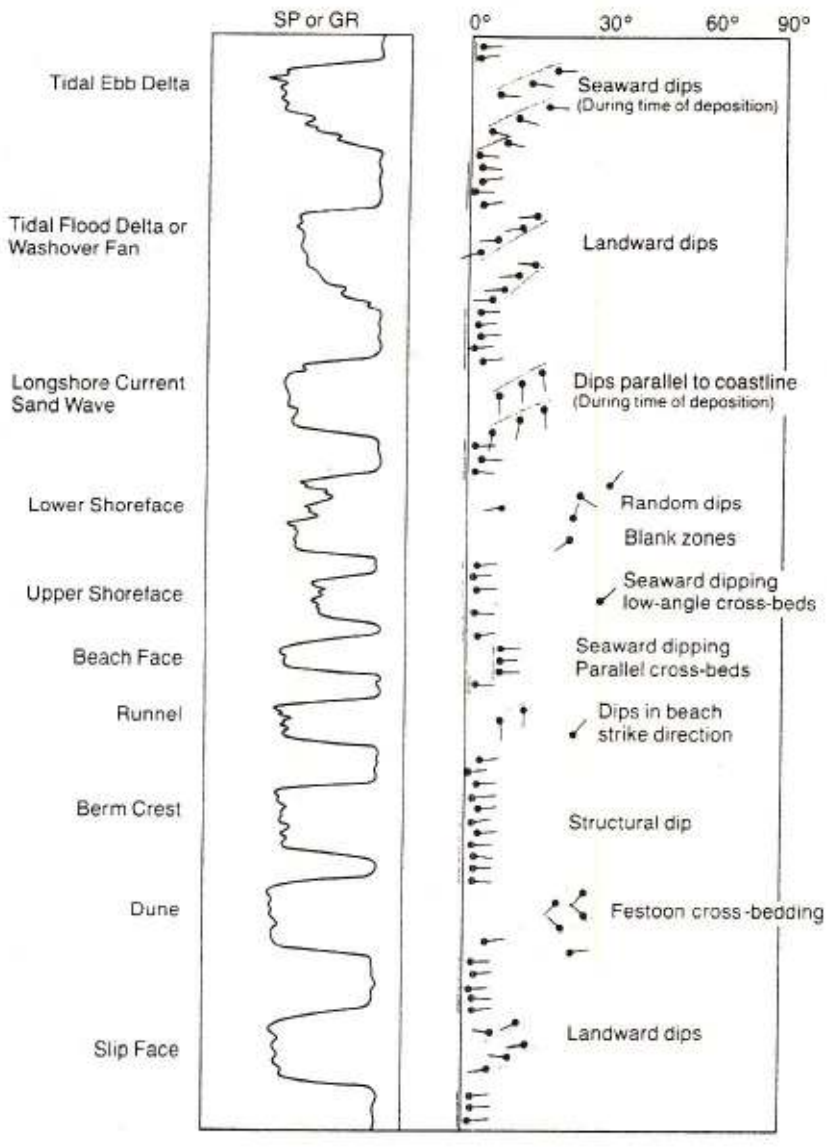

Continental Slope and Abyssal

Sediments in the deep waters of the continental slope and beyond often undergo post-depositional movement that produces random dips. Structural dip, consequently, is difficult to determine in these environments. Dips that appear to be structural can indicate the most common flat-lying features — submarine fans and feeder channels.

Reading the log from the bottom, the yellow pattern suggests either a debris flow or upper slope deposits that were deformed after deposition. Distinguishing between the two requires data from a core or a Formation MicroScanner* (FMS) log. Above them, the structural dip and evidence in the SP/GR log of alternating sand/shale layers suggest the low-lying outer edge of a submarine fan. Farther up, the appearance of blue patterns from cross-bedding suggests either the axis of a feeder channel or the mid-fan. Mid-fan deposits, however, are much more common. Sediment transport is in the downdip direction of the blue pattern (north to south).

Independent information from cores indicated this second yellow pattern results from highly deformed sediments, probably from a debris flow. The following patterns suggest the various parts of a submarine feeder channel. Red indicates the edge of the channel, with the dip toward the channel axis (axis to the east) and normal to channel strike (north–south). The two blue patterns above suggest the channel axis, with transport direction downdip (toward south–southwest). Finally, the blue over red patterns, with dips 90 degrees apart, indicate an area of the channel between the axis and the edge. The red pattern, again, dips toward the channel axis and normal to channel strike, and the downdip direction of the blue pattern indicates the transport direction. The decline in SP/GR values with depth in the mid-fan suggests the sand is getting coarser with depth. This occurs because the first deposits of a fan are the finest, then, as the fan builds out, coarser sediments are carried farther. Finally, the uppermost layer, which was nearest shore, will be the coarsest. The numerous SP/GR excursions in the outer fan indicate alternating sand-shale layers.

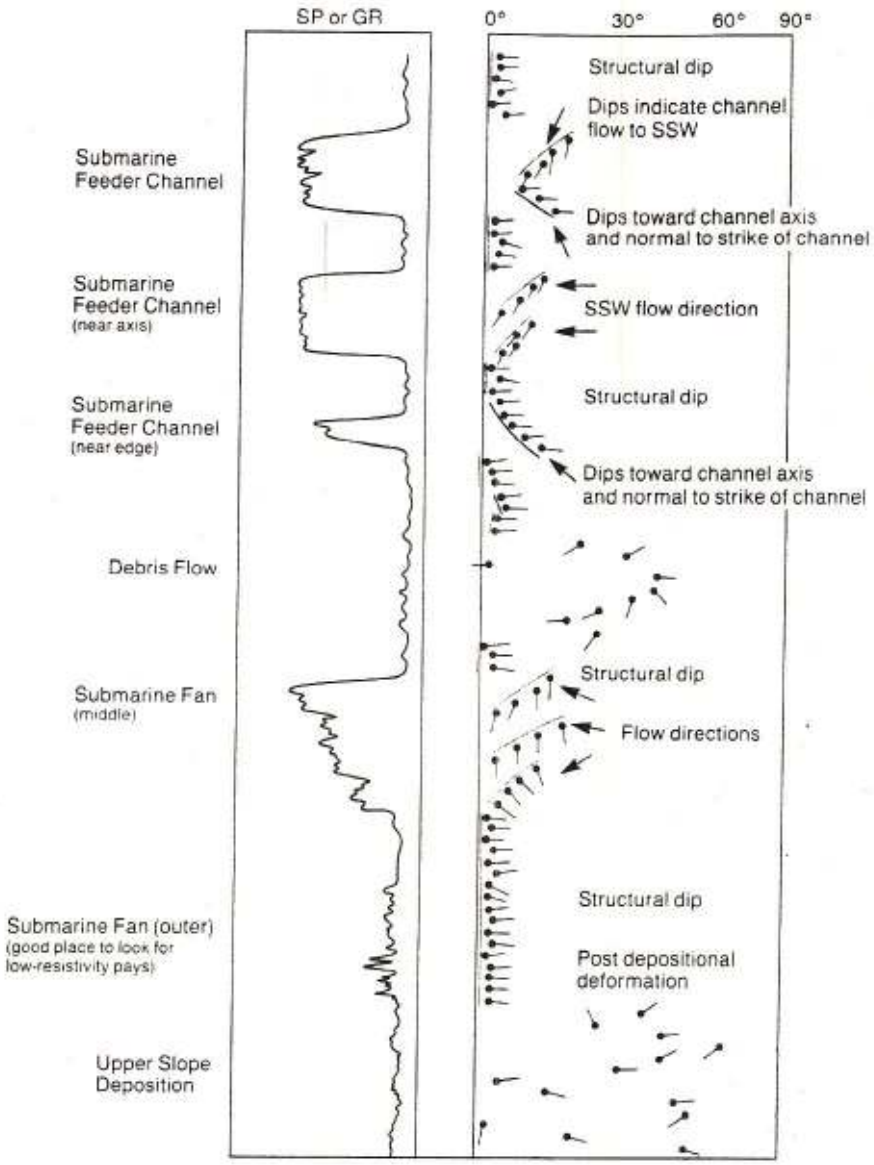

* Mark of Schlumberger

Strategies for Dipmeter Interpretation

Part 1
(First of Two Parts)

J.A. Gilreath
New Orleans

The dipmeter is one of the most enduring, versatile tools in well logging. Introduced more than 50 years ago, it was first used in exploration for identifying large-scale geologic structures that might be oil traps. Gradually, refinements in dipmeter hardware, data processing, and interpretation enabled the tool to resolve small-scale features, such as texture, *laminations*, and intrabed sedimentary structures (See "A Glossary for Dipmeter Interpretation," page 40, for definitions of terms in italics). Today, dipmeter interpretation routinely integrates information about small-scale sedimentary features and large-scale structure to describe the stratigraphy around a wellbore. This stratigraphic model enables the interpreter to estimate a reservoir's shape, extent, preferential permeability and clay-rich zones — some of the crucial information needed for getting the most from a single well or a field of wells.

Dipmeter logs are made with a family of tools that spun off from the first pad-mounted dipmeter introduced in 1935.[1] Early dipmeters measured only the direction, or azimuth, of the slope of sedimentary features, such as *bedding* planes. Although this remains one of the dipmeter's primary functions, modern dipmeters also measure the magnitude of *dip*, borehole geometry, deviation (inclination from vertical), direction, and roundness.

Dip is computed from formation resistivity measured by button electrodes on four orthogonal pads pressed against the borehole wall. This article focuses on interpretation of logs made with the Stratigraphic High Resolution Dipmeter (SHDT*) tool, also called the Dual Dipmeter* tool, or the older High Resolution Dipmeter (HDT*) tool. The application of a relative of the SHDT tool, the Formation MicroScanner (FMS) tool, has been covered elsewhere.[2]

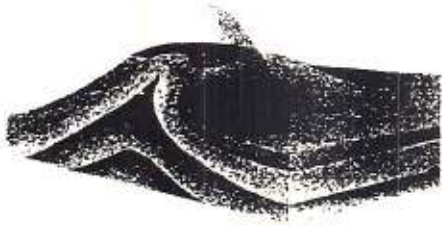

☐ *Idealized structural and stratigraphic hydrocarbon traps. A recumbent anticline (above) is one type of structural trap. It will hold hydrocarbon if it is capped by impermeable strata. Structural traps also form in folds created by thrust-faulting (right). Channel sand deposits*

Strategies of dipmeter interpretation vary with the requirements of the client, knowledge of the area's geology, and the bent of the interpreter. At one extreme are reductionists, who interpret dipmeter logs in the context of a few other logs they consider pertinent, weighting their interpretation with their experience and detailed study of local context. At the other extreme are synthesizers, who interpret dipmeter logs in conjunction with many other logs, taking a broad, integrative approach. Many interpreters, of course, take a middle road and augment dipmeter data with as many or as few logs as they need for confident interpretation.

This article reviews a reductionist approach that evolved in the US Gulf Coast in the 1950s and meets the diverse needs of independents and majors working there. The synthetic approach evolved later. One such approach was developed in the North

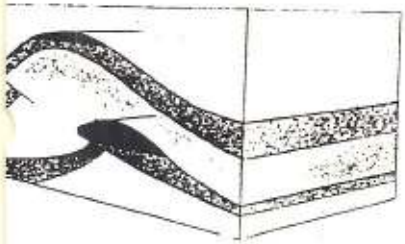

are a common type of stratigraphic trap. nel is first cut (top), then filled (middle). If tion continues, channel sands will be com- l by draping, overlying sediments (bottom). ke Maracaibo reservoirs in Venezuela are type.

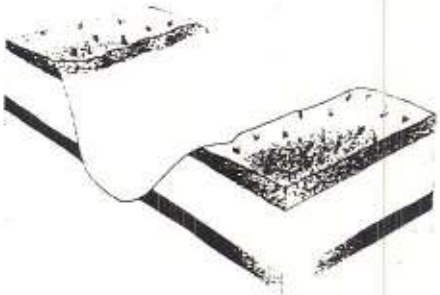

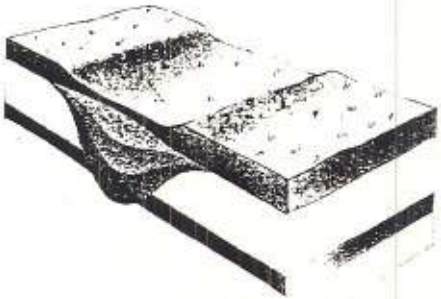

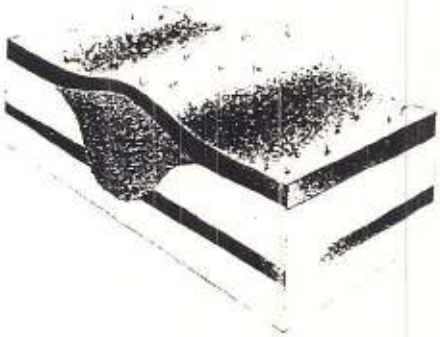

ea in the 1980s and meets the fairly singu- ar needs of majors, the only oil producers who can afford to work the North Sea fields. his will be described in the second article f the series.

The reductionist method pioneered by Al Gilreath can be fairly called rule-based, ince it applies a set of dip patterns that have ee hown, through thousands of inter- re ns, to indicate certain geologic tructures.

The goal of dipmeter interpretation is to dentify reservoir traps, of which there are vo broad categories, *structural* and *strati- raphic (above and right)*. Structural traps e defined by *faults*, folds, and other fea- ires caused by tectonic forces, such as onconformities. Stratigraphic traps are oduced by sedimentary processes and hologic changes that alter the porosity d permeability of rock layers — changes mineralogy, grain size, sorting, and ce- entation. These traps reflect the condi- ns under which sediments were

1. C. and M. Schlumberger and H.G. Doll, "The Electromagnetic Telechinometer and Dipmeter," First World Petroleum Congress, London, July 19-25, 1933: 424-430.

C. and M. Schlumberger and H.G. Doll, "The Electromagnetic Dipmeter and Determination of the Direction of Dip of Sedimentary Strata Crosscut by Drilling," Congrès international des mines, de la metallurgie et de la geologie appliquée, 7th, Paris (October) 1935.

2. P.M. Lloyd, C. Dahan, and R. Hutin, "Formation Imaging with Micro-electrical Scanning Arrays: A New Generation of Stratigraphic High Resolution Dipmeter Tool," *Transactions of the SPWLA 10th European Formation Evaluation Symposium*, Aberdeen, April 23-24, 1986, paper L.

Michael P. Ekstrom, Claude A. Dahan, Min-Yi Chen, Peter M. Lloyd, and David J. Rossi, "Formation Imaging with Microelectrical Scanning Arrays," *Transactions of the SPWLA 27th Annual Logging Symposium*, Houston, June 9-13, 1986, paper BB.

L.M. Grace, S.M. Luthi, and R.C. Pirie, "Stratigraphic Interpretation Using Formation Imaging and Dipmeter Analyses," SPE paper 15611, presented at the 61st Annual Technical Conference and Exhibition of the Society of Petroleum Engineers, New Orleans, October 5-8, 1986.

R.A. Plumb and S.M. Luthi, "Application of Borehole Images to Geologic Modeling of an Eolian Reservoir," SPE paper 15487, presented at the 61st Annual Technical Conference and Exhibition of the Society of Petroleum Engineers, New Orleans, October 5-8, 1986.

For a review:

Steve Brown, Philip Cheung, Christian Clavier, et al., "Fracture Detection With Logs," *The Technical Review*, 35, no. 1 (January 1987): 24-26.

deposited, consolidated, or eroded. In general, stratigraphic features are those whose shape and extent are defined by depositional forces; structural features are those whose shape and extent are defined by tectonic forces.

Parallel meanings are assigned to *structural dip* and *stratigraphic dip* patterns. Structural dip is imposed on the formation by tectonic forces after sediments are deposited and consolidated. Stratigraphic dip, produced by sedimentary processes, is that seen in stratigraphic features such as *dunes*, channel deposits, or *deltaic* deposits.

Gilreath was among the early log interpreters in the Gulf Coast to grasp the importance of this distinction in analyzing dipmeter logs. He began to work with dipmeter logs in 1951, developed his interpretation scheme in 1958, and first published on the subject in 1960.[3]

Gilreath's interpretation is based on patterns he noted on tadpole plots (also called arrow plots), the main graphic device of the dipmeter interpreter. The position of the tadpole head shows dip magnitude and the tail points downdip. Gilreath recognized that geologic features form distinct patterns of tadpoles of constant azimuth. He reduced the number of patterns to four and color coded them red, blue, green, and yellow for easy recognition *(below)*.

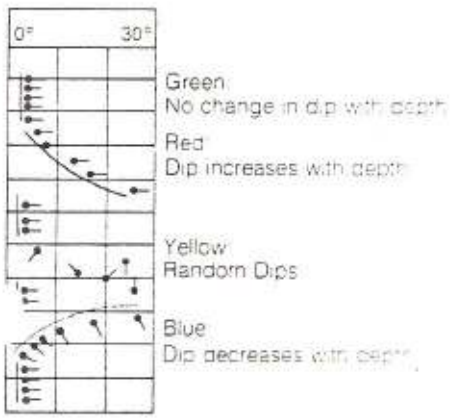

☐ *The four color-coded dip patterns identified by Gilreath. The position of the tadpole head represents dip magnitude and depth. The tail projects downdip.*

3. J.A. Gilreath, "Interpretations of Dipmeter Surveys in Mississippi," *Transactions of the SPWLA 1st Annual Logging Symposium*, Tulsa, May 16-17, 1960. *Transactions — Gulf Coast Association of Geological Societies*, 10 (1960), 267-275.

The Gilreath Approach: A Gulf Coast

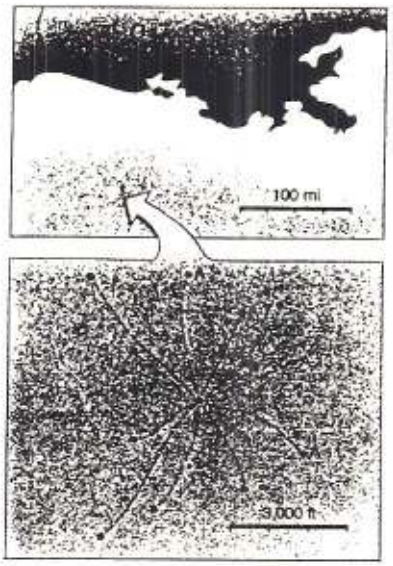

In 1971, Pennzoil Offshore Gas Operations, Inc., Mobil Oil Corp., Mesa Oil Co., and Texas Production Co. began jointly developing East Cameron Block 270, located about 100 miles southwest of Lafayette, Louisiana, 65 miles offshore in the Gulf of Mexico *(above)*. Three years after the first well was drilled, two platforms were producing 500 million cubic feet of gas per day from eight sand zones.[1]

This field was unusual because it involved one of the early uses of the dipmeter to predict reservoir geometry during development. This application of dipmeter interpretation contributed to another surprising aspect of the field's development: Only one well was junked and sidetracked, and none of the remaining 23 wells were dry holes.

During development drilling, the logging program was designed to accommodate a complete evaluation of the field. Most logging runs included resistivity, density, and neutron logs; for reasons of ecomomics, dipmeter and sonic logs were run in selected wells. The resulting structural and stratigraphic dipmeter interpretation assisted in deciding where to drill. Structural interpretation focused on the identification of fault zones and fault plane orientation. Stratigraphic interpretation included probable sand geometry, strike of producing sand bodies, and shale-out and sediment transport directions of each producing sand layer.

Estimates of sand geometries locally were made after each dipmeter run, and isopach maps indicating sand thickness and geometry of the area drilled to that point were revised after every third well was logged. This was an early application of well-to-well dipmeter correlation.

Here is an example of how logs in one well helped develop a model of depositional environment, which was then used to pick the location for the next well.

The log *(right)* shows some characteristics used to infer the types of sedimentary features present in well A-7. The major red trend from 8,375 to 8,515 feet indicates a channel. Since the dips are north-northeast, the channel axis, which is always normal to dip, lies downdip to the north-northeast and strikes west-northwest by east-southeast. Log readings of high permeability and low clay content are also evidence for the channel.

The logs show from 8,345 to 8,375 feet a slight reduction in permeability and slight increase in clay content in the sand overlying the channel. Dips in this sand suggest that it was deposited in a low-energy environment and capped by a distributary

s_ Study

front sand above 8,345 feet. Interpretation of the distributary front was based primarily on the blue dip pattern, and on Pennzoil's field study evidence of a deltaic environment. The permeability and spontaneous potential logs and the fairly constant level of clay neither support nor conflict with the distributary front interpretation. The blue pattern was probably produced by cross-bedding, the downdip direction of which indicates current flow to the r ›–northwest, opposite that of t. ›ain channel.

The goal of the dipmeter interpretation was to find the channel, which would indicate the location of oil-rich distributary sands and might itself contain producible hydrocarbons. Gilreath correctly predicted the azimuth of the channel sand from the red pattern. By following this trend, Pennzoil was able to place the next well, A-11, in both the channel and an oil-rich overlying distributary deposit.

Similar logging runs with the dipmeter were made in wells A-11 and A-2 into this sand horizon. Interpretations here indicated that the wells penetrated the southwest sides of the channel. Based on these dipmeter interpretations, the path of th annel was estimated and well A vas drilled to intersect the body ›nce again. The estimate was on tar-ɜet — well A-13 proved to be a pro-ducer *(right)*.

The Pennzoil and Schlumberger eam repeated this process for the ›ther sand layers in Block 270, build-ng up similar models for deposi-ional environment and current ransport. Using these models, they ssembled four maps — a porosity ›ap, a hydrocarbon map, a per-›eability map, and a silt map - that helped them decide where › drill next.

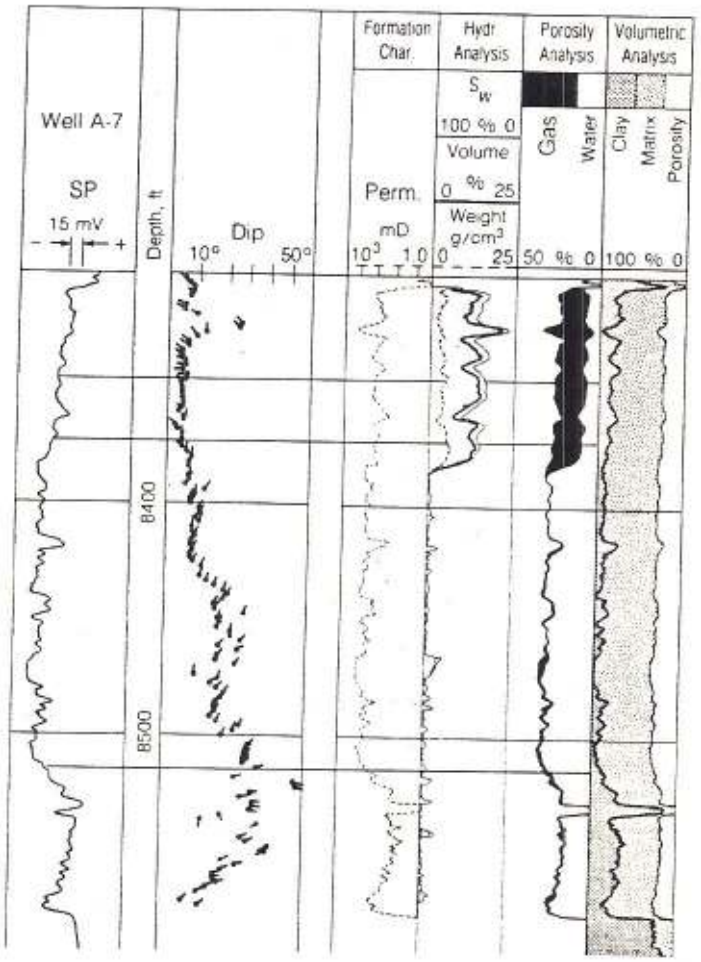

1. D.S. Holland, Clark E. Sutley, R.E. Berlitz, and J.A. Gilreath, "East Cameron Block 270, a Pleistocene Field," *Transactions of the SPWLA 16th Annual Logging Symposium*, New Orleans, June 4-7, 1975, paper DD; *Transactions — Gulf Coast Association of Geological Societies*, 24 (1974): 89-106.

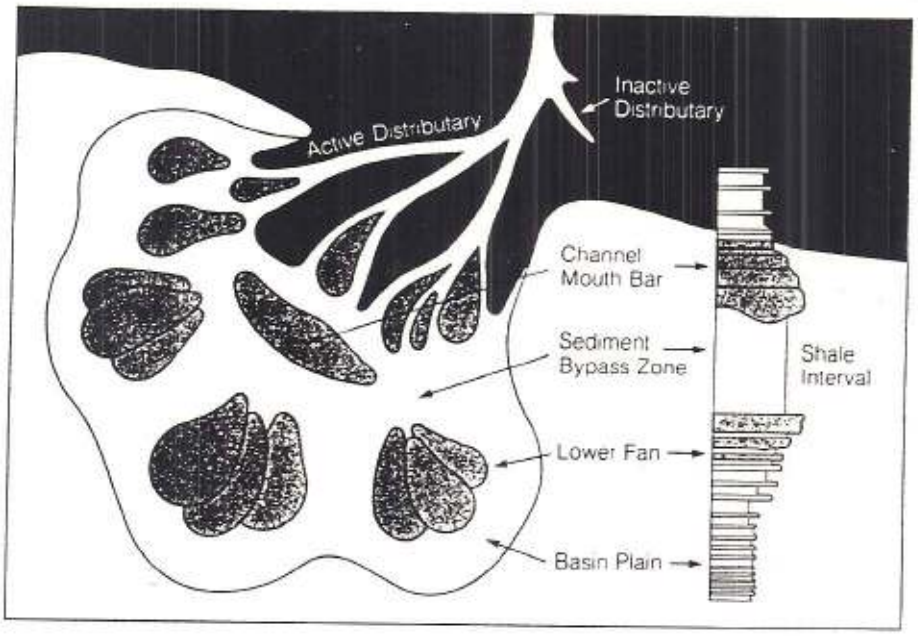

Components of an ancient submarine fan, which resemble those of a deltaic environment. Major components include active and inactive distributary branches, channel mouth bars, and sand lobes.

Red denotes dip increasing with depth, blue denotes dip decreasing with depth, green is no change in dip with depth, and yellow is random dips (a "bag-of-nails" pattern). Blank zones, with an absence of dip patterns, often indicate marshes or swamps where sediments have been disturbed by plants and animals. For any given geologic context, each color and combination of patterns denotes likely structural or stratigraphic features. For example, green (no change in dip with depth) almost always denotes postcompaction tilting, or structural dip. Depending on the setting, blue (dip decreasing with depth) over red (dip increasing with depth) suggests a *distributary channel* or a *submarine feeder channel* (*above*).

Since the 1950s, Gilreath has refined his approach to dipmeter interpretation drawing on his work around the world — in the US Gulf Coast, Africa, South America, the North Sea, and Far East. Here, step by step, are highlights of his strategy.

Before Gilreath looks at a dipmeter log, he spends a day or so with the client, learning the details of the region's geology. This skull session mainly establishes two or three likely depositional environments, and is the first step in narrowing the dipmeter interpretation. It establishes the types of faulting present and the existence of *unconformities* or *domes*.

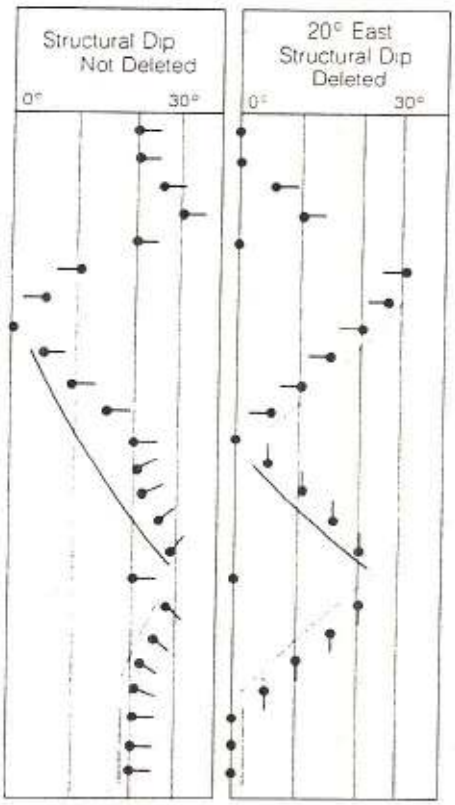

Tadpole plots before and after gross structural dip is deleted. Ideally, gross structural dip should always be deleted and two tadpole plots presented for every job. Structural dip should be deleted if the dips in the zone of interest are less than structural dip or have an azimuth different from that of structural dip.

Gilreath interprets the dipmeter log with a spontaneous potential or gamma-ray log, which differentiates permeable from shale zones, and a resistivity log, when available. In the US Gulf Coast, shale resistivities less than 0.8 ohm-meters indicate a deep-water depositional environment; in other areas subtle changes in resistivity logs can indicate faults and unconformities.

Gilreath begins interpreting a dipmeter log by recognizing gross structural dip. This initial step is important for several reasons. First, it helps differentiate structural from stratigraphic traps. Second, it allows the vectorial subtraction of gross structural dip, which can overprint and distort stratigraphic dip (*below*). This subtraction is especially important when stratigraphic dip is less than structural dip or the two kinds of dip have different azimuths. Third, interpretation of faults often requires subtracting gross structural dip because the structural dip may be altered by a dip pattern generated by the fault.

Picking out gross structural dip can be tricky. In areas that have undergone only postdepositional uplift, structural dip is indicated by tadpoles of constant azimuth and dip magnitude. In tilted structures, structural dip is represented by tadpoles of changing azimuth and dip (*opposite top left*). An approximate structural dip is easiest to pick out initially on a reduced-scale log (1 or 2 inches to 100 feet; 1:1200 or 1:600 scale). Once an approximate trend (or trends) is selected, the final trend can be made on an expanded scale log (5 inches to 100 feet, 1:240 scale).

The most common error in picking structural dip is selecting an interval of dips that is too short to represent the true structural dip. Dip trends that extend only a few hundred feet don't represent structural dip, except in intensely faulted areas. The most likely candidate for structural dip is a dip pattern that remains constant or changes gradually over the longest interval, usually on the order of 1,000 feet. Another common error, conversely, is extending a dip trend too far horizontally, especially when structural trends change frequently (as in intensely faulted areas). When selecting a location for the next well, a safe rule of thumb is that a dip trend extends horizontally no farther than it does vertically.

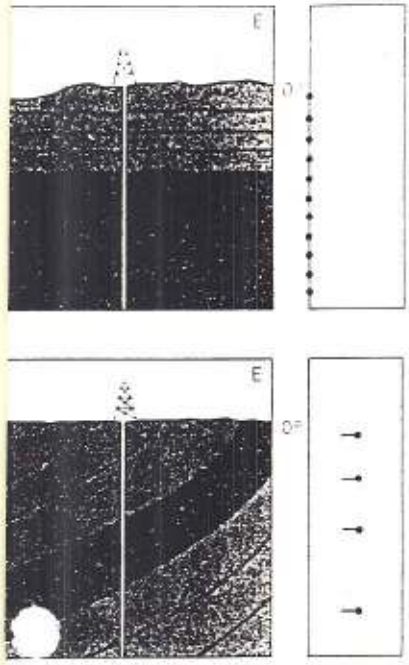

...ology, structure and tadpole plots in wells ...rating a disconformity, an area of uplift ...and of postdepositional deformation ...ure. A disconformity is formed after a depositional hiatus and an interval of erosion when ...are deposited parallel to underlying beds.

Landward-dipping cross-beds sandwich bed between horizontal beds in a trench cut at Plum Island, Massachusetts, a barrier island. The horizon is to the southeast, the Atlantic Ocean to the left.

...ructural dip is difficult or impossible to ...ermine when *beds* are deposited with ...ly variable dips or are deformed before ...mpaction (*above, right*). Continental ...e deposits, for example, undergo much ...ortion from precompaction creep (clay ... creep on a 2-degree slope). It is there- ... essential to determine structural dip ...n beds that were deposited horizontally ... have undergone little postdepositional ...ormation.

...) ... the gross structural dip is accounted ... ...gs are examined for both *missing* ... *repeat sections* (*right*). A missing sec- ... appears in one well but is missing from ...ther nearby. A repeat section appears at ... depth and reappears at a greater depth ... the same well. Repeat sections often ...ate folding or *reverse* faulting. Distin- ...shing missing and repeat sections helps ...mble a picture of the faults, unconformi- ...s, and stratigraphic features around the ...lls that can be later identified from ...meter trends.

... missing section may indicate that a ...le crosses a *normal fault* — a section that ...ears in a well away from the fault will be ...sing in the well that crosses the fault. A ...sing section may also indicate a feature ...h as an *angular unconformity* or a ...conformity.

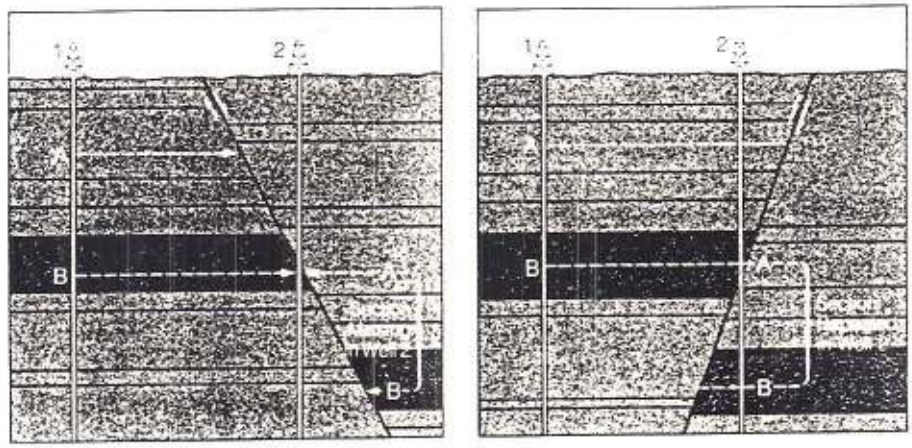

Missing (left) and repeat sections (right) due to faulting.

A common error in interpreting a missing section from a well is to infer a *rollover* from every lengthy red pattern that appears to dip into the upthrown block (page 64, *top left*). These patterns reliably indicate faulting only when the missing section can be independently confirmed with seismic data or well-to-well correlations. Dips near fault zones often involve bedding plane distortion near the fault plane. The distortion results from motion along the fault, warping bedding planes into *drag* and *growth* features. Faults not associated with bedding

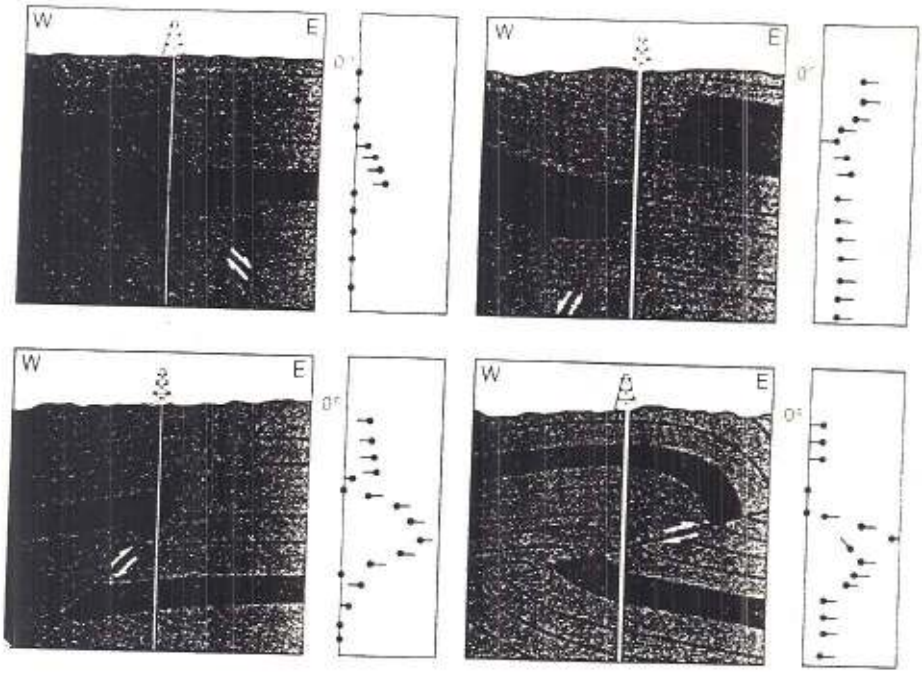

Growth (top left) and drag features associated with different types of faulting. In a rollover (top left), dip displacement increases with depth. In a reverse fault (left, right), dips in the drag zone are in the same direction as the overthrust and are normal to the strike of the fault.

distortion are more difficult to confidently identify by dipmeter. One fairly strong sign of faulting, however, is a sudden change in gross structural dip, indicating a tilted fault block.

Structural features that produce missing sections are often difficult to identify by dipmeter. A disconformity producing a missing section may go undetected because it produces changes in dip less than ½ degree (*page 33, top left*). Angular unconformities can be confused with faults (*right*). But two features can help distinguish angular unconformities from faults: beds overlying an angular unconformity tend to parallel the surface of the unconformity, and the rocks below the unconformity usually dip more steeply than the younger rocks above. Angular unconformities are indicated by a blue pattern, produced by weathering or fracturing just below the unconformity.

Missing and repeat sections can be corroborated by changes in borehole drift. Changes in drift occur for many reasons — often when the drill bit encounters a sudden change in formation compaction — but always at or near a missing or repeat section. The relationship of borehole drift to dip direction varies from place to place and no general rules apply.

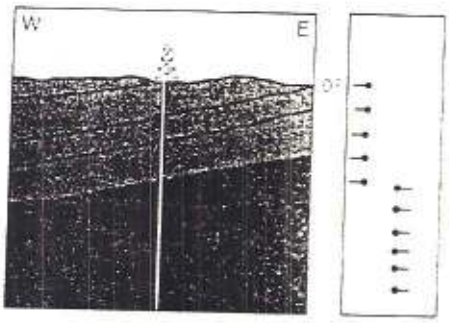

An angular unconformity is formed after a depositional hiatus and an interval of erosion in which older beds are tilted before new strata are deposited.

If the repeat or missing sections are caused by faulting (structural), the next step is to determine whether the faulting is normal, reverse, or *thrust*. Red patterns on the downthrown side generally indicate normal faulting. Red patterns dipping toward the fault plane indicate a rollover from a growth fault; patterns dipping in the same direction as the fault plane indicate a drag zone (*top*). Drag and rollover produce similar dip patterns and are sometimes difficult to distinguish. Patterns that extend 200 feet or more, however, usually indicate a rollover. When patterns stretch less than 200 feet, distinguishing one from the other often depends on seismic studies, well-to-well correlation or local knowledge.

Reverse and thrust faults produce red over blue patterns dipping in the same direction as the overthrust. Dip patterns often show drag on both sides of the fault. The overthrust block, however, usually has the most distinctive dip patterns: dip azimuth is normal to fault *strike* and dip magnitude increases downward, approaching the fault plane (*bottom left and right*). One major pitfall, horizontal (strike-slip) displacement overprinting reverse and thrust faulting, can introduce error in interpretation because it rotates the drag zone dips, usually in the direction opposite horizontal movement.

Once faults are identified, or unconformities suspected by default, stratigraphic interpretation begins. Gilreath finds that, with a few exceptions, the dipmeter can help interpret sedimentary features of most reservoirs. Each environment has a set of commonly occurring sedimentary features. It is the exception rather than the rule that a borehole penetrates only one environment; most penetrate two or three environments.

Among the many important decisions that depend on determination of depositional environment are estimates of reservoir reserves, selection of drilling and production procedures (e.g. mud composition and weight, perforation intervals), and location of future wells. Preferential permeability, one input for many of these decisions, can be roughly estimated from dipmeter logs. For example, the zone of highest permeability in *foreset* bedding (indicated by a blue pattern) will generally be between beds and normal to dip. Preferential permeability in laminated beds (red patterns; see *page 33, top right*) will also be normal to dip. In highly *cross-bedded* sands, greatest permeability is at the sand – shale interface.[4]

An important early step in stratigraphic interpretation is examining lithology logs (neutron, density, sonic, gamma ray, spontaneous potential) to broadly distinguish sand, carbonate, and shale. Once faults, unconformities, and lithologic zones are identified, Gilreath returns to the dipmeter plots to find key dip signatures of features characteristic of four main depositional environments — nonmarine/continental; continental shelf, delta dominated; continental shelf, tide, wave, and current dominated; and continental slope and abyssal.[5] Here are brief summaries of the important features of each.

4. K. S. Kunz and M. P. Tixier, "Temperature Surveys in Gas-Producing Wells," *Journal of Petroleum Technology*, 204 (July 1955): 171-176.

5. J. A. Gilreath, J. S. Hicks, and J. S. Yelverton, "Depositional Environments Defined by Dipmeter Interpretation," [illegible] (October 1981): [illegible].

NONMARINE/CONTINENTAL

Eolian sands: Transverse dunes are the most common eolian (wind-produced) features. They are usually expressed as groups of green patterns overlying blue patterns *(right)*. The azimuth of both patterns parallels the prevailing wind direction during deposition.

Point bar sands: A number of dip patterns can indicate point bar sands. A common feature is *foreset beds in trough cross-bedding*. These produce blue patterns with azimuths diverging from the downcurrent direction by up to 60 degrees *(below)*. These spoon-shaped beds may be a yard or so thick, with the downdip direction of the trough indicating the direction of current flow. Current dding may point downstream, or ue patterns from acretion deposits will point toward the *thalweg* (longitudinal axis) of the stream channel. As a rule, a blue pattern extending more than 3 feet indicates an acretion deposit. A *clay plug* in a cut-off *meander loop* can produce *drape* over a point bar that mimics a buried *beach ridge*.

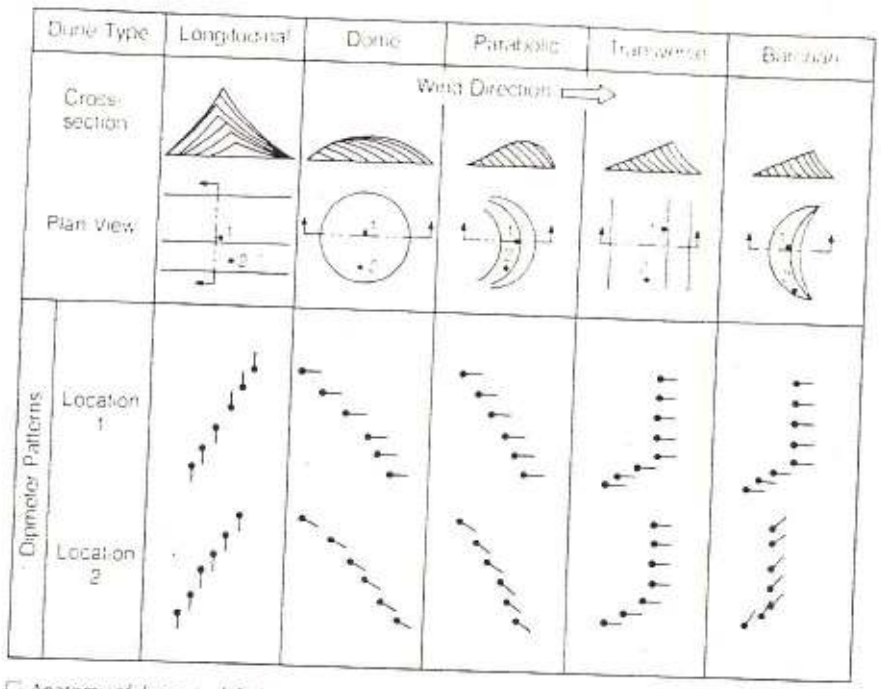

Anatomy of dunes and their measurement.

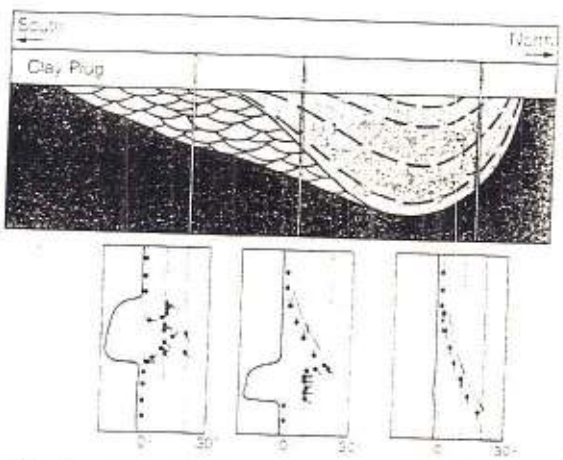

Point bar sands and their common dipmeter signatures.

Eolian sands	Green over blue, or red dip directions generally the same as the prevailing wind direction
Point bar sands	Red often over blue; blue dips in direction of current flow, ± 60°
Stream channel fill	Blue dips in direction of current flow; red dips toward thalweg and normal to strike
Delta plain deposits	Green or strong blue
Flood plain deposits	Yellow
Swamp/marsh deposits (peats or coals)	Blank zone

CONTINENTAL SHELF: TIDE, WAVE, AND CURRENT DOMINATED

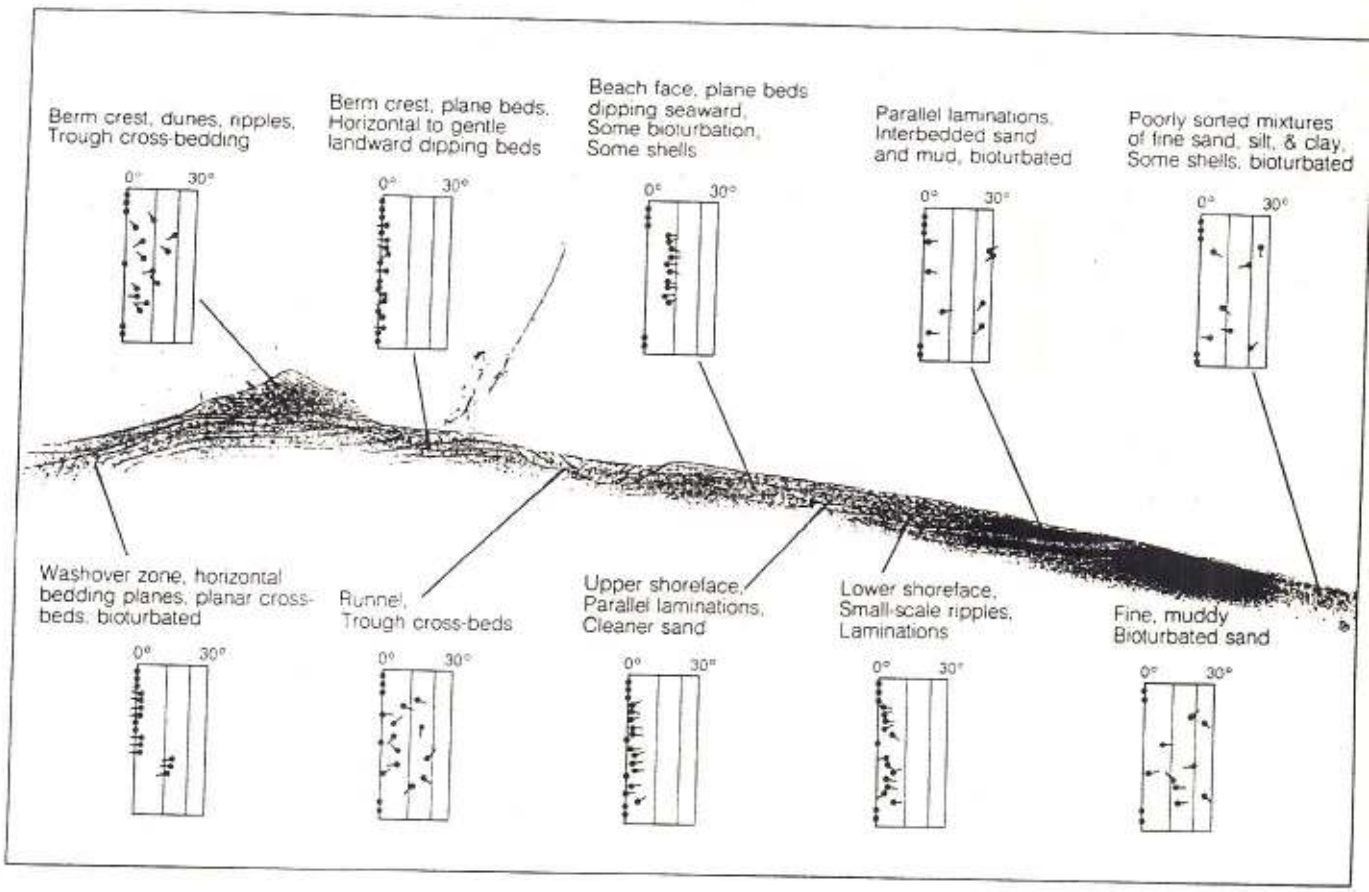

☐ *Depositional environments and typical dipmeter responses for various parts of a cross section reaching from the nearshore to the wash-over zone landward of the berm crest.*

This environment has the largest collection of sedimentary features and so the largest array of dip patterns. A few of the more complex ones are described below.

Tidal deltas: Interpretation of tidal deltas requires knowing the direction to land during deposition. Internal foreset beds in ebb tidal deltas, for example, produce blue patterns dipping seaward; the same feature in flood tidal deltas has blue patterns dipping landward.

Tidal channels: These produce the same dip patterns as distributary channels. Point bars within tidal channels create the same dip patterns as those within stream channels, with dip azimuth paralleling current flow.

Beach ridges and barrier islands: These are identified by the drape of overlying sediments: drape-related dips are normal to the strike of the sand body and point in the direction of shale-out. Numerous internal dips characterize beach ridges and barrier islands, distinguishing them from *breakpoint bars*, which have few internal structures because they have been reworked by waves.

Beaches: A variety of dip patterns indicate a beach *(above)*. The landward side of the beach, behind the *berm*, is indicated by landward dipping blue patterns, created by landward dipping foreset beds. These blue patterns, like those of tidal flood deltas, suggest a *washover fan*. Scattered, high-angle dips (up to 40 degrees) suggest the high-energy deposition and frequent bioturbation of *shoreface* sands. Seaward dipping parallel cross beds indicate the area from the swash zone to mean low water. Blue patterns alternating with blank zones indicate small *ripples* and *megaripples* in *runnels*. Blue patterns with azimuth parallel to the paleoshoreline indicate *longshore current sand waves*.

idal delta	Blue dipping seaward
tidal delta	Blue dipping landward
channel	Blue over red
flat	Green or adjacent blue of opposite azimuths
bar	Red often over blue; blue dips in direction of current flow, ± 60°
h	Blank zone
h ridge	Red dips toward shale-out and strikes normal to beach ridge
h face	Green from seaward dipping parallel cross-beds
over fan	Blue dipping landward
kpoint bar	Red dips toward shale-out and normal to strike of bar
ir nel margin bar	Same as breakpoint bar
shore current sand waves	Blue dips parallel to shoreline strike; stronger blue patterns than in ridges and runnels
shore sands or shales	Yellow
hrock	Green from parallel cross-beds dipping seaward about 20°
	Above reef, red dips toward pinch-out and normal to reef strike; blank zone within reef; blue below reef

Both reefs and sand bars have
tterns dipping toward the
out, created by sediments
g over the flanks *(right)*. But a
as several distinguishing fea-
nc lid dips in the middle;
a is pointing toward the
nter are often found in under-
ediments; and blue patterns
ntly seen dipping away from
ef, the result of reef detritus
g foreset beds. A reef usually
more extensive drape than a
ar, extending some distance
d its margins. This characteris-
netimes allows the interpreter
l a reef missed by the borehole.

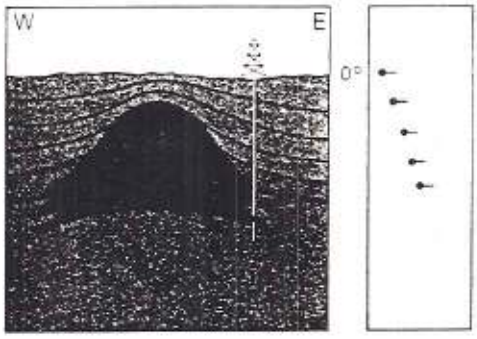

Dip patterns associated with reef deposits. Dip increases with depth and drape.

Continental Shelf: Delta Dominated

Deltaic deposits are marked by sweeping blue patterns with a number of strong red patterns. Blue foreset dip patterns often dominate *(right)*. These dips are derived from distributary mouth bars, crevasse splays, and sediments deposited at or near the axis of distributary channels. Distributary channel deposits and their drape generally produce blue patterns in the thickest section, the middle of the channel, and blue over red patterns away from mid-channel and red patterns near the channel edge *(below)*.[6] The red patterns point downdip to the channel axis; the downdip direction of the blue patterns indicates the direction of current flow.

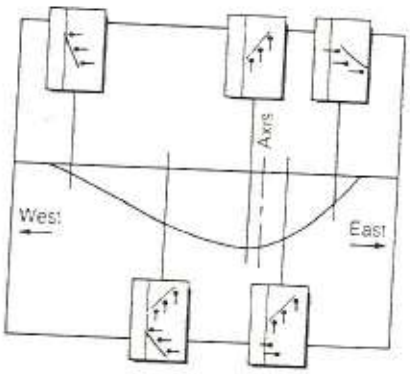

☐ *Common dip patterns associated with channels. Red patterns dip toward the axis; blue patterns indicate the direction of current flow.*

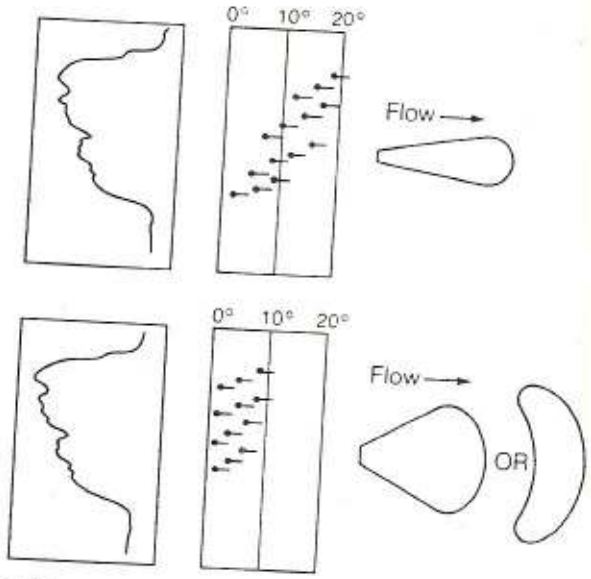

☐ *Dip patterns and geometries of distributary mouth bars. Long, narrow deltas (right, top) form when the magnitude of dips exceeds 10° Crescent or lobate deltas (right) form when dip magnitude is less than 10°*

Sedimentary Features	Common Dip Patterns
Distributary mouth bar	Blue dips in direction of current flow
Distributary channel fill	Blue over red; blue indicates current flow direction, red dips normal to strike of channel
Crevasse splay	Blue
Scour channel	Red
Linear channel margin bar	Red
Breakpoint bar	Red dips toward shale-out and normal to strike of bar
Interdistributary sediments	Yellow
Marsh (peat)	Blank zone
Shoreface sands	Green seaward dipping low-angle cross-beds
Longshore current sand waves	Blue dips parallel to shoreline strike; stronger blue patterns than in ridges and runnels

6. J.A. Gilreath and R.W. Stephens, "Distributary Front Deposits Interpreted from Dipmeter Patterns," *Transactions — Gulf Coast Association of Geological Societies*, 21 (1971): 233-243.

Continental Slope and Abyssal

Sediments laid down in deep water (>600 feet) are structurally simpler than those deposited in shallow water. Most deep-water sands are deposited as fill in feeder channels or fans *(right)*. Feeder channel dip patterns are the same as those in tidal and distributary *channel fills* — a blue over a red pattern dipping toward the channel axis, or red if the well is near the channel edge. Fans lie downdip at the end of feeder channels. The midfan is marked by blue patterns. Dips in the outer reaches of the fan parallel structural dip because outer fan sediments were deposited flat. — JMK

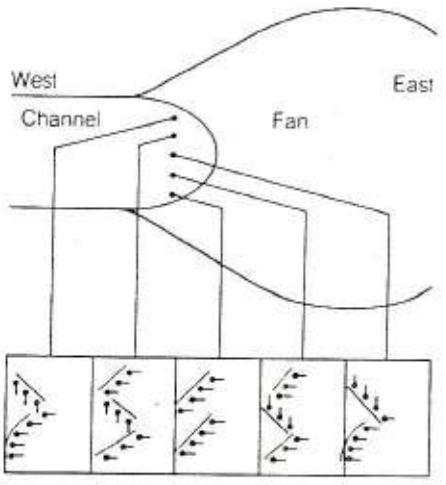

☐ *Dip patterns typical of the junction of a channel and fan.*

Submarine feeder channel	Blue over red
Submarine fan	Blue grading into green
Debris flow (random structure)	Yellow
Creep and slump features	Yellow

ESEMPIO n° 15

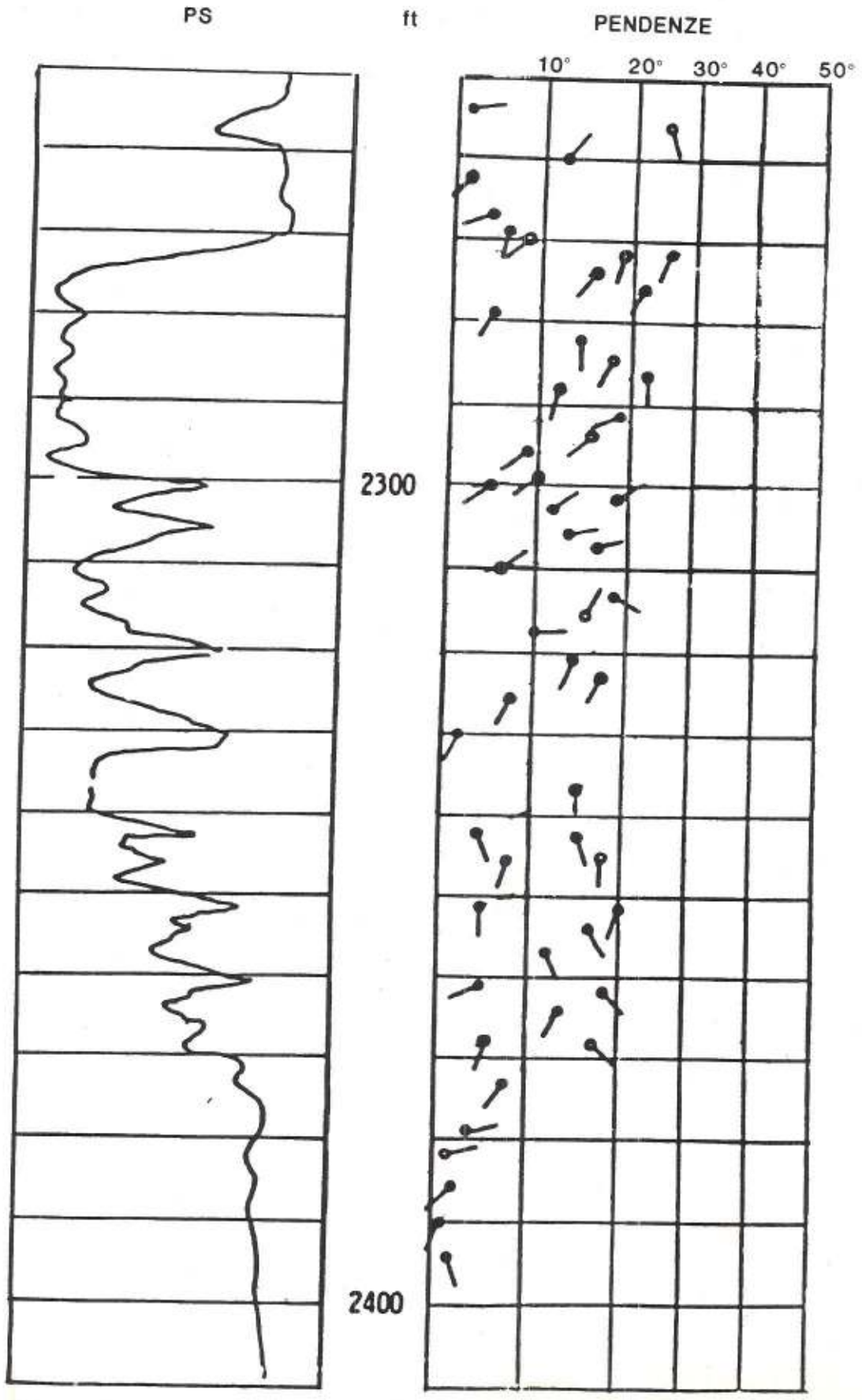

ESEMPIO n° *14*

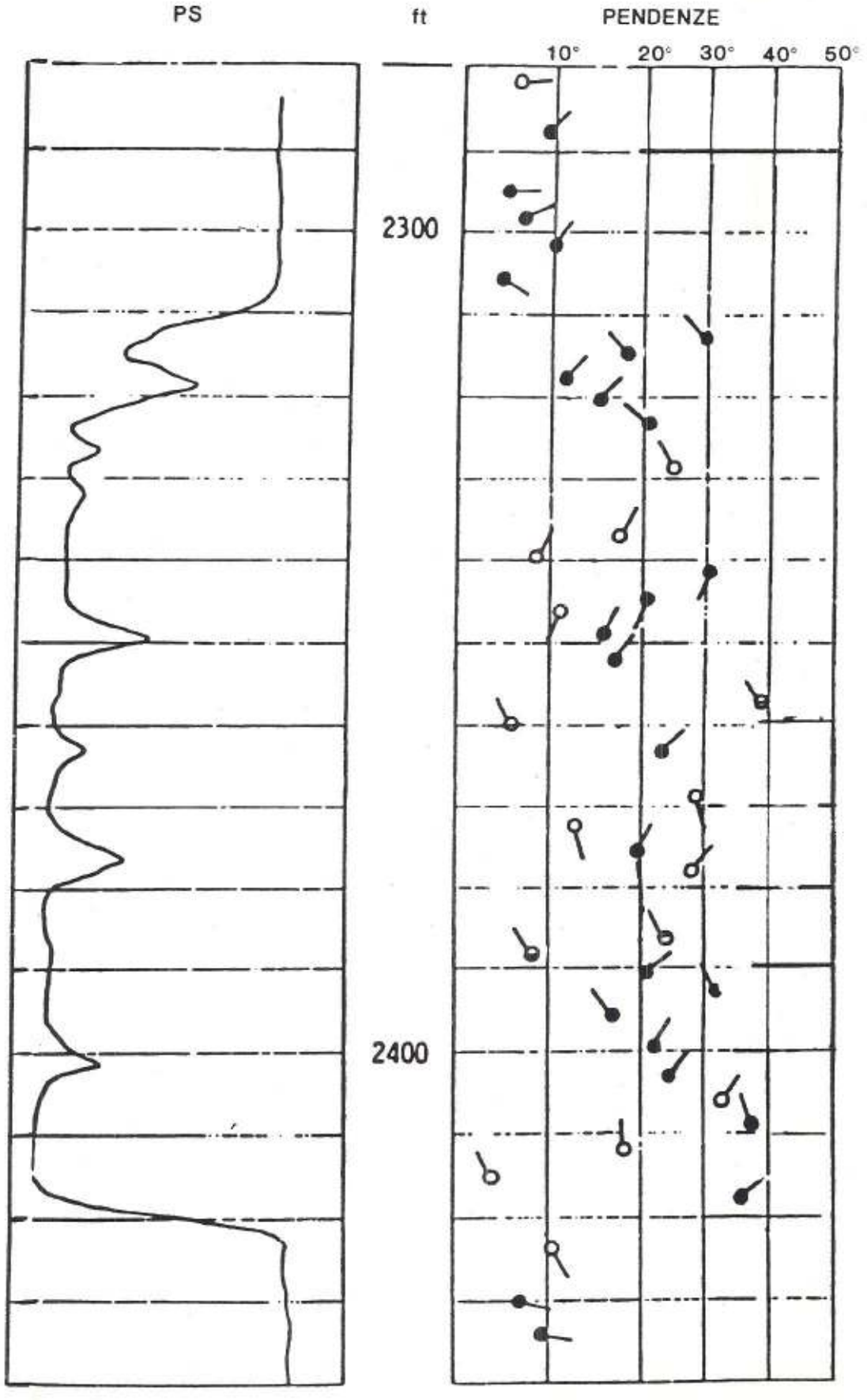

6.4. FLUVIAL ENVIRONMENT : BRAIDED SYSTEM

6.4.1. DEFINITION

A continental environment characterized by deposits resulting from a river system of an interlaced network of low sinuosity channels. The style of a braided system is shown in Fig. 6.4-1, and representative vertical sections in Fig. 6.4-2.

6.4.2. GEOLOGICAL FACIES MODEL

6.4.2.1. Lithology

Two parameters must be considered separately.

6.4.2.1.1. *Composition*

Braided river deposits are typically composed of texturally and chemically immature gravels and sands with a sand-shale ratio greater than 1. They can be classified as *lithic arenites to lithic wackes* (Pettijohn *et al.*, 1972). Only minor amounts (some 10 %) of silt are found and correspond to abandoned channel deposits (Selley, 1976). Gravels and pebbles are rock fragments, the composition of which depends on the source areas. Shale pebbles and reworked clay-ironstone concretions may be present. Common mineral constituents are quartz, feldspars, micas. Glauconite is absent (non marine deposit). Carbonaceous organic matter is very rare, due to the oxidizing nature of the environment (Selley, 1976). Alteration of iron-rich minerals to haematite or limonite is frequent. Uranium bearing minerals may accumulate along with gold as placer deposits (e.g. Blind River in Canada and Witwatersand basin in South Africa). These minerals concentrate at the bases of channels (Minter, 1978).

Fig. 6.4-1. - Aerial photograph of a braided stream choked with erosional debris, near the edge of a melting glacier (Photo by B. Washburn, in Press & Siever, 1978, Fig. 7-25).

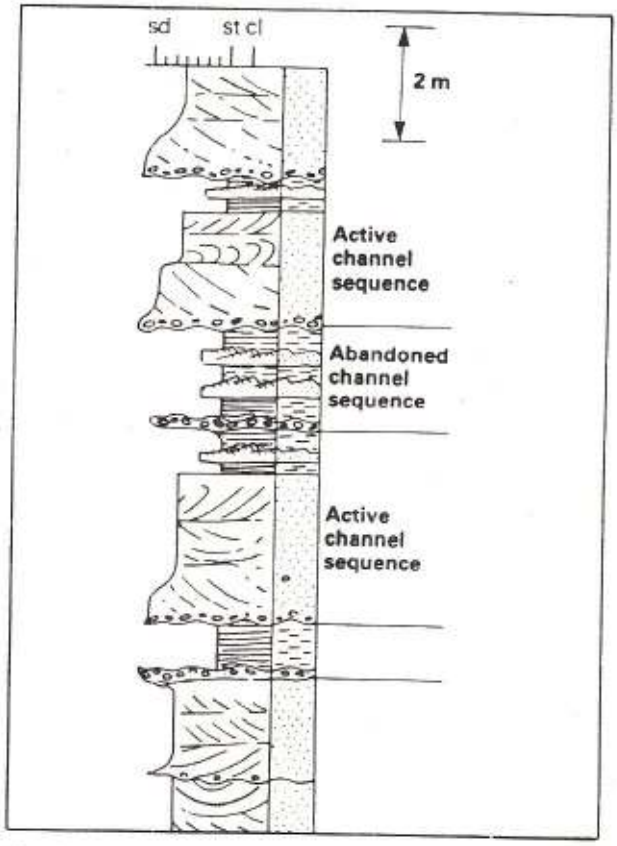

Fig. 6.4-2a. - Theoretical vertical cross-section of a braided alluvial channel system deposits. Sedimentation occurs almost entirely in the rapidly shifting complex of channels. A flood plain is absent (from Selley, 1976, Fig. 101).

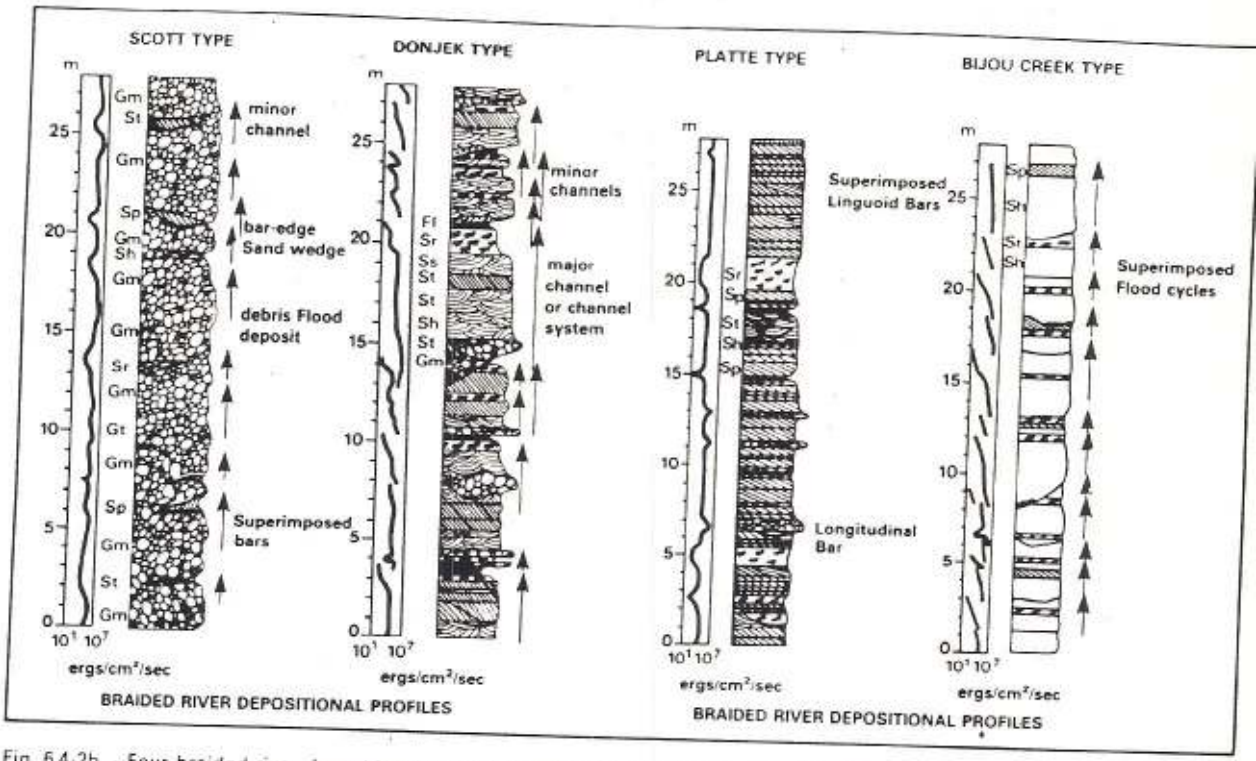

Fig. 6.4-2b. - Four braided river depositional profiles representing the four models of braided river systems related to the energy involved during deposition, and consequently to the proximity to the apex (from Miall, 1977).

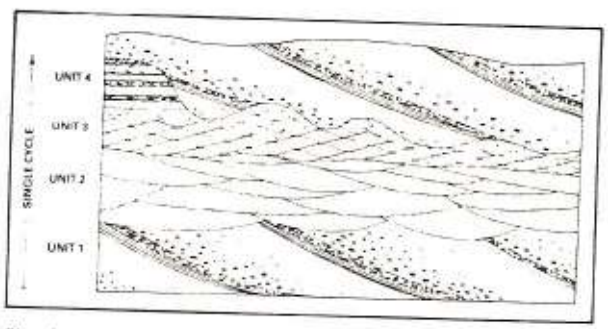

Fig. 6.4-3. - Schematic vertical sequence of a braided river deposit. Unit 1 : large scale cross-bedding with pebbles. Unit 2 : medium sand megaripple bedding. Unit 3 : fine sand small ripple bedding. Unit 4 : fine sand and mud horizontal bedding, occasional convolute bedding (from Reineck & Singh, 1975, based on data of Doeglas, 1962).

6.4.2.1.2. *Texture*

Poor to moderate sorting (gravel to sand) with low sphericity and with moderate to low grain-matrix ratio is observed; abundant silt in fine end tail (Pettijohn *et al.*, 1972). Conglomerates range from clast-supported matrix-free, through clast-supported with interstitial sandy matrix, on to sandy conglomerates with dispersed clasts. Matrix-free conglomerates are reasonably well sorted and unimodal; conglomerates with sandy matrix show a bimodal distribution; matrix-supported conglomerates are unimodal with poor sorting.

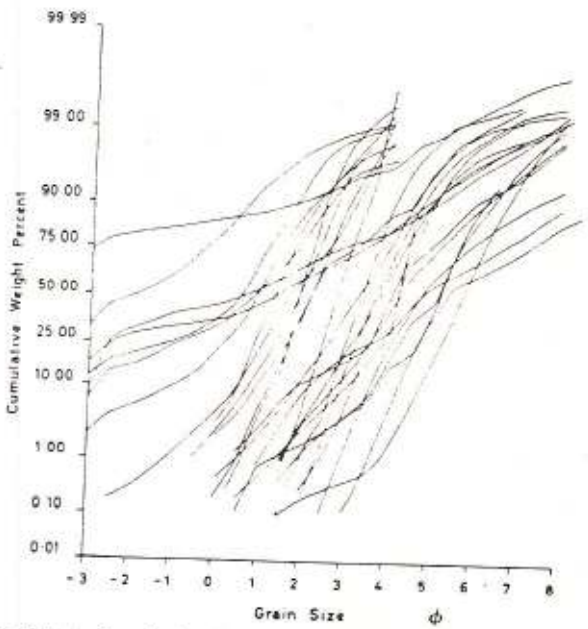

Fig. 6.4-4. - Cumulative size frequency curves of samples from braided river systems (from Williams & Rust, 1969, Fig. 4). For a given sample the range of grain size reflects the poor sorting.

6.4.2.2. Structure

Table 6.4-1 summarizes the principal sedimentary structures and their abundance found in a braided river deposit. Asymmetrical small scale

Table 6.4-1

Principal sedimentary structures and their relative abundances

(from Williams & Rust, 1969, Table 1).

Level / Stream Channel	Lamination, Cross-Lamination				Ripples							Bedding		Large Scale Structures				Small Scale Structures																
					Small Scale					Large-Scale				Erosional		Depositional		Surface								Cross Section								
	Parallel	Lenticular	Small Scale X-L	Large Scale X-L	Straight	Sinuous	Lunate	Linguoid	Wave	Lunate	Linguoid	Massive	Graded	Scour Hollows	Channels	Bar, Avalanche Face	Bars	Rill Markings	Current Crescents	Grain Lineation	Plant Lineation	Rain Pits	Deformation Tracks	Silt Undercuts	Trails and Trails	Bedded Organics	Color Banding	Bioturbation	Imbrication	Rank Slippage				
4	O	R										O		R	C		C																
3	C	O	A	O			A			O		O	O	C	A	O	A	R	C	R	R	O	C		R	A	C	A					
2	C	R	A	C			A			R		O	O	C	A	R	A	R	A	O	R	C	O	O	C	R		R	O	R			
1	O	R	A	C			A			R		O	R	C	A	O	A	R	A	O	R	C	O	O	R	R		R	O	O			
Overall (1-4)	C-O	O-R	A	C	O	A	A	A	C	R	R	O	O-R	C-R	A	O-R	A	R	A	O-R	R	C-O	C-O	O	C-R	A-R	C-R	A-R	O	O-R				

A = Abundant, C = Common, O = Occasional, R = Rare.

ripples and abundant well oriented cross-bedding, commonly unimodal, are observed, as well as small scale cross-laminations. The bedding may be either massive or graded. Beds tend to be lenticular with erosional scour; infrequent tracks and trails. Depositional bars are abundant.

6.4.2.3. Boundaries

Lower contact of the sand is erosional. Upper contact is also frequently abrupt.

6.4.2.4. Sequences

Four units or facies can be distinguished. They are arranged as shown in Fig. 6.4-3 to compose a theoretical vertical sequence.

Unit 1: large scale cross-bedding mostly coarse-grained with pebbles, with erosional lower contact. Discontinuous lenses of sand, silt and clay can be present. This unit is related to lateral and downstream advance of channel bars.

Unit 2: megaripple bedding in medium sand; large and small scale cross-stratifications and ripples. They correspond to migrations of channel sand bars.

Unit 3: small ripple bedding in fine sand composed of banded sands and silts. Ripple laminated or massive. Small scale ripples, microbars and scours. They may be related to recently abandoned channel deposits.

Unit 4: fine sand and mud showing horizontal or convolute bedding. This unit corresponds to abandoned channels.

Such fining upward sequences are best developed in channel fill sediments. The grain size gradually decreases upward and the sorting improves upward. Coarse- and fine-grained units may be interbedded. Small grain size reversals can occur. They are due to fluctuating river stages.

In relation to the energy involved during deposition, Miall (1977) proposed four models of braided river sediments, which are shown in Fig. 6.4-2b.

6.4.2.5. Geometry of the Body

"Braided channel systems are characterized by a network of constantly shifting low-sinuosity anastomozing courses" (Selley, 1976).

Both sandy and gravelly braided rivers migrate laterally leaving sheet-like or wedge-shaped deposits of channel and bar complexes preserving only minor amounts of floodplain material (Cant, 1982).

In detail, three main geomorphological bodies are recognized : channels, bars and islands (Williams & Rust, 1969) (Fig. 6.4-5).

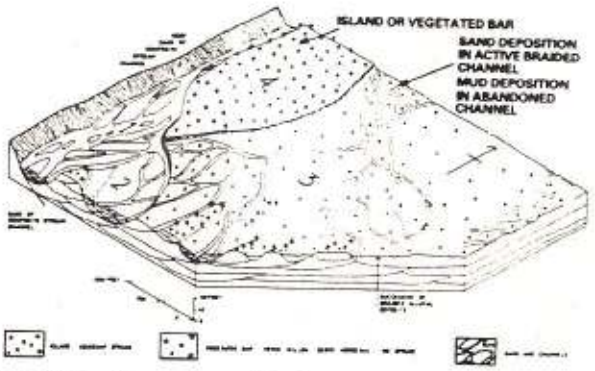

Fig. 6.4-5. - Composite model of a braided river deposit (from Williams & Rust, 1969, Fig. 27).

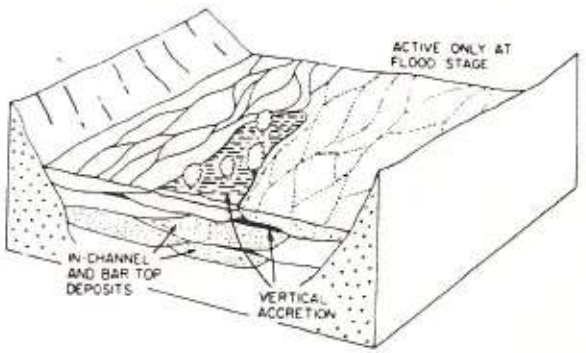

Fig. 6.4-6. - Block diagram of a braided sandy system with low sinuosity channels. Vertical accretion can occur during flood stage (from Walker, 1969).

Channels vary considerably in size and are arranged in five hierarchical orders. *A composite stream channel* is straight with an average width of one mile (1.6 km). *Stream channel* is characterized by a braided network of three finer order channels. These smaller channels - width up to hundreds of feet - are generally of low sinuosity. The basic sedimentary fill succession is fining-upward. In cross-section the channels are erosional, occurring in a very high frequency association. The main channel is divided into several channels which meet and redivide (Fig. 6.4-5 to 6.4-7). Channel bars, which divide the stream into several channels at low flow, are often submerged during high flow. They are commonly composed of coarse-grained lag deposits of the stream (often gravels) which could not be carried by the flow.

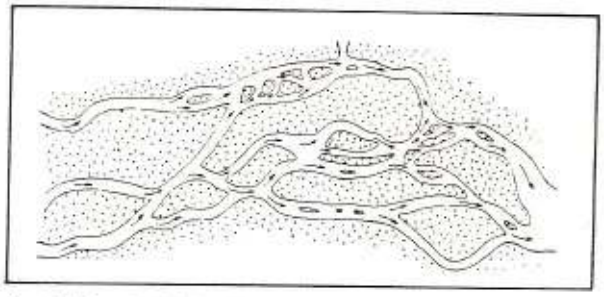

Fig. 6.4-7. - Aerial distribution of a braided system showing hierarchical organization of channels and bars (from Allen, 1965)

Once such a channel bar is formed, it may stabilize by the deposition of fine-grained sediment on its top during high flows and may later be colonised by vegetation forming an island.

Three types of *bar* are present : longitudinal, transverse, and point bars. Longitudinal bars are the most abundant (95 %) and occur as lateral bars along channel sides and central bars in mid-channel areas. They are invariably elongate downstream. Maximum length and width vary from a few feet to hundreds of feet. The surface of the bar is never smooth, including a very wide range of large- and small-scale structures. They are composed of gravel, sand, and silt-mud admixtures. Bars tend to be built up by lateral accretion down stream. The upstream end is partly eroded.

Islands are the most permanent features on the valley floor within a braided system. They are elongate downstream. Root evidence or carbonaceous material can be present.

Braided rivers are characterized by wide channels of changing position, and rapid and continuous shifting of the sediment. Consequently, an individual unit may be between . 5 and 8 km wide. Their length may commonly range from 10s to 100s km. The thickness of an individual unit ranges from several decimetres to 30 metres. The width-depth ratio is high. The area occupied by braided rivers may be very wide (100s km) and coalescing bars and sand-flats will result in a laterally continuous and extensive sand sheet, unconfined by shales (Walker, 1979).

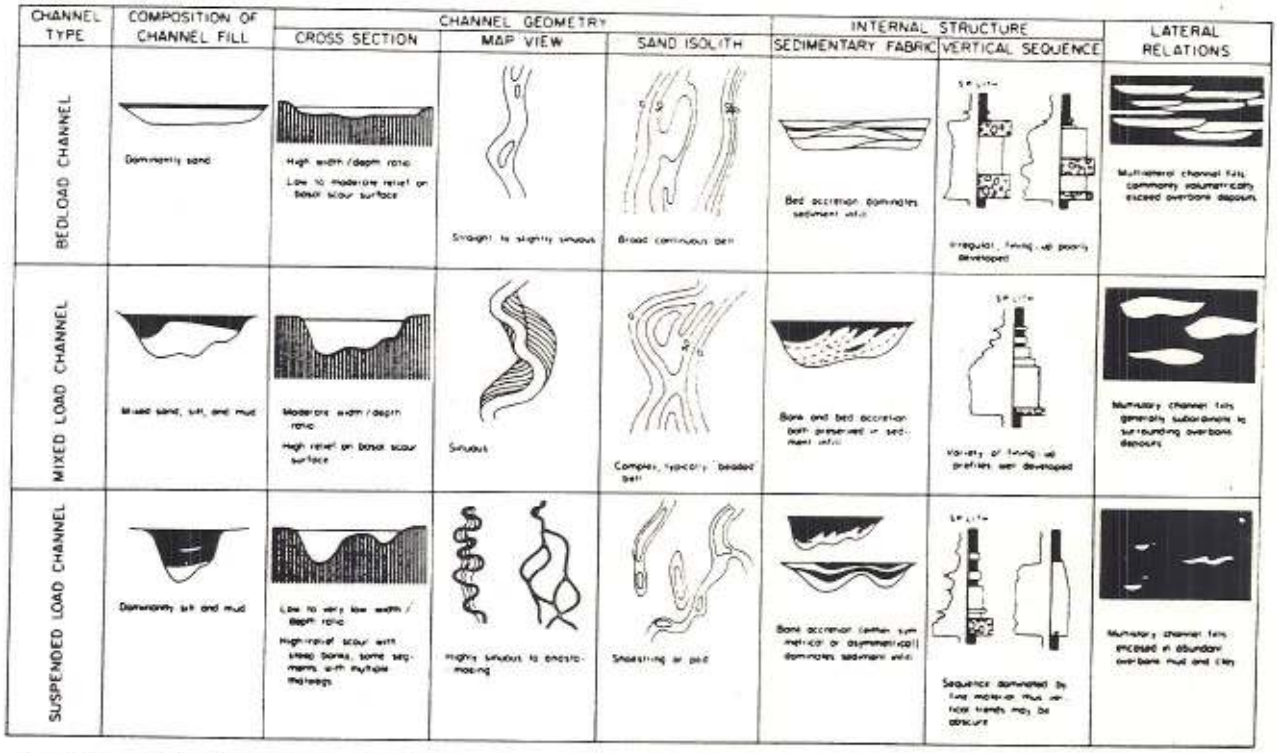

Fig. 6.4-8. - Geomorphological and sedimentary characteristics of bed-load, mixed-load, and suspended-load stream channel segments (from Galloway, 1977, and in Galloway & Hobday, 1983, Fig. 4-13)

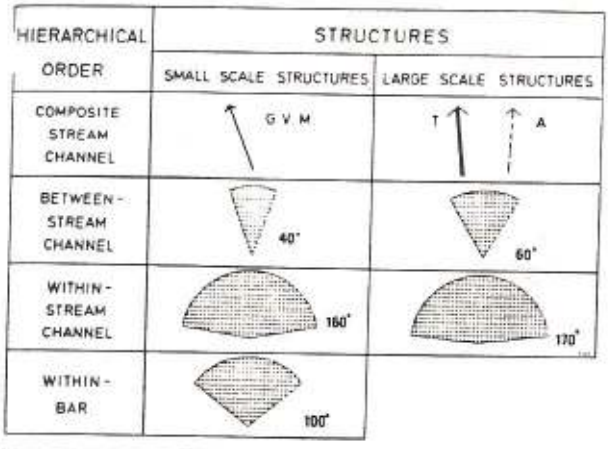

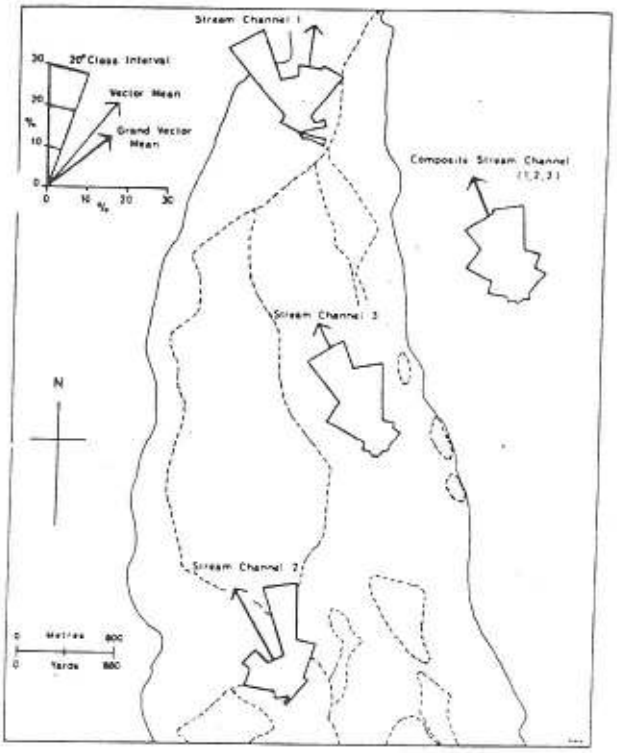

Fig. 6.4-9. - Dispersion of the azimuth of the directional current flow from the structures (from Williams & Rust, 1969, Fig. 28 & 23).

6.4.2.6. Directional Current flow Model

The ranges of directional current data for the hierarchical orders of small scale and large scale structures are summarized in Fig. 6.4-9. They show a characteristic unimodal azimuth distribution with a moderate to low scatter, along the down dip direction of the palaeoslope.

6.4.2.7. Reservoir Characteristics

Braided river deposits may constitute potentially good reservoir rocks with up to 30 % porosity and permeabilities of thousands of millidarcys. The

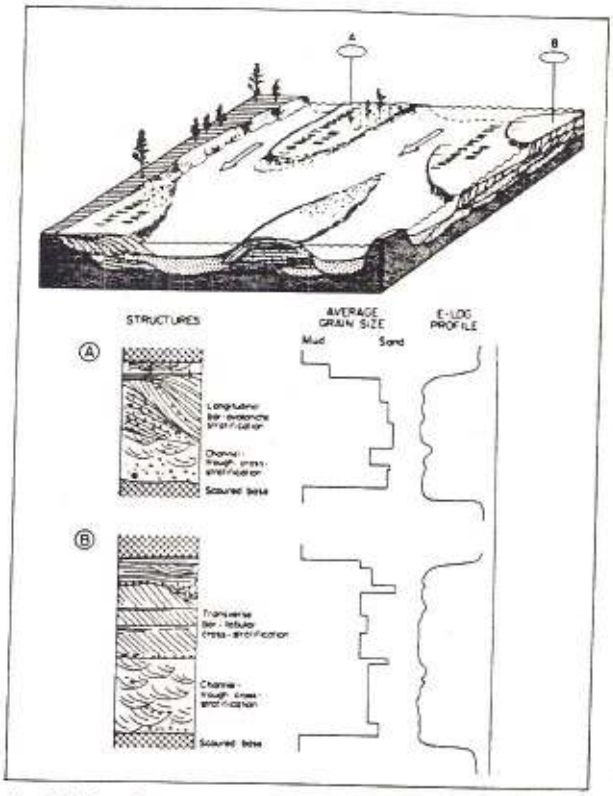

Fig. 6.4-10. - Generalized depositional model, vertical sequences of grain size and sedimentary structures, and S.P. log profiles produced by a low-sinuosity, braided channel. Sequence (A) is dominated by migration of a gravelly longitudinal bar. Sequence (B) records deposition of successive transverse bar cross-bed sets upon a braided channel fill (from Galloway & Hobday, 1983, Fig. 4-4).

shales are of limited lateral extend and do not play a major role in blocking fluid migration. They do not commonly form stratigraphic traps.

6.4.3. WELL-LOG RESPONSES AND CHARACTERISTICS

Galloway & Hobday (1983) proposed a generalized depositional model for a braided channel with theoretical S.P. log response (Fig. 6.4-10). The S.P. shape is typically a smooth cylinder. The responses and characteristics of the other logs will be illustrated by a case-study : The Upper Tipam Formation (Assam, India), the composite-log of which is represented by Fig. 6.4-11.

6.4.3.1. Electro-Lithofacies

A detailed study of the various crossplots was made in order to define the mineralogical composition of the formation.

The ρ_b vs ϕ_N crossplots (Fig. 6.4-12) with S.P. (Fig. 6.4-12b) and EATT (attenuation of the electromagnetic wave) (Fig. 6.4-12c) on the Z-axis

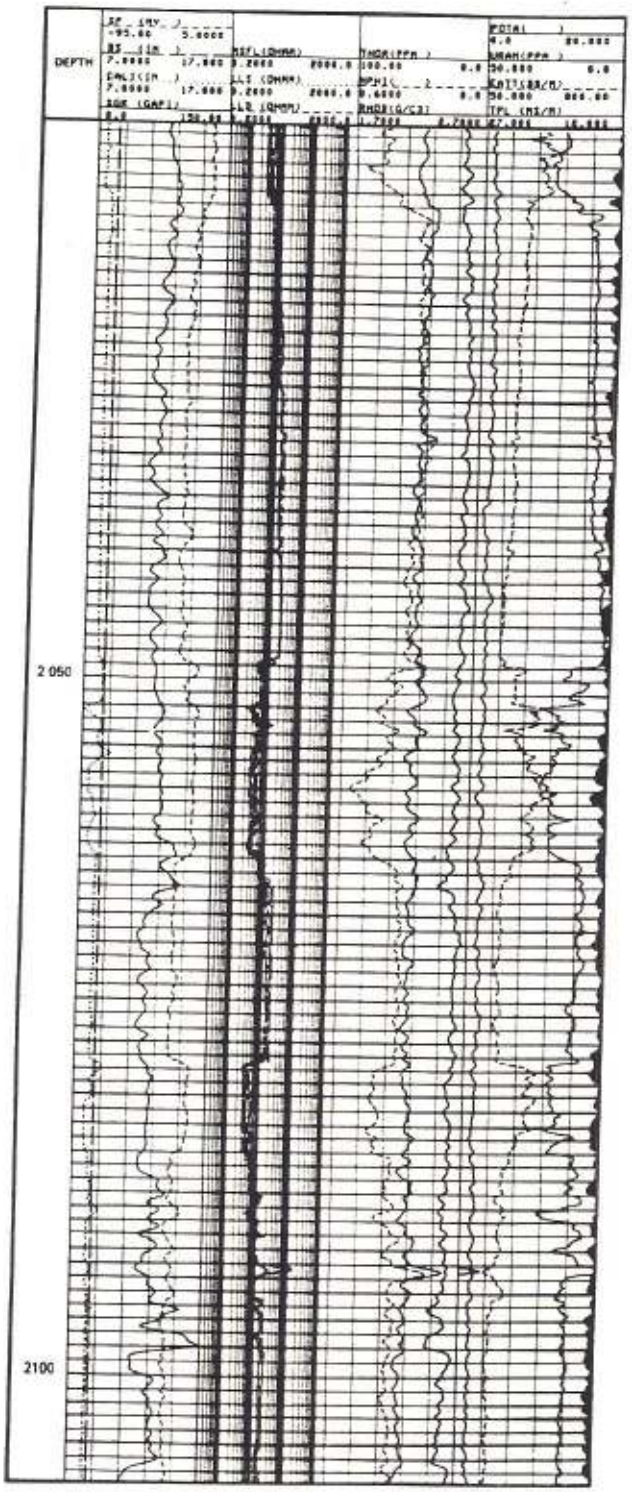

Fig. 6.4-11. - Typical log responses over a braided river system (from Schlumberger, Well Evaluation Conference, India, 1983).

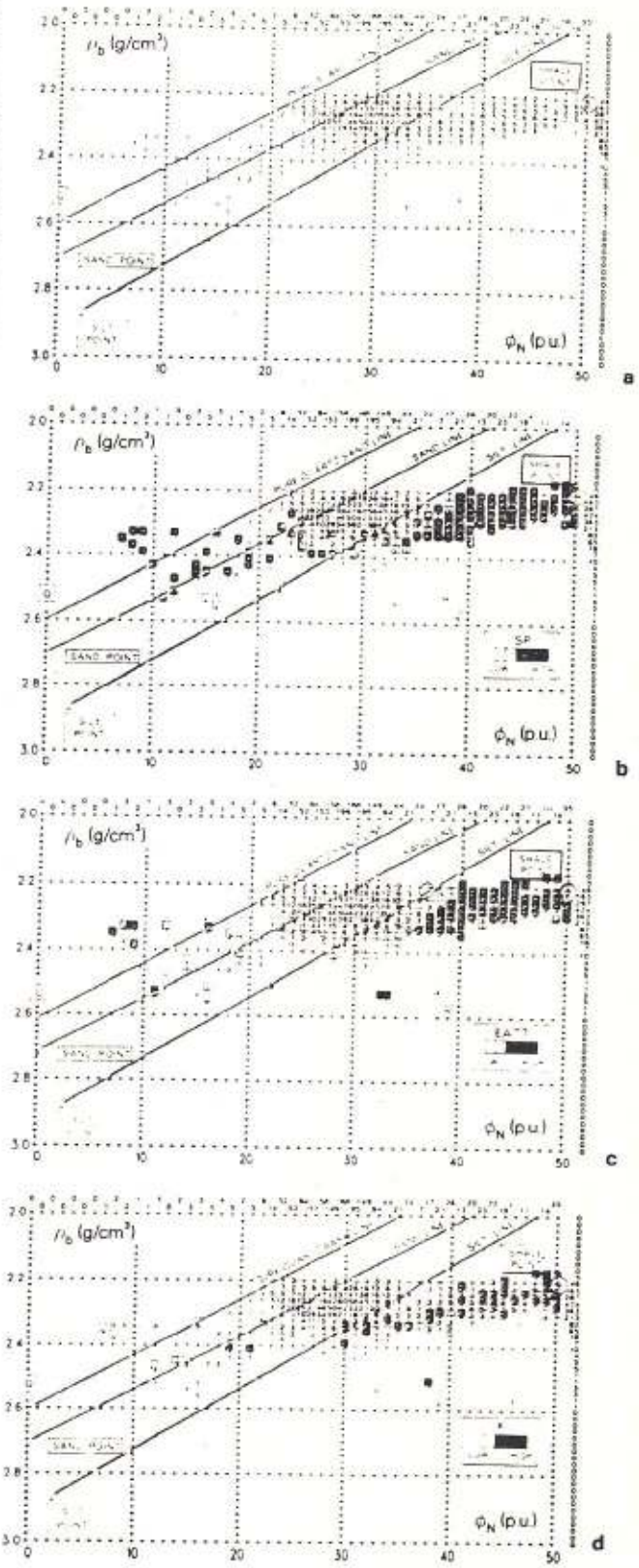

Fig. 6.4-12. - Density-neutron porosity crossplots with (a) frequency, (b) SP, (c) EATT and (d) potassium content on Z-axis (interpretation from Serra, in Schlumberger, Well Evaluation Conference, India, 1983).

show, very clearly, the change of grain size in the sands. The sandstone line corresponds to the line from the fluid point ($\rho_b = 1.$, $\phi_N = 100\,\%$) going through the most north-westerly points with low SP and EATT values. Similarly, the siltstone line

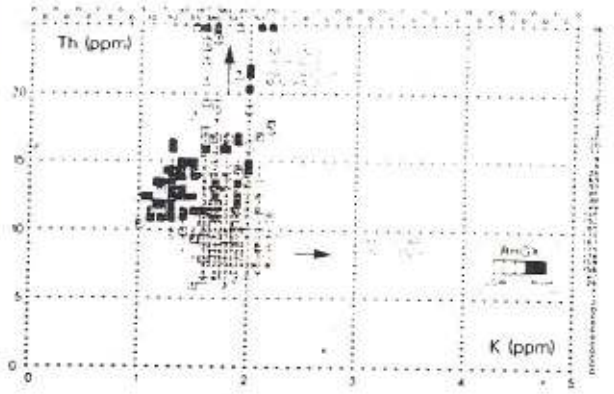

Fig. 6.4-13. - Thorium vs potassium with grain density on the Z-axis (interpretation from Serra, in Schlumberger, Well Evaluation Conference, India, 1983).

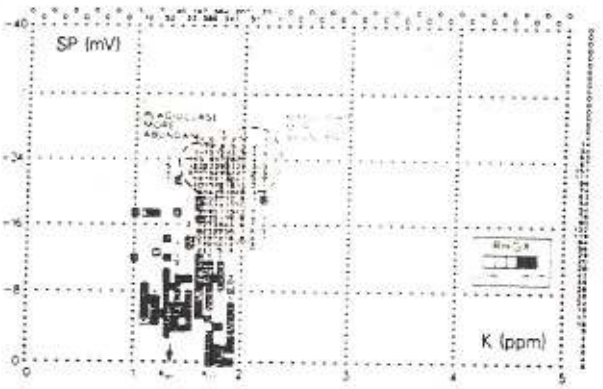

Fig. 6.4-14. - SSP vs potassium with grain density on the Z-axis (interpretation from Serra, in Schlumberger, Well Evaluation Conference, India, 1983).

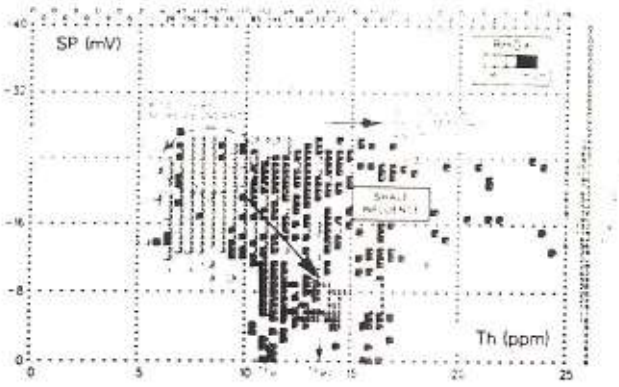

Fig. 6.4-15. - SSP vs thorium with grain density on the Z-axis (interpretation from Serra, in Schlumberger, Well Evaluation Conference, India, 1983).

can be drawn from the fluid point through the lowermost points with low to moderate SP and EATT values. The "sand point" corresponds to $\phi_N = 0$ on the sandstone line, and the "silt point" is obtained from the intersection of the siltstone line with a line drawn from the sand point parallel to the equiporosity line for the sand-silt mixture.

The moderately high and constant potassium values on the corresponding density-neutron crossplot (Fig. 6.4-12d) for all the sand and silt points suggest an *immature rock* composed of quartz, feldspar and plagioclase with mica and heavy radioactive minerals (e.g. zircon).

The potassium vs thorium crossplot (Fig. 6.4-13) confirms the presence of feldspar and also highlights the high thorium concentration from heavy radioactive minerals such as zircon.

The variation in the feldspar and biotite concentration in the sands can be recognized by analysing the evolution of the potassium content with respect to grain density ($(\rho_{ma})_a$) on the Z-axis (Fig. 6.4-14). The cluster of points with a high SSP deflection corresponds to sand. Within this cluster, plagioclases are more abundant when the potassium contentis lower (1.5 to 1.8 %) and the density higher, while K-feldspar concentration increases with higher potassium content (1.8 to 2.2 %) and lower density. The shale trend is clearly observed toward the low SSP values and high grain densities. In fact, over the interval studied, it is possible to identify two types of shale, one which appears in thick beds, and the other which is present as thin intercalations around 2260 and 2180 m. The corresponding K_{sh} can be selected for each shale from this crossplot.

On the SSP vs thorium (Th) crossplot (Fig. 6.4-15) the K-feldspar is more abundant in the sand cluster with lower thorium values (6.5 to 10 ppm) and lower densities (2 to 3 on the Z-axis). The increase in the content of biotite and heavy radioactive minerals corresponds to higher thorium values (10 to 18 ppm) and higher densities. The presence of the two type of shale is confirmed, and the general shale trend is clearly indicated. Core analysis confirmed the mineralogical composition deduced from the study of the crossplots.

6.4.3.2. Dipmeter curve Shape and Dip Patterns

From the GEODIP analysis (Fig. 6.4-16) the following conclusions can be done :

- Each sand starts with an abrupt lower contact, often non planar (four dip computation or no dip on GEODIP display). This feature could be related to possible erosional scoured surfaces.
- The sands are massive, apparently homogeneous, but with a few randomly distributed highly resistive peaks appearing only on 1, 2 or 3 curves. The resistive intervals show low GR, t_{pl} and hydrogen content, and high density. The mineralogy associated with such levels is not obvious, but chert or hydrated silica (opal) could possibly be present. If $(\rho_{ma})_a$ is higher than 2.65 a late diagenetic calcite formation may be involved.

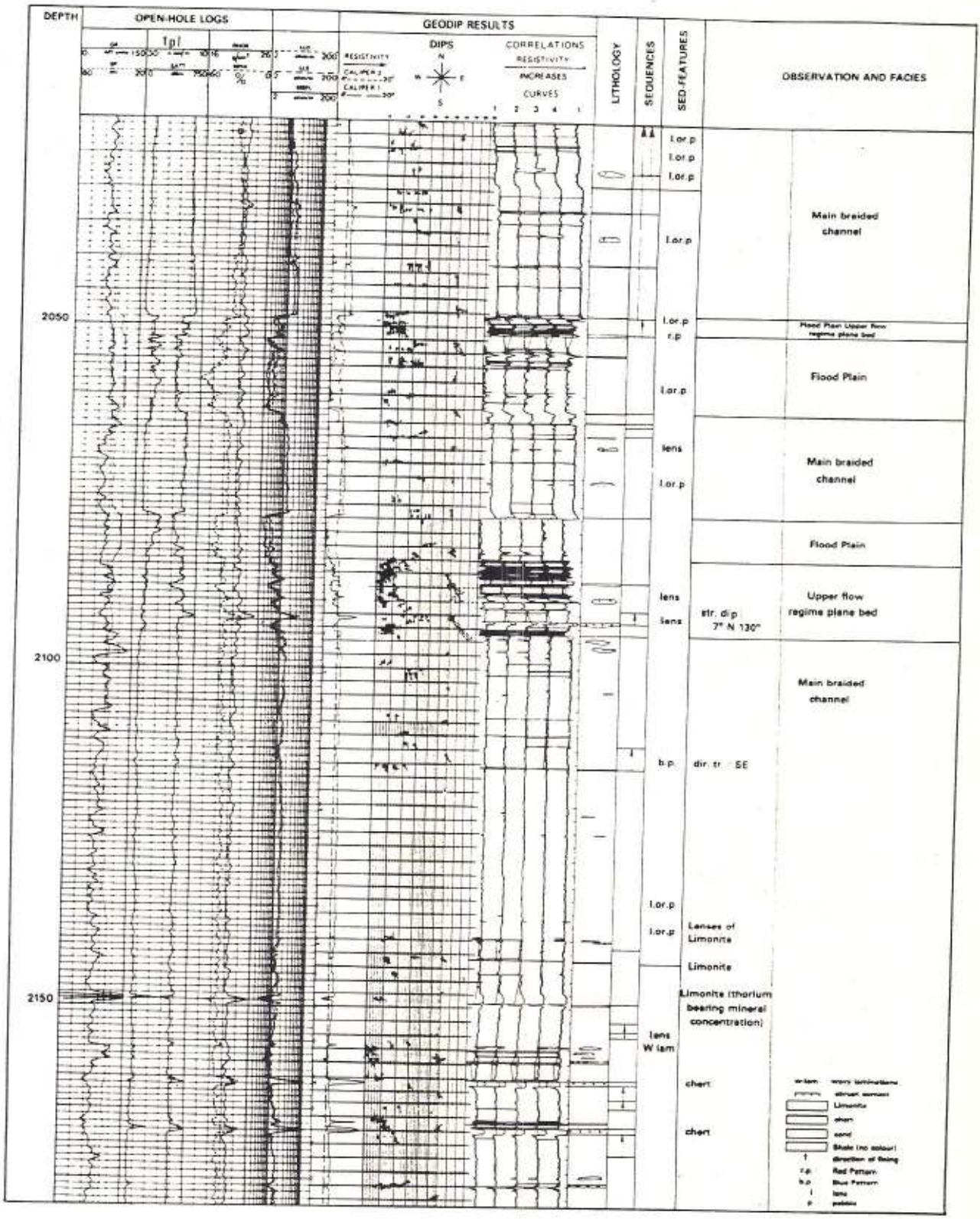

Fig. 6.4-16. - GEODIP arrow-plot on the same well and its interpretation (interpretation from Serra, in Schlumberger, Well Evaluation Conference, India, 1983).

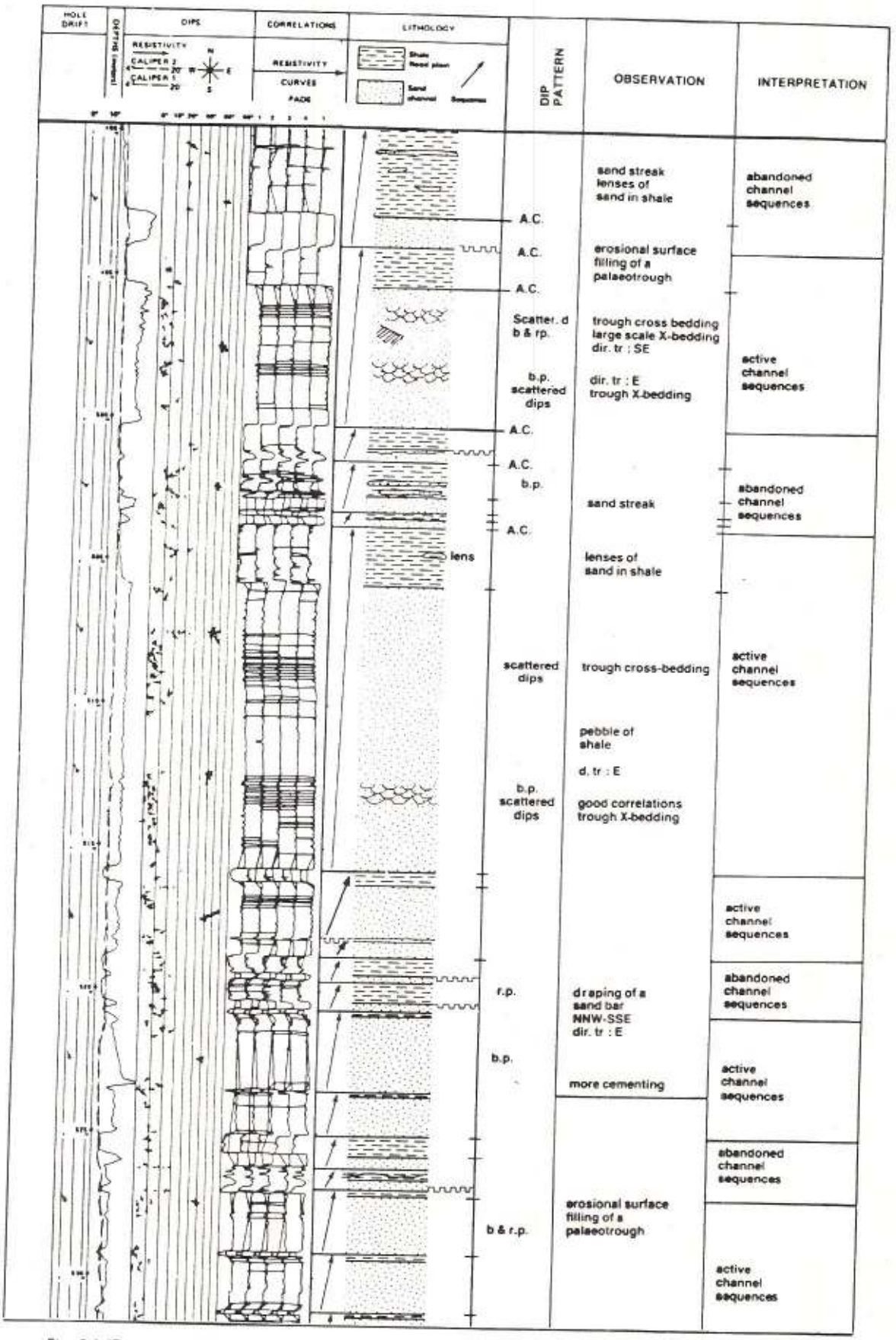

Fig. 6.4-17 - Other example of a braided river system from Africa as can be interpreted from GEODIP.

- Some thin, very conductive spikes are seen within the sands. Such features have high density, hydrogen content, EATT, t_{pl} and GR values. This could be limonite with concentration of thorium-bearing minerals (zircon).
- The sand-shale ratio is high.
- The general tendency within the sands appears to be fining upward.
- The upper intervals of the different sands show thin laminations.
- Few blue patterns can be seen. They generally indicate a S to SE direction of transport.

6.4.3.3. **Boundaries**

As it can be easily seen on the dipmeter resistivity curves the lower and upper sand boundaries are sharp or abrupt giving a general cylindrical shape.

6.4.3.4. **Electro-Sequences**

The general evolution of the resistivity curves indicates a fining upward sequence in the sands.

6.4.3.5. **Thickness**

Thickness of sand bodies is variable, but generally important in this example.

Another example from Africa, illustrated by Fig. 6.4-17 shows very variable thicknesses. As can be observed from the GEODIP analysis, all the other features are similar to the Tipam ones.

6.4.3.6. **Confusion with other Environments**

Cylinder shape of braided channels can be confused with the same features found in chute-bars (see Fig. 6.5-11).

DISTRIBUTARY FRONT DEPOSITS INTERPRETED FROM DIPMETER PATTERNS

J. A. Gilreath[1] and R. W. Stephens[2]
New Orleans, Louisiana

ABSTRACT

Continuing studies of high-resolution dipmeter data suggest that dipmeter patterns can be used to identify at least three different major depositional environments. Dipmeter patterns differentiate sediments deposited (1) in the neritic environment between beaches and the seaward edge of the continental shelf, (2) on the slope between the outer edge of the shelf and the abyssal zone, and (3) near active deltas where distributary-front sands may accumulate.

Distributary-front sands tend to be deposited in one of three general shapes: (1) elongate, (2) crescent, or (3) fan. Dipmeter patterns in distributary-front deposits are mainly influenced by current-induced cross-stratifications rather than structural dips. These "current patterns" record the dip of foreset beds, giving a characteristic dip pattern that can be readily identified. The direction of dip in these current patterns defines the direction of transport, and the magnitude of the dip indicates the probable shape of the sand body.

INTRODUCTION

Many dips that appear on a high-resolution dipmeter plot reflect environmental energy conditions existing at the time of deposition rather than structural dip. Beds deposited in a high-energy marine environment tend to exhibit great scatter of dip magnitudes. In contrast, low-energy environments lead to "layer-cake" deposition and tend to show uniform dip magnitudes.

Gilreath, Healy, and Yelverton (1969) describe a method for estimating water depth during deposition by analyzing the dip-magnitude spread on dipmeter plots. A dip-magnitude spread of 40 degrees suggests deposition in a water depth of 0 – 50 feet; a dip-magnitude spread of 15 degrees suggests deposition in a water depth of 50 – 300 feet; and a dip-magnitude spread of 2 degrees suggests deposition in a water depth of more than 300 feet. In each of these three depth zones, deposition is affected by different energy levels. A high-energy level exists in the inner shelf; a medium-energy level exists in the middle shelf, and a low-energy level exists in the outer shelf.

Recent investigations show in some areas a second band of three energy levels lying seaward of the band described previously (Fig. 1). The "high-energy" dipmeter pattern of the seaward band exists along the upper continental slope, the medium-energy dipmeter pattern exists along the lower continental slope, and the low-energy pattern exists in the abyssal environment.

Dip-magnitude spread is similar for shoreward and seaward energy bands. Energy for the shoreward band is provided mainly by current and wave action, while that for the seaward band is provided by gravity in the form of submarine slump, mudflow, and creep. The gravity-fed downslope movement results in high-energy dip-magnitude scatter in water depth equated to a low-energy paleoecologic zone. A clue to differentiation between deposition of shoreward and seaward bands is the cyclic nature of dipmeter-derived energy zones in the seaward or deep-water bands. This cyclic effect may be a function of periodic loading of the continental slope. Unless data from paleontology or other sources indicate otherwise, the dipmeter-derived energy level is assumed to be for the shoreward, or more-shallow-water energy band.

Characteristic dipmeter patterns are also seen near distributary mouths in active delta environments (Fig. 2). Dipmeter plots in beds deposited just seaward of distributary mouths reflect foreset bedding and are referred to as "current patterns". The current pattern is a characteristic dip pattern that can be identified readily (Gilreath, Healy, and Yelverton, 1969). Although characteristic dip patterns make possible the recognition of distributary-front deposits, they also may mask the effects of other depositional agents. Therefore, the rules for water depth identification in the shoreward and seaward energy bands do not apply.

[1]Schlumberger Offshore Services.
[2]Louisiana State University in New Orleans.

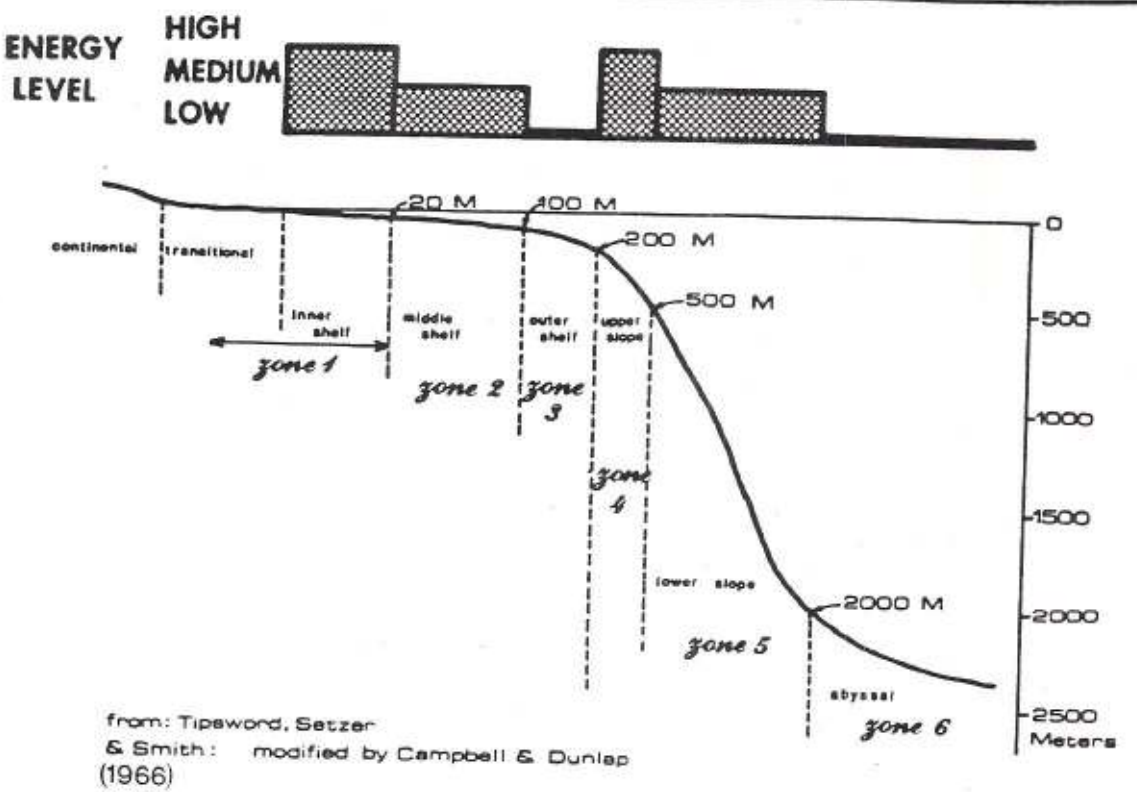

Fig. 1 — Dipmeter-derived energy levels equated to paleoecological zones.

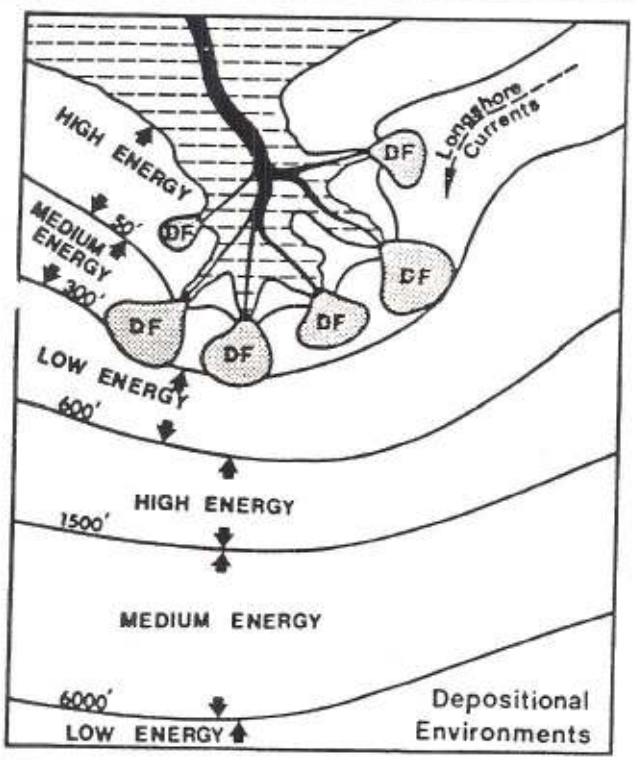

Fig. 2 — Environment for distributary-front deposits.

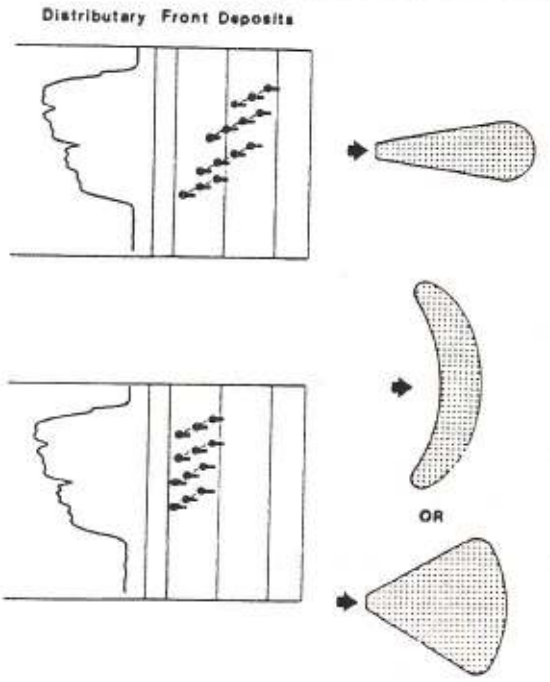

Fig. 3 — Theoretical shapes of distributary-front deposits and their associated dip patterns.

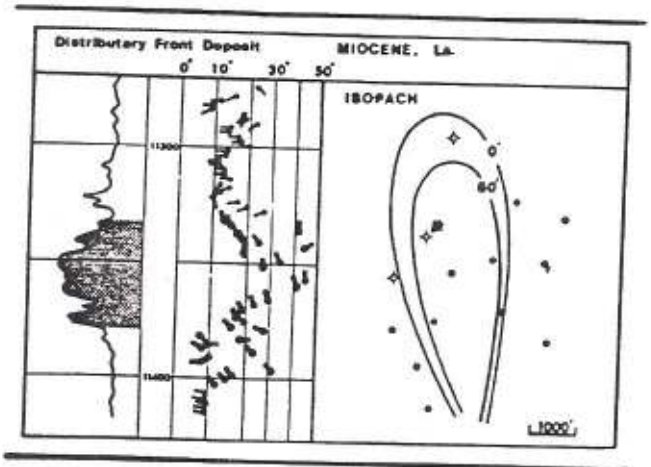

Fig. 4 — Spontaneous potential, dipmeter plot, and isopach map of a Miocene elongate distributary-front deposit.

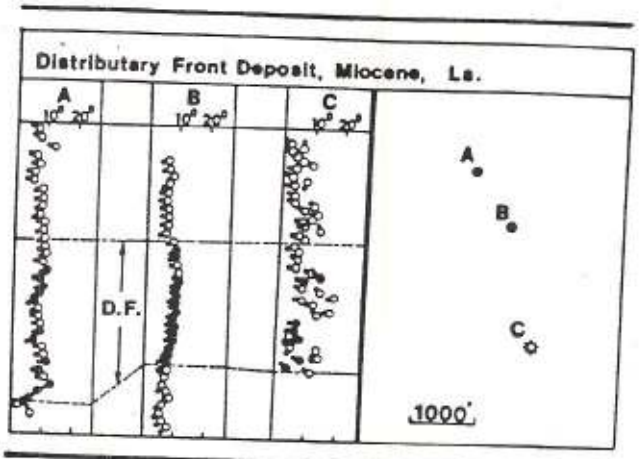

Fig. 5 — Dipmeter plot characteristic of crescent- or fan-shape distributary-front deposit (Miocene, La.).

DISTRIBUTARY FRONT DEPOSITS

Distributary-front sands are deposited as discrete sand lenses up to a mile or more offshore from rivers, and they will be preserved if the distribution is diverted or abandoned or if the rate of subsidence is sufficiently rapid for the sands to be buried before the distributary channel progrades through their site of deposition. Distributary-front sands tend to be deposited in one of three general shapes: (1) elongate, (2) crescent, or (3) fan (Fig. 3).

Study of dipmeter data suggests elongate sand bodies are characterized by current patterns having a dip magnitude spread greater than 10°. The direction of current-pattern dips is the same as sediment-transport direction and coincides with the long axis of the sand body. The elongate shape is indicative of rapid deposition, rapid subsidence, and lack of reworking.

Crescent- and fan-shaped sand bodies are identified by current patterns having a dip-magnitude spread less than 10°. The direction of the current-pattern dips is the same as sediment-transport direction. However, the long axis of a crescent-shaped sand body and an axis through the wings of a fan-shaped sand body are normal to the transport direction. The crescent or fan shape is indicative of slow deposition, slow subsidence, and possible reworking by wave action and longshore currents.

Distributary-front sediments are not always sand. Shale and silt distributary-front deposits also have been noted.

MIOCENE DISTRIBUTARY FRONT DEPOSITS

Figure 4 illustrates dipmeter plots of a Miocene distributary-front deposit from Louisiana. The high angle (greater than 10°) current patterns identify this sand as elongate in shape with transport from south-southeast to north-northwest.

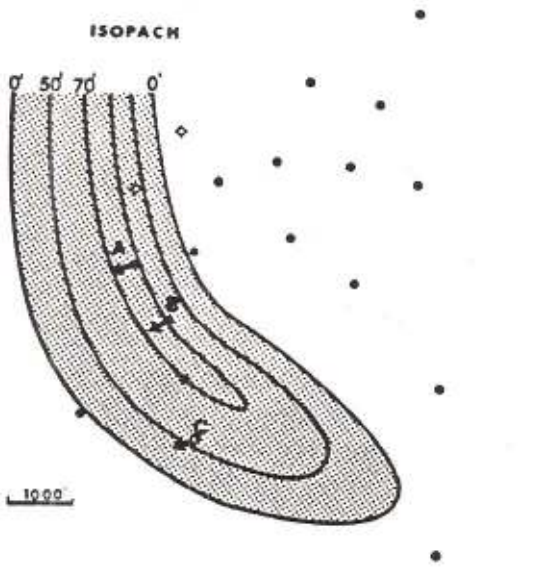

Fig. 6 — Isopach map of the Miocene crescent-shaped distributary-front deposit identified by dipmeter plots (see Figure 5).

An isopach map using available well control confirms the elongate shape with long axis from south-southeast to north-northwest.

Figure 5 depicts another plot of a Miocene distributary-front deposit. The dip plots from wells A, B, and C exhibit low-angle current patterns (less than 10°) opposite the sand. Low-angle patterns indicate that the probable shape of the sand is crescent or fan. The isopach map (Fig. 6) shows this distributary-front deposit to be crescent shaped with the long axis of the crescent normal to the direction of sediment transport. The current patterns on a dipmeter plot confirm a northeast-to-southwest direction for sediment transport.

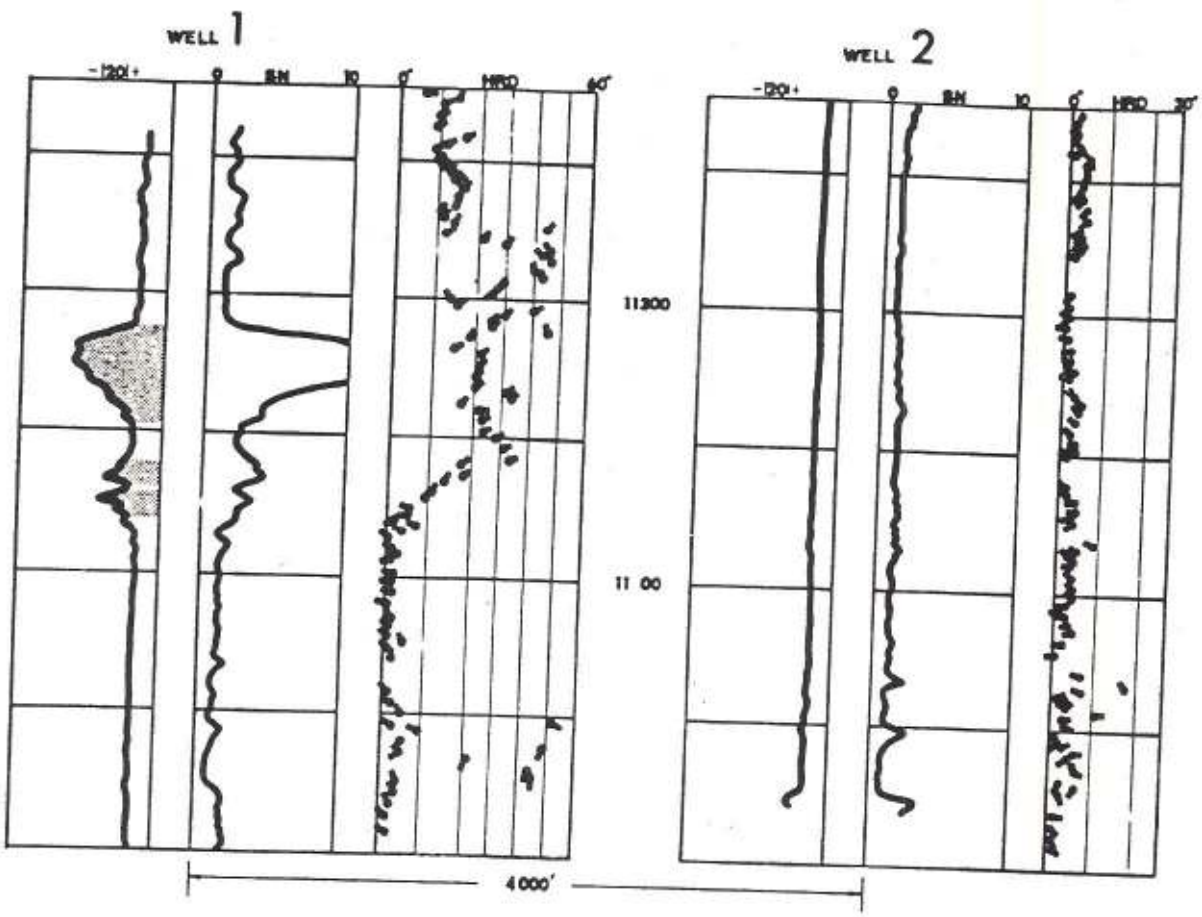

Fig. 7 — Dipmeter plot of distributary-front deposit from the Oligocene of Louisiana.

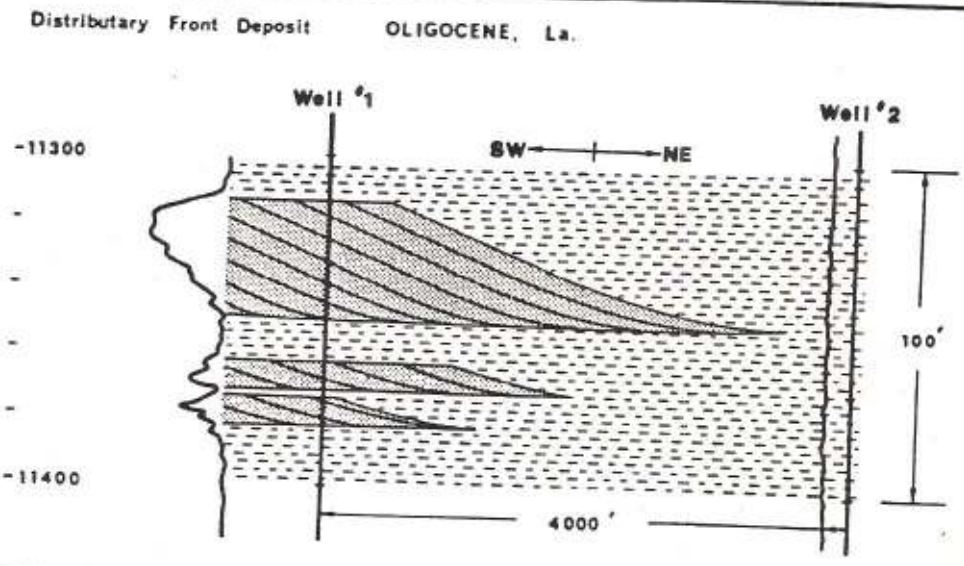

Fig. 8 — Cross section showing interpreted relationship of distributary-front deposits in wells #1 and #2 of Figure 7.

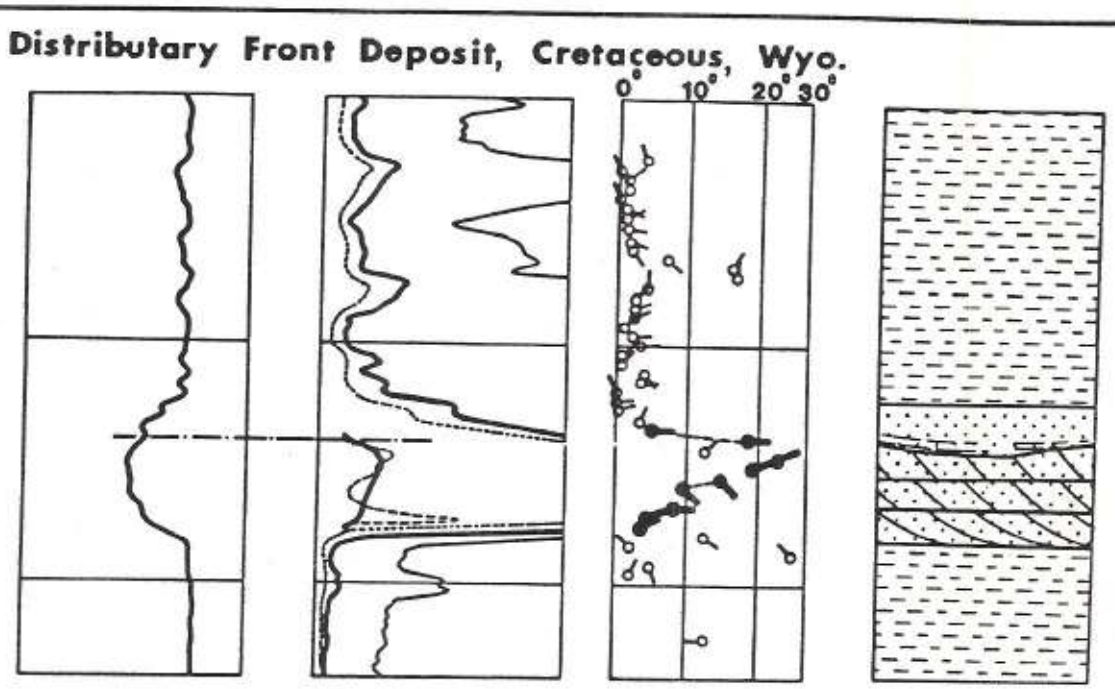

Fig. 9 — Dipmeter plot of distributary-front deposit from the Cretaceous of Wyoming.

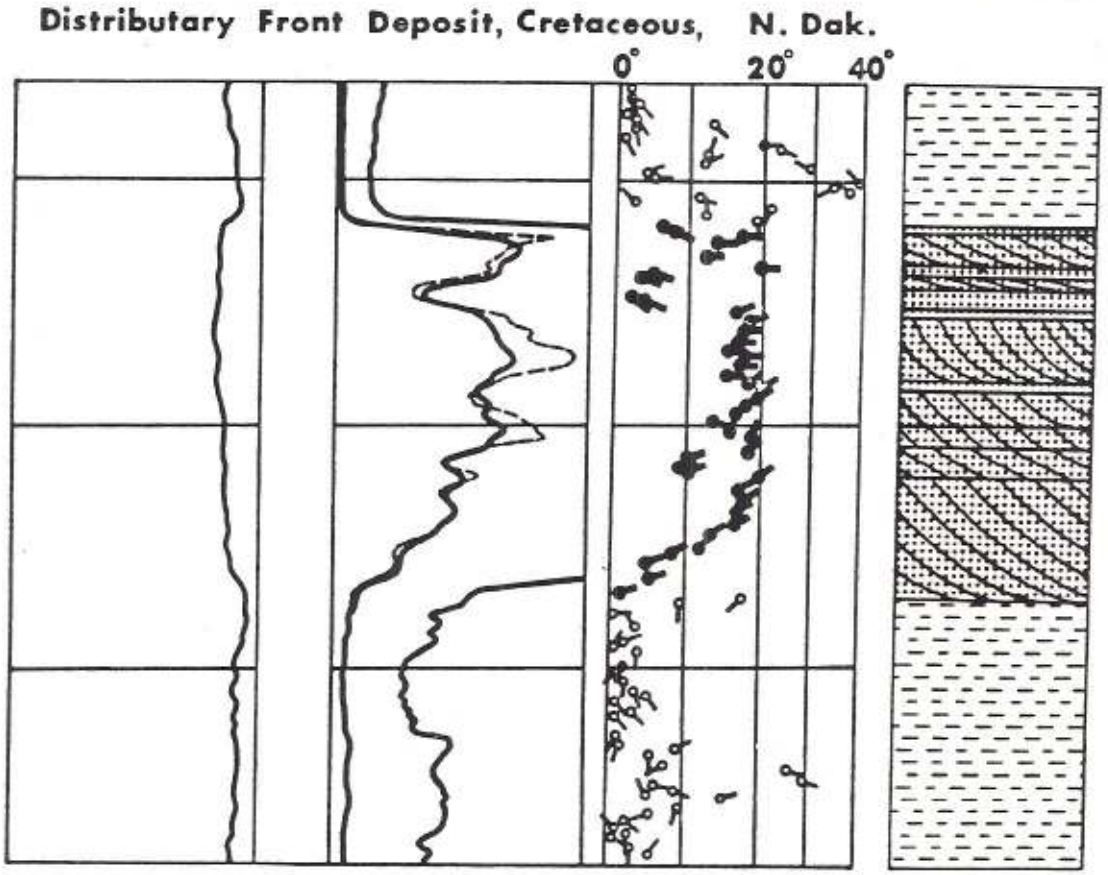

Fig. 10 — Dipmeter plot of distributary-front deposit from the Cretaceous of North Dakota.

OLIGOCENE DISTRIBUTARY FRONT DEPOSITS

Figures 7 and 8 depict plots of a series of Oligocene distributary-front sands from Louisiana. Well #1 contains three sand members. The current patterns seen on dip plots opposite these sands suggest two distributary-front sand shapes. The current-dip patterns from the lower sand member exhibit a dip magnitude spread of less than 10 degrees and suggest a crescent- or fan-shaped sand deposit with sediment transport from southeast to northwest. The middle and upper sand members exhibit a dip-magnitude spread greater than 10 degrees and suggest an elongate sand deposit with sediment transport from southwest to northeast.

Well #2 was drilled 4000 feet northeast of Well #1 and is flat structurally. The lack of sand in the distributary-front interval suggests this location is beyond the seaward limits of this particular distributary-front system. The dipmeter "current patterns" indicate a slow rate of deposition with sediment transport from southeast to northwest, the same direction seen in the beds below the distributary-front system in Well #1.

CRETACEOUS DISTRIBUTARY FRONT DEPOSITS

Figures 9 and 10 represent dipmeter plots of distributary-front deposits confirmed by examination of conventional cores from the Cretaceous of Wyoming and North Dakota. The presence of high-angle current patterns indicates that both deposits are elongate with sediment transport direction from southwest to northeast.

In these examples, small cut-and-fill sedimentary structures are noted at the top of each distributary-front sequence. The axes of the cut-and-fill structures are normal to the direction of original sediment transport, suggestive of cut-and-fill action by longshore currents.

MIOCENE DISTRIBUTARY FRONT DEPOSITS WITH CHANNEL SAND

Plots of two other Louisiana Miocene distributary-front sands and an associated channel sand are illustrated in Figure 11. All three probably were deposited by a distributary system which prograded through the area of the well location. Though three sand members are present, only one sketch is used to illustrate the relative positions of the system as it moved across this location. The lower member is typical of the seaward fringe of a delta deposit. From bottom to top there is a gradation from shale to silt to a very fine sand. The current patterns are low angle suggesting a relatively slow rate of deposition. The middle member is a less-shaly sand and the dipmeter current patterns are high angle indicating rapid deposition.

The upper member was deposited in the distributary channel. Instead of "current patterns", "slope patterns" are present on the dip plot. These "slope patterns" indicate that this member is a sand body that is convex downward and strikes northeast-southwest; the same as the sediment-transport direction of the lower members.

CONCLUSIONS

Successful development drilling in oil and gas fields requires the prediction of reservoir limits with a minimum of dry holes. Proper utilization of dipmeter data can aid in identifying distributary-front sand reservoirs and in predicting probable reservoir boundaries.

Other depositional environments, such as deltaic interdistributary-marsh, fluvial-flood-plain and lagoonal, also should produce characteristic dip patterns. Dipmeter patterns in these and other environments will be the subject of future studies.

SELECTED REFERENCES

1. Bonham – Carter, G. F., 1967, Diffusion and settling of sediments at river mouths: A computer simulation model: Gulf Coast Assoc. Geol. Socs. Trans., V. 17, p. 326-338.
2. Curtis, Doris M., 1970, Miocene deltaic sedimentation, Louisiana Gulf Coast, *in* J. P. Morgan Ed., Deltaic Sedimentation, Modern and Ancient: Society of Economic Paleontologists and Mineralogists, Special Publication No. 15, p. 293-308.
3. Fisk, H. N., 1961, Bar finger sands of Mississippi Delta, *in* Geometry of sandstone bodies: Tulsa, Oklahoma, Am. Assoc. Petroleum Geologists, p. 29-52.
4. Gilreath, J. A., 1960, Interpretation of dipmeter surveys in Mississippi: Gulf Coast Assoc. Geol. Socs, Trans., V. 10, p. 267-275.
5. Gilreath, J. A. and J. M. Maricelli, 1964, Detailed stratigraphic control through dip computations: Am. Assoc. Petroleum Geologists Bull., V. 48, No. 12, p. 1902-1910.
6. Gilreath, J. A., J. S. Healy, and J. N. Yelverton, 1969, Depositional environments defined by dipmeter interpretation: Gulf Coast Assoc. Geol. Socs. Trans., V. 19, p. 101-111.
7. Rainwater, E. H., 1963, The Environmental control of oil and gas occurrence in terrigenous clastic rocks: Gulf Coast Assoc. Geol. Socs. Trans., V. 13, p. 79-94.
8. Tipsword, H. L, F. M. Setzer, and Fred L. Smith, 1966, Interpretation of depositonal environment in Gulf Coast petroleum exploration from paleoecology and related stratigraphy: Gulf Coast Assoc. Geol. Socs. Trans., V. 16, p. 119-130.

Fig. 11 follows.

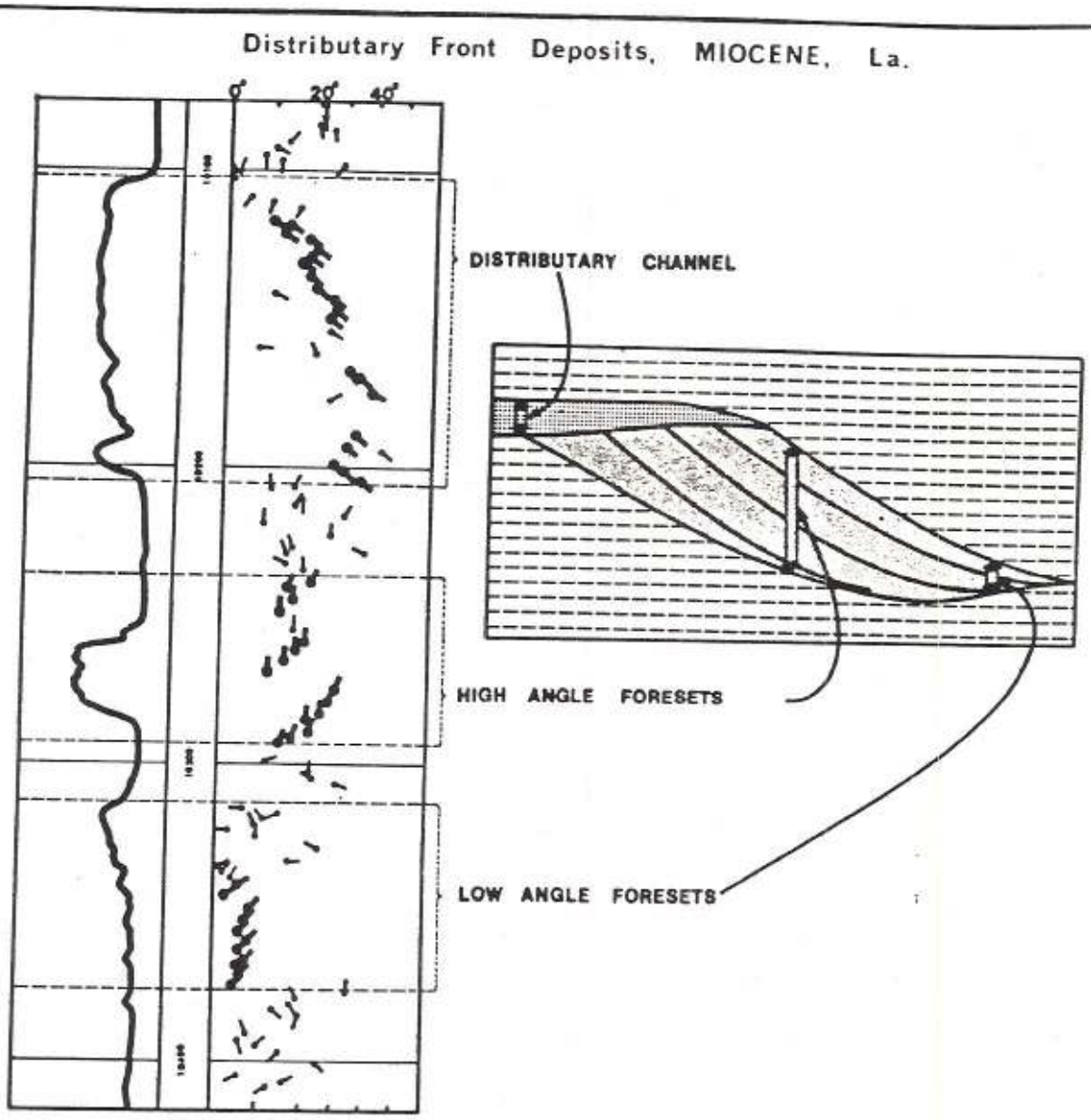

Fig. 11 — Left: Spontaneous potential and dipmeter plot of two distributary-front sands and associated distributary-channel sand. Right: Hypothetical diagram of distributary channel prograding through the site of the distributary-front deposits.

Schlumberger

SEDIMENTOLOGICAL ANALYSIS OF SHALE-SAND SERIES FROM WELL LOGS

by

O. Serra and L. Sulpice

Geological Engineers, ELF-RE

PURPOSE

In reconstructing depositional environments, the sedimentologist needs representative samples (lithology, fossils), as well as a continuous picture of the series.

In subsurface regions, 'core samples' alone meet these two requirements.

For both technical and economic reasons, core samplings are becoming increasingly rare, particularly in shale-sand series.

For his analytical work, the sedimentologist thus has to be content with an examination of side wall cores and drill cuttings.

The former present the drawback of sampling discontinuities, together with the limited size of the sample, which generally prevents the observation of sedimentation patterns. As for drill cuttings, these are often difficult to interpret, owing to their limited size and also due to cavings.

These considerations led G.S. Visher (1), 1965, W.C. Krueger (2), 1968, L. Fons (3), 1969, S.J. Pirson (4), 1970 and K.J. Weber (5), 1971 to the idea of employing well logs as a sedimentological tool, as the recorded parameters are closely associated with lithology and vary in relation to it. Furthermore, well logs provide a source of

variation of a physical parameter reflects a progressive modification in the corresponding geologic characteristic. Any sudden change indicates a sudden lithologic or physical change.

On the other hand, a curve which exhibits no changes - one which is homogeneous or smooth - denotes persistence of the characteristics of the rock, and hence the various conditions prevailing in the depositional phase.

PRINCIPLE OF SEDIMENTOLOGICAL ANALYSIS OF WELL LOGS IN SHALE-SAND SERIES

The facies of detritic shale-sand series are conditioned partly by the dynamic conditions of the environment of deposit and by their variations, and partly by the action of gravity.

In either case, it is generally accepted that the study of grain size distribution and sorting provides one means of identifying the facies. If, moreover, the detritic argillaceous phase is considered to constitute a grain size fraction, a knowledge of the clay percentage and its variation provides an idea of the facies.

Thus in the special case of detritic shale-sand series, any well log the response of which can be linked, directly or not, to the clay percentage, or any method enabling a calculation of this percentage, can be used as a tool in sedimentological analysis.

Two well logs in particular are employed as indicators of argillosity: spontaneous polarization and natural radioactivity.

In 1958, Shell engineers appear to have been the first to develop the idea of characterizing sand masses from the appearance of the spontaneous polarization curve.

By analyzing the lower and upper bedding contacts and the shape of the curve, this suggested the classification illustrated in figure 1, and associated certain patterns or 'electro-facies' with sedimentological phenomena (figure 2).

Similarly, by comparing the grain size and natural radioactivity (gamma-ray) curves, it is possible in certain cases to observe excellent agreement between them (figure 3), thereby enabling the use of natural radioactivity for the same purpose as spontaneous polarization as a faciologic analysis tool.

METHODOLOGY OF SEDIMENTOLOGICAL WELL LOG ANALYSES IN SHALE-SAND SERIES

In order to give sedimentological analyses carried out from well logs their full effectiveness, and to make their results absolutely reliable, it is wise to follow the procedure that we describe below, constituting a sort of methodology of this type of interpretation.

1. Establishment of the fundamental composite log

On the basis of the foregoing observations and actual experience, we recommend, whenever possible, the use of all well logs for every sedimentological well log analysis. This requires plotting well logs and dip measurements on a single document - with dips derived from optical correlations if need be - as well as natural gamma-ray spectrometry, if possible, with readjustment in depth on a single reference log.

This document is called the fundamental composite log. Its scale depends on the type of study and desired degree of accuracy. If it covers the entire series crossed by the bore hole, it is advisable to use a scale of 1:1000 or preferably 1:2000. This permits a better appreciation of the overall well logs and facies traversed, thereby leading to better identification of partial and general sequential variations (cf. figure 5).

However, a scale of 1:500 or preferably 1:200 is necessary in order to determine the finer details of an elementary sequence, together with the use of micro-devices if necessary (cf. figure 4).

In certain cases of thin elementary sequences, or to better appreciate the homogeneous character of a formation, it is preferable to employ micro-devices, particularly the microlog at 1:40 scale.

2. Faithful, precise and detailed lithologic reconstruction

This must be carried out by relying on descriptions of the cuttings as well as a qualitative and quantitative interpretation, with calculation of porosity and determination of the major constituents in the matrix: quartz, calcite, dolomite, clay. At this stage, the lithologic reconstruction can be improved by the interpretation of micro-devices. The example in figure 4 shows that an interpretation based on SP and induction curves alone would not have revealed the existence of

By a combination of the various parameters, this permits identification of a certain number of characteristic electro-facies.

Nine major electro-facies were thus identified in the illustration given in the following chapter.

4. Examination of breaks in curves

The term break is applied to any sudden change in value, the vertical extension of which does not exceed the spacing or diameter of the sphere of influence of the tool (this corresponds to abrupt contact in the Shell classification).

The analysis of these breaks involves examining the various possible hypotheses to determine the one which is most compatible with known data on lithology and on the general context.

In effect, any break in a shale-sand environment generally reflects a lithologic change. This can:

. Logically fit into the sequential evolution: examples:

- Sand bed surmounting a marine shale in a deltaic sequence.
- Passage into the different units of the evaporitic sequence dolomite - anhydrite - salt.
- Lignite bed interbedded with a tidal flat shale.

Not fit logically into the sequential evolution. In this case the explanation must be found among the following hypotheses:

- Diagenetic influences: cementation, dissolution, transformation.
- Passage of a fault.
- Transgression period.
- Erosion phenomena.
- Turbidites.
- Volcanic flow.

7. Faciologic analysis: environmental reconstruction

Only after having calibrated the electro-facies and verified the reliability of the electro-facies - facies relationship can one go on to the final stage of the sedimentological well log analysis, namely, the faciologic well log analysis and reconstruction of the depositional environment, the latter being derived from the combination of electro-facies and sequential evolution.

ILLUSTRATION OF THE METHOD: EXAMINATION OF A DELTAIC BASIN

In order to illustrate the above method of sedimentological well log analysis, we selected a series of examples derived from investigation carried out by ELF in the Niger delta. These examples show how the application of the method permits identification of a certain number of characteristic electro-facies which, once located in the sequential evolution, lead to reconstruction of the depositional environment and the examination of its variations with time.

To set the geologic framework of this illustration, we shall borrow the deltaic sedimentation model of J.R. Allen (6) (cf. figure 12), and, from K.J. Weber (5), the units characterizing the depositional environments identified.

The elementary deltaic sequence generally overlays a frequently thin bed comprising a sandstone-carbonate sediment, sometimes sideritic, often lumachellic, slightly porous, compact, and generally clearly distinguishable on porosity logs (neutron, density, acoustic) and resistivity logs, at least if it is sufficiently thick; if not, it can only be detected by micro-devices (mainly microlog, and possibly HDT resistivity). It may sometimes be radioactive if it includes glauconite and/or phosphatic debris. If the bed is sufficiently thick, it may exhibit a positive sequence.

This bed corresponds to deposits of the marine transgression phase on the deltaic shelf (cf. figures 9 to a).

The elementary deltaic sequence proper corresponding to the regressive phase begins with clays (cf. figures 9 to b). These are characterized by: very stable (within statistical limits), high radioactivity, but not necessarily the highest of the sequence; a neutron hydrogen index which is also stable, and increases with clay purity; resistivity and sonic velocity which decrease with increasing purity. It is at this level that

in fine argillaceous laminations, or to radioactive carbonate deposits. In the first instance, the SP log matches the variations in the gamma-ray log; in the second case, it continues to respond as a sand; in the final case, these deposits are identified by porosity and resistivity logs.

The porosity of these sands is often substantially lower than that of barrier bar sands (cf. figures 9 to e), owing to poorer sorting.

Moreover, the passage from one sand to another is sudden, reflecting the erosive character of tidal channel sands. This contact is sometimes emphasized by a lumachellic sandstone level (cf. figures 8 to i) clearly identified on the resistivity and porosity logs; in fact, this is a means of distinguishing tidal channel sands from fluvial sands. They also exhibit a more serrated curve and a frequently more clearly marked positive sequence ('bell' shape, cf. figures 7 to f).

Their resistivity is often significantly greater than that of littoral sands, partly owing to their lower porosity, and mainly to the far less saline formation water (10 to 15 g/l as compared with 25 to 35 g/l for littoral sand formation waters, cf. figure 5).

As for the argillaceous deposits, these behave in SP in a manner comparable to pure clays (cf. figures 8 to h), while the neutron hydrogen index is significantly lower, the density and resistivity higher, indicating a heterogeneous sediment composition (sandy or silty lens or veins, carbonate levels, plant debris). The radioactivity frequently exhibits high response instability, with frequent strong radioactive peaks probably corresponding to beds which are richer in humic organic matter or to radioactive silt beds. It is also not rare to encounter lignite beds (cf. figures 8 to g) which stand out clearly in neutron logs (IH_N = 50%), density logs (ρ_b oscillating between 1.2 and 1.7) and acoustic logs (Δt as high as 170 $\mu s/ft$). These argillaceous deposits correspond to swamp facies.

In the event that progradation continues, following the marginal-littoral deposits described above, one can find continental deposits generally consisting of thick sandy series exhibiting characteristic 'cylinder' shapes in the well logs (cf. figures 11 to j), corresponding to meander-belt sands or to stacking of bed deposits.

The argillaceous deposits corresponding to natural levees or the flood plain (cf. figures 11 to k), are generally very rare, as they are eroded by continuous changes in the course of the river. When neutron or acoustic density recordings are available, they exhibit

They also permit identification of radioactive reservoirs in the absence of SP curves.

Differentiation of pure, homogeneous shales from the others is also very useful for clay compaction studies, leading to a better choice of well logging parameters (Δt_{sh}, ρ_{sh}, R_{sh}) whose variations are observed with depth, and thus helping to avoid errors of interpretation caused by a faulty appreciation of lithology.

They also facilitate the interpretation of dip measurements by permitting a distinction between regional and sedimentary dips.

These analyses lead to a better orientation of the choice of side wall core sampling zones for sedimentological, geochemical and paleontological studies, as well as a restriction of the types and number of these samples.

They also lead to the rapid preparation of electro-facies cards based on the appearance of the curves or arising from quantitative processing.

It is possible that after a minimum of research work on the question, they will help to develop an idea of the covering quality of certain shales. In effect, only marine shales seem to exhibit good cover characteristics, owing to their homogeneity, purity and wide extension. On the other hand, tidal flat shales cannot provide very effective cover owing to their heterogeneous composition: veins, sand, pebbles, abundant plant debris, carbonate levels, slight lateral extension.

In the same sense, these analyses should help to provide an idea of the oil-bearing potential of the series crossed, especially if accompanied by spectral well logging. Heterogeneous shales, rich mainly in organic matter of humic origin, will tend preferably to generate dry hydrocarbons, whereas the purer and more radioactive marine shales will generate heavier hydrocarbons (oil, condensate gas), owing to the sapropelic nature of the organic matter entrapped therein.

ADVANTAGES OF SEDIMENTOLOGICAL WELL LOG ANALYSES

Well logs provide the only means of obtaining a continuous view of the series crossed by a well. Hence they provide the only means of observing faciologic variations without any hiatus.

They also permit very fine, detailed analysis, particularly at a scale of 1:200 or 1:40, or by the exploitation of micro-devices.

BIBLIOGRAPHY

(1) Visher, G.S., 1965, Use of vertical profiles in environmental reconstruction: B.AAPG, v.49, No.1.

------ 1969, How to distinguish barrier bar and channel sands: World Oil, May.

(2) Krueger, W.C., 1968, Depositional environments of sandstones as interpreted from electrical measurements. An introduction: Transactions of Gulf Coast Association of Geological Societies, 18th annual meeting, v.18.

(3) Fons, Sr., L., 1969, Geological application of well logs: Transaction of 10th annual logging symposium, SPWLA meeting.

(4) Pirson, S.J., 1970, Geologic well log analysis: Gulf Publishing Co., Houston, Texas.

(5) Weber, K.J., 1971, Sedimentological aspects of oil fields in the Niger delta: Geol en Mijnbouw, v.50.

(6) Allen, J.R., 1965, Late quaternary Niger Delta and adjacent areas: sedimentary environment and lithofacies: B.AAPG, v.49, No.5.

------ 1965, Coastal geomorphology of Eastern Nigeria: beach ridges barrier island and vegetated tidal flats: Geol en Mijnbouw, v.44.

------ 1970, Sediments of the modern Niger Delta in 'Deltaic sedimentation modern and ancient': SEPM, No.19.

Dailly, G., 1967, Delta du Niger, 'Quelques exemples de facies électriques': Rapport interne SAFRAP, inédit.

Serra, O., 1974, Interprétation géologique des séries deltaïques à partir des diagraphies différées: Rev. AFTP, No.227.

Norwood, Jr., E.M., and Holland, D.S., 1974, Lithofacies mapping. A descriptive tool for ancient delta systems of the Louisiana outer continental shelf: Tr. of Gulf Coast Assoc. of Geol. Societies, v.24.

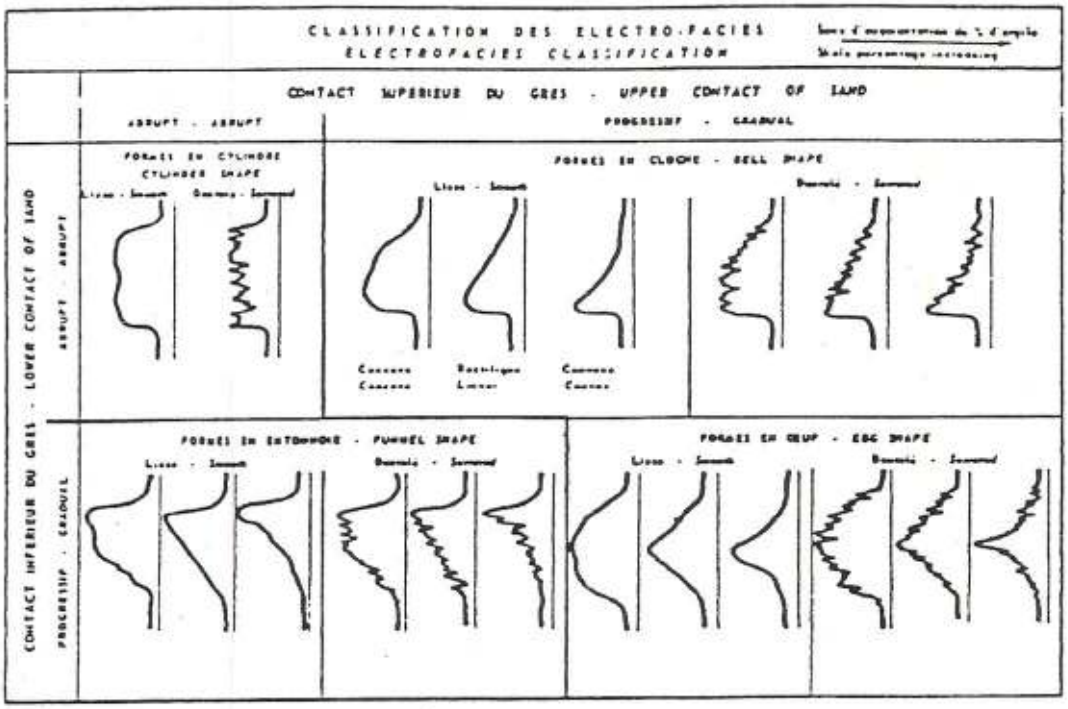
CLASSIFICATION DES ELECTRO-FACIES
ELECTROFACIES CLASSIFICATION
CONTACT SUPERIEUR DU GRES - UPPER CONTACT OF SAND
ABRUPT - ABRUPT
PROGRESSIF - GRADUAL
CONTACT INFERIEUR DU GRES - LOWER CONTACT OF SAND
ABRUPT - ABRUPT
PROGRESSIF - GRADUEL
FORME EN CYLINDRE
CYLINDER SHAPE
FORME EN CLOCHE - BELL SHAPE
FORME EN ENTONNOIR - FUNNEL SHAPE
FORME EN OEUF - EGG SHAPE
Lisse - Smooth
Dentelé - Serrated
Concave
Rectiligne
Convexe
Linear

Fig 1

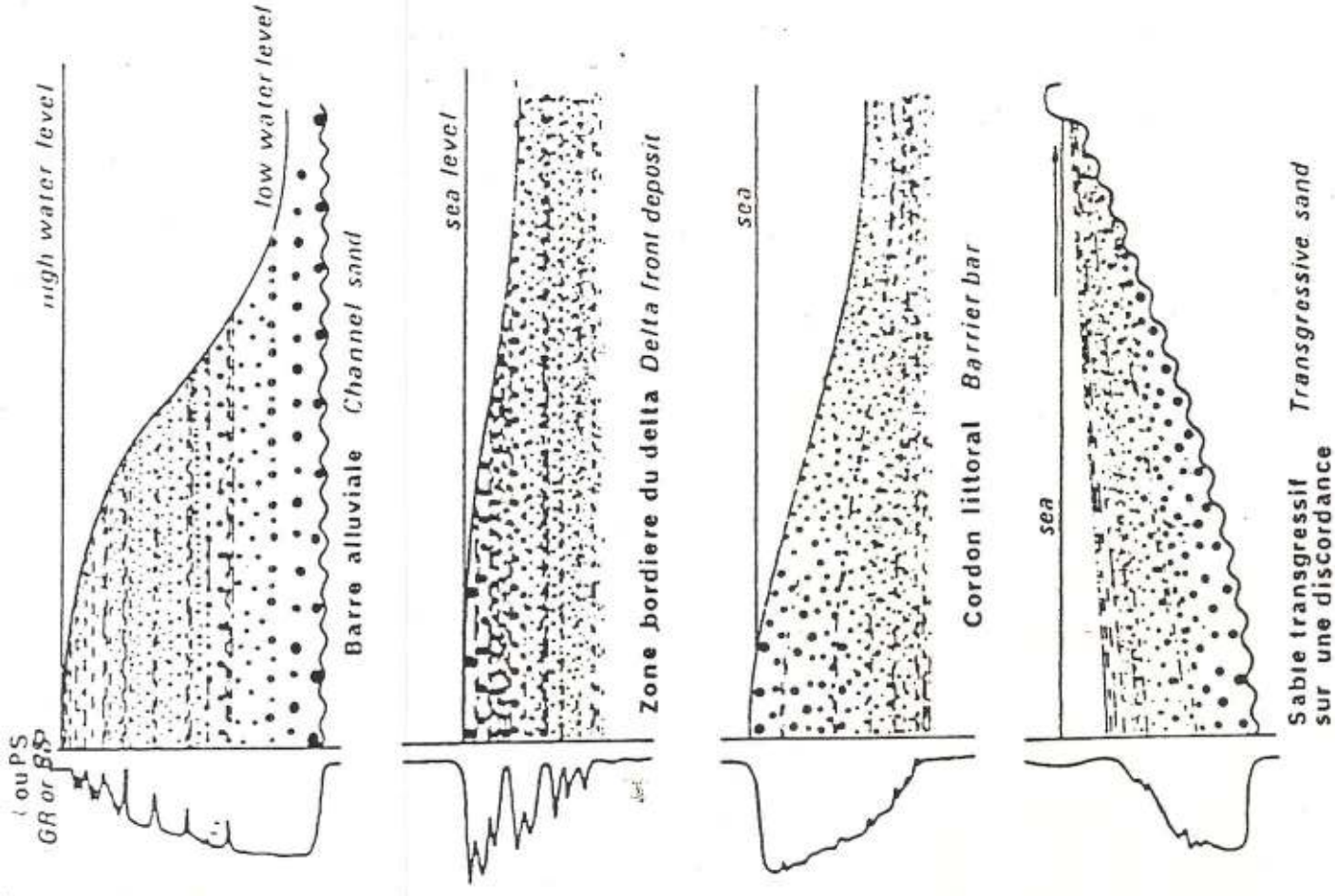
high water level
low water level
Barre alluviale Channel sand
sea level
Zone bordiere du delta Delta front deposit
sea
Cordon littoral Barrier bar
sea
Sable transgressif Transgressive sand
sur une discordance
ou PS
GR or SP

Fig 2

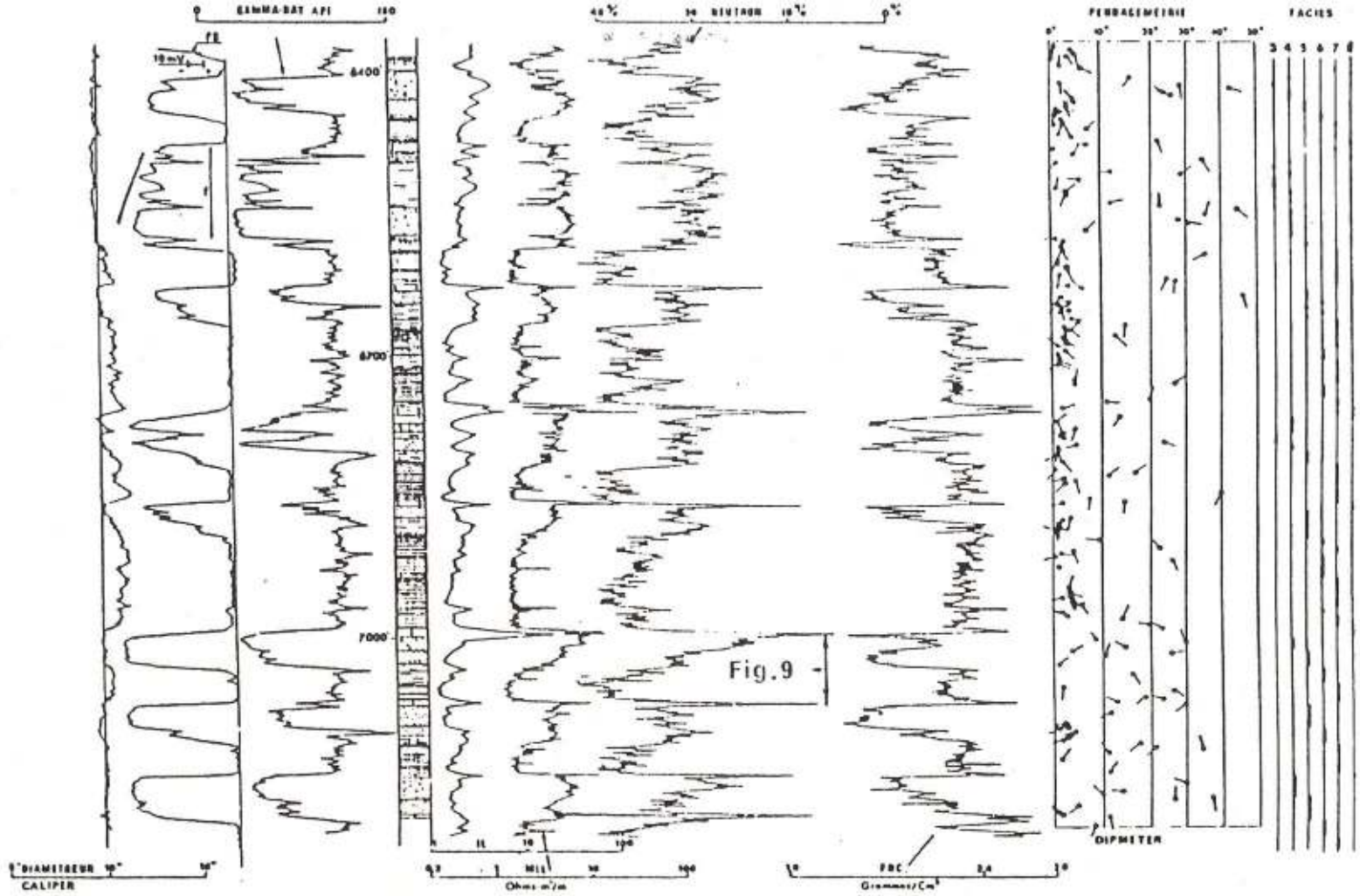
GAMMA-RAY API
NEUTRON
PENDAGEMETRIE
FACIES
DIPMETER
CALIPER
Ohms m²/m
Grammes/Cm³
Fig.9
LITHO
FACIES
SABLES HETEROGENES POREUX
HETEROGENEOUS SANDS
ARGILES HETEROGENES
HETEROGENEOUS SHALES
SABLES HOMOGENES POREUX
HOMOGENEOUS SANDS
SILT OU SABLE & ARGILEUX
SILT OR VERY FINE SANDS
SILT ARGILEUX
SHALY SILT
ARGILES SILTEUSES
SILTY SHALES
ARGILES FRANCHES HOMOGENES
HOMOGENEOUS SHALES
NIVEAUX CARBONATES
CARBONATES
LIGNITE
LIGNITE
1 - PLAINE D'INONDATION - LEVEE NATURELLE
FLOOD PLAIN - NATURAL LEVEE
2 - CHENAL FLUVIATIL - BARRE DE MEMBRE
CHANNEL - POINT BAR
3 - REPLAT DE MARE
TIDAL FLAT
4 - CHENAL DE MARE
TIDAL CHANNEL
5 - SABLES DE FRONT DE DELTA
DELTA FRONT SANDS (BARRIER BAR)
6 - PLATEFORME DELTAIQUE
BARRIER FOOT
7 - ARGILE MARINE
MARINE SHALE
8 - NIVEAUX TRANSGRESSIFS
TRANSGRESSIVE BEDS

Fig. 7

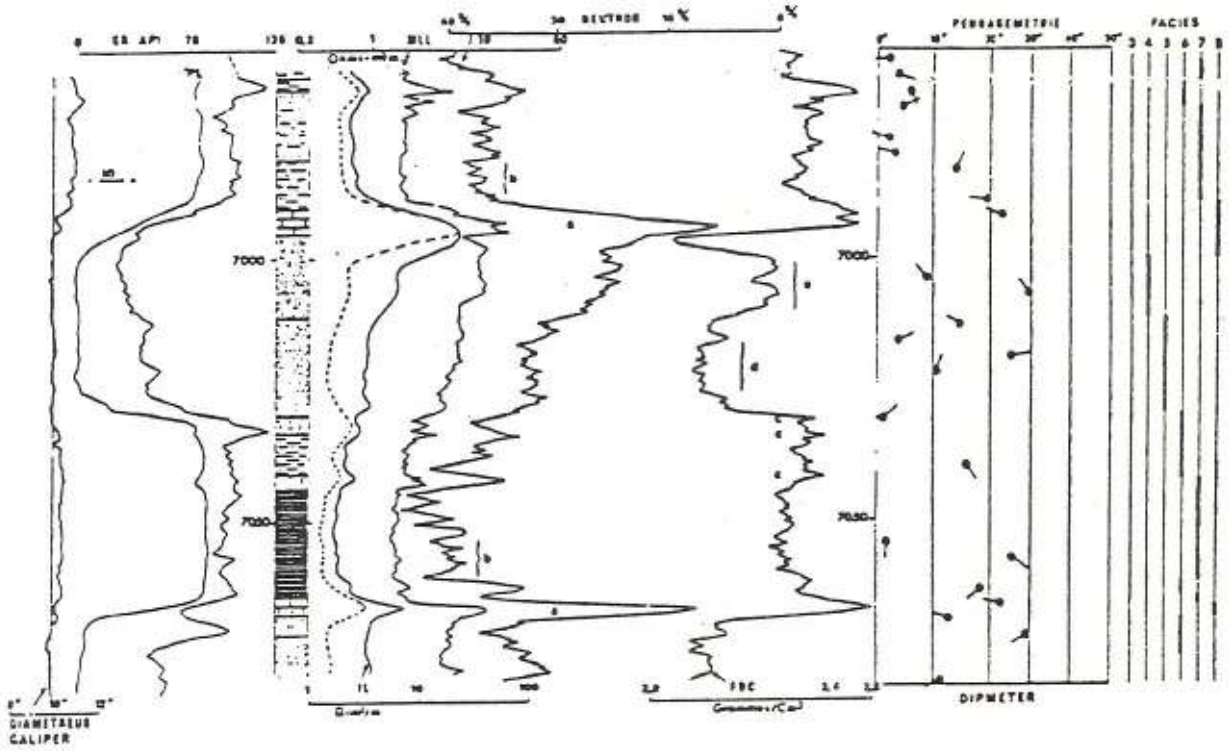
PERMEAMETRIE
FACIES
7000
7050
DIPMETER
DIAMETRE
CALIPER

Fig. 9

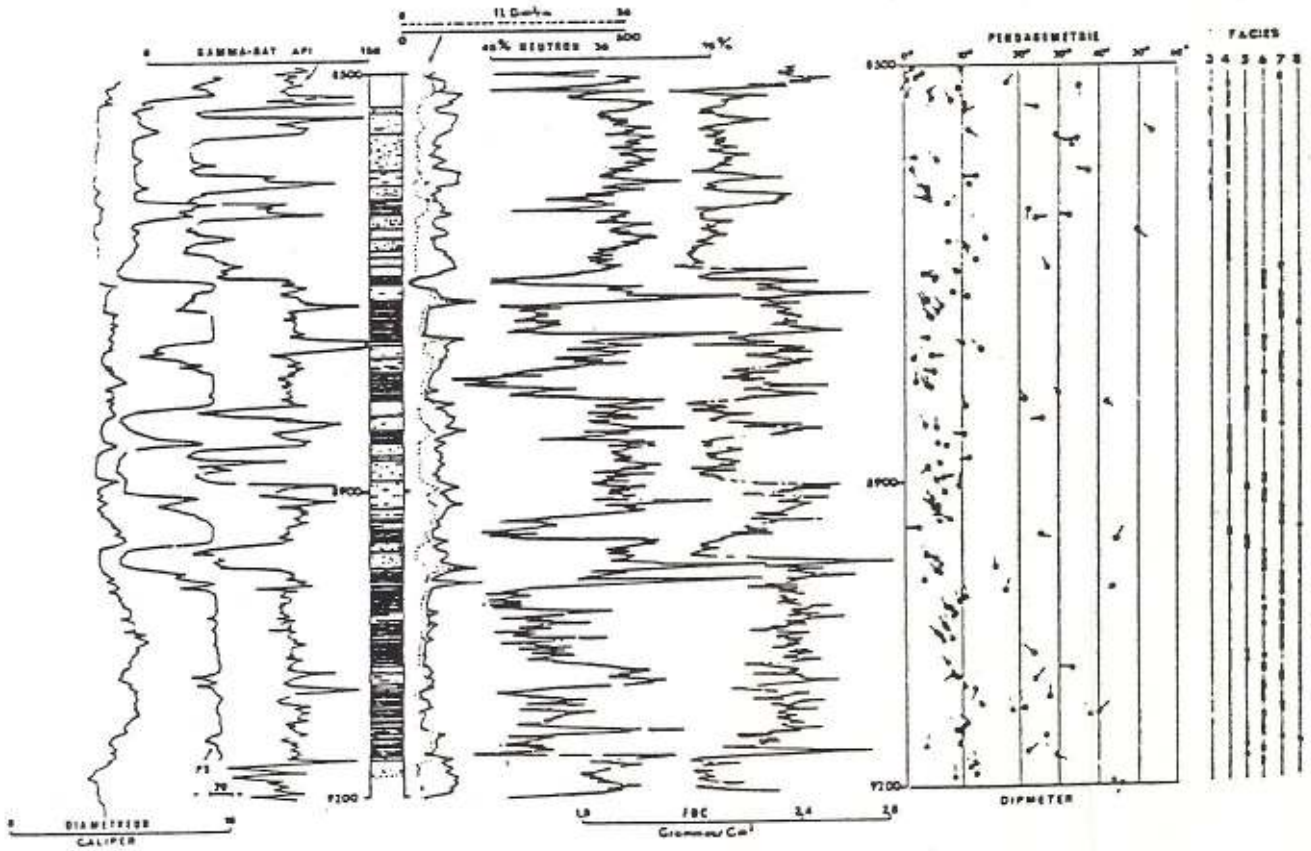
PERMEAMETRIE
FACIES
8300
8900
9200
DIPMETER
DIAMETRE
CALIPER

Fig. 10

Fig. 5

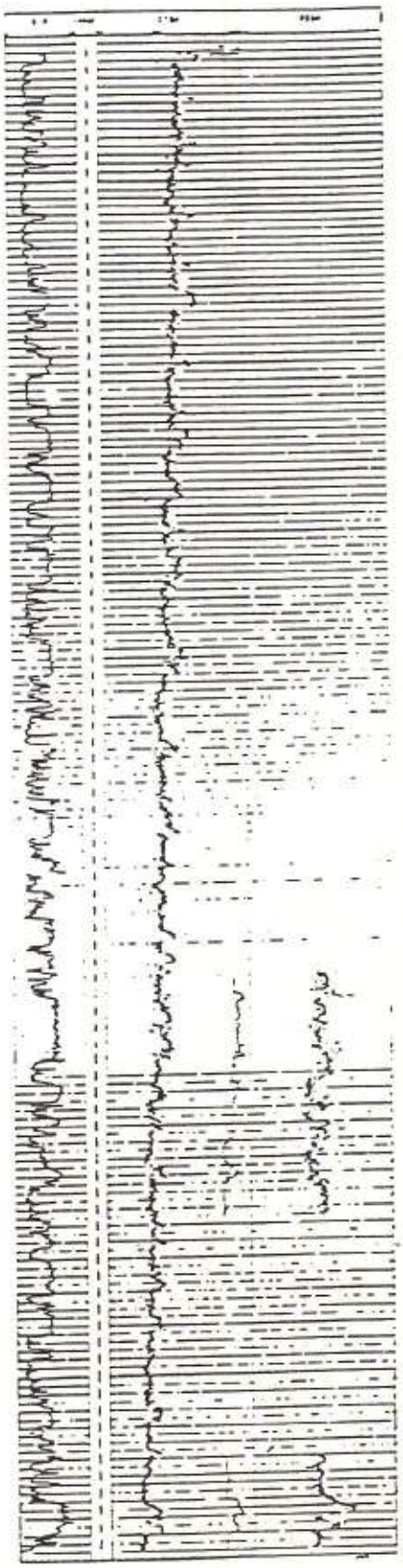

Fig. 13

6.7. SHALLOW SILICICLASTIC SEA ENVIRONMENT

6.7.1. DEFINITION

Environments characterized by detrital deposits in moderate water depth (10-200 m), or on nearshore continent (at the exclusion of deltas), under tides, waves, wind, longshore currents, or storms as dominant sediment-moving forces. They include deposits such as : estuarine, tidal ridges, tidal flats, sand waves, sand ribbons, intertidal sand bars, strand plains, barrier islands, beach ridges, cheniers, shorelines, storm deposits ("tempestites" as defined by Ager, 1974), offshore bars.

6.7.2. GEOLOGICAL FACIES MODEL

Because of the difficulties to recognize all of these environments in ancient records, only three main environments will be described and illustrated hereafter.

6.7.2.1. Tidal sand Ridges

6.7.2.1.1. *Definition*

Tidal sand ridges are elongated sand bodies formed by tidal currents.

6.7.2.1.2. *Composition*

Detrital quartz is dominant and the sand is mineralogically mature; argillaceous rock fragments, skeletal shell debris can occur especially as a basal lag conglomerate. Some glauconite and authigenic feldspar are mentioned. Peat, clay galls and wood fragments are common. Detrital and authigenic cement can be present.

6.7.2.1.3. *Texture*

Well-sorted (Fig. 6.7-1), medium-grained sand is the dominant feature, with moderate to high grain-matrix ratio. Grain size distribution across the ridges is relatively uniform. Grain size may decrease upward within a ridge, and on a regional scale in the direction of net tidal current transport.

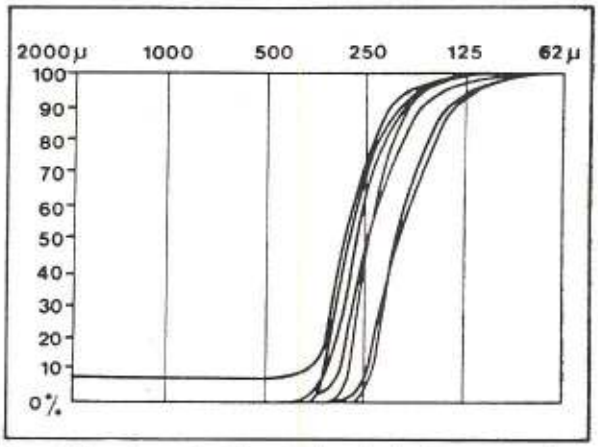

Fig. 6.7-1. - Example of grain size distribution curves from North Sea tidal sand ridges (from Houbolt, 1968).

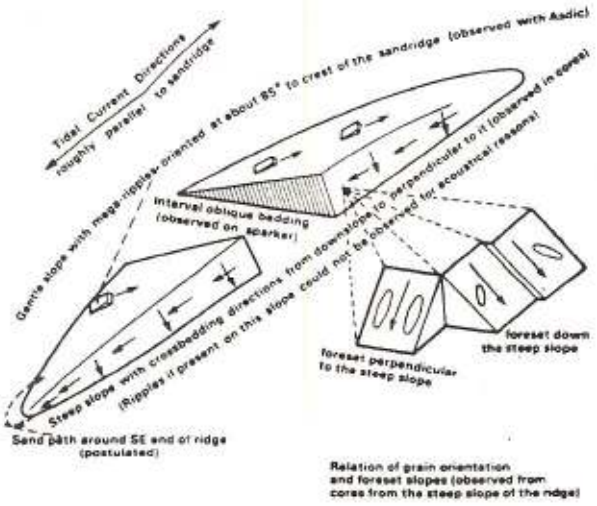

Fig. 6.7-2. - Schematic diagram of sedimentary features of a tidal ridge in the North Sea (from Houbolt, 1968).

6.7.2.1.4. *Structure*

Tidal ridges are composed of large-scale foreset beds with flanks dipping at angle of repose (30°), parallel to the steep ridge flank (Fig. 6.7-2). These cross sets are commonly draped by clay

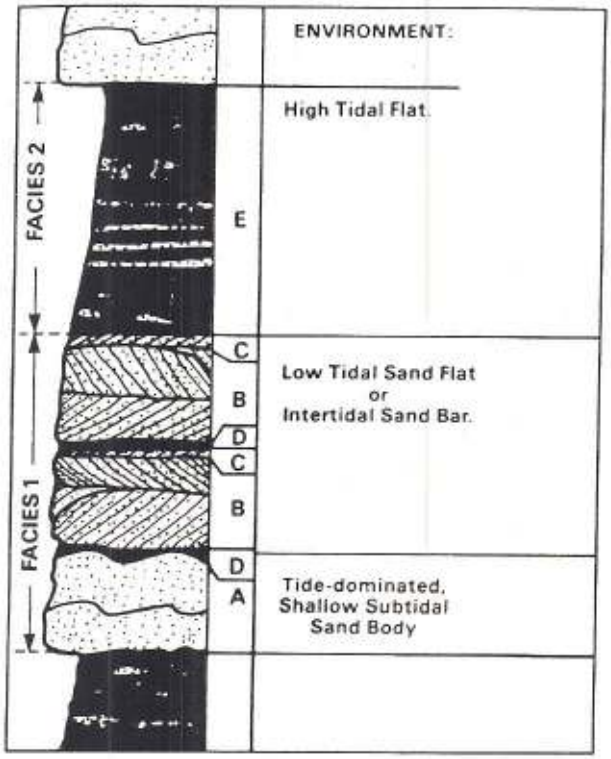

Fig. 6.7-3. - A fining upward sequence and its interpretation. This sequence includes alternation of facies 1 and 2, comprising tide-dominated shallow, subtidal sand body (massive sandstone of interval A) with basal lag conglomerate, grading into a low tidal sand flat or low tidal intertidal sand bar (cross-stratified sandstone of interval B) which has been reworked by late-stage, sheet-runoff tidal flow (sandstone of interval C), draped by clay produced by mud suspension settlement during slack water (interval D) occurring on top of both intervals A and C. Interval E consists of mudstone and siltstone with lenticular bedding, tidal bedding, and burrowing structures, all deposited in a high tidal flat environment (adapted from Klein, 1970).

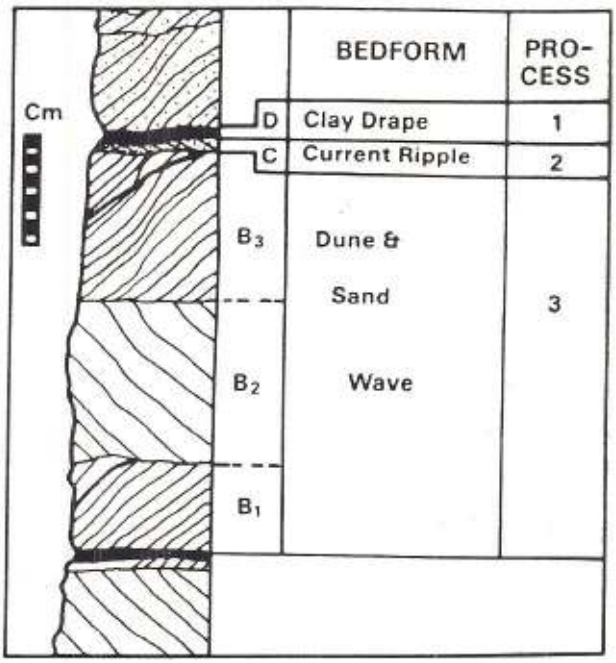

Fig. 6.7-4. - Sequence in facies 1 (see Fig. 6.7-3) showing vertical change from cross-stratified sandstone (interval B) into micro-cross-laminated sandstone with dips oriented at 90° to 180° to underlying cross-stratification dip orientation (interval C) and clay drape (interval D). Depositional processes are indicated on the side (from Klein, 1970).

laminae (mud suspension settlement during slack water : Fig. 6.7-3). Small foreset strata (sand waves) on the gentle ridge slope overlie the large cross sets. Asymmetrical ripples overlie the sand wave cross sets. Tracks, trails and burrows are abundant. A strong vertical decrease in grain size and bed thickness is generally observed.

6.7.2.1.5. *Boundaries*

An abrupt, erosional lower contact is the rule. Gradational contact toward the top is frequently observed.

6.7.2.1.6. *Sequences*

Vertical sequences within a tidal sand ridge may include (Spearing, 1971) : (1) a thin, basal lag conglomerate, rich in shell fragments, separating sand from underlying older marine clays; (2) large scale cross sets composed of well sorted sand; (3) thin, short silty-clay laminae draped over the cross sets; (4) upward grain size reduction; (5) sand wave cross sets near the top overlain by (6) asymmetrical ripple stratification. Klein (1970) recognizes sharp-based, fining upward sequences, which he interprets as shallow subtidal, tide-dominated facies which grade upward into low-tidal sand flat or low-tidal sand bar facies (Fig. 6.7-3 and 6.7-4).

6.7.2.1.7. *Geometry of the bodies*

Present day tidal sand ridges in the North Sea (Fig. 6.7-5) are long and straight, up to 40 m high, 65 km long and 5 km wide. Ridges are asymmetric in cross section with a steep lee slope and gentle stoss slope (Fig. 6.7-2).

Other associated sand bodies may exist. They are described hereafter.

Sand waves are much smaller and are oriented normal to tidal current directions. They are between 1 and 10 m high, asymmetrical, and spaced a few hundred metres apart.

Sand ribbons are elongated bodies that run parallel to the strongest tidal current flow. They are up to 15 km long, 200 m wide and not greater than 1 m thick.

Intertidal sand bars are linear, asymmetrical, about 5 to 6 km long, 1 km wide, and 6 to 10 m high. The steep slopes average 8° and gentle slopes 2°. Texture is fine to medium sand on steep bar faces. Bed forms are dominantly current ripples and dunes. Texture is medium to coarse sand on gently sloping bar faces. Bed forms are simple and complex dunes and sand waves.

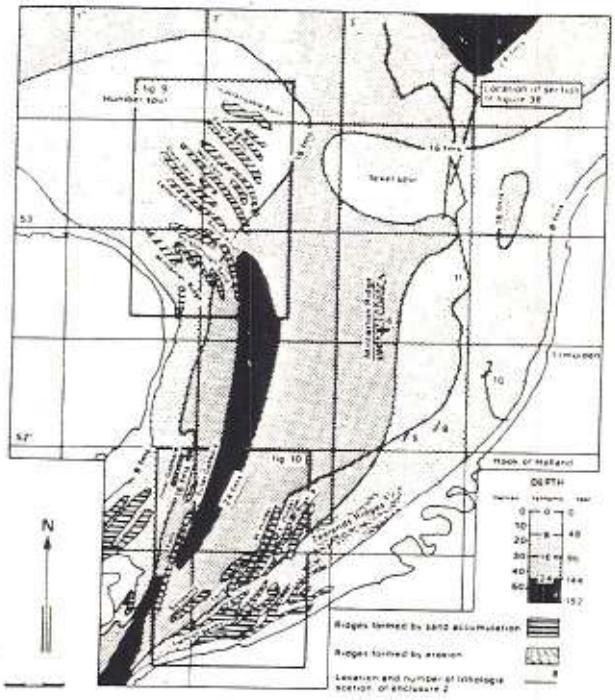

Fig. 6.7-5. - Tidal sand ridges location in the southern North Sea (from Houbolt, 1968).

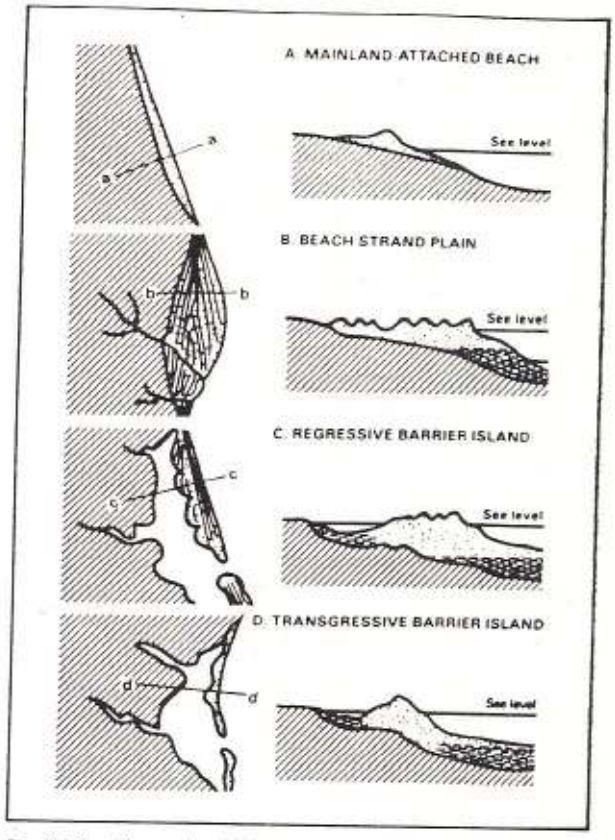

Fig. 6.7-6. - Generalized diagram illustrating the morphological relationship between beaches, strand plains and barrier islands (from Reinson, 1984).

6.7.2.1.8. *Directional current flow*

The long axis of tidal sand ridges is roughly parallel to the tidal current directions (Fig. 6.7-2).

6.7.2.1.9. *Surrounding facies*

Tidal sand ridges and other associated sand bodies (sand waves, sand ribbons and intertidal sands) may be surrounded by marine muds, tidal-flat silts and muds, barrier island, beach, or fluvial-estuarine deposits.

6.7.2.2. Clastic Shoreline, Barrier Island, and Associated Systems

6.7.2.2.1. *Definition*

According to Reinson (1984) "wave-dominated sandy shorelines in interdeltaic and non-deltaic coastal regions are characterized by elongated, shore-parallel sand deposits. These can occur as a single mainland-attached beach, a broader beach-ridge strand plain consisting of multiple parallel beach ridges and intervening swale zones or as barrier islands partially or wholly-separated from the mainland by a lagoon, estuary or marsh (Fig. 6.7-6)".

Considering a barrier island system three major geomorphic elements can be recognized (Fig. 6.7-7) : (1) the sandy barrier island chain itself; (2) the enclosed body of water behind it (lagoon or estuary); (3) the channels which cut through the barrier and connect the lagoon to the open sea (tidal inlets). They correspond to three major subenvironments : (1) the sub-tidal to sub-aerial barrier-beach complex; (2) the back-barrier region or subtidal-intertidal lagoon; and (3) the subtidal-intertidal delta and inlet-channel complex (Reinson, 1979). These subenvironments can in turn be subdivided into several zones. Their main characteristics (composition, texture, sedimentary features) are summarized in Fig. 6.7-8 and illustrated by the vertical profiles of Fig. 6.7-9 to 6.7-11.

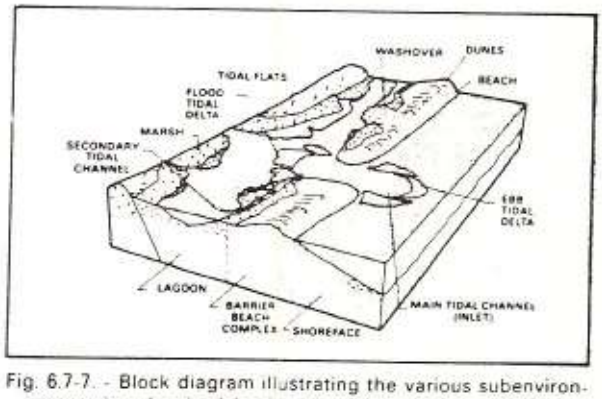

Fig. 6.7-7. - Block diagram illustrating the various subenvironments in a barrier-island system (from Reinson, 1979).

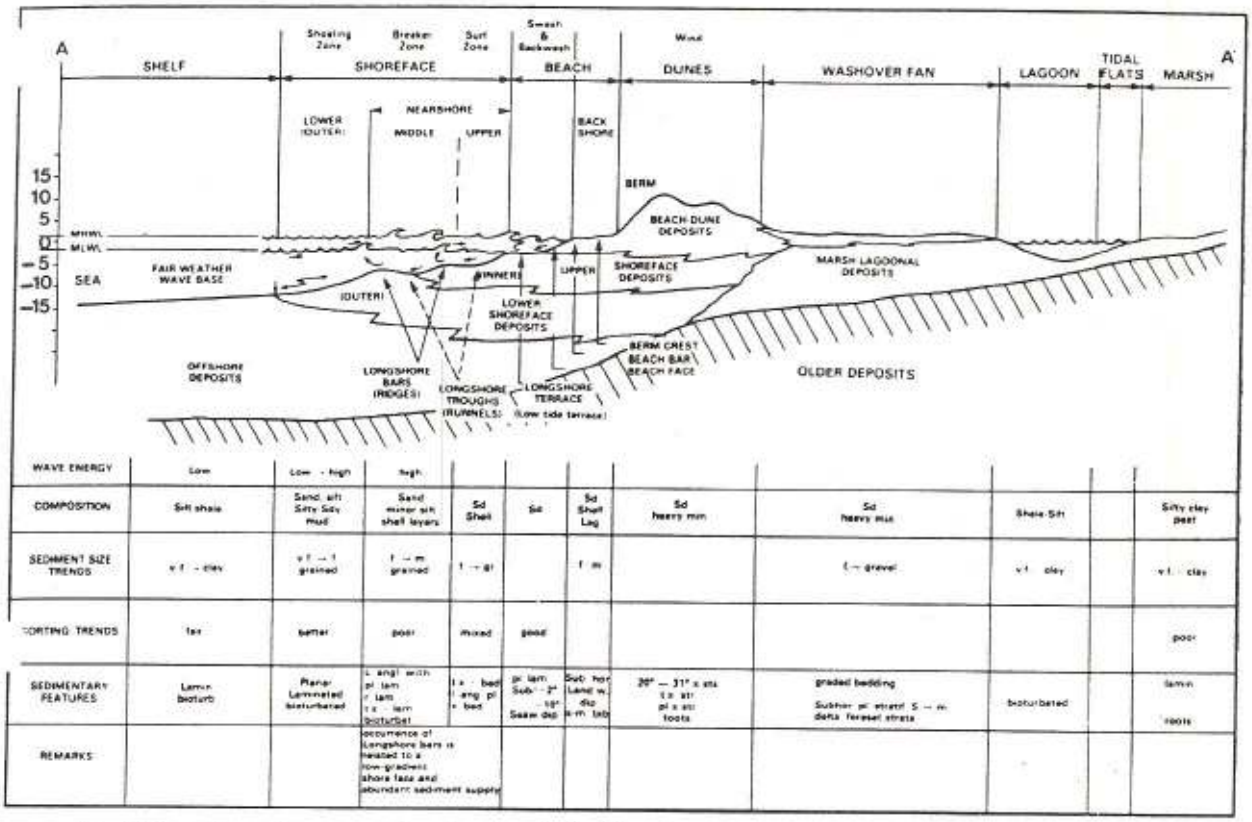

Fig. 6.7-8. - Schematic cross-section through a barrier-island system with indications of the main characteristics.

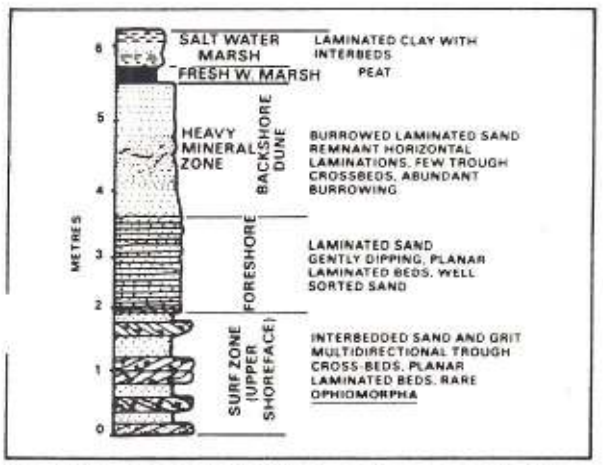

Fig. 6.7-9. - Generalized vertical profile in a barrier-island system from observations made in the Upper Tertiary Cohansey Sand of New Jersey (modified from Carter, 1978).

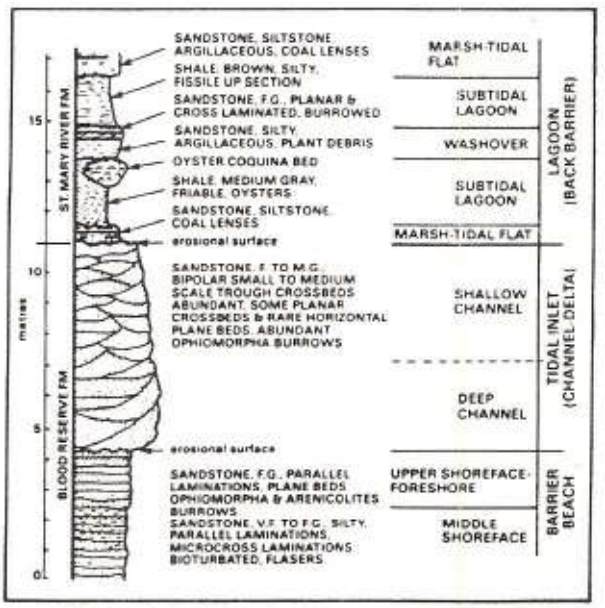

Fig. 6.7-10. - Composite stratigraphic section of the Upper Cretaceous Blood Reserve - St. Mary River Formations, Alberta, illustrating a sequence of barrier beach, tidal inlet and lagoonal deposits (from Young & Reinson, 1975).

6.7.2.2.2. *Sequences*

The general trend of barrier bar sands is coarsening upward. But following the subenvironments several more detailed lithologic, textural and sedimentary feature sequences have been described in several papers from which are extracted Fig. 6.7-12 to 6.7-16. Those figures are sufficiently explanatory to have not to develop sequence description by a long text.

6.7.2.2.3. *Geometry of the bodies*

The geometries of the bodies are schematically represented in the block diagram of Fig. 6.7-7.

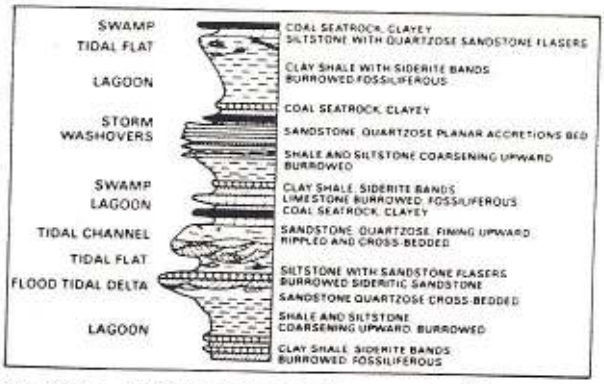

Fig. 6.7-11. - Generalized lagoonal sequence as illustrated by Carboniferous deposits of eastern Kentucky and southern Virginia (from Horne & Ferm, 1978).

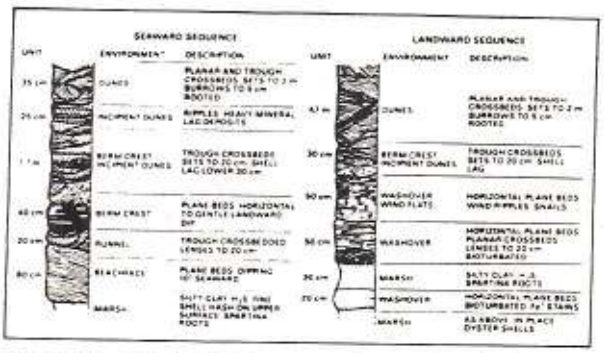

Fig. 6.7-12. - Lithological sequences observed on the landward and seaward edges of a Kiawah Island (South Carolina) beach ridge (from Barwis, 1978).

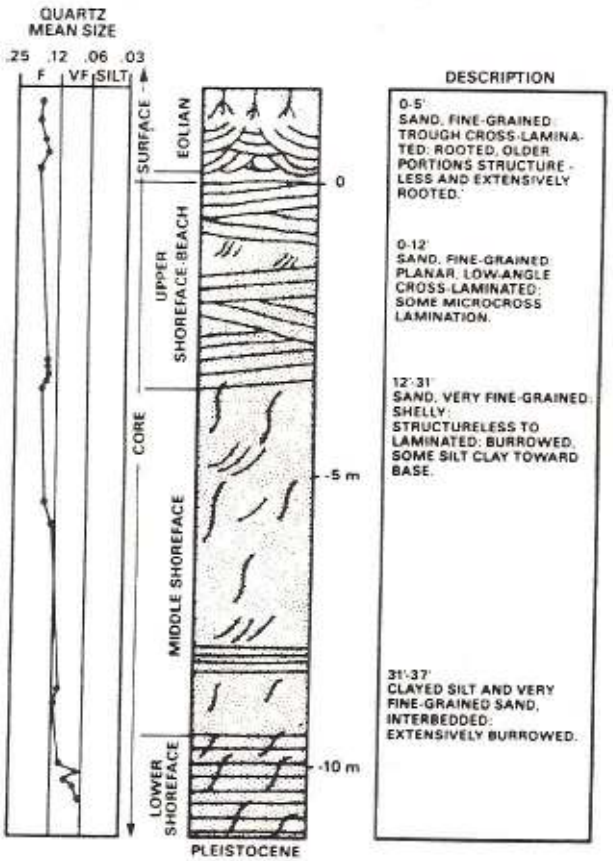

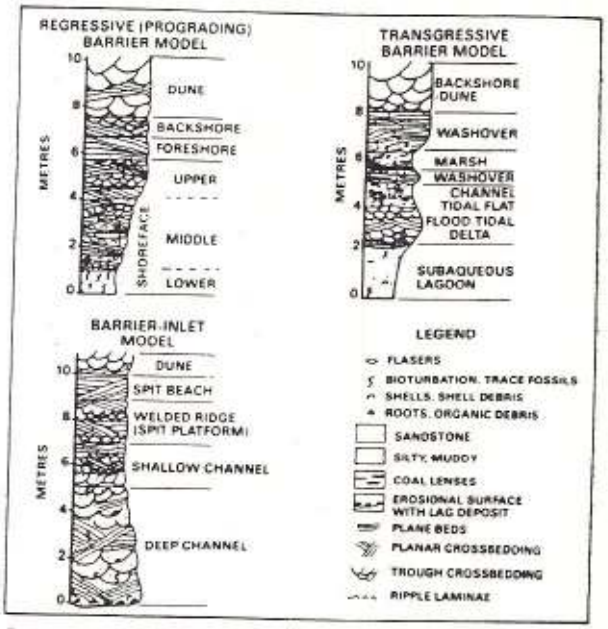

Fig. 6.7-14. - Three "end-member" facies models of barrier island stratigraphic sequences (from Reinson, 1979).

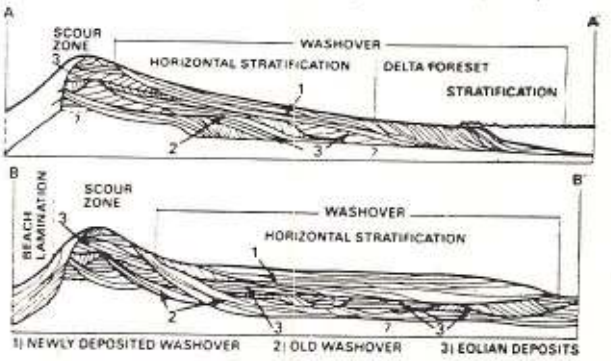

Fig. 6.7-15. - Two sequences of sedimentary structures through washover fans (from Schwartz, 1973).

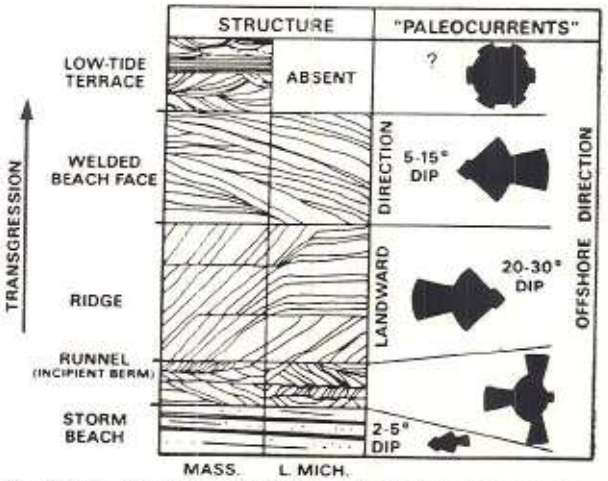

Fig. 6.7-16. - Transgressive sequence formed by the landward migration of ridge-and-runnel during beach construction phase. Vertical sequence would be about 1 m thick (from Davis *et al.*, 1972).

◄ Fig. 6.7-13. - Sequences of sedimentary structures, textures and lithology in a core through Galveston Island (from Davies *et al.*, 1971).

6.7.2.3. Linear Submarine sand Bars

6.7.2.3.1. *Definition*

They correspond to isolated elongated sand ridge, in a shallow marine environment (subtidal), occurring at some distance from, and extending generally parallel with, the shoreline, built chiefly by tidal, oceanic, storm- or wave-generated currents (Fig. 6.7-17).

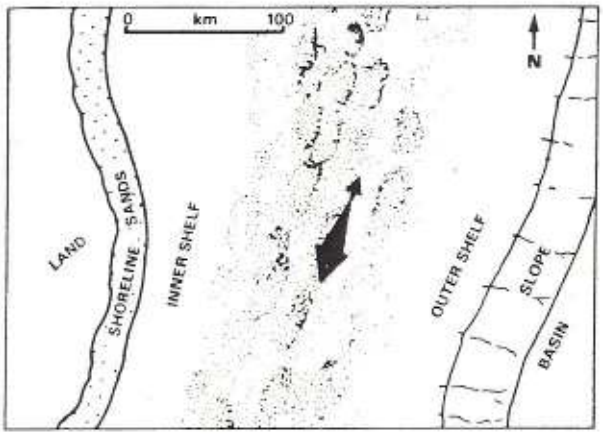

Fig. 6.7-17. - Hypothetical palaeogeographic reconstruction showing Shannon sand patches migrating south-southwest parallel to the shoreline (from Spearing, 1976).

6.7.2.3.2. *Composition*

Sand deposits of this environment are composed of quartz, shell debris, glauconite, chamosite (iron silicate) associated with limonite (or haematite) oolites or siderite, and phosphates.

6.7.2.3.3. *Texture*

The deposits have a textural maturity due to long periods of transport with winnowing of fines. Consequently the sands are well sorted.

6.7.2.3.4. *Structure*

Sedimentary structures are rarely environmentally diagnostic. Lenticular, wavy and flaser bedding, cross laminations, cross- and horizontal bedding are described. Bioturbation is minor.

6.7.2.3.5. *Boundaries*

The lower contact of the sequence is abrupt.

6.7.2.3.6. *Sequence*

The general sequence is coarsening upward (Fig. 6.7-18). It is composed of bioturbated mudstone and silty sandstone at the base, overlain by ripple cross-laminated fine-grained sandstone, capped by large-scale festoon cross-bedded, medium-grained sandstone. Bioclastic rich units form thin sheetlike units with erosional bases.

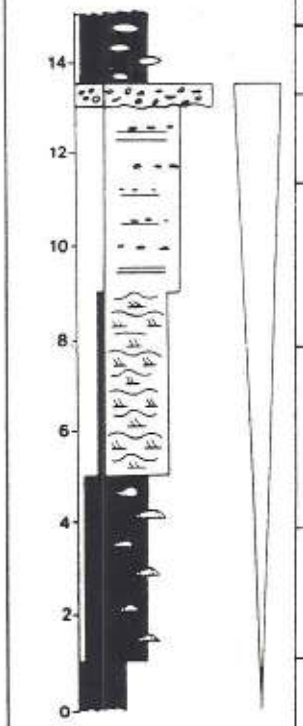

Units of Berg, 1975	Thickness	Description	Interpretation of the Facis	Interpretation of the Sequence
1	1.5-2.5 m	Bioturbated muds with reworked sand & granules. Horizontal bedding	Shelf muds with storm deposited sand layers.	Sudden cessation of active sand transport. Shelf muds blanket the linear sand bars
2	0.30-1.0 m	Pebbly sandstone with chert & mudstone pebbles. Chert pebbles concentrated in top layer.	Wave reworked sands. Related to wave processes concentrated on bar crest	Gradual increase in wave & current activity in response to a prograding linear tidal (?) sand body. Elongate geometry of several sand bodies parallel to shoreline & to current transport path suggests they may represent linear tidal (?) sand ridges which formed topographic highs. Coarsening upward sequence reflects both progradation & preferential reworking of bar crest & flanks
3	1.5-5.5m	Cross bedded & flat bedded sandstone. Cross bed sets ca. 5-20 cm thick. Numerous mudflakes & occasional mud-drapes. Rare cross-laminated sands	SE (?) migration of dunes in response to tidal currents, possibly enhanced by storms. Abundant penecontemporaneous erosion of mud. Sands deposited on upper bar flanks.	
4	1.8-5.0 m	Cross laminated fine grained sandstone with numerous mud-drapes. Occasional mudflakes & cross-bed sets. Minor bioturbation.	Deposition by current ripples in response to tidal (?) currents. Currents of fluctuating strength. Abundant fine grained suspended sediment. Deposition on lower bar flanks & troughs.	
5	0.9-4.0 m	Muds with rippled sandstone lenses & sandstone interbeds 1-5 cm thick. Minor bioturbation.	Suspension deposition of muds alternating with periodic sand influxes (? distal storm layers). Deposition downcurrent of the sand bars.	
		Massive marine muds but with little bioturbation.	Shelf muds.	

Fig. 6.7-18. - Description and interpretation of the Upper Cretaceous Sussex Sandstone, Wyoming (from Berg, 1975)

6.7.2.3.7. *Geometry of the body*

The sandstone bodies are elongate, between 3-30 m thick, 4-60 km wide and up to 160 km long, have planar bases and convex-upward tops.

6.7.2.3.8. *Direction of current transport*

The current is generally unidirectional parallel to the bar crest.

6.7.2.3.9. *Surrounding facies*

The linear sand bars are either surrounded by, or interfinger with, marine muds.

6.7.2.4. **Reservoir Characteristics**

Sand bodies have, generally, good reservoir characteristics but their volume is limited.

6.7.3. WELL-LOG RESPONSES AND CHARACTERISTICS

It is not always easy to distinguish between the shallow siliciclastic and the deltaic environments. Consequently, only some of the previously described deposits will be illustrated by examples of composite-logs and dipmeter results.

The first example is taken in the Muddy Formation, Granerous Group, Powder River Basin, Wyoming. This formation is sometimes and somewhere (Bell Creek Field, Montana) described as a typical ancient barrier island (Davies *et al.*, 1971). The composite-log (including gamma ray, neutron and density logs) of one well (no location reference) is given in Fig. 6.7-19b. From the shape of traditional open-hole logs a coarsening upward sequence followed by a fining upward seems quite evident. Now, by looking at in detail the LOCDIP arrow-plot (obtained from SHDT, Fig. 6.7-20b), several abrupt lower contacts followed by fining upward sequences appear clearly. An interpretation of the dipmeter has been done following the barrier island hypothesis. But some of the observations which can be done on the dipmeter (abrupt lower contacts, fining upward sequences, thin shale drapes) do not fit completely with the general continuous coarsening upward trend described in barrier island. Consequently, another interpretation, based on a tidal sand ridge hypothesis (Klein, 1970), can be proposed (compare with Fig. 6.7-3).

A second example is from the Shannon Sandstone in the Hartzog Draw Field, Powder River Basin, Wyoming. The composite-log (including SP, gamma ray, neutron, density, sonic, DIL-SFL and GEODIP arrow-plot) is reproduced in Fig. 6.7-21 alongside the core description and the interpretation in terms of facies and subenvironments. A general coarsening upward sequence is observed as expected in a linear submarine sand bar. Low ϕ_D peaks (9387, 9395 ft) correspond to levels richer in

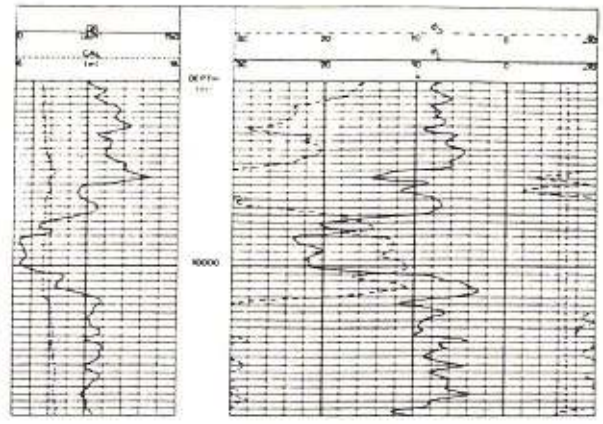

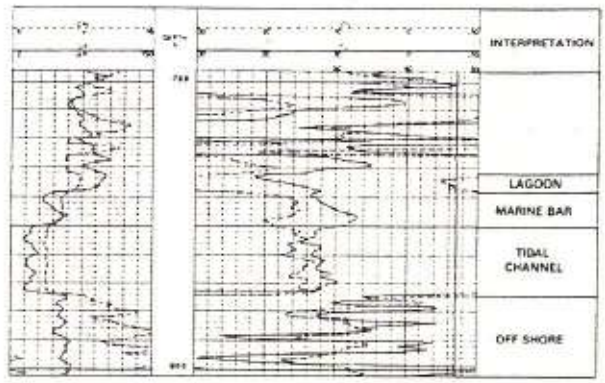

Fig. 6.7-19. - Two composite-logs of the Muddy Formation, Powder River Basin.

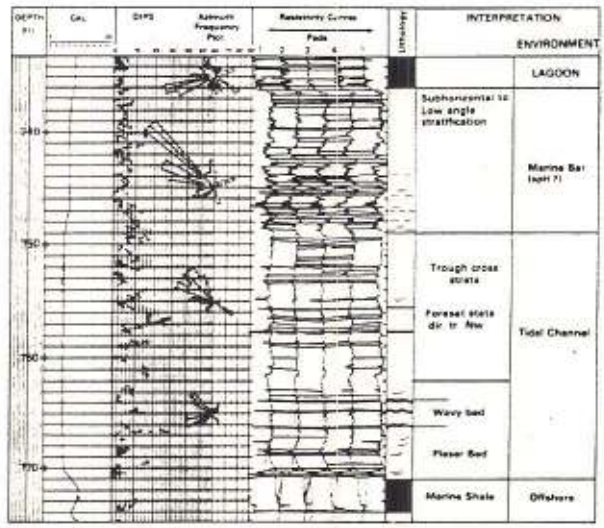

Fig. 6.7-20a. - GEODIP arrow-plot of the Muddy Formation in the well represented by the composite-log 6.7-19a, and its interpretation in terms of facies and environment.

siderite and glauconite (confirmed by core analysis). The analysis of the GEODIP arrow-plot (low sand character option) at an expanded scale (Fig. 6.7-22 to 6.7-24) permits a more detailed observation. The lower interval (9443-9412.5 ft) is very

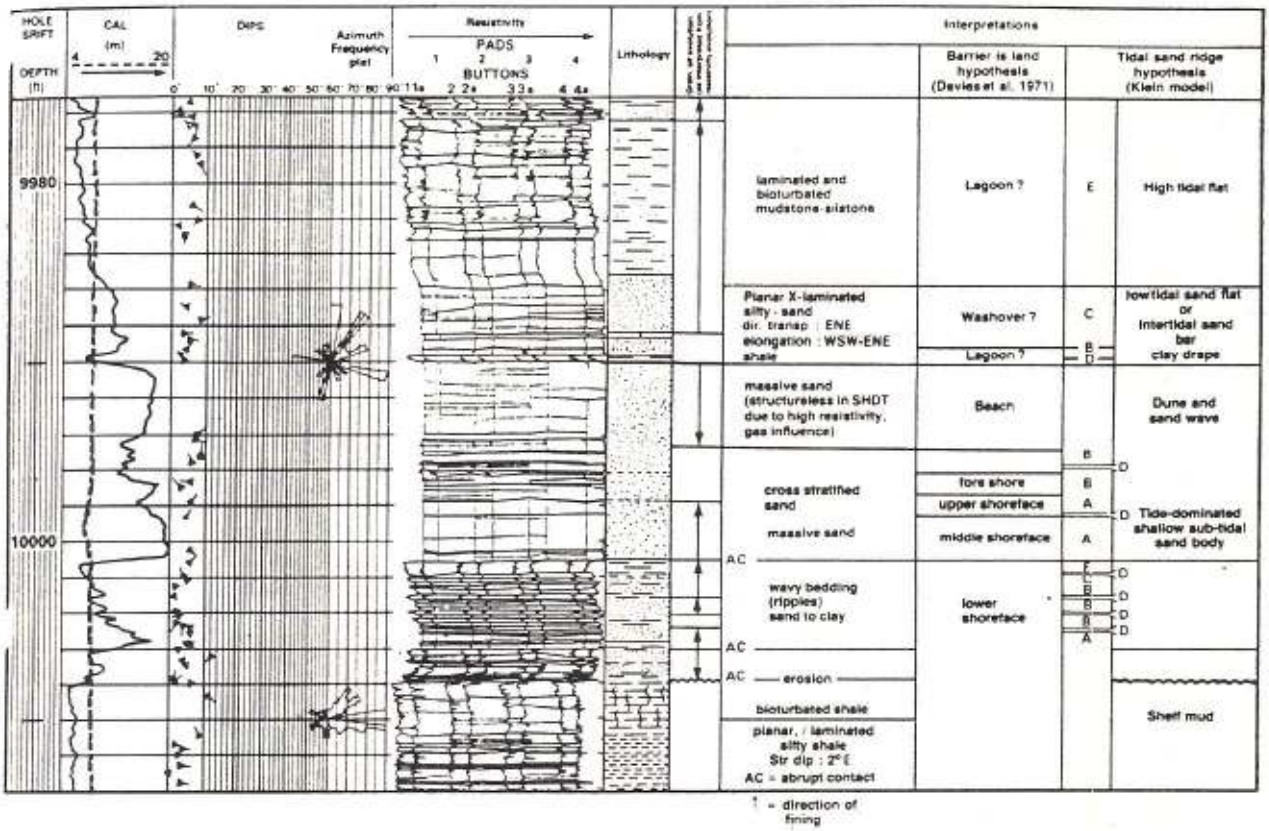

Fig. 6.7-20b. - LOCDIP arrow-plot of the Muddy Formation in the well represented by the composite-log 6.7-19b, and its interpretation in terms of facies and environment.

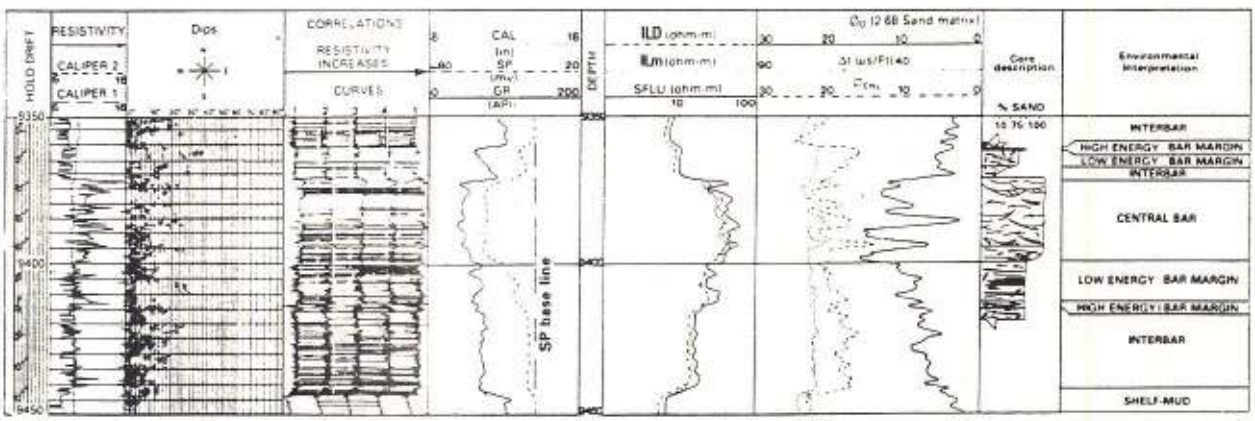

Fig. 6.7-21. - Composite-log of the Shannon Sandstone in the Hartzog Draw Field.

laminated on the HDT resistivity curves (a lot of very thin events) at a medium resistivity level, generating a lot of dips with scattered azimuth (observe the azimuth frequency plots), with low SP deflection, moderate radioactivity. In some places an erratic aspect of the curves can be observed. It could reflect some bioturbations. All these observations suggest a very thinly laminated, sometimes bioturbated interval, with small lenses (uncorrelated events seen only on one or two curves), with a relatively high clay percentage. Consequently one can deduce numerous intercalations of thin silt or sand beds (corresponding to more resistive continuous events) in the shale. This is confirmed by core photographs (Fig. 6.7-22). The following interval (9413-9400 ft) is more resistive, with a higher SP deflection (lower shale content), and slightly less radioactivity. On the dipmeter resisti-

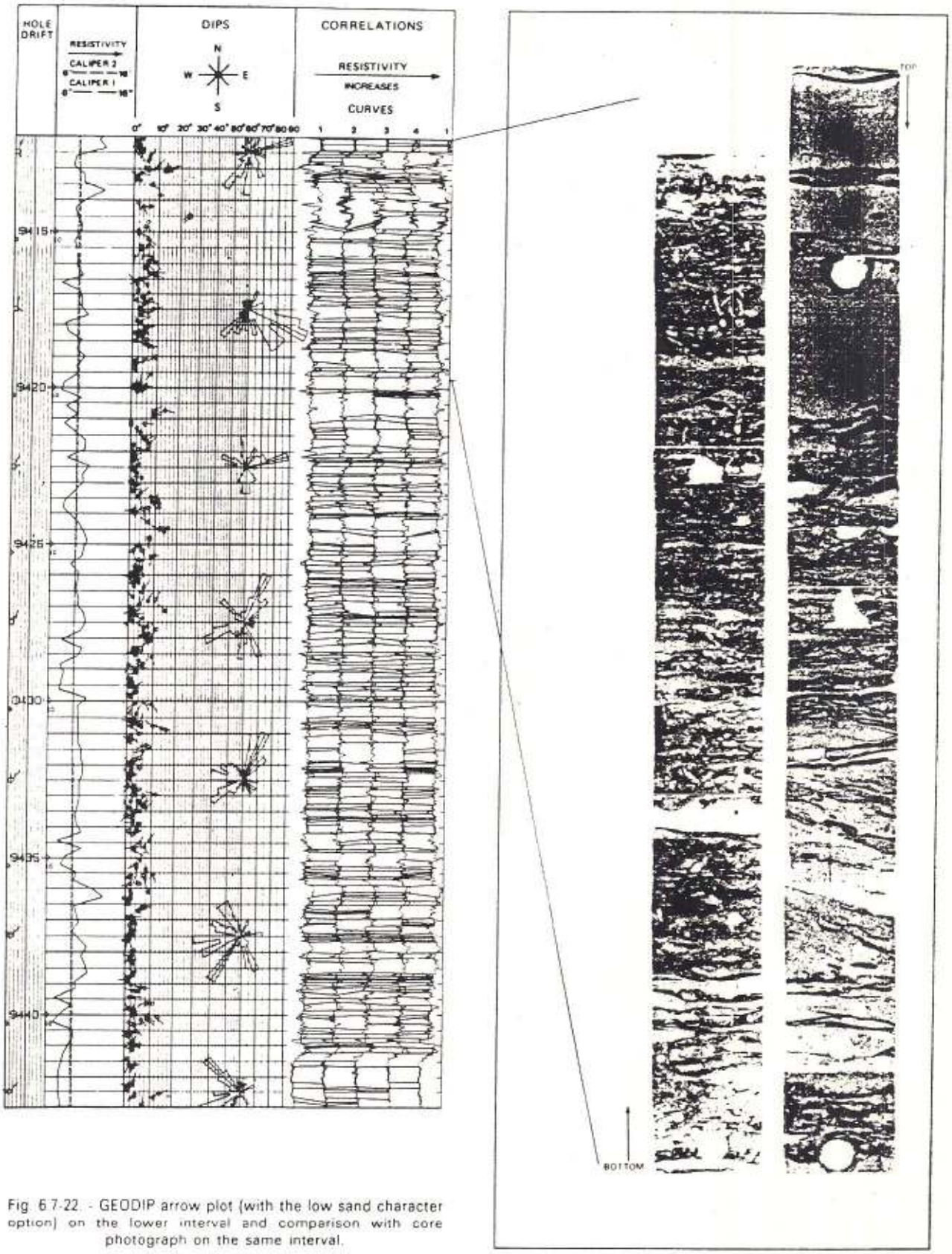

Fig. 6.7-22. - GEODIP arrow plot (with the low sand character option) on the lower interval and comparison with core photograph on the same interval.

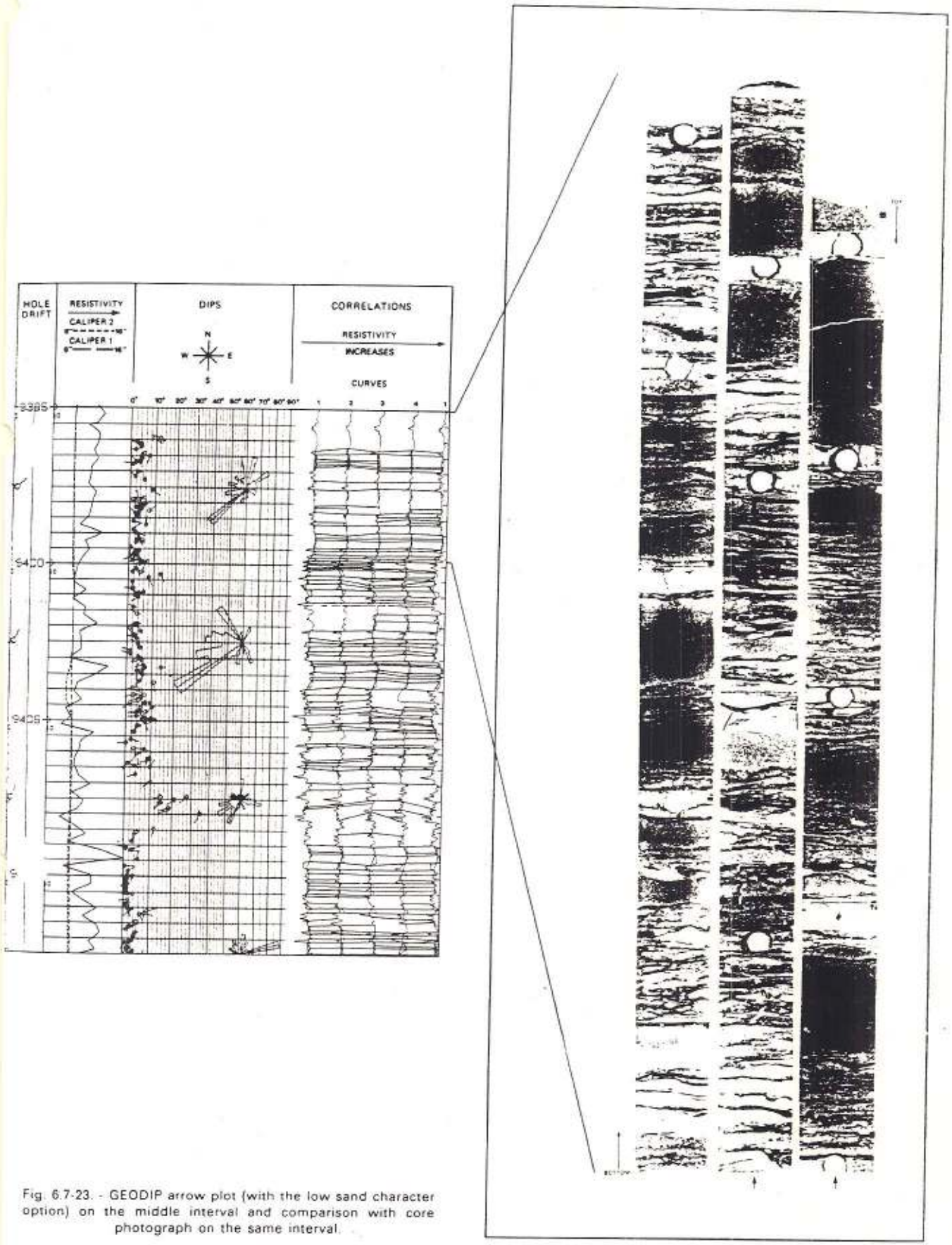

Fig. 6.7-23. - GEODIP arrow plot (with the low sand character option) on the middle interval and comparison with core photograph on the same interval.

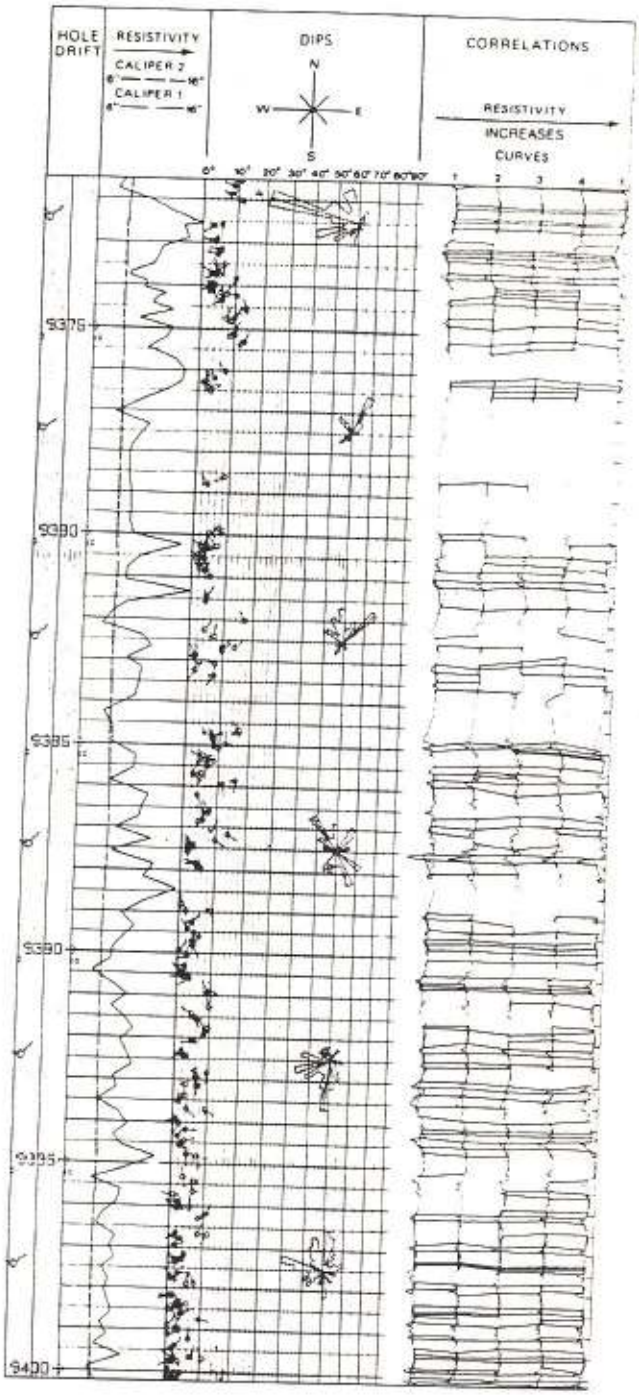

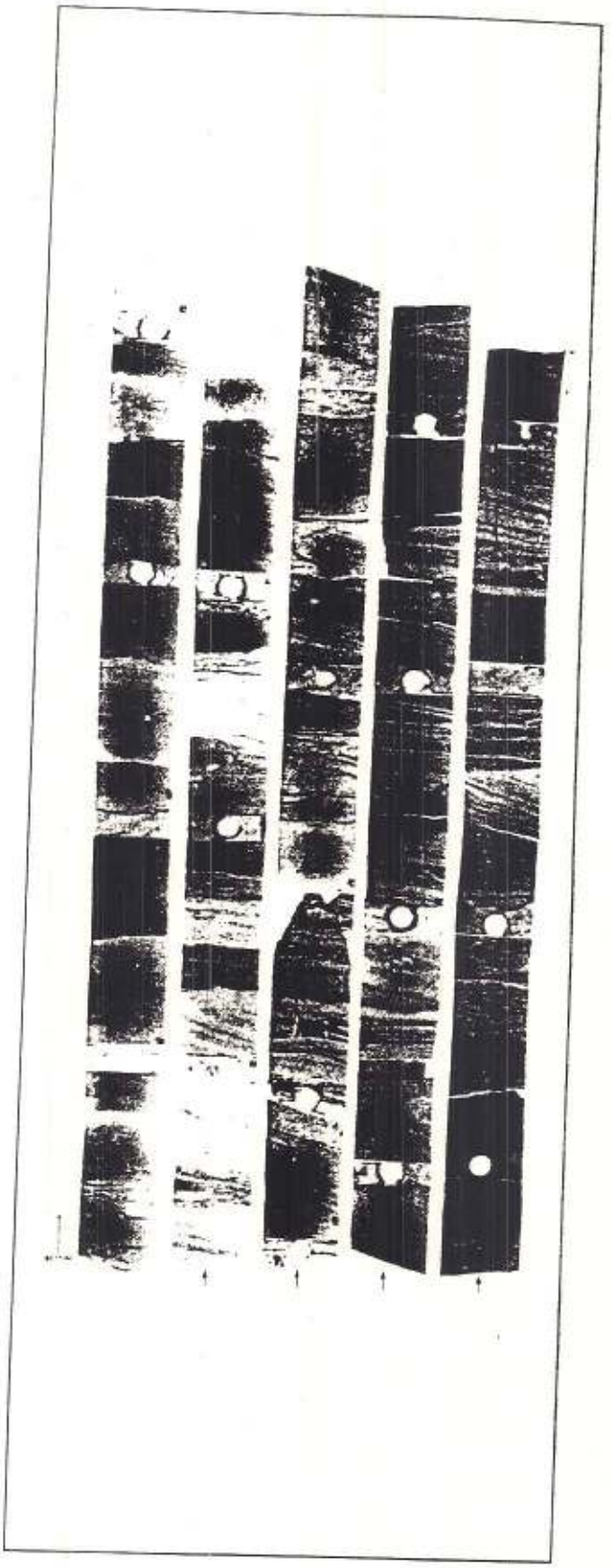

Fig. 6.7-24. - GEODIP arrow plot (with the low sand character option) on the upper interval and comparison with core photograph on the same interval.

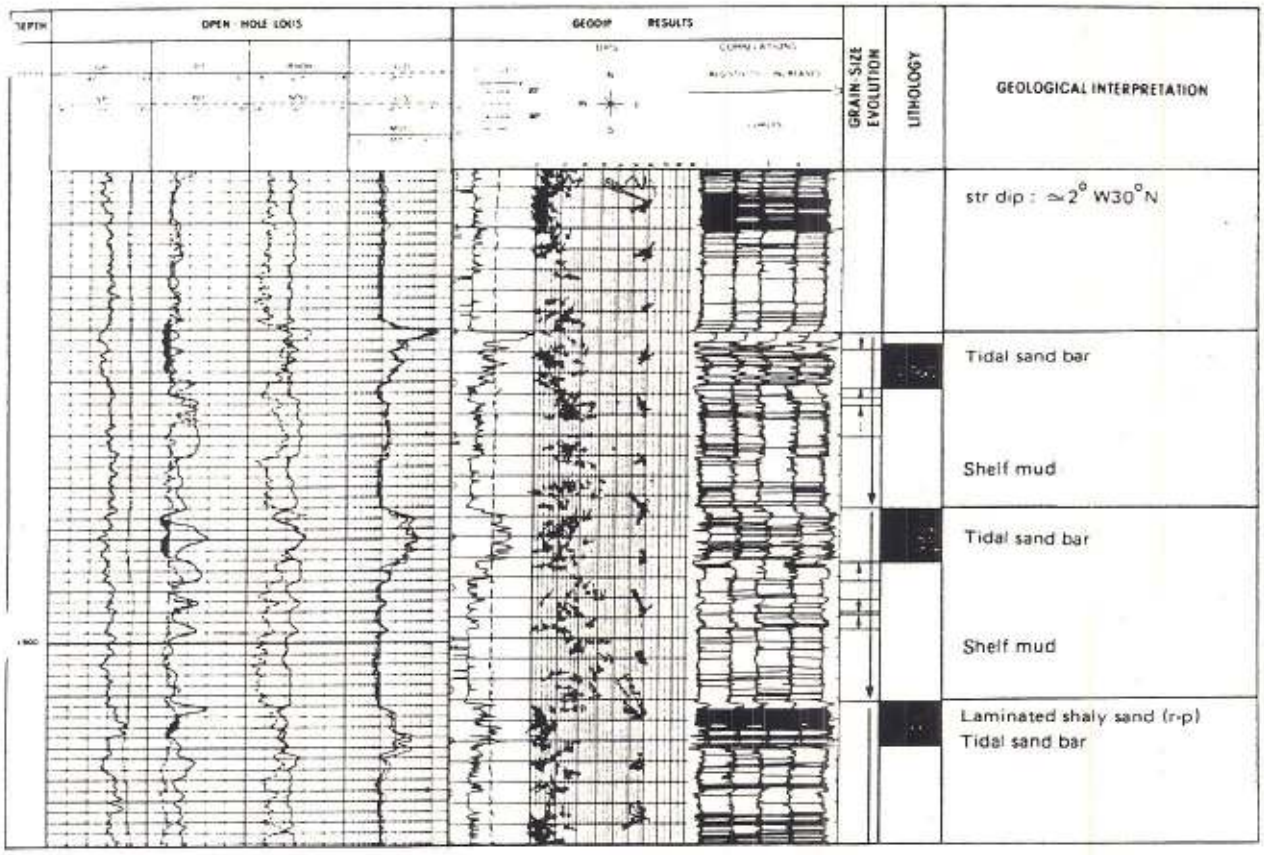

▲ Fig. 6.7-25. - Composite-log of three submarine sand bars in the Godavari Basin, India, and its interpretation (from Schlumberger, Well Evaluation Conference. India, 1983).

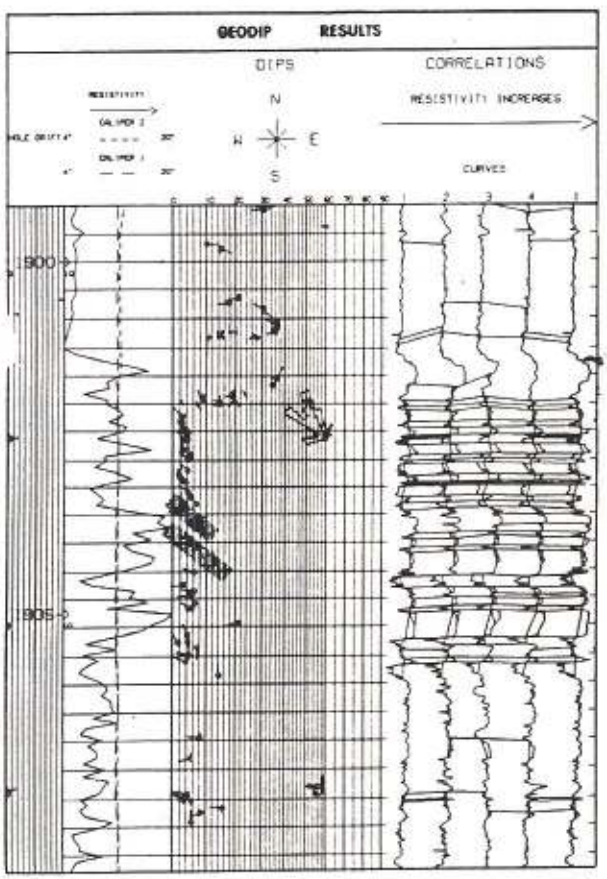

◀ Fig. 6.7-26. - GEODIP arrow plot of the lower sand at an expanded scale (from Schlumberger, Well Evaluation Conference. India, 1983).

Fig. 6.7-27. - Crossplot ρ_b vs ϕ_N showing the shale-silt-sand trend (boomerang shape) and the sandstones rich in shell fragments (from Schlumberger, Well Evaluation Conference. India, 1983). ▼

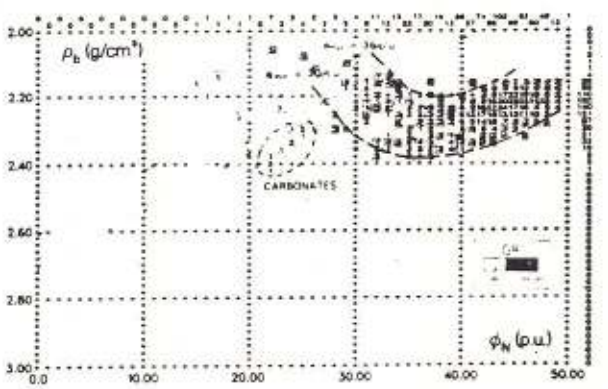

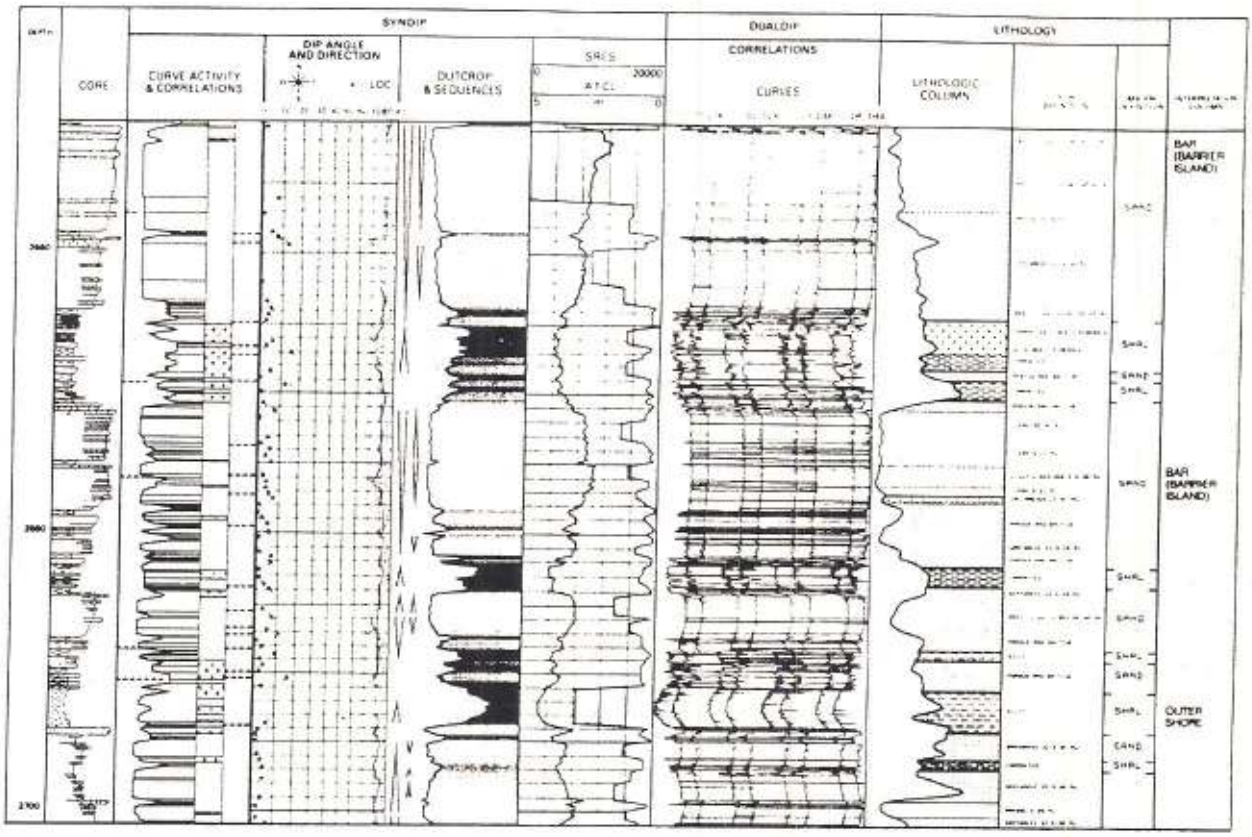

Fig. 6.7-28. - Interpretation of the studied sequences from LITHO, LOCDIP and SYNDIP results (from Schlumberger, Well Evaluation Conference. Nigeria, 1985).

vity curves, resistive beds are thicker and more continuous, with very thin conductive levels (shale laminae), which, when they are correlated, generate dips with variable magnitude (between 0° and 14°) and scattered azimuth, suggesting wavy bedding and sometimes flaser bedding when events are not seen on all curves (Fig. 6.7-23). Some blue and red patterns occur which can correspond to foresets or cut and fill features. The overlying interval (9400-9372 ft) is characterized by thicker resistive beds, with less frequent conductive levels, high SP deflection and lower radioactivity (Fig. 6.7-24). The top interval is more resistive (cemented) and is overlapped by gradually less resistive thin levels. The dips suggest a draping of the previous deposit (bar).

Another example is extracted from the Godavari Basin (India) and represented by the composite-log of Fig. 6.7-25 (GR-LDT-CNL-BHC-DLL-MSFL-SP and GEODIP at 1/200 scale), and the enlarged GEODIP arrow-plot on the lower interval (Fig. 6.7-26). Log evolutions suggest three coarsening upward sequences from shale to sand as interpreted from the ρ_b vs ϕ_N crossplot (Fig. 6.7-27). The thickness of each sequence is roughly 17 to 18 metres. Some thin limestone beds are present and confirmed by Pe values. They may correspond to sandstones very rich in shell fragments. The top of the two upper sand bodies is gas bearing. The direction of transport, as interpreted from the blue patterns, is N to NNW, giving the long axis orientation of the submarine bar.

The last example is from Nigeria. LOCDIP, SYNDIP and LITHO programs have been processed on one well on which a core description was available. The typical features of barrier bar can easily be observed (Fig. 6.7-28).

A case history : "TURBIDITES RECOGNIZED THROUGH DIPMETER"

by { Xavier PAYRE (1)
Oberto SERRA (2)

A B S T R A C T

The comparison between cores and dipmeter microconductivity curves reveals turbidites in two boreholed formations. The association of a particular turbidite sequence with the corresponding character of curves has allowed to recognize the same sequences without any use of the cores. Verifications made afterwards prove the validity of the method.

The study of the curves at a detailed depth scale (1/5) for a particular sequence shows the quality of recording made by H.D.T. : parts of the sequence are easily determined thanks to evolution of the density of optical and computed correlations (determined by GEODIP) with the depth.

---

(1) Mining Engineer (Ecole des Mines de Paris)

(2) SNEA(P) now Schlumberger Technical Services (Paris)

TURBIDITES RECOGNIZED THROUGH DIPMETER

XAVIER PAYRE[1] AND OBERTO SERRA[2]

1) DEFINITION OF THE TURBIDITES

1.1.) Introduction

Turbidites are those types of sedimentary rocks deposited by a turbidity current (fig. 1) the definition of which is :

> "density current..., caused by different amount of matter in suspension ; specifically a bottom-flowing current laden with suspended sediment, moving swiftly (under the influence of gravity) down a subaqueous slope and spreading horizontally on the floor of the body of the water, having been set and/or maintained in motion by locally churned - or stirred-up sediment that gives the water a density greater than that of the surrounding or overlying clear water..." (in Glossary of Geology).

Several figures (fig. 2 to 5) borrowed from sedimentologists who have worked on the submarine fan deposits or turbidites are enclosed to explain and illustrate briefly those sedimentary rocks and the way by which they have been deposited.

The figure 5 shows the complete "Bouma sequence" -or cycle- of a turbidite unit as described by Bouma (1962), a dutch sedimentologist.

In the ideal complete model of the Bouma sequence, five zones and several characteristic features can be described.

(1) *Mining Engineer (École des Mines de Paris).*

(2) *SNEA(T) at the time of those studies ; now with Services Techniques Schlumberger(Paris,*

2) EXAMPLES

1° First well

It is located in the Aquitaine Bassin.

The interval (2100-2170m) corresponds to an Eocene formation the composite log response of which is shown by figure 6. The interpretation of the upper part of the interval indicates a succession of porous (Ø ≃ 18 p.u.)sandstones with intercalations of tight sandstones (Ø between 1 and 7 p.u.) sometimes a little shaly or limy (fig. 7). The microlog proximity log analysis shows several sequences, (fig. 8) the sedimentological interpretation of which is not clear.

By adding the Geodip output and the simultaneous analyse of curves and dips (fig 9, 10, 11) we find approximately the same sequences and we can recognize that almost each of them, between 2142 and 2110m, starts by an abrupt contact, overlaid by an erratic interval, which can correspond to a conglomerate, itself overlaid by a massive unit, showing sometimes a progressive evolution on resistivity curves suggesting a graded bedding.

At the bottom this massive unit shows some low resistivity peaks which can correspond to soft flat shaly pebbles.

Above the massive unit we observe an interval which starts by laminated beds with parallel boundaries (same dip and azimuth values), overlaid by unparallel boundaries (variable dip values), and ends by parallel boundaries again. This interval grades up into a low resistivity level (perhaps an equivalent of pelagic clays).

The average thickness of each sequence is equal to 2 meters (minimum 1.5, maximum 3).

...

2° Second well

This deviated well is located in Italy on the Adriatic coast.

The interval understudy corresponds to a folded and faulted formation of the "Scaglia Rossa" (paleocene) which has been cored.

Figure 14 shows the composite log. Its interpretation gives, as lithology, a limestone, sometime lightly dolomitic or shaly, the porosity of which varies between 0 and 10 %.

Several sequences seem to be recognizable but their sedimentological interpretation is difficult.

The integration of the GEODIP output over this interval (Fig. 15) aids to recognize several sequences starting by an abrupt contact and a massive unit which correspond to a high resistivity limestone.

This unit could be the equivalent of the A unit of the Bouma sequence.

It grades up into a laminated interval of lower resistivity with parallel bounderies at the lower part, unparallel boundaries in the middle and parallel boundaries at the upper part. Those three zones could corresponds to the B, C and D units, the characteristics of which they have.

The sequential evolution is very clear on resistivity curves.

This well logging sequence can be easily compared to that one described by DUVERNOY and REULET, from outcrops and core analysis (fig. 16).

...

- a cyclic repetition of sequences the thickness of which is not higher than few meters.

The recognition of this environment is very important for reservoir analysis and delineation. The reservoir with the best characteristics (porosity permeability) correspond to the massive unit.

The current direction can be derived from the lamination dips study and the structural dip must be taken in laminations showing parallel boundaries.

Aknowledgement

The authors would like to express their appreciation to the Société Nationale ELF-AQUITAINE (Production) for permission to present and publish this paper.

TEN HAAF, E (1959)

Graded beds of the Northern Apprennines Rijksuniversiteit Groningen, thesis, 102 p.

WALKER, R.G. (1967)

Turbidite sedimentary structures and their relationship to proximal and distal depositional environments :
Jour. Sedimentary Petrology, V; 37, p 25-43.

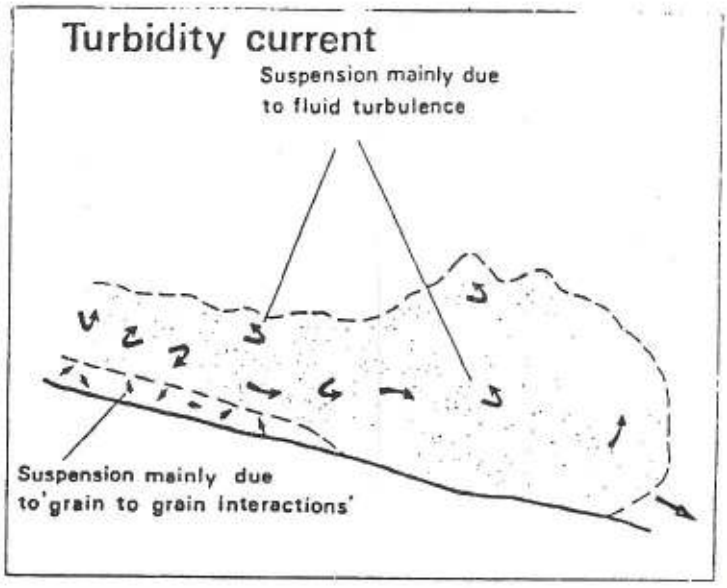

Fig. 1 - Mechanism of transportation by gravity : the turbidity current (from Middleton 1969).

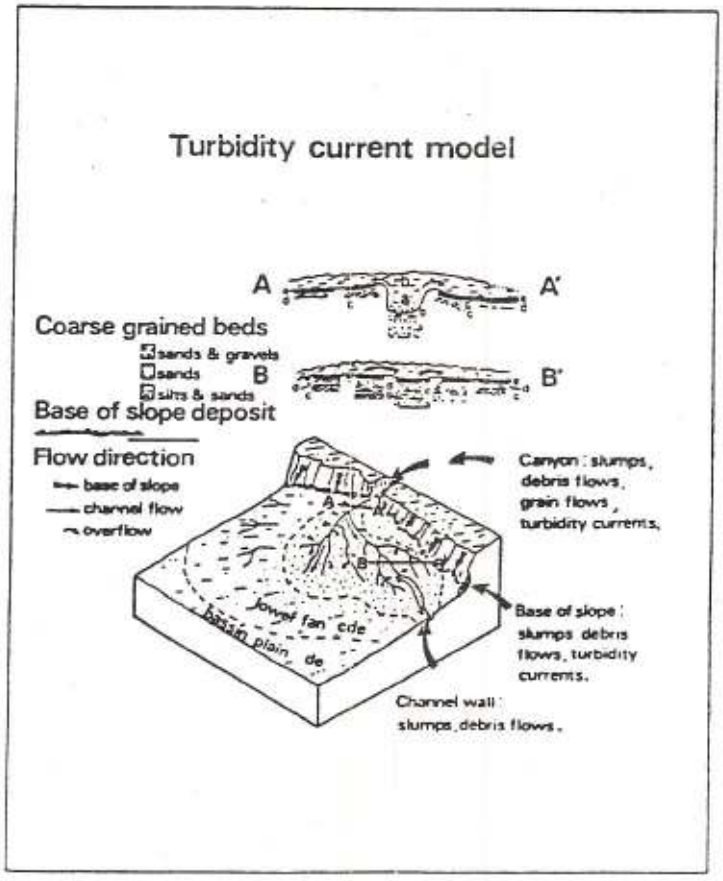

Fig. 2 - A block diagram showing a model of turbidity current processes on submarine fans.

Cross section A.A'. and B.B'. indicate hypothetical(1) distribution of sediment in the flow and (2) pattern of sedimentary structures in deposits laid down by a single flow. Plan view shows expected sediment dispersal patterns of turbid layer and turbidity current flows (from Nelson 1972).

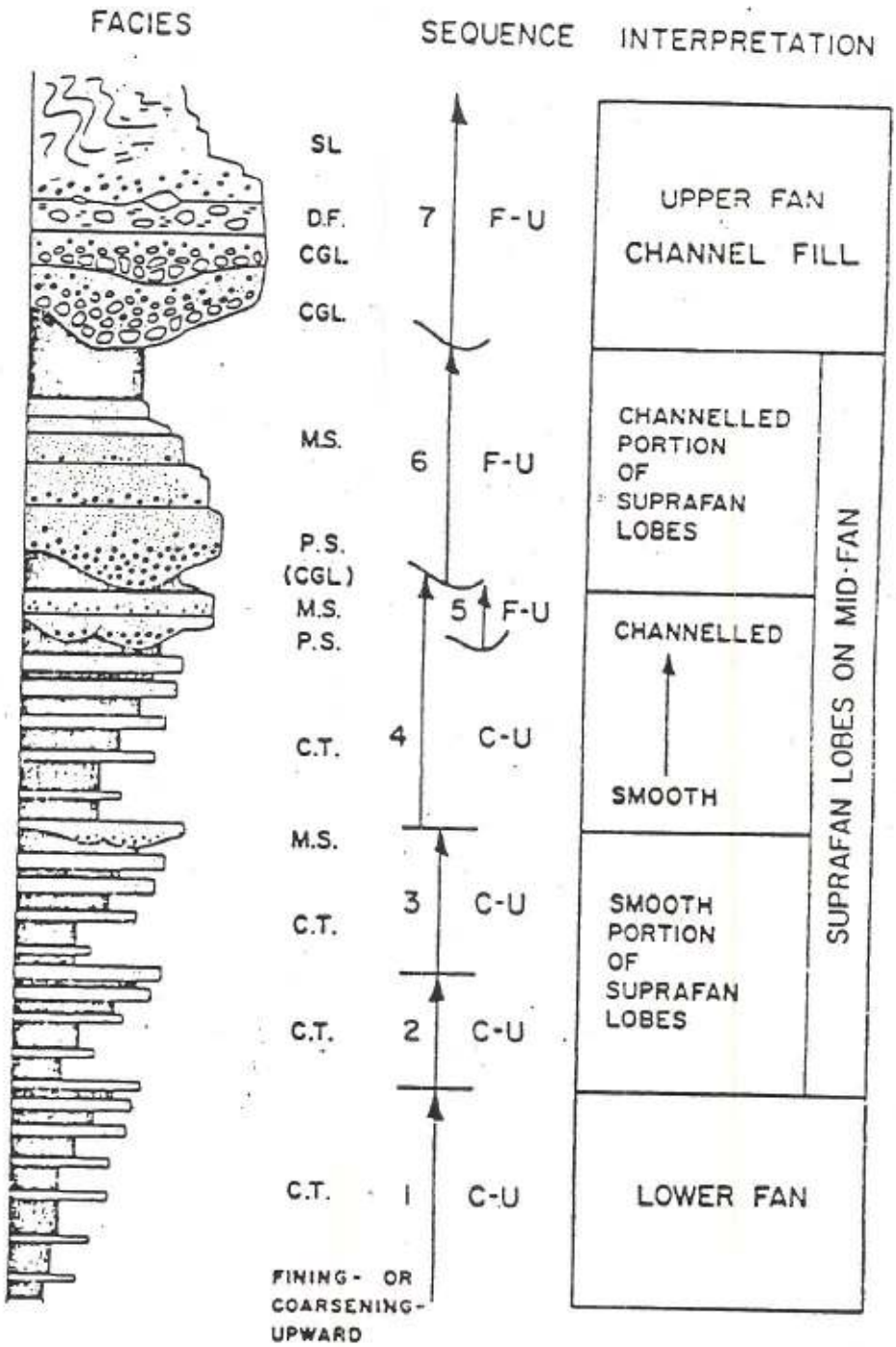

FIG.4 —Hypothetical stratigraphic sequence that could be developed during fan progradation. *C-U* represents thickening- and coarsening-upward sequence; *F-U* represents thinning- and fining-upward sequence; *C.T.*, classic turbidites; *M.S.*, massive sandstones; *P.S.*, pebbly sandstones; *CGL*, conglomerate; *D.F.*, debris flows; *SL*, slumps. Numbered sequences discussed in text.

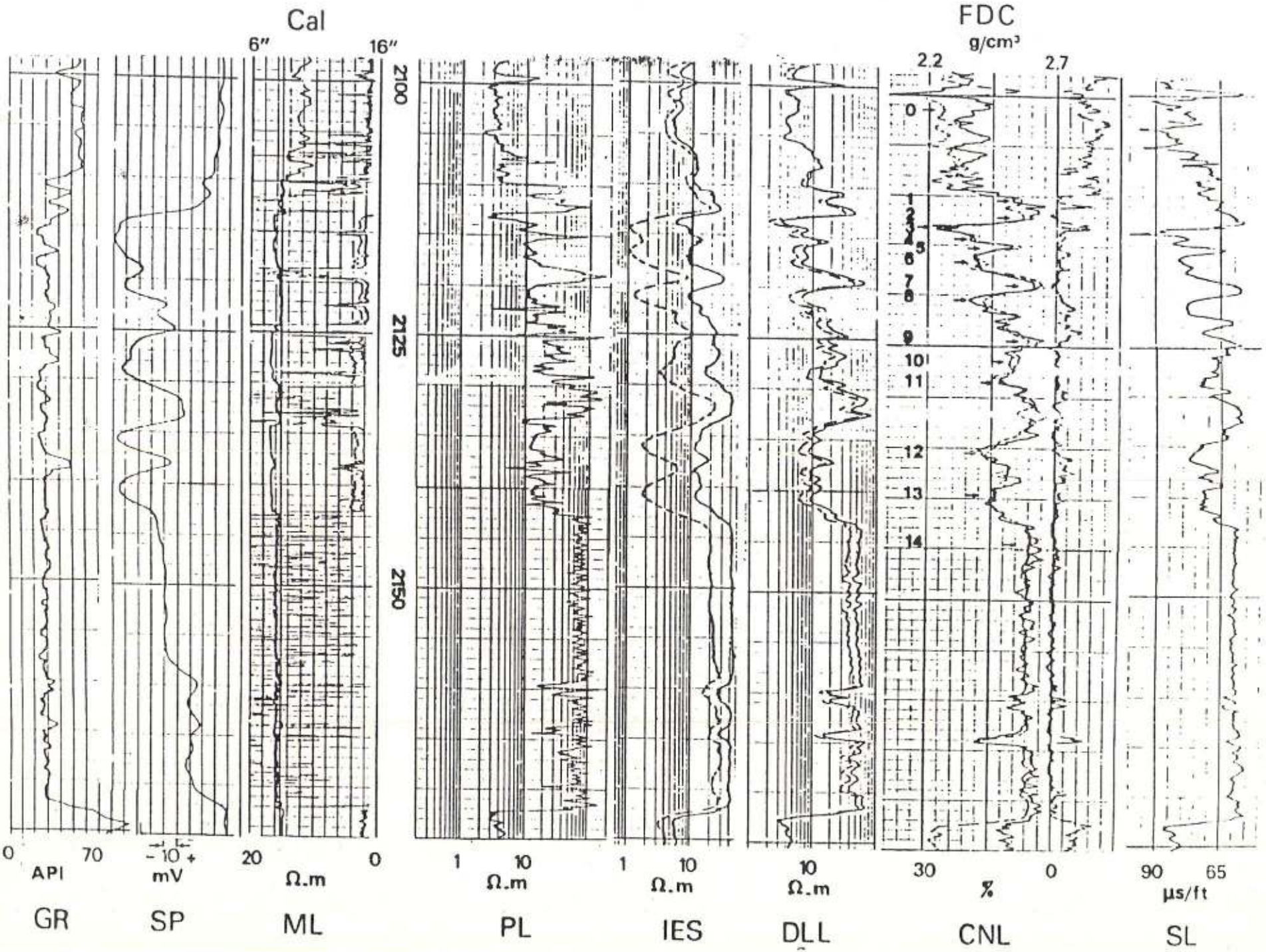
Cal
6"
16"
2100
2125
2150
FDC
g/cm³
2.2
2.7
0
1
2
3
4
5
6
7
8
9
10
11
12
13
14
0
70
API
GR
- 10 +
mV
SP
20
0
Ω.m
ML
1
10
Ω.m
PL
1
10
Ω.m
IES
10
Ω.m
DLL
30
0
%
CNL
90
65
µs/ft
SL

Figure 6

Figure 8

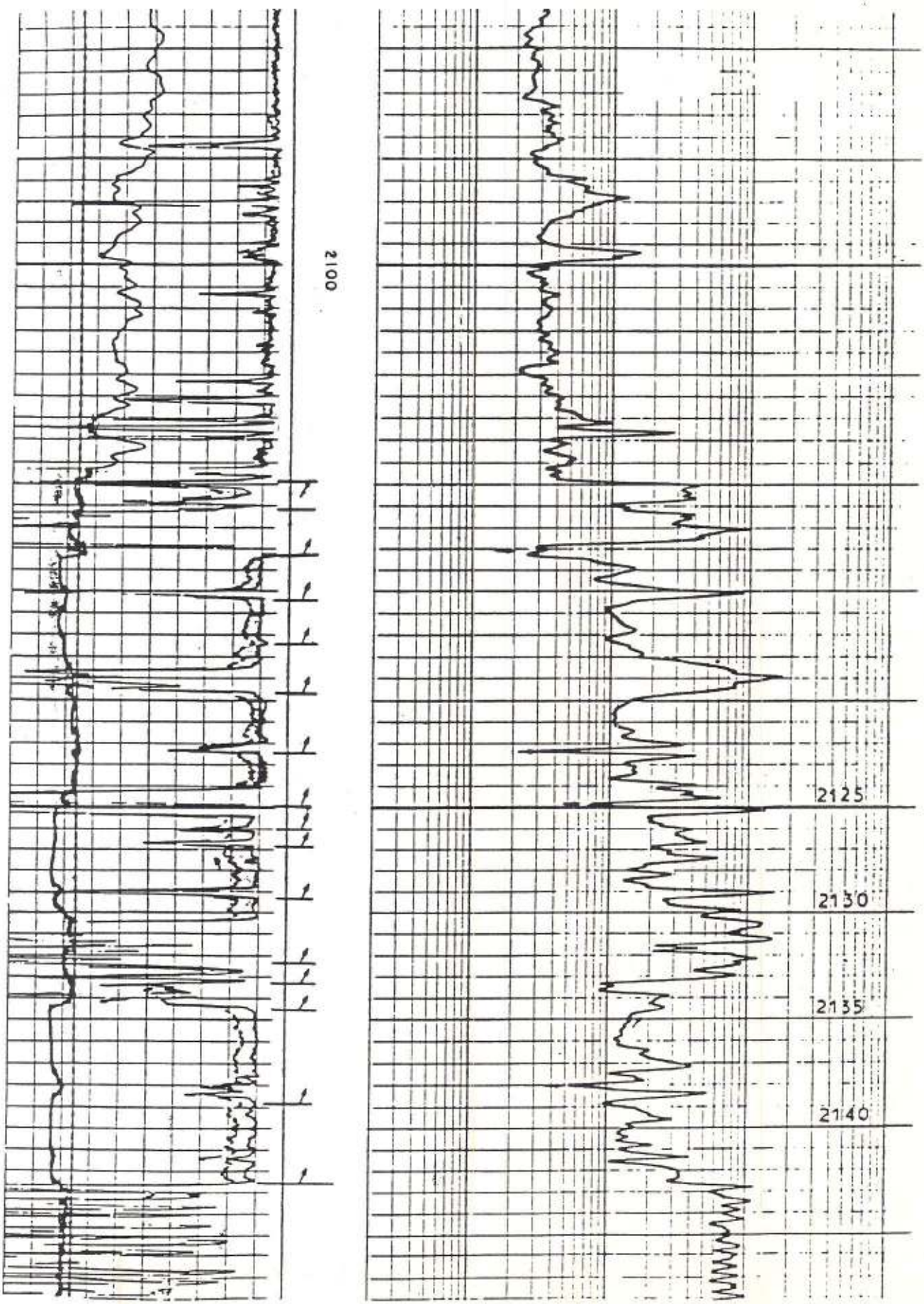

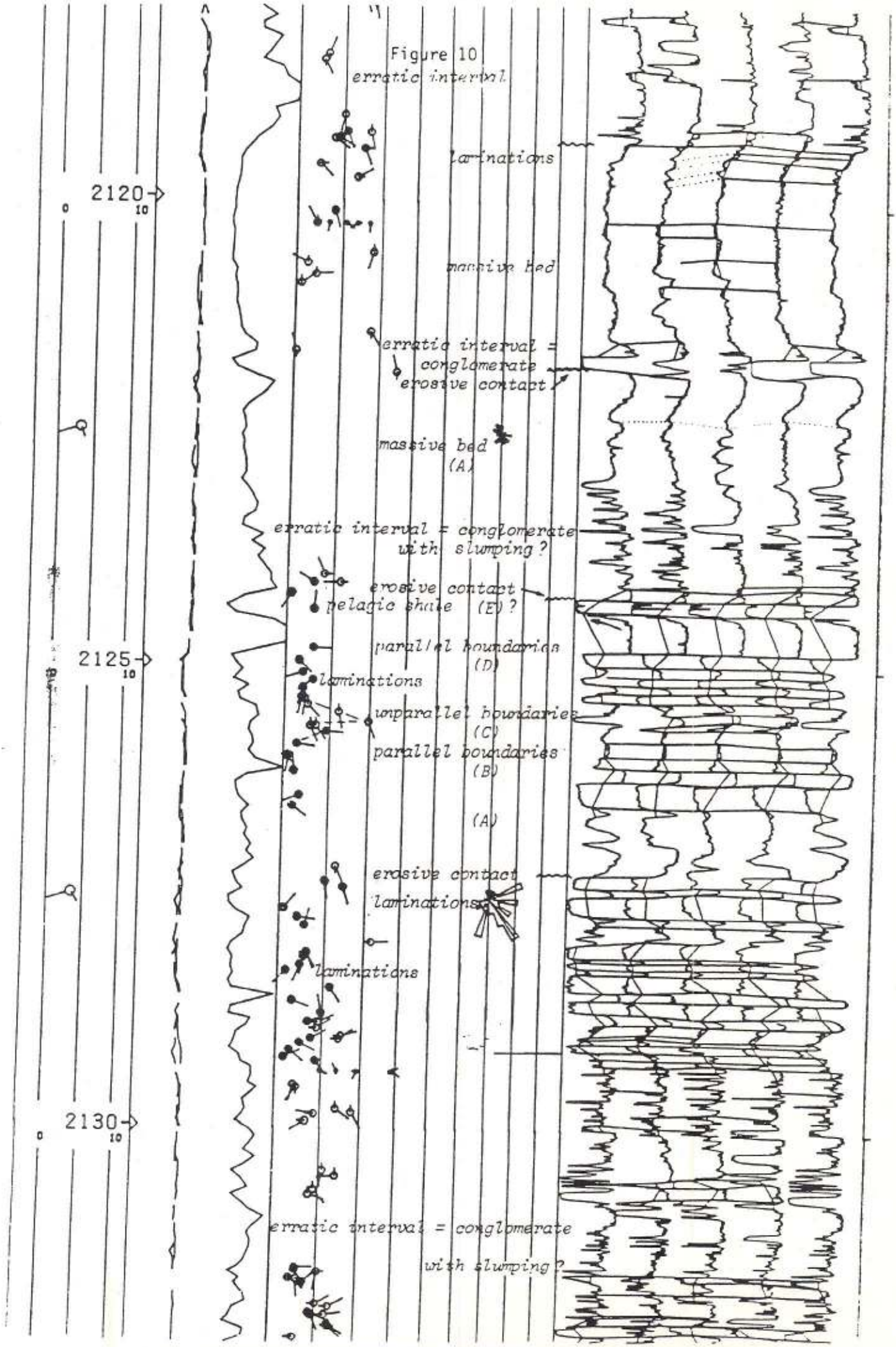
Figure 10
erratic interval
laminations
massive bed
erratic interval =
conglomerate
erosive contact
massive bed
(A)
erratic interval = conglomerate
with slumping?
erosive contact
pelagic shale (E)?
parallel boundaries
(D)
laminations
unparallel boundaries
(C)
parallel boundaries
(B)
(A)
erosive contact
laminations
laminations
erratic interval = conglomerate
with slumping?
2120
2125
2130
0
10

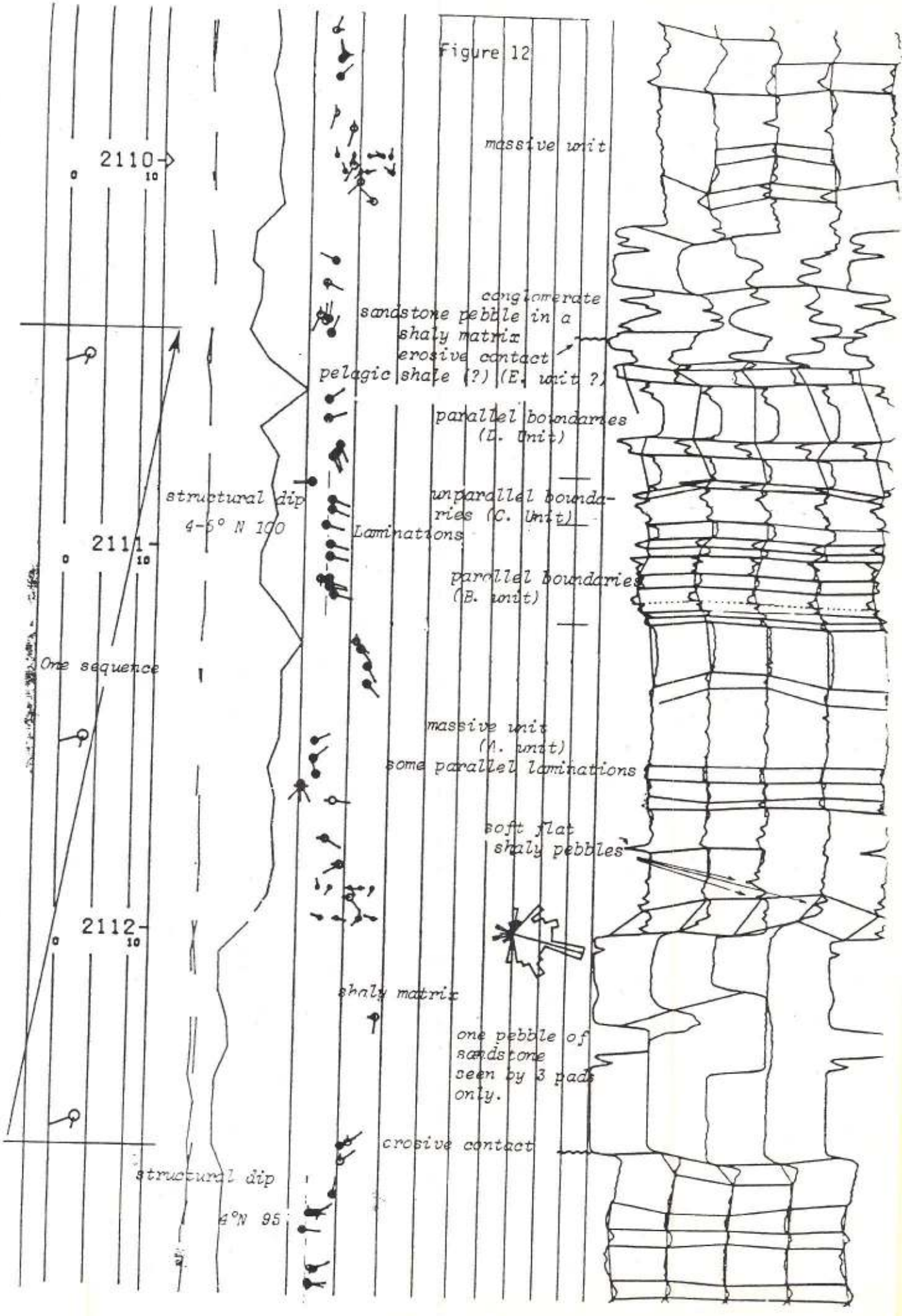
Figure 12
massive unit
2110
conglomerate
sandstone pebble in a
shaly matrix
erosive contact
pelagic shale (?) (E. unit ?)
parallel boundaries
(D. Unit)
structural dip
4-5° N 100
unparallel boundaries (C. Unit)
Laminations
2111
parallel boundaries
(B. unit)
One sequence
massive unit
(A. unit)
some parallel laminations
soft flat
shaly pebbles
2112
shaly matrix
one pebble of
sandstone
seen by 3 pads
only.
erosive contact
structural dip
4°N 95

Figure 13

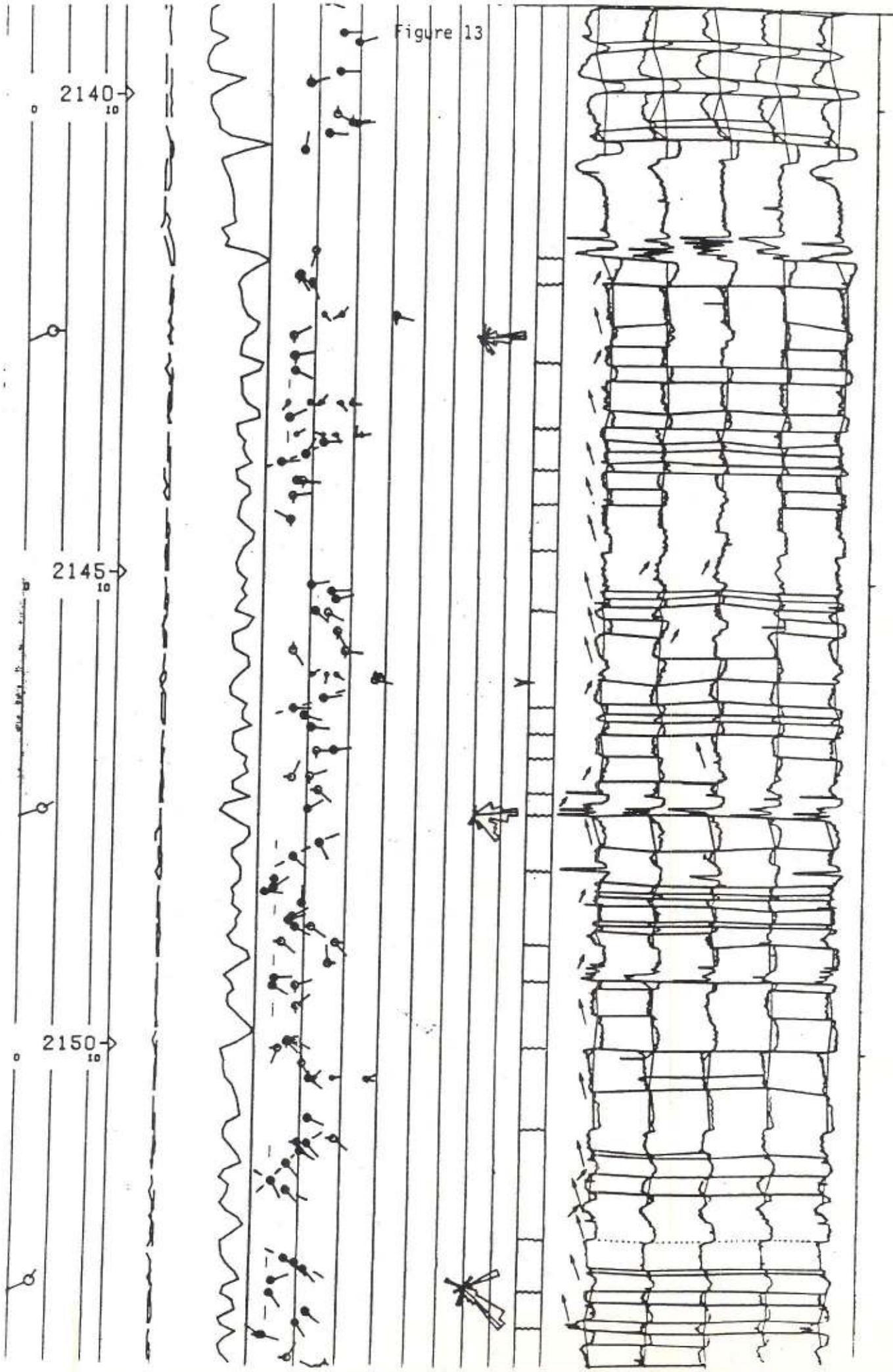

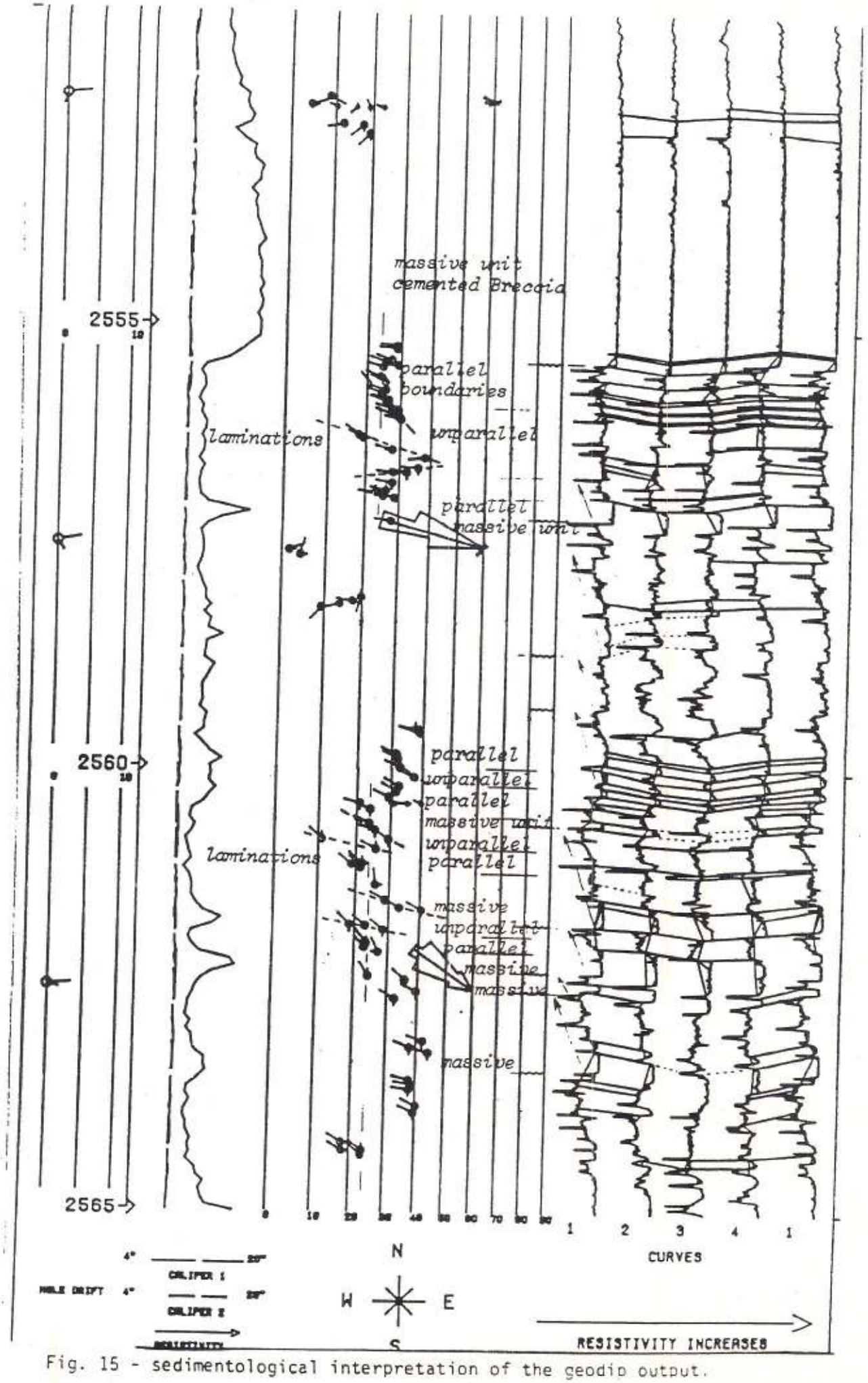

Fig. 15 - sedimentological interpretation of the geodip output.

XAVIER PAYRE, born in 1955, carried out this study at the Société Nationale ELF-AQUITAINE (Production) during his last year at Ecole des Mines de Paris, from which he graduated in 1978 as mining Engineer.

OBERTO SERRA obtained a science degree in Geology and graduated as an engineer from ENSPM (IFP). He joined the ELF-AQUITAINE GROUP in 1958, where he worked in the Sahara and the Paris Basin as a field geologist. Transferred to the well logging department in 1966, which he headed since 1969.
He is since 1978, with Services Techniques Schlumberger (Paris), in the Market Development Department. He is a member of SPWLA and AFTP.

USE OF DIPMETER IN CARBONATES FOR DETAILED SEDIMENTOLOGY AND RESERVOIR ENGINEERING STUDIES

BY

P. THEYS, S. LUTHI, O. SERRA

ABSTRACT

The Dipmeter survey has the reputation of being more characteristic of siliciclastic than carbonate formations. Since roughly half of the known world oil reserves are contained in carbonates, it is obvious that efforts must be directed towards a better interpretation of Dipmeter in those rocks.

In addition to its ability to discern structural features, the Dipmeter can be used for sedimentology and reservoir engineering analysis.

Dipmeter-derived results, used independently or in conjunction with other open hole logs, match with the overall sedimentary history of the reservoirs and offer a direct parallelism with lithofacies description. Dipmeter recognizes facies such as reef, fore-reef, back-reef, in the Middle East fields.

On the other side, the lateral extent and continuity of small sedimentary features are evaluated through the well-to-well correlation of the Dipmeter micro-resistivity curves.

Finally, the sharp vertical resolution of the Dipmeter electrode, one order of magnitude better than the other open hole sensors, allows the recognition of the fine bedding events, hydraulic barriers such as shaly zones, tight streaks and stylolites on one side and very permeable zones such as fractures on the other side. Thus the Dipmeter can provide a continuous record of semi-quantitative permeabilities which allow the implementation of more accurate reservoir simulation and the anticipation of channelling and fingering.

GENERAL

VERTICAL RESOLUTION OF THE LOGGING TOOLS SUPERIORITY OF THE DIPMETER SENSORS

A close scrutiny of cored sections point out the high degree of heterogeneity of the rocks, and moreover so in carbonate formations (Fig. 1). The petrophysical characteristics of the reservoirs are therefore bound to vary on minute distances. Accurate evaluation of essential parameters such as porosity and permeabilities is closely tied to the vertical resolution of the logging devices.

The sharpest deep resistivity tool has a resolution of 2 feet. Nuclear tools resolution vary between 6" and 18". Open hole logging data is sampled every 6" (or 15 cm).

In some areas attempts have been successful to reach a sharper resolution. Short spacing sonic (10 cm or 4"), long spacing density and sampling rates five times increased provide a better definition of the formations(Fig. 2).

These high resolution tools are still one order of magnitude less effective than the dipmeter electrodes (Fig. 3) which scan the formation with highly focussed currents and detect textural contrasts with a vertical resolution of 5mm (or .2"). To take advantage of the sensor resolution, sampling rates of 5mm (or .2") are used to format the data transmitted up hole from the tool.

Fig 1 : Microphotography of a carbonate formation

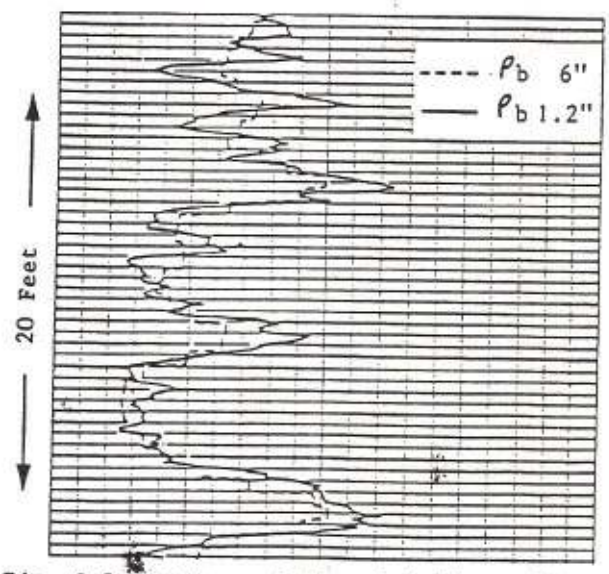

Fig. 2 Comparison of 6" and 1.2" sampling rates on a density log

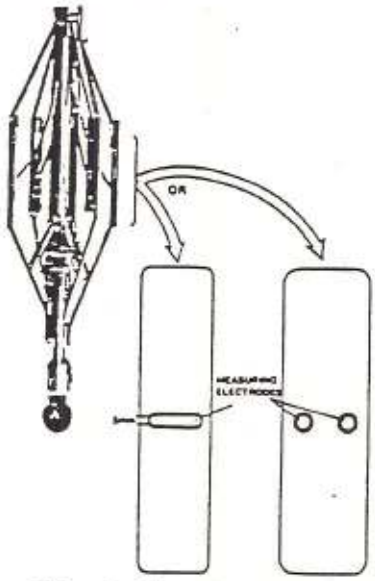

Fig. 3 Dipmeter sensor configuration

GEODIP PRESENTATION

The Geodip results are displayed on a depth scale of 1/40 or 1/20 . The print includes three groups of results (Fig. 5, 6 and 7). In the left track a resistivity curve, correlatable with an induction or a laterolog, and two caliper curves are shown. The second track displays an arrow plot similar to the one used in correlation programs. The original resistivity curves are plotted in the right-hand track, the curve corresponding to pad one being repeated at the right of the curve measured with pad 4. This presentation gives an idea of the continuity of the formation around the borehole. Straight lines drawn between the curves join elements which have good likeness. Subvertical lines join the top and bottom of an element within the same curve.

METHOD OF ANALYSIS

The Geodip record exhibits a large density of results. The following method of analysis is recommended :

(1) Check of the caliper quality : as the tool does not have very deep investigation care must be exercised to isolate washed-out and rugose sections which generate signals unrelated to the formation.

(2) Observation of the resistivity curves - qualitative evaluation of the density of correlation. It is possible to compute the density of correlation (number of correlations/foot) for beds of interest (Fig. 5)

(3) Observation of the resistivity curves : Evaluation of the activity of the curves. Activity is not always related to good correlation as shown in Fig. 6. In some cases, the curve has a high frequency content which is characteristic of specific lithologies (Fig. 7 : the lower part of the section is mainly dolomitic).

(4) Observation of the shape of the resistivity curves. They can be funnel-shaped, bell-shaped or flat/massive. These trends represent textural changes such as grain size increase/decrease with depth (fining upwards - coarsening upwards). See Fig. 7.

(5) Observation of non-correlatable anomalies appearing on only one or two of the resistivity curves. They can be associated to pebbles, nodules, large bioclastics or very commonly in carbonates, to fractures.

(6) Analysis of the azimuth frequency diagram. Modes, directions with a high concentration of dip azimuths, may be recognized. The diagram can be unimodal, bimodal or scattered. A single mode may be superimposed if the regional dip removal has not been performed.

(7) Check of the quality of the arrows. The dip representation, or tadpole may have three ratings :

(a) The four curves exhibit a good likeness and the derived dip is coherent (good planarity). The tadpole has a black (full) head (Fig. 6 / feature B).

(b) Good likeness of three curves only is obtained. The dip is derived from them and no planarity check can be made. The tadpole is shown with an empty head. The curve (or pad) number not participating in the computation is indicated as a dash on the tadpole head (feature C).

(c) Likeness between the four curves is good but the resulting planarity is only fair. One best-fit dip is shown. But, in addition, four 3-pad dips, derived from three by three combinations are shown. To distinguish them from type (a) dips, the represented tadpoles are smaller. Non-planar boundaries may indicate erosional surfaces, bedform effects, burrowed surfaces etc. (feature D).

(8) Observation of patterns formed by sequence of dips on the arrow plots : Dips with the same azimuth are considered. Classical nomenclature, e.g. the distinction between blue, red and green patterns is used.

(9) Observation of the rhythm of the detected features : repetition, cycles need then to be recognized.

Fig. 8 shows a check list of the different Geodip characteristics which should be analysed in zones of interest.

APPLICATIONS

SEDIMENTOLOGY

A good correspondence between Geodip features and lithofacies extracted from cores is generally found in siliciclastic sequences. Comparison of cores with Geodip in carbonates show that similar relations can be drawn.

The most efficient approach to Geodip interpretation starts with core-Geodip comparison : each Geodip signature or set of characteristics (specify density or correlation, activity, arrow pattern etc.) is related to a lithofacies obtained from the core. Core-derived information is then projected on uncored sections or uncored wells if a dipmeter has been run, thus allowing a saving of core costs and rig time. In some cases dipmeter information can improve core data : a more reliable depth matching and a more definite identification of missing core sections are possible. Futhermore, the dipmeter supplements dip measured or unoriented cores by giving the dip azimuth.

In the total absence of cores, the dipmeter data can still be interpreted. Extreme care must be exercised as there is a limited number of dipmeter signatures for a large number of different lithofacies.

Fig. 9 gives a non exhaustive list of the correspondence between signature and facies. This list has to be locally extended with the help of core-log comparison.

GEODIP SIGNATURE		LITHOFACIES
DENSITY OF CORRELATION ACTIVITY	LOW LOW	CHALKY TEXTURE UNCONSOLIDATION, HIGH MATRIX POROSITY). CALCILUTITE
DENSITY OF CORRELATION ACTIVITY	MEDIUM MEDIUM	OFF REEF ENVIRONMENT, INTERMEDIATE WATER DEPTH, MEDIUM ENERGY CALCARENITE
DENSITY OF CORRELATION ACTIVITY	HIGH MEDIUM	LAMINATED SHALES OR MARL STREAKS IN LIMESTONES
DENSITY OF CORRELATION ACTIVITY DIP PATTERN	LOW HIGH ERRATIC	NEAR-REEF, REEF DEBRIS, HIGH ENERGY CONGLOMERATES, CALCIRUDITE DISTURBATION
MODE DIP MAGNITUDE	SINGLE HIGH	FORESET BEDDINGS. REEF TALUS FORESETS. OOLITE SHOALS DIP AZIMUTH INDICATES THE MAIN CURRENT DIRECTION
MODE DIP MAGNITUDE ARROW PATTERN DENSITY OF CORRELATION	SINGLE MEDIUM RED HIGH	BLANKETING SHALES, MARLS
MODE ARROW PATTERN	SCATTER BLUE	CROSS BEDDING, DIRECTION INDICATES CURRENT OF DEPOSITION

Fig. 9 Correspondence between Geodip Signature and Lithofacies

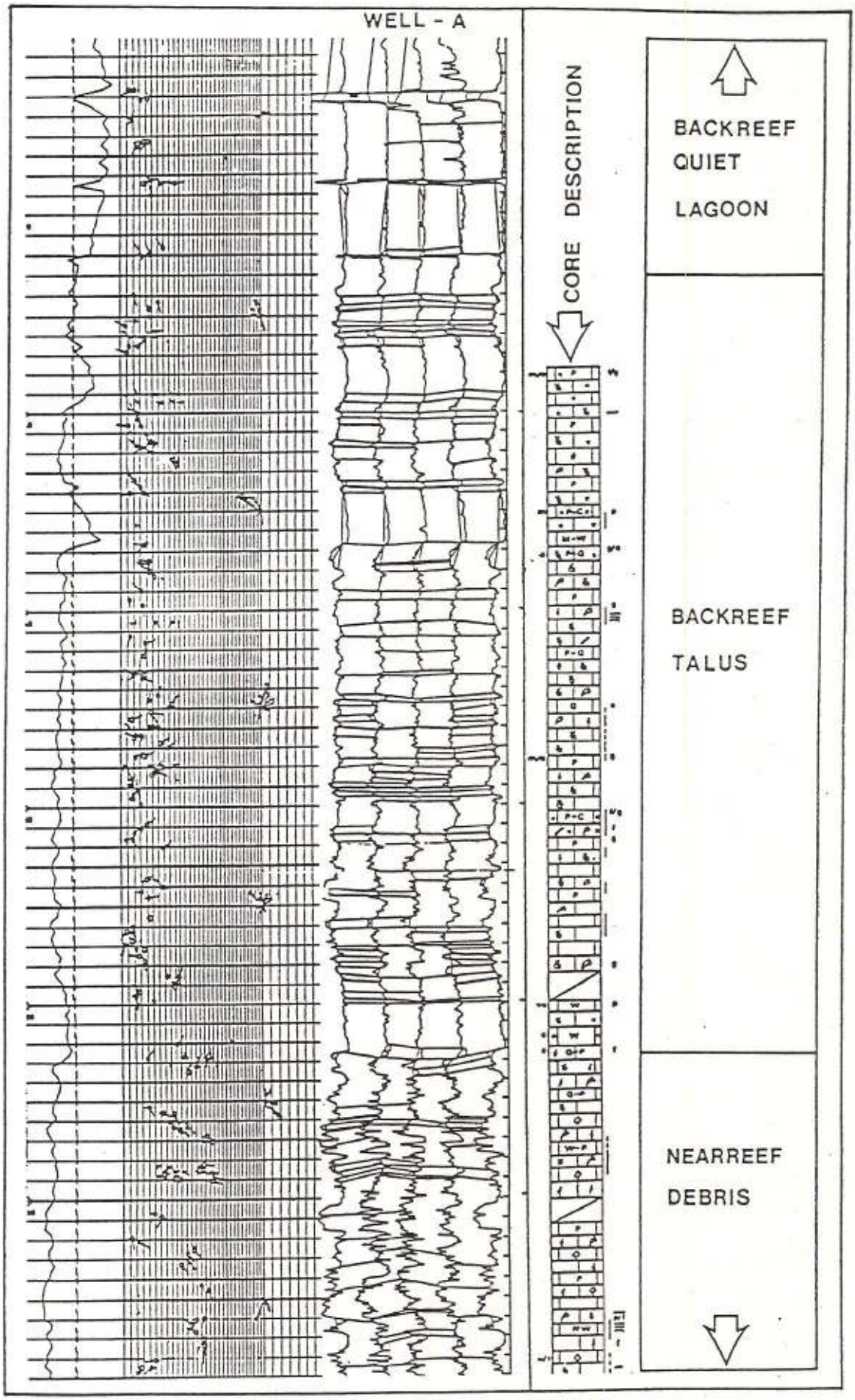

Fig. 11 : Well A Geodip and Core Description

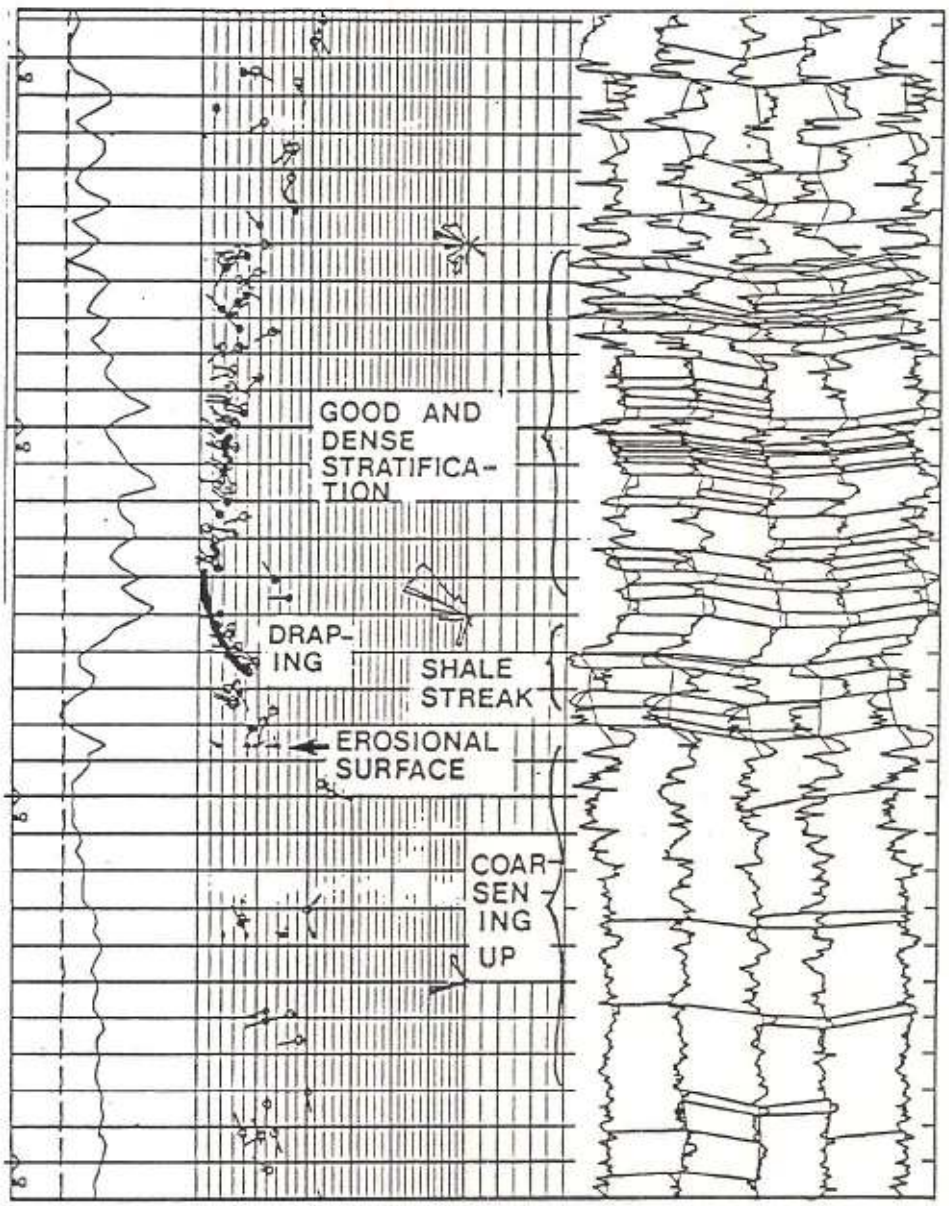

Fig. 13 : Geodip on Well B

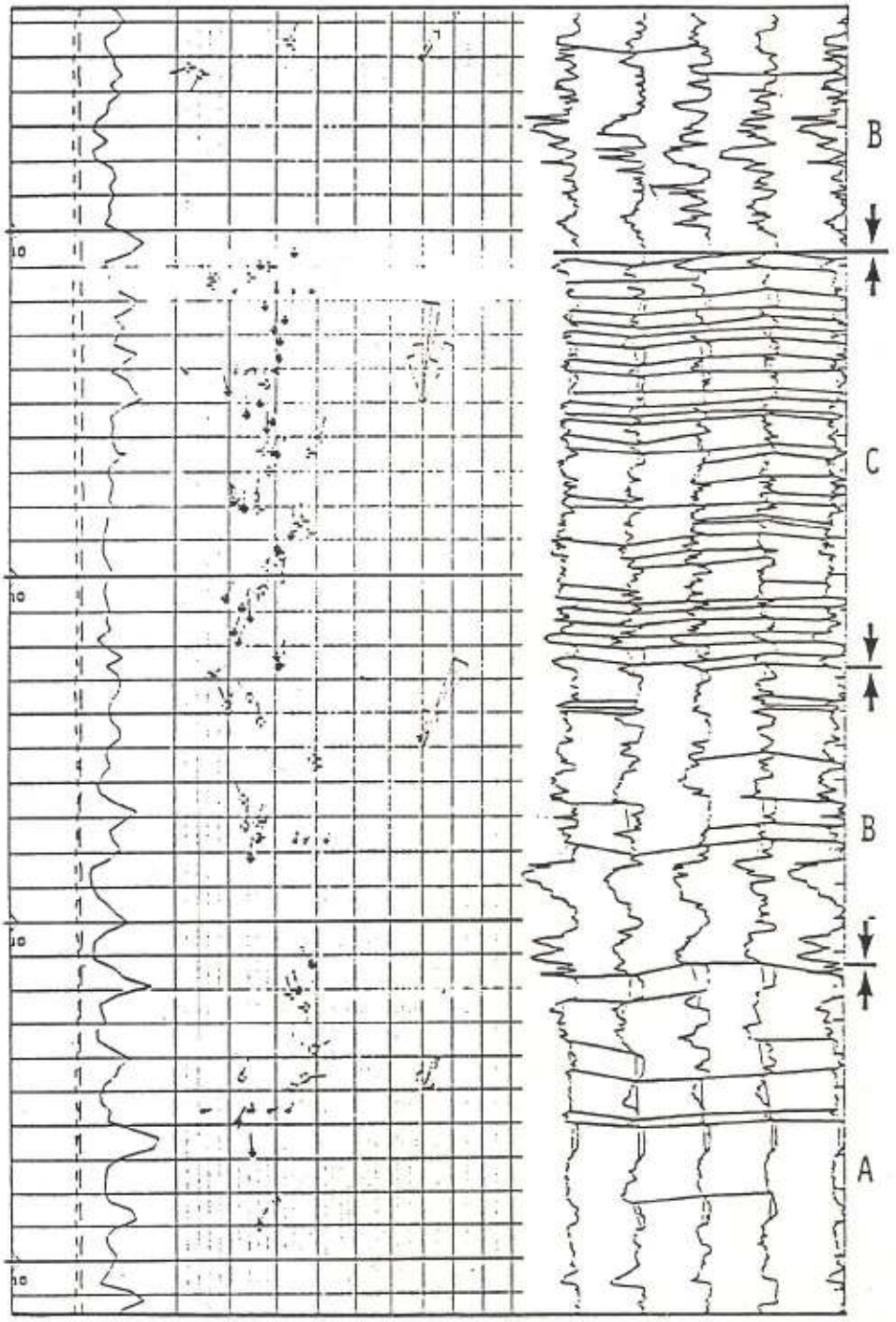

Fig. 14 : Four Facies (One is repeated) are identified within forty feet

PERMEABILITY EVALUATION

The high vertical resolution of the dipmeter sensor is coupled with a shallow depth of investigation. Eventual hydrocarbons, unless quite heavy or moved with difficulty are flushed by mud filtrate beyond the radius of investigation of the tool.

In these conditions the dipmeter resistivity curve behaves in a way similar to the Spontaneous Potential curve and variations of the dipmeter resistivity curves correspond to changes of horizontal permeability. A non deflecting curve is associated to a tight bed. A large deflection corresponds to a highly permeable formation. The noticeable advantage is that features as small as few inches are sensed by the dipmeter (Fig.16).

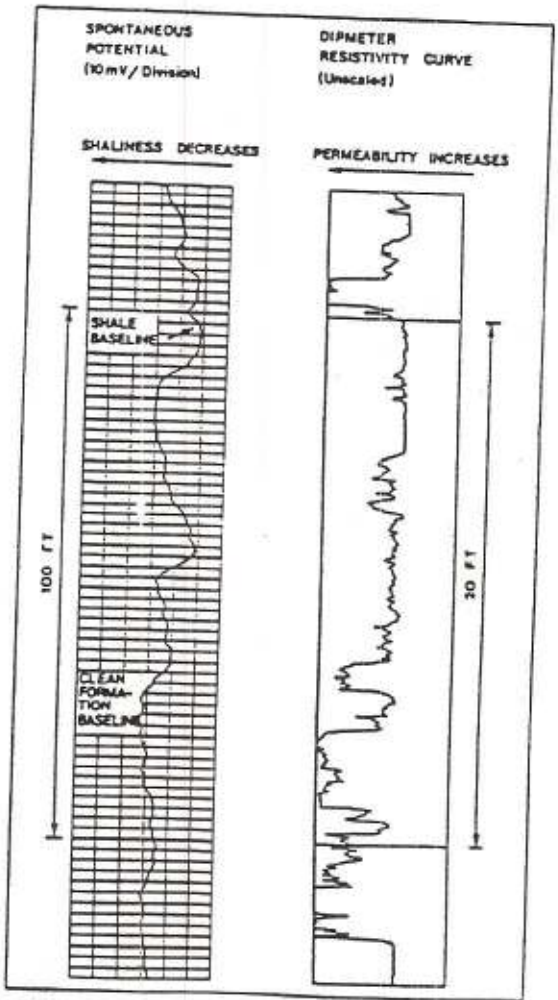

Fig. 16 : Spontaneous potential and Microresistivity curve comparison

EXAMPLES

WELL A

Well A has been described in the facies recognition section. Pressure tests have been taken over the potential reservoir. Hydrostatic pressures line up on a coherent gradient and confirm the validity of the data.

Formation pressure points seem to plot accurately on three distinct gradients : the first one identifies water with a density of .94 g/cc, the second light hydrocarbons with a density of .37 g/cc (Fig. 18). On the other hand, the third gradient yields an unreasonable value of 1.32 g/cc. The dipmeter sheds some light on these measurements. The curve spot three obvious tight streaks (zones A, B and C on Fig. 17) with high resistivities, massive profiles and lack of correlation. A fourth potential barrier is seen around XX10 (zone D).

The RFT interpretation of the original third gradient can then be modified to reflect the presence of the hydraulic barriers. The reservoir can be described as five independent hydraulic units (top zone not shown on the pressure diagram).

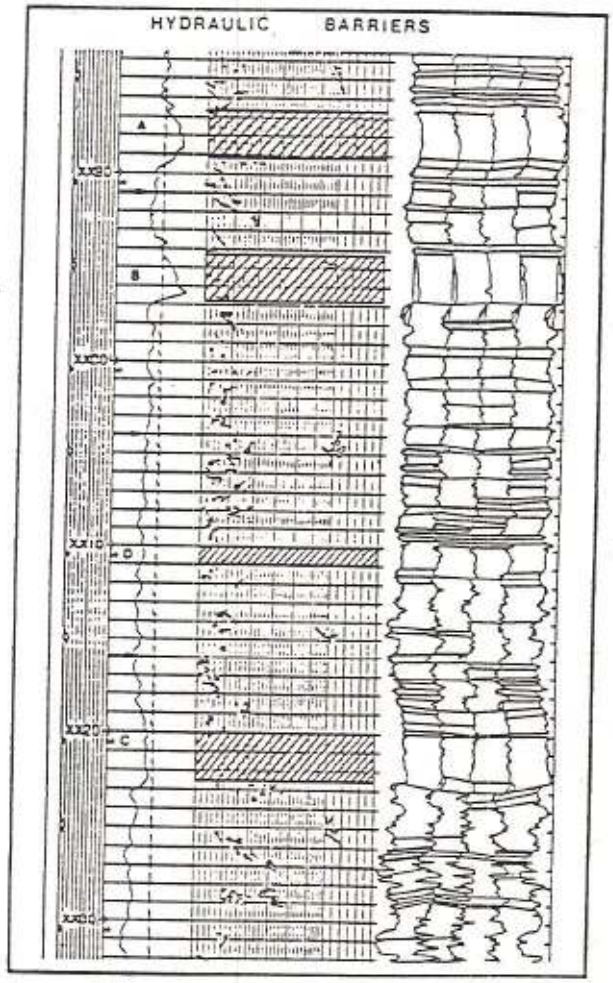

Fig. 17 : Recognition of tight barriers

WELL B

The second example relates to a hundred foot oil reservoir with porosities ranging between 0 and 25 p.u. We focus our interest to the 22 bottom feet of the reservoir. The porosity curve derived from open hole logs is fairly constant and reads around 20 p.u. The dipmeter curves show a serrated fining up sequence of 3 feet, followed by a permeability tunnel of 3.5 feet topped by a tight anhydrite zone. Two more permeable zones are present but amid the original 22 feet zone only half has a better than poor permeability and 3 feet have excellent permeability. Production logging confirms that most production takes place in zone A and injected water breakthrough is a potential problem in this field.

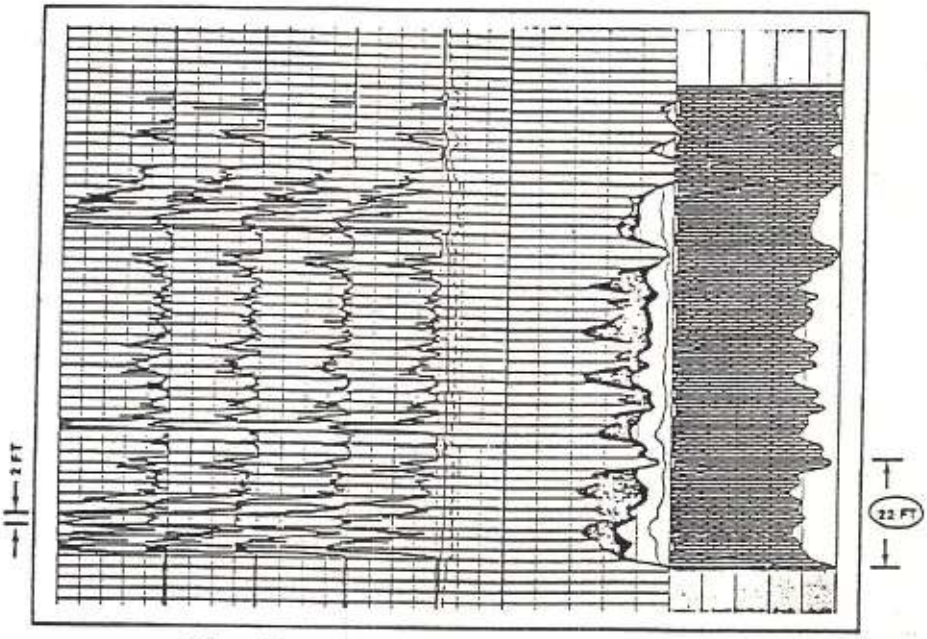

Fig. 19 : Well B Reservoir

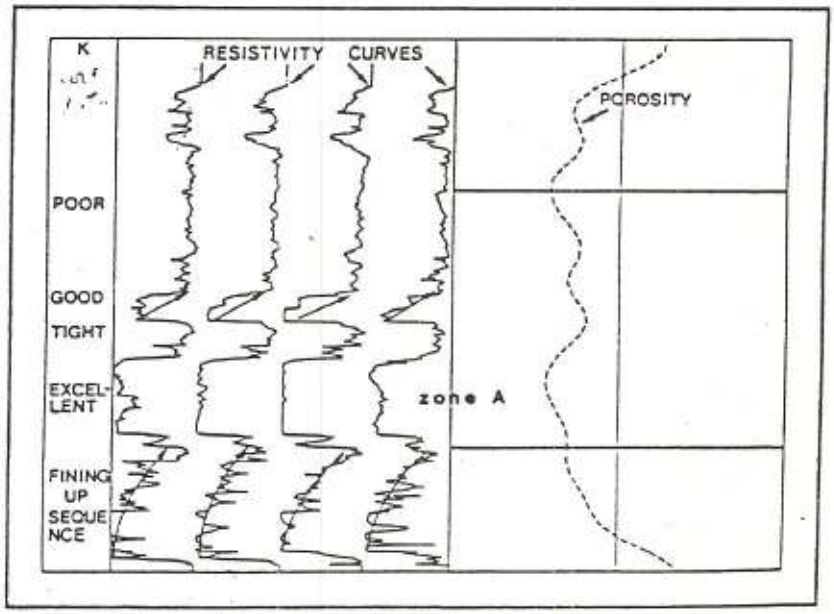

Fig. 20 : Core Permeabilities are shown in the left column

Philippe Theys is Sales Manager for Schlumberger South Gulf Division. After a degree in engineering (Ecole Centrale de Paris) he obtained a Ms Sc in Plasma Physics at the University of Orsay in 1972 and a Bsc in economical sciences from the University of Paris. After one year research work with the French Atomic Commission he joined Schlumberger and served in Europe, North America and Far East. Before holding his present position, he headed the interpretation studies group for Eastern Hemisphere and South America. He is a member of SPE of AIME and SPWLA.

Stefan Luthi obtained a diploma in geology from the ETH Zurich in 1973. He worked as a production geologist for OSCO Iran in 1974/5 and then went back to Switzerland to get a Ph.D degree in geology at the ETH Zurich in 1978. Since then he was working as a consultant petroleum development geologist. He is currently based in Schlumberger Middle East Headquarters in Dubai.

Oberto Serra obtained a science degree in Geology and graduated as an engineer from ENSPM (IFP). He joined the Elf-Aquitaine group in 1958 where he worked in the Sahara and the Paris Basin as a field geologist. He was transferred to the well logging department in 1966, which he has headed since 1969. He joined Schlumberger in 1978 and worked in Paris Headquarters before transfering to Singapore. He is a member of SPWLA and AFTP.

REFERENCES

(1) An approach to Detailed Dip Determination Using Correlation by Pattern Recognition by P. Vincent, J.E. Gartner and G. Attali (SPE 6823)

(2) Applications Sedimentologiques de la Pendagemetrie by O. Serra, J. Harry and J. Gartner.

(3) Reservoir Delineation by Wireline Techniques by J. Goetz, W. Prins, J. Logas.

(4) Sedimentological Analysis of Shale Sand Series from Well Logs by O. Serra and L. Sulpice (SPWLA 16th Symposium, New Orleans).

(5) A Case History : Turbidites recognized through Dipmeter by X. Payre and O. Serra. (SPWLA, 6th European Symposium).

(6) Application of Sedimentological Studies in the Reservoir Geological Modeling of the Al Huwaisah Field, Oman by A. Baumann (SPE 11452).

(7) Idd El Shargi field study : Shuaiba Reservoir by J.L. Chardac, P. Theys, S. Dingley and S. Kimminau.

(8) The Reservoir Engineering aspects of waterflooding by F. Craig Jr. (SPE monograph, volume 3).

(9) Fracture Detection from the logs by J. Suau and J. Gartner.

(10) Fracture Detection in the Middle East by J.C. Minne and J. Gartner (SPE 7773).

(11) Application of Repeat Formation Tester Pressure Measurements in the Middle East by J. Pelissier Combescure, D. Pollock and M. Wittmann (SPE 7775).

The American Association of Petroleum Geologists Bulletin
V. 72, No. 11 (November 1988), P. 1323-1333, 9 Figs.

Multiple Applications of Dipmeter Curves for Analyzing Evaporite Formations: Examples from Paleogene of Bresse Trough, France[1]

ALAIN CURIAL[2]

ABSTRACT

The microresistivity curves recorded by dipmeters give much diverse information about evaporitic formations because these curves have a fine vertical resolution (approximately 1 cm) and show the very high contrast in resistivity between evaporites (with high resistivity) and clay and carbonate rocks, which are porous and conductive. Examples are taken from the Paleogene salt sequence and its overlying formations of the Bresse Trough in southeastern France.

The consistency of the 4 to 8 dipmeter curves allows clear recognition of different salt facies (primary salt, secondary salt, and mixed patches of clay and carbonate within displacive halite layers) and sulfate facies (massive anhydrite, nodular anhydrite, etc). The correlation of thin continuous carbonate and clastic beds using resistivity curves discloses, with a high degree of precision, the geometry of the various formations between wells. Examples show the detection of small-magnitude halite dissolution (a few meters vertically) and the lateral effect of anhydrite hydration.

In this paper, a method is proposed for determining structural dip of salt beds by computing dip angle and azimuth of thin conductive beds within the salt using the DUALDIP computer program. A frequency distribution plot of these dip angles and azimuths gives a good indication of the dip of the salt beds.

INTRODUCTION

Dipmeter logging consists of the simultaneous recording of several microresistivity curves (3, 4, or more, depending on the tools) in particular directions, perpendicular to the borehole axis. Dip values (angles and azimuths) are obtained by deciphering the data with appropriate computer programs (curve-by-curve correlations of the resistivity contrasts, calculation of the depth difference between these correlated contrasts, etc).

The merit of these records resides not only in the estimation of the dip but also in their microresistivity curves. These curves represent a major information source for recognition of the rock fabrics and textures because they have high resolution (of the order of 1 cm compared with several 10s of centimeters for other well logs), and high vertical sampling frequency (every 5 to 2.5 mm, whereas the standard distance between two measurements for other recording devices is about 15 cm and, more exceptionally, 3 cm).

These dipmeter curves are commonly used in petroleum sedimentology, for instance, in analyzing turbidite sequences (Payre and Serra, 1979; Harry, 1981). However, these curves are seldom used in certain other lithological environments, such as evaporite sequences, despite the amount of information they provide. Dipmeter curves can indicate the location of the different mineral components because of the great electrical contrast existing between compact resistive constituents (halite, anhydrite, gypsum, etc) and conductive constituents. The conductivity may be related to the chemical character of certain disseminated minerals such as metallic sulfides (e.g., pyrite, galena, etc). However, in most cases, conductivity is primarily induced by water present within the rock pores, which is the case in claystones and porous-matrix lithologies (carbonates, sands, and sandstones).

In this study, comparisons between dipmeter curves and cores have been carried out within the Paleogene salt sequence of the Bresse Trough (southeast France) and continuing through the overlying rocks (Curial, 1986b). A few examples are presented showing the merit of these records for lithofacies recognition within both halite environments (Serra and Curial, 1985) and carbonate-sulfate (anhydrite) environments. Two further examples are given regarding information derived from well-to-well correlations obtained by joint use of microresistivity curves and other well logs. The recognition of slight (a few meters) syndepositional dissolution of halite is discussed. Then, the effect of hydration processes of anhydrite are presented, followed by a discussion on recognizing the structural dip in a diagenetic salt environment.

[1]Manuscript received, July 29, 1987; accepted, May 12, 1988.

[2]Centre des Sciences de la Terre, Université Claude Bernard, Lyon I, 27-43 Bd du 11 Novembre, 69622, Villeurbanne Cedex, France. U.A. 1209 (C.N.R.S.): "Nature et genèse des faciès confinés."

I express my thanks to B. C. Schreiber, O. Serra, M. L. Helman, G. G. Dromart, and J. G. Reed for critical review of the manuscript. The examples presented in this paper are from my PhD thesis (University of Lyon), which has partially been supported by Schlumberger (Services Techniques, Paris). I also thank Gaz de France company for providing cores and well log data and for permission to publish this study.

REGIONAL GEOLOGY AND STRATIGRAPHY

The Bresse Trough (east and southeast France), oriented east N15°-N20°, is a portion of the intracontinental West European Rift, which extends from Holland to the Mediterranean Sea and Spain. This rift began to form in the Eocene. Subsidence was very active during the late Eocene and Oligocene, particularly in areas filled with evaporite deposits. The Bresse Trough passes into the Rhine graben to the north (a transform fault separates these basins) (Bergerat, 1977a, b) and into the Valence Trough to the south. The Paleogene salt basin is located in the southern part of the Bresse Trough (Figure 1). The stratigraphy of the salt sequence has been established in the center of the salt basin (Etrez area) where the greatest thickness of halite deposits exists.

The salt deposits are divided into three main series: the lower salt series, the intermediate series, and the upper salt series. The lower salt series (630 m) is composed of halite with variable amounts of carbonate, anhydrite, and clay material. Generally, terrigenous deposits are sparse.

The intermediate series (220 m) begins with 50 m of alternating claystone and halite in beds that commonly range from 1 to 10 m thick. This section is named "Argilites de base." The upper part of the intermediate series consists of alternating halite and laminated carbonates. The thicknesses of these beds are similar to those of the "Argilites de base." Throughout this series, minor anhydrite intercalations are present. Both the lower and intermediate series are considered to be late Eocene, based upon palynology (Moretto, 1986).

The upper salt series (420 m) is of early Oligocene age (Stampian), and is mainly composed of halite with sporadic clay beds up to 4 m thick (e.g., seismic marker horizons: "Stérile" H5, H4A in Figure 1). Above the upper salt series lies the "Marno-calcaire" (180 m), also of Stampian age. This sequence consists of carbonate, gypsum, and anhydrite. The most important gypsum and anhydrite are referred to as "Barre Sulfatée." The overlying Neogene sequence is composed of carbonates and siliciclastic material.

DIPMETER CURVES AND EVAPORITIC LITHOFACIES

Comparison of dipmeter records with core has been done using the microresistivity curves recorded by the Stratigraphic High Resolution Dipmeter Tool (SHDT) (Schlumberger, 1983a). This tool has four cross-linked arms, each equipped with one pad. Each of the four pads carries two electrodes, located in the same horizontal plane and spaced 3 cm apart. There are thus four couples of measurement electrodes that record a total of eight microresistivity curves in four perpendicular directions. The sample spacing is 2.5 mm, providing 400 measurements per meter. The resolution is on the order of the electrode diameter itself (1 cm).

Halitic Environment

Main halite macrofacies.—Within the salt deposits of the Bresse area, two fundamental salt types can be distinguished by reference to the fairly well-developed diagenetic alterations of the original depositional structures. The term "primary salt" (or syngenetic salt) corresponds to layers slightly to moderately transformed since deposition (or precipitation) on the bottom of the brine pool. However, the term "secondary salt" is linked to deposits in which halite is mainly diagenetic in origin (intrasedimentary precipitates) and in which the depositional structures have been strongly disrupted or destroyed.

The primary salt (Figure 2A) consists mainly of milky halite, rich in fluid inclusions. This halite is composed of several different fabrics: pyramidal hoppers, chevrons, and rare rafts of halite crystals (Moretto, 1986). The pyramidal hoppers initiate at the air/brine interface, group together into rafts, then, under certain conditions, sink and accumulate upon the floor (Dellwig, 1955; Arthurton, 1973). The halite with chevron fabrics is generated in subaqueous conditions by upward growth on the bottom of a brine pool (Shearman, 1970; Arthurton, 1973). The milky halite is occasionally colored because of the presence of clay particles scattered within the crystals. In addition, the primary porosity of the milky halite has commonly been filled by clear halite devoid of fluid inclusions (Moretto in Curial and Moretto, 1985; Moretto, 1986). This clear halite cementation is believed to have been early, probably during the period of sedimentation. The halite beds that compose this facies are somewhat variable in thickness and are rhythmically intercalated with shale-carbonate layers forming a characteristic bedded sequence with layers on the order of 1 mm to several meters thick. Generally, the halite beds are somewhat thicker than the shale-carbonate layers.

The secondary salt is the more dominant type within the sedimentary sequence of the Bresse area. This salt is composed of clear halite macrocrystals separated from each other by clay-carbonate material commonly containing anhydrite ("halite phénoblastique," term proposed by Moretto, 1985) (Figure 2B). The secondary salt has a rubbly appearance produced by the crystallization of halite within an original soft clay-carbonate sediment. Usually crystals have pushed the host sediment aside during their growth (displacive halite). Sometimes, part of the matrix has been incorporated within the halite macrocrystals (incorporative halite) (Moretto, 1986). Very similar phenoblastic halite has been documented in Permian formations of Texas (Handford, 1981; Presley and McGillis, 1982). Modern equivalents of displacive and incorporative halite have been observed within the Dead Sea deposits (Gornitz and Schreiber, 1981) and within Bristol Dry Lake deposits in California (Handford, 1982).

Comparisons Between Cores and Dipmeter Curves

A rapid inspection of the microresistivity curves permits ready determination of the halite facies by the recog-

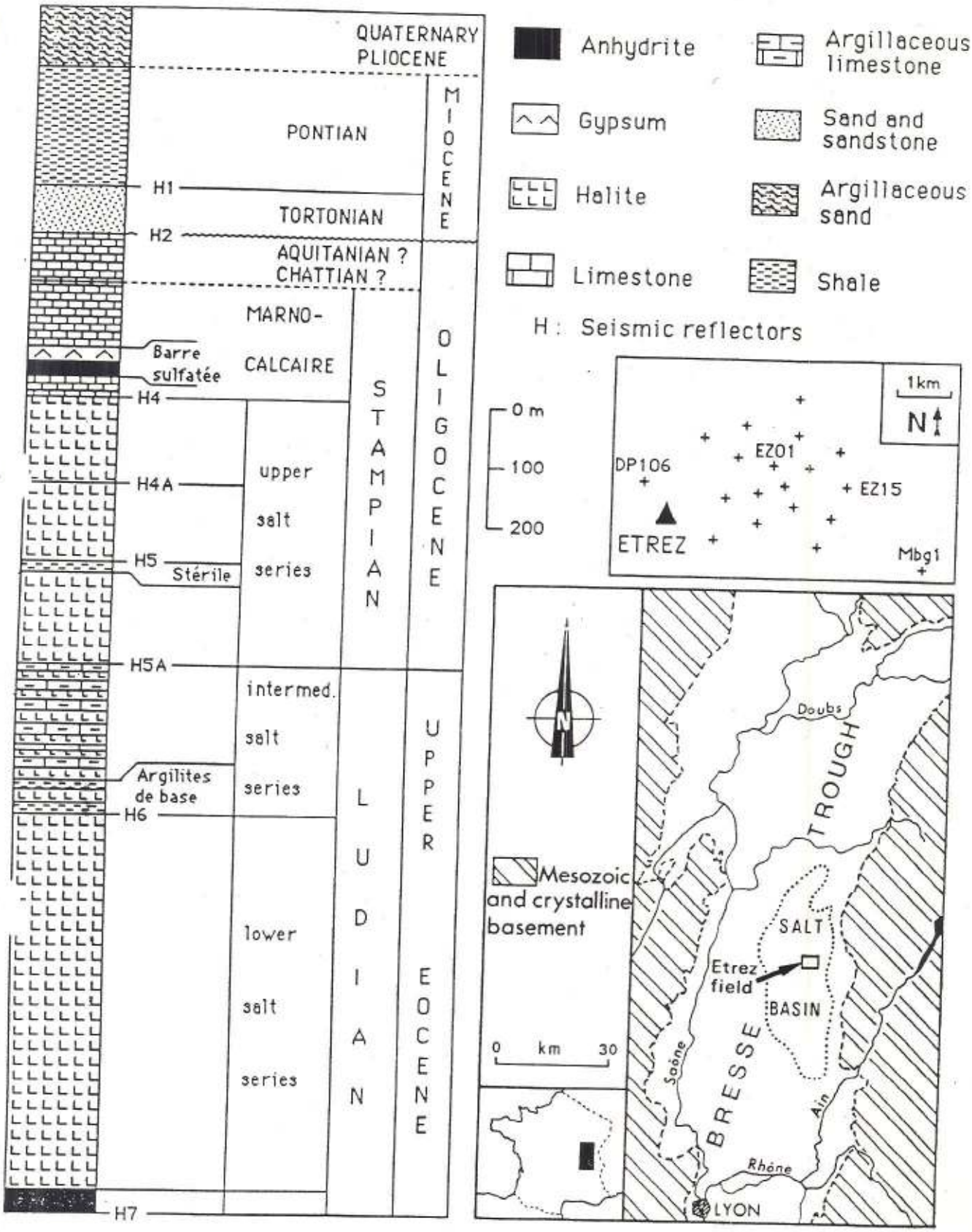

Figure 1—Cenozoic lithologic column over Etrez field, location of Paleogene salt basin in Bresse Trough (France), and map of Etrez field (underground storage in salt cavities, Gaz de France) with well locations.

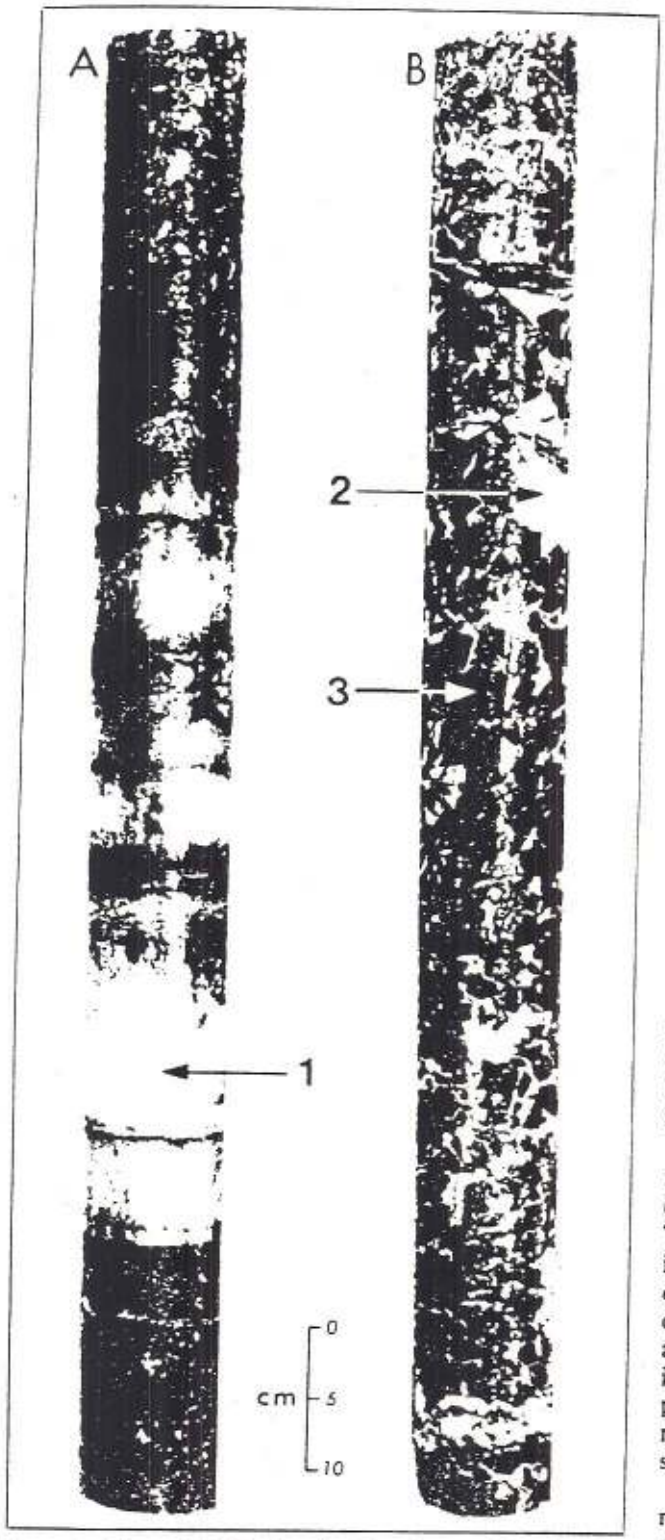

Figure 2—Cores of halite deposits from lower salt series. (A) Primary salt facies showing well-bedded halite composed of milky halite (rich in fluid inclusions) with interfingering thin clay layers (this core corresponds to interval 2 in Figure 3). 1 = milky halite. (B) Secondary salt facies formed of mixed clear halite and clay-carbonate material and having a typical rubbly appearance (interval 5 in Figure 3). 2 = clay-carbonate matrix aligned along intercrystal planes, 3 = clear halite.

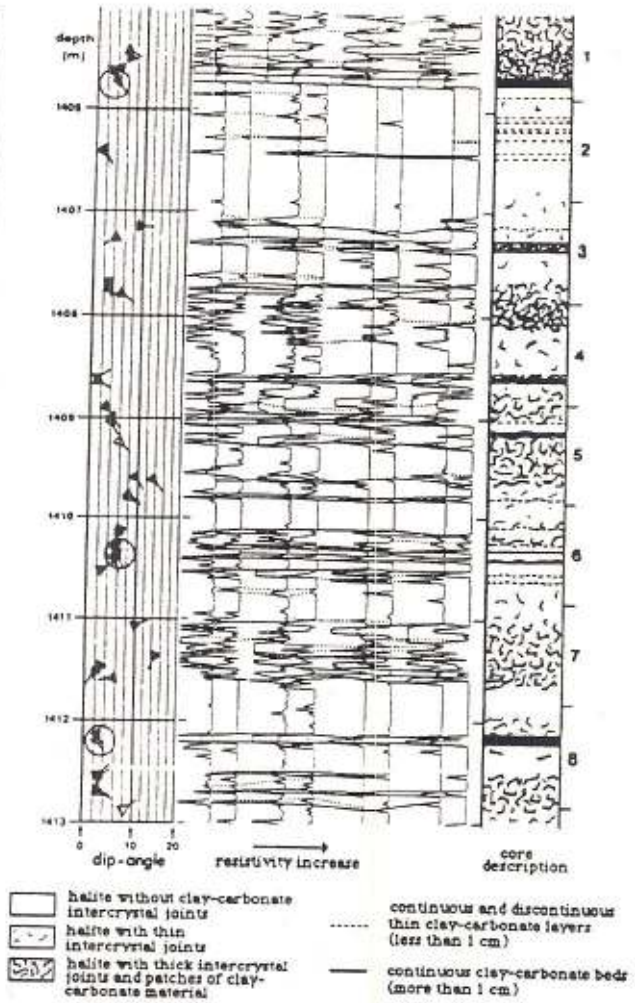

Figure 3—Comparison of cores and microresistivity curves (SHDT). Graphic presentation (curves, correlation lines between curves, and dip values) is given by DUALDIP program. Interval numbers refer to discussions in text.

nition of intervals through which the resistivity is high (flat curves with rare resistivity decreases) (Figure 3). These layers are composed of pure halite and halite that includes a small amount of porous material (shales and/or carbonates). These layers alternate with intervals that display a number of resistivity deflections with a variable amplitude. The latter correspond to salt layers enriched in shale-carbonate material that is either well bedded or present as aligned fragments along intercrystal boundaries pushed aside during halite crystal growth within a soft sediment.

Several halite facies can be distinguished based on the microresistivity curves mainly because of the distribution of the porous (conductive) material. If these components occur as continuous beds whose thickness exceeds only a few millimeters, they will be detected by all measurement electrodes. The resistivity contrasts will thus be easily correlatable among eight curves. If the porous sediments occur as scattered patches, only a few curves will show a resistivity decrease. In this case, the general curve pattern will be controlled by the abundance and size of the

patches of sediment located within the intercrystal planes.

Characterization of Primary Salt

The preservation of original bedding, recognized from the analysis of the dipmeter curves, is a reliable indicator of the primary salt deposits. Interval 2 (Figure 3) is composed of milky halite (syngenetic), rich in fluid inclusions, enclosing very thin discontinuous shale beds (less than 1 cm thick) (see Figure 2A). In this type of halite, all curves exhibit maximum resistivity. The discontinuous shale beds induce decreases in resistivity only on certain curves. These resistivity contrasts can be easily correlated and reveal a vertical succession of parallel planes, which characterize salt deposits little altered during diagenesis. If the porous beds are thick enough, they are simultaneously detected by each electrode. Thus, the dipmeter curves show the bedded appearance of primary salt layers and variations in the depositional rhythm with great clarity (Figure 4). The presence of incidental displacive crystals of halite, veins of fibrous halite, and centimeter-size anhydrite nodules within shale-carbonate beds causes increases in resistivity detectable only by one or two electrodes.

Characterization of Secondary Salt

Because of their heterogeneity, the diagenetic salt deposits are recognized by their mixed or variable resistivity signals. Secondary salt differs from primary salt in that resistivity contrasts cannot be correlated between all curves. Different types of secondary salt, which vary in the abundance and size of porous impurities along intercrystal planes, can be distinguished by examining the curves.

When the amount of clay-carbonate material is high (30 to 50% in volume), intercrystal accumulations are thick (a few centimeters) and form a network that wraps around the halite crystals. Therefore, the resistivity increases, and deflections are numerous and very closely spaced vertically (e.g., interval 7, Figure 3). These dipmeter curves have a rubbly appearance (as does the rock itself).

When porous material is less abundant (around 20% in volume), the resistivity curves show very few deviations (e.g., the central part of interval 4, Figure 3) corresponding to isolated intercrystal accumulations. Each of these accumulations is detected by one or two electrodes on one of the pads, and by more electrodes in the case of large porous patches. The vertical pattern of these contrasts never shows any succession of parallel planes. This characteristic permits us to distinguish this kind of secondary salt from a primary salt, including thin and discontinuous clay-carbonate beds.

Certain salt layers show both primary features (halite locally rich in fluid inclusions, well-bedded deposits) and secondary features (abundant clear halite with the presence of rare and very thin intercrystal accumulations of

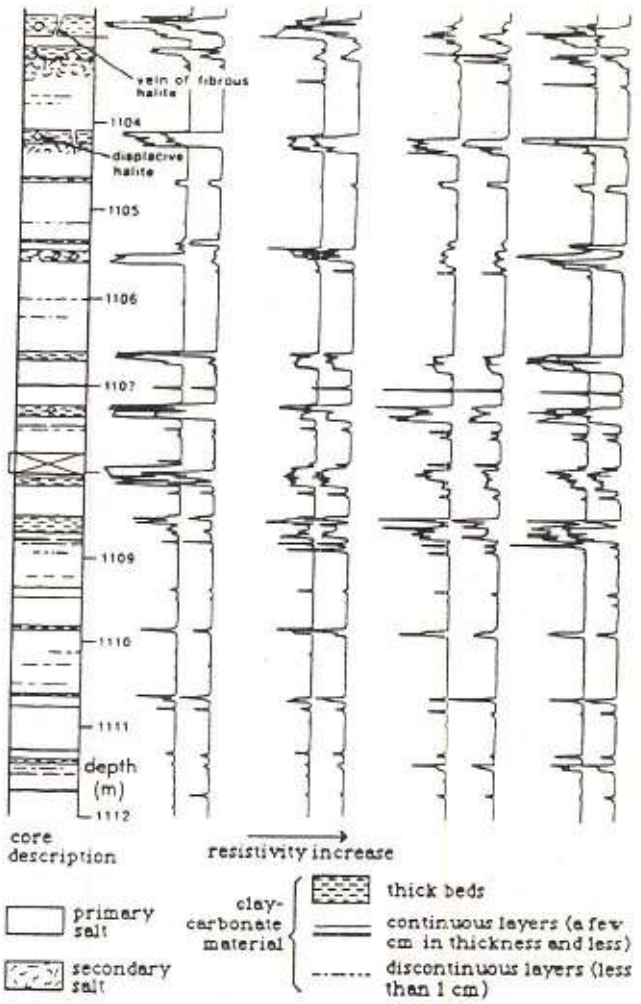

Figure 4—SHDT field log within mainly primary salt (bottom of upper salt series). Deflections of resistivity exhibit vertically successive parallel planes that characterize preservation of original bedding.

porous sediments). In addition, these layers contain nodular anhydrite. This composite facies results from a fluid-filled halite that is altered by an early precipitation of clear halite filling the primary porosity. This causes a weak alteration of the original bedding. In this case, the dipmeter curve pattern is similar to the pattern obtained from typical primary salt.

Extensive nodular anhydrite can give a high resistivity to associated carbonates; such carbonates are thus not detectable by electrodes. The use of other well logs (e.g., density logs) allows one to detect anhydrite and specify salt facies deduced from the microresistivity curves.

Shale-Carbonate-Sulfate Environment

The formation that overlies the halite sequence ("Stampien marno-calcaire") is mainly composed of variable argillaceous limestones. These deposits are very porous and, therefore, act as conductors. In contrast, those zones with anhydrite and gypsum have a very high

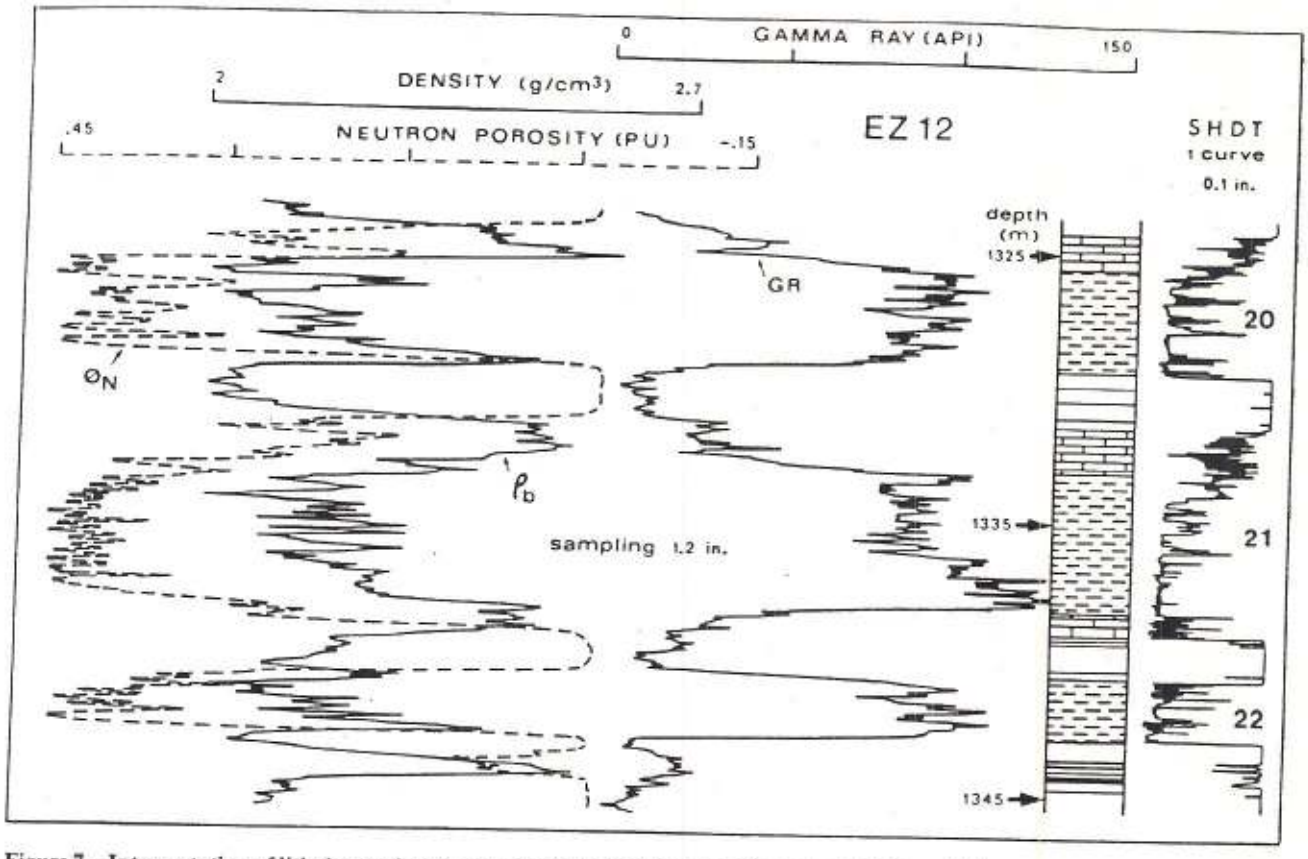

Figure 7—Interpretation of lithology using standard well logs (precise sampling every 1.2 in.) and dipmeter curves (only one SHDT curve is shown). This interval corresponds to upper part of "Argilites de base" (intermediate salt series). Thin carbonate beds included within primary salt layers are precisely detected by dipmeter. See Figure 6 for lithology explanation.

relatively continuous and are useful lithological markers that can be correlated from one well to the other. Using correlations based on these beds, the upper part of the salt sequence clearly is truncated by solution. This dissolution truncation affected a considerable part of the salt to the south. Below claystone layer 21 (Figure 6), carbonate deposits rich in anhydrite can be recognized. Their thickness decreases from the south (well EZ 12) to the north, and they are missing in wells EZ 07 and EZ 10 (northern area). These deposits represent a local accumulation of residual material resulting from the dissolution of the halite matrix before deposition of the next terrigenous unit (Curial, 1986b).

Anhydrite Hydration Processes

Despite the relatively small size of the Etrez field (about 10 km^2), well-log examination reveals important lateral lithological changes within the carbonate-sulfate formation overlying the salt sequences (Curial, 1986b). Some of these changes correspond to a lateral transition of anhydrite to gypsum, which is believed to be the result of a late diagenetic hydration of anhydrite. This hydration affected a particular layer approximately 20 m thick (the "Barre sulfatée"). Supporting evidence for such an anhydrite hydration process (and not a gypsum dehydration) is available from the well-to-well comparisons of dipmeter curves.

The north-northwest–south-southeast section of the "Barre sulfatée" (Figure 8) shows a dominant gypsum lithology above a dominant anhydrite lithology. The gypsum-anhydrite contact is sharp but oblique to general bedding. Interbedded thick shale-carbonate layers (about 10 cm or more) are laterally continuous between wells, irrespective of the host sulfate lithology. When the lithology is anhydrite, the thinnest shale-carbonate beds are also easily correlated between wells; however, when the lithology becomes gypsiferous, most of these beds disappear from the logs. This fact suggests a later anhydrite hydration that caused the destruction of the thinnest and most fragile beds.

DIP ESTIMATE IN DIAGENETIC SALT ENVIRONMENT

Within the diagenetic halite formations, dipmeter logs show a wide scattering of dip-angle and dip-azimuth values (Figure 3). This scattering suggests that the recognition of structural dip may be impossible because of the heterogeneity of the lithofacies. However, a few horizons have been preserved from the general diagenetic effects. Thus, information on structural dip exists sporadically in

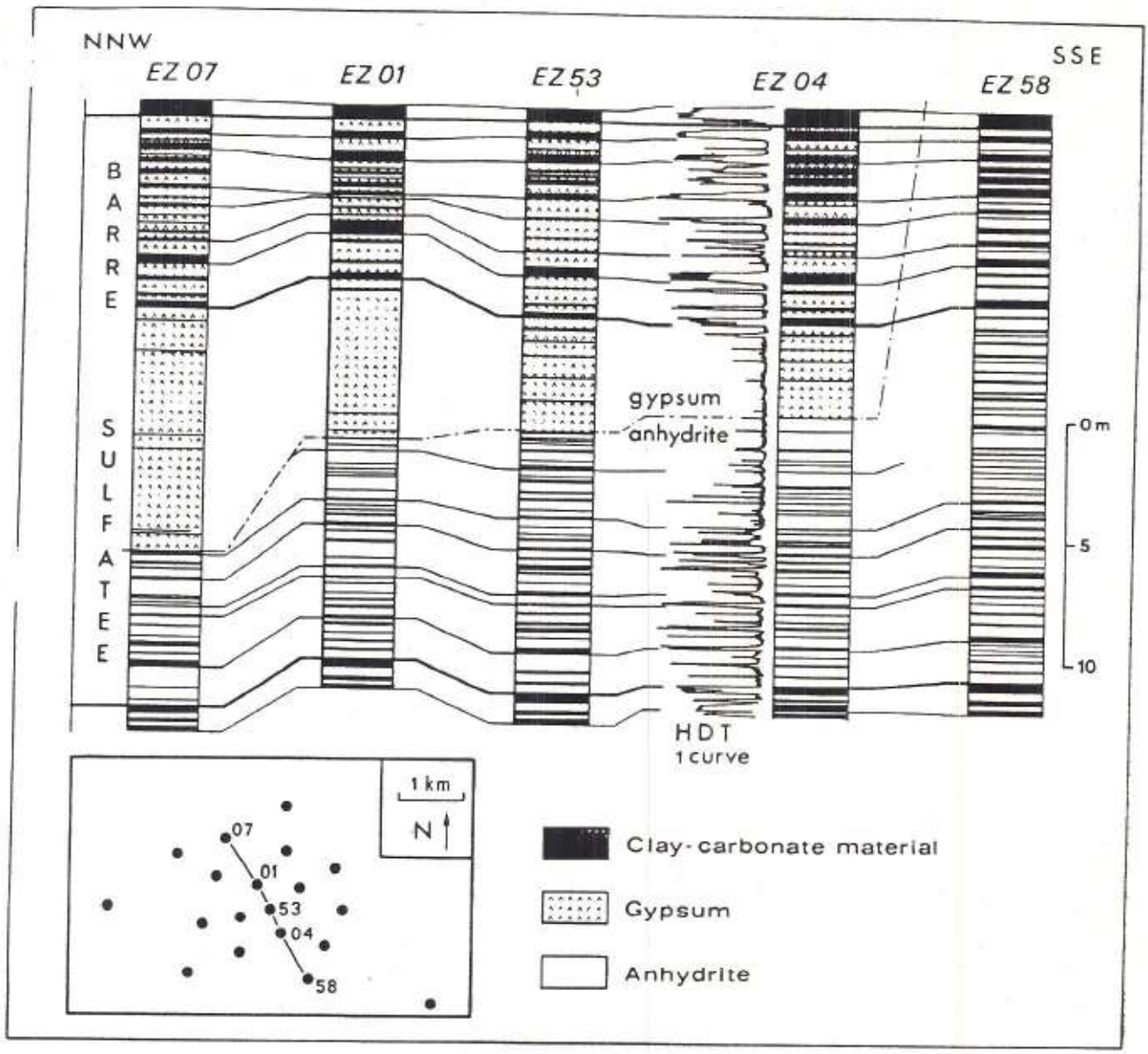

Figure 8—North-northwest-south-southeast section across five wells of Etrez field for "Barre sulfatée" member ("Stampien arno-calcaire") showing lateral passage from gypsum into anhydrite. Lithology is interpreted from well logs and dipmeter curves. Most of thin clay-carbonate beds disappear from dipmeter curves when lithology becomes gypseous, suggesting an anhydrite hydration process rather than a transformation from gypsum into anhydrite.

the records and can be extracted from the welter of non-significant values.

Raw Data Computed by Interpretive Programs

The resistivity measurements recorded by the SHDT have been computed using two different programs: DUALDIP (the SHDT Dipmeter tool uses four dual electrodes to record eight correlation curves giving a high density of dip results; three types of computations are made for the DUALDIP plot: pad-to-pad interval correlations, pad-to-pad feature correlations, and side-by-side interval correlations [Schlumberger, 1983b]) and MSD (mean squared dip, used for interval correlations), which produced dip-angle and dip-azimuth values. The graphic presentations of results obtained from these programs differ in that DUALDIP presents correlations between curves whereas MSD does not. The azimuths computed by each of these programs are reported on frequency charts (Figure 9A). For a given stratigraphic interval, DUALDIP and MSD have computed a little over 700 dips and 135 dips, respectively. The values produced by the MSD program indicate a bimodal azimuth distribution: first mode is oriented south-southeast (30% of dips), the second mode northeast-east-southeast (28% of dips). The remaining 42% are irregularly distributed in all other directions. The data from the DUALDIP pro-

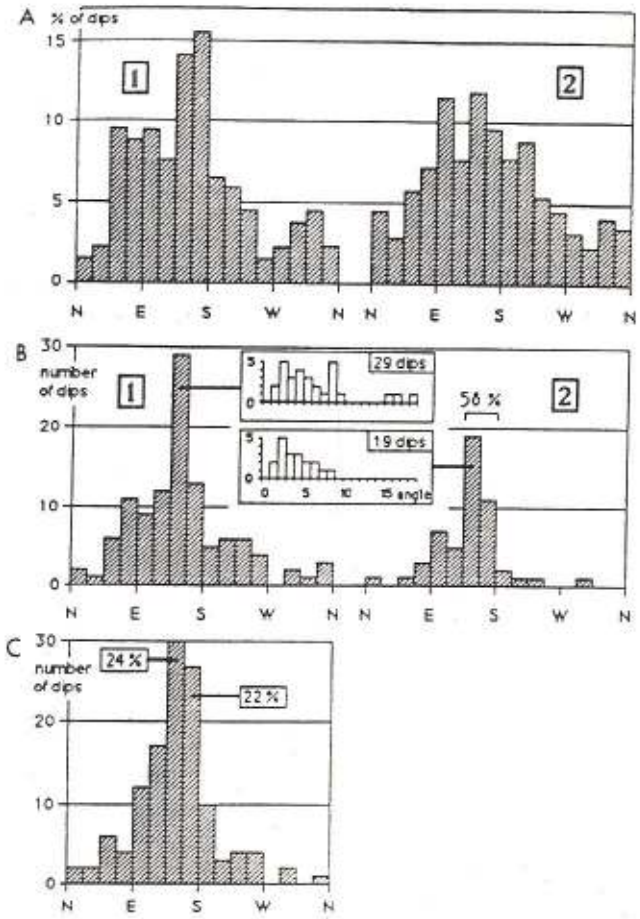

Figure 9—(A) Frequency charts (% of dips) of azimuth values: (1) raw data given by MSD program, (2) raw data given by DUALDIP program. (B) Frequency charts (number of dips) of azimuth values after selection of dips corresponding to well-bedded layers recognized in cores: (1) dips corresponding to all well-bedded layers, (2) dip values after discriminative selection from previous data set (values computed from doubtful correlations and established due to layers having irregular surfaces have been omitted). (C) Frequency chart (number of dips) of azimuth values selected from visual analysis of dipmeter curves without reference to core data.

gram are more scattered but general trends are similar to those of the MSD results.

Selected Results

Only the well-bedded porous beds bear information relative to the structural dip of the sediments in contrast to beds composed of displacive halite with marked intercrystal impurities. Where such well-bedded layers were recognized in cores, dips and azimuths were extracted from DUALDIP processed logs. The azimuths were plotted on a frequency chart (Figure 9B1), and a mode is noted between southeast and south-southeast with corresponding dips ranging from 1° to 18°.

A discriminative selection has been made from this data set consisting of a visual verification of the curve-by-curve correlations given by DUALDIP. Dips computed from doubtful correlations or from layers having irregular surfaces have been omitted (e.g., Figure 3). The azimuths of beds whose thickness exceeds a few centimeters show a marked preferential orientation, again between south and southeast (Figure 9B2); indeed, 58% of the data point south-southeast. However, the azimuths corresponding to thinner beds do not point in a particular direction because thin beds are more susceptible to diagenetic processes. Hence, their original bedding is easily altered. The dip angles for the data set range from 1° to 8°, with the mode at 2° and the average about 4°. These results are consistent with the structure contour maps constructed over the Etrez field (Curial, 1986b).

Application to Dip Estimation Without Core Data

If no core data are available, structural dip may be estimated. A simple technique consists of visually selecting certain dip values according to the shape of the microresistivity curves. A selection must be made omitting all dips computed from horizons in which the lateral continuity is limited or absent. Thus, only the resistivity contrasts that can be correlated among all curves are retained. By examining microresistivity curves, we can rule out many nonsignificant values. Two selection criteria prevail in this examination: (1) verification that the curve-by-curve correlations performed by the program are the only ones possible (if another correlation is possible, that dip value has to be eliminated), and (2) the contrasts of resistivity correlated between all curves have to show similar shapes and thicknesses. The latter is a morphological criterion and, therefore, is the most important.

Although this selection method is subjective, it gives rather reliable results. From a little more than 700 raw dips computed by the DUALDIP program, 123 dips were selected using this technique (Figure 9C). The principal orientation determined from the core inspection, south-southeast, is confirmed here by 46% of selected dip-azimuth values. A comparison of graphs A2 and C in Figure 9 indicates this selection method appears to provide reasonable estimates of the structural dip within a diagenetic salt environment.

CONCLUSIONS

Different salt facies may be distinguished using dipmeter curves because they provide a picture of the distribution of porous deposits in the borehole. Primary salt facies, and those slightly altered by intrasedimentary halite crystallization, are recognized from a particular geometry of the dipmeter curves: the resistivity contrasts exhibit a vertical succession of parallel planes. This characteristic reveals the depositional rhythm of the primary salt deposits. In contrast, secondary salt deposits are never well bedded, thus, the dipmeter curves take on a more or less rubbly and broken appearance relative to the abundance and size of the porous patches. Within a

carbonate-sulfate environment, the dipmeter curves provide information on the macrostructure of nonconductive minerals such as anhydrite (e.g., discrimination between a massive structure or scattered nodules).

The high vertical resolution of dipmeters permits detailed correlations between different wells. The examination of the laterally continuous thin shale-carbonate beds reveals the salt-layer geometry. In this way, halite dissolution of even small magnitude (a few meters vertically and a few square kilometers in area) can be detected. In addition, precise correlation of rhythmic beds may allow long-distance correlation that presently may be achieved by tedious "varve" correlation.

Where diagenetic processes altered original well-organized bedding (by intrasedimentary halite crystallization, anhydrite-gypsum transformation, etc), the dipmeter curves provide accurate information not revealed by other well logs. The recognition of anhydrite hydration phases (e.g., in the "Barre sulfatée") exemplifies the application of the dipmeter curves for establishing or supporting interpretations of diagenetic processes. By comparison with other logs, diagenetic zones oblique to bedding can be identified.

The altering of original primary structures induced by early diagenetic intrasedimentary growth of halite crystals explains widely scattered dip values (angles and azimuths) calculated by computer programs. A method has been proposed for estimating the structural dip despite the heterogeneity of the secondary salt deposits. This method consists of a discriminative selection of significant dips, computed by the DUALDIP program, by inspecting the dipmeter curves.

REFERENCES CITED

Arthurton, R. S., 1973, Experimentally produced halite compared to Triassic-layered halite-rocks from Cheshire, England: Sedimentology, v. 20, p. 145-160.

Bergerat, F., 1977a, Le rôle des décrochements dans les liaisons tectoniques entre le fossé de la Saône et le fossé Rhénan: Comptes Rendus Sommaires de la Société Géologique de France, v. 4, p. 195-198.

——— 1977b, La fracturation de l'avant pays jurassien entre les fossés de la Saône et du Rhin: Revue de Géographie Physique et de Géologie Dynamique, v. 19, p. 325-337.

Curial, A., 1986a, Les dissolutions dans la partie supérieure du Salifère paléogène de Bresse (SE de la France): Chronologie, extension et mécanismes: Revue de Géographie Physique et de Géologie Dynamique, v. 27, p. 225-235.

——— 1986b, La sédimentation salifère et suprasalifère du Paléogène bressan (France): comparaison entre les données diagraphiques et lithologiques. Etude diagraphique du champ d'Etrez et synthèse du bassin: Documents de l'U.A. 1209 (C.N.R.S.), v. 11, 251 p., and Documents des Laboratoires de Géologie de Lyon (1987), v. 100, 192 p.

——— 1987, Le détritisme durant la sédimentation salifère paléogène en Bresse méridionale: Géologie Alpine Mémoire hors série, v. 13, p. 391-395.

——— and R. Moretto, 1985, Le Paléogène salifère de Bresse (département de l'Ain, SE de la France). Etude diagraphique et sédimentologique: Documents du GRECO 52 (C.N.R.S.), v. 5, p. 93-153.

Dellwig, L. F., 1955, Origin of the Salina salt of Michigan: Journal of Sedimentary Petrology, v. 25, p. 83-93, 95-102, 107-110.

Gornitz, M. V., and C. B. Schreiber, 1981, Displacive halite hoppers from the Dead Sea: some implications for ancient evaporite deposits: Journal of Sedimentary Petrology, v. 51, p. 787-794.

Handford, C. R., 1981, Coastal sabkha and salt pan deposition of the lower Clear Fork Formation (Permian), Texas: Journal of Sedimentary Petrology, v. 51, p. 761-778.

——— 1982, Sedimentology and evaporite genesis in a Holocene continental sabkha-playa basin—Bristol Dry lake, California: Sedimentology, v. 29, p. 239-253.

Harry, J., 1981, Utilisation des courbes de pendagemétrie en sédimentologie pétrolière: Mémoires Géologiques de l'Université de Dijon, v. 7, p. 275-284.

Moretto, R., 1985, Sédimentologie de la série salifère du Paléogène de la Bresse (France): Bulletin de la Société Géologique de France, v. 1, p. 849-855.

——— 1986, Etude sédimentologique et géochimique des dépôts de la série salifère paléogène du bassin de Bourg-en-Bresse (France): PhD thesis, University of Nancy I, Nancy, France, 312 p., and Mémoires Sciences de la Terre (1987), v. 50, 252 p.

Payre, X., and O. Serra, 1979, A case study: turbidites recognized through dipmeter: Society of Professional Well Log Analysts 6th European Logging Symposium Transactions, paper K, 27 p.

Presley, M. W., and K. A. McGillis, 1982, Coastal evaporite and tidal-flat sediments of the upper Clear Fork and Glorieta formations, Texas panhandle: Bureau of Economic Geology Report of Investigations 115, 50 p.

Schlumberger, 1983a, Stratigraphic high resolution dipmeter tool: Schlumberger, 24 p.

——— 1983b, Openhole services catalog: Schlumberger, p. 36.

Serra, O., and A. Curial, 1985, Progrès récents dans la reconnaissance des accumulations salines par diagraphies: Bulletin de la Société Géologique de France, v. 1, p. 797-806.

Shearman, D. J., 1970, Recent halite rock, Baja California, Mexico: Institute of Mining and Metallurgy Transactions, v. 79, p. 155-162.

Wellbore Breakout Stress Analysis Within the Central and Eastern Continental United States

Richard L. Dart: U.S. Geological Survey, Denver, Colorado
Mary Lou Zoback: U.S. Geological Survey, Menlo Park, California

Abstract: Using readily available petroleum exploration dipmeter and fracture identification well logs, the orientations of stress-induced and stress-related wellbore enlargements were analyzed to determine horizontal crustal stress directions. Data were from more than 200 selected wells in 15 structurally diverse areas within the continental interior and along the Atlantic continental margin. A variety of genetically diverse types of stress- and nonstress-related wellbore enlargements were observed. Factors controlling or contributing to their formation include not only horizontal stress differences and rock strength but possibly drilling history, intersecting natural fractures, and rock-fabric properties.

Our findings agree closely with results of previously published studies, indicating that (1) stress-induced borehole elongations (breakouts) can develop in a wide variety of rock types in regions with differing tectonic histories; (2) breakout shape is elliptical in cross section with the long axis oriented parallel to the inferred direction of minimum horizontal compressive stress (Sh_{min}); (3) elliptical wellbore enlargements resembling breakouts can be mechanically induced during drilling in boreholes that deviate vertically; (4) in weakly consolidated formations or in rocks that are easily eroded, stress-induced breakouts are likely to be further enlarged by the action of circulating drilling fluids; (5) breakout orientations in wells within a given structural environment are generally consistent in orientation; and (6) stress directions inferred from breakout orientations often agree with the results from other types of stress data.

INTRODUCTION

A number of recent studies comparing wellbore-breakout cross-sectional long-axis orientations with known directions of horizontal stress from areas in North America and Europe have yielded results supporting the conclusion that wellbore breakout enlargements are stress induced and that their azimuths of borehole enlargement parallel the Sh_{min} orientation (Bell and Gough, 1979, 1982; Gough and Bell, 1981, 1982; Mastin, 1984; Hickman et al., 1985; Plumb and Hickman, 1985; Teufel, 1985; Zoback et al., 1985). These studies, using field data as well as laboratory results and theoretical analysis of breakout formation, indicate that breakouts are elliptically shaped, vertically elongated zones of wall spalling (Figure 1) formed primarily by compressional shear failure caused by the unequal concentration of horizontal compressive stresses about the wellbore (Teufel, 1985; Zoback et al., 1985). This finding is supported by the overall excellent agreement in breakout orientations in both individual well data sets and composite data sets of wells within the same structural setting, and by the consistency between stress orientations inferred from breakout data and the results from other types of stress data (Gough and Bell, 1981, 1982; Hickman et al., 1985; Plumb and Hickman, 1985), i.e., earthquake focal mechanisms and hydrofrac measurements.

Knowledge of in situ stress conditions is essential in evaluating hazards associated with both seismic and aseismic deformation and the potential for slip on preexisting zones of weakness. Such knowledge is also important to the petroleum industry in the mitigation of certain drilling problems and in hydraulic fracturing (hydrofrac) treatment design. The analysis of breakout data has become an important tool in understanding present-day stress conditions in regions where log data are available (areas of petroleum exploration).

This report focuses on the results of several recent breakout stress studies involving primarily breakout orientation data from a variety of tectonic settings within the central interior and along the eastern continental shelf of the United States (Dart, 1985, 1987; Dart and Zoback, 1987). The results of these stress studies are compared with other types of stress data from the areas studied and from the surrounding regions.

BREAKOUT STUDIES IN THE UNITED STATES

We have completed the analysis of stress-induced, stress-related, and nonstress-related wellbore enlargement data from more than 200 wells located in 15 structural settings, primarily sedimentary basins, within the midcontinent and along the modern Atlantic continental shelf margin of the United States (Dart, 1985, 1987; Dart and Zoback, 1987) (Figure 2). The term "wellbore enlargement," as used in this report, is an interval of vertical borehole elongation of some length where the cross-sectional size of the wellbore in at least one direction exceeds the calibrated bit size. Data analyzed consist of over 62,000 vertical feet of borehole elongation in 1,240 wellbore enlargement features (primarily breakouts). The areas studied include (1) the west-central part of the Denver basin in Colorado and the southern half of the Illinois basin in Illinois, and adjoining parts of Indiana and Kentucky; (2)

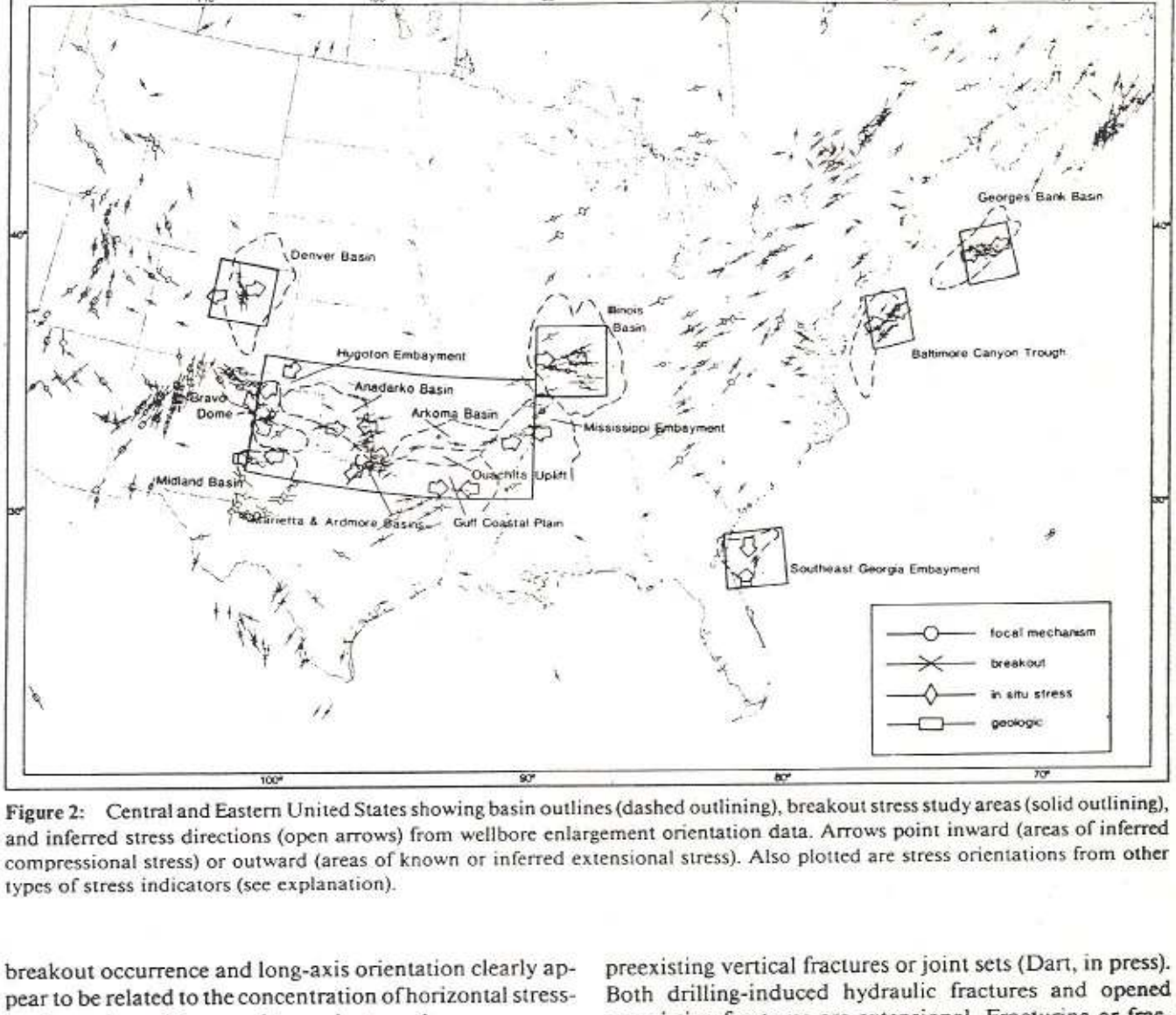

Figure 2: Central and Eastern United States showing basin outlines (dashed outlining), breakout stress study areas (solid outlining), and inferred stress directions (open arrows) from wellbore enlargement orientation data. Arrows point inward (areas of inferred compressional stress) or outward (areas of known or inferred extensional stress). Also plotted are stress orientations from other types of stress indicators (see explanation).

breakout occurrence and long-axis orientation clearly appear to be related to the concentration of horizontal stresses about the wellbore and to rock strength.

Elliptically shaped, deviation-induced wellbore enlargements (Figure 4B) appear to form as a result of the eccentric wobble of drill string when the vertical axis of the borehole deviates from vertical during drilling (Plumb and Hickman, 1985). If the amount of deviation is more than a few degrees, enlargement-orientation data are considered to be of questionable value as stress data. This seems to be true when the enlargement long-axis orientation is within $\pm 10°$ of the azimuth of hole deviation (Figure 3). Log records of enlargements of this type closely resemble log records of breakouts.

Fracture-related enlargements, inferred to be stress-related, are also elliptically shaped in cross section and are generally oriented normal to the trend of breakouts within the wellbore. Fractures associated with their formation are likely drilling-induced hydraulic fractures or opened preexisting vertical fractures or joint sets (Dart, in press). Both drilling-induced hydraulic fractures and opened preexisting fractures are extensional. Fracturing or fracture opening may occur when the hydrostatic pressure within the wellbore exceeds the confining strength of the rock drilled. The hydrostatic pressure is the weight of the vertical column of drilling fluid plus the pumping pressure. A likely mechanism for the formation of fracture-related enlargements may involve the mechanical "chipping out" or enlarging of an interval of the borehole weakened by extensional fractures (D. G. Davis, personal communication). That is, through the dynamic drilling process and the erosional effect of circulating drilling fluid, the fractured wellbore may become enlarged. Possible examples of fracture-related wellbore enlargements involving preexisting and drilling-induced extensional fractures are shown in Figures 4C and 4D, respectively. Figure 5 is a schematic example comparing the cross-sectional structure of breakout and fracture-related wellbore en-

Table 1: Continued.

Study area	Total number of wells	Total number of breakouts	Total vertical feet of breakout	Depth interval from sea-level datum (ft) From	To	SH_{max}	Angular deviation	Geologic age	Generalized stratigraphy	Geologic references
Hugoton embayment[1]	6	13	420	140	−3,300	35	15	Paleozoic (Permian to Mississippian)	Interbedded DOLO with LS and SS with SH	Hill and Clark (1980)
Bravo dome area[1]	33	98	2,583	−800	−7,000	47	18	Paleozoic (Permian to Pennsylvanian) and Precambrian basement	Redbeds, interbedded ANHY, DOLO, LS, granite wash, and SH. Granite	Dutton et al. (1982)
Midland basin	5	24	986	−2,300	−8,400	86	24	Paleozoic (Permian to Pennsylvanian)	LS, DOLO, SS, and SH	Galley (1978)

SS, sandstone; SH, shale; LS, limestone; ANHY, anhydrite; DOLO, dolomite; ST, siltstone. SH_{max} is inferred from breakout data. SH_{max} is not inferred for data sets having angular deviation greater than 30°. —, indicates no inference made.
[1] In study areas with bimodal–orthogonal well-dated sets, SH_{max} is inferred from the breakout portion of these data sets. SH_{max} and angular deviation are in degrees.

largements. Also shown are the orthogonal long-axis orientations of these two types of wellbore enlargements. It has been observed (Dart, 1987) in data from a number of study areas in the southern midcontinent study region (Figure 2) that breakout and fracture-related wellbore enlargements together form data sets of enlargement orientations having orthogonally oriented bimodal trends.

A type of elliptical borehole enlargement, possibly associated with plastic deformation of the borehole, was observed at depths of less than 5,000 ft in soft or poorly consolidated basin sediments in wells along the Atlantic continental margin (Dart and Zoback, 1987) (Figure 4E). Wellbore enlargements of this type were typically elliptical, were often oriented orthogonal to the trend of "true" breakouts that occurred in consolidated formations at greater depths, and may have been stress related. However, because of apparent randomness in orientations and occurrence at shallow depths in poorly consolidated strata, this type of enlargement was not considered to be a reliable stress indicator. Although no theoretical or experimental studies exist to explain the inferred deformation of the wellbore, the difference in horizontal stresses and the lack of sediment consolidation at shallow depths may cause the wellbore to become plastically deformed in the SH_{max} direction. Circulating drilling fluid may then rapidly erode the borehole, resulting in the formation of an elliptically shaped, deformation-related wellbore enlargement.

Preferentially oriented washouts (POW's) are wellbore enlargements exhibiting an increase in borehole size in two directions while maintaining a pronounced elliptical cross-sectional shape. Their long-axes orientations may be subparallel or orthogonal to the mean orientation of "true" stress-induced breakouts within the well (Figure 4F). POW's, so oriented, are considered oversized or enlarged breakouts or fracture-related wellbore enlargements, respectively. Fracture-related POW's may be associated with either drilling-induced hydrofractures or preexisting natural fractures or joint sets intersecting the borehole. Because POW's are enlargements of the wellbore in two directions, they are usable but are considered less reliable stress indicators than breakouts.

Washouts (random enlargement of the wellbore) do not exhibit a preferred cross-sectional orientation (Figure 4G; also Figures 4A, 4F) and are therefore not stress indicators. Washout enlargement shape and vertical length of elongation may be affected by circulating drilling fluid, changes in lithologic type, and variety of rock-fabric properties present (Babcock, 1978). Washouts often occur at shallow depths because the upper part of the borehole will likely be an area of limited sediment compaction and will have had a longer exposure time to drilling activity. Washouts were observed to vary in vertical length within the wellbore from a few feet to several hundred feet.

We have evaluated wellbore enlargement data quality in two ways. Initially, a log copy is graded according to the readability of recorded traces (trace clarity) and wellbore roughness. Wellbore roughness or rugosity refers to how badly washed out or otherwise damaged the borehole appears on the log record. Wellbore roughness will affect

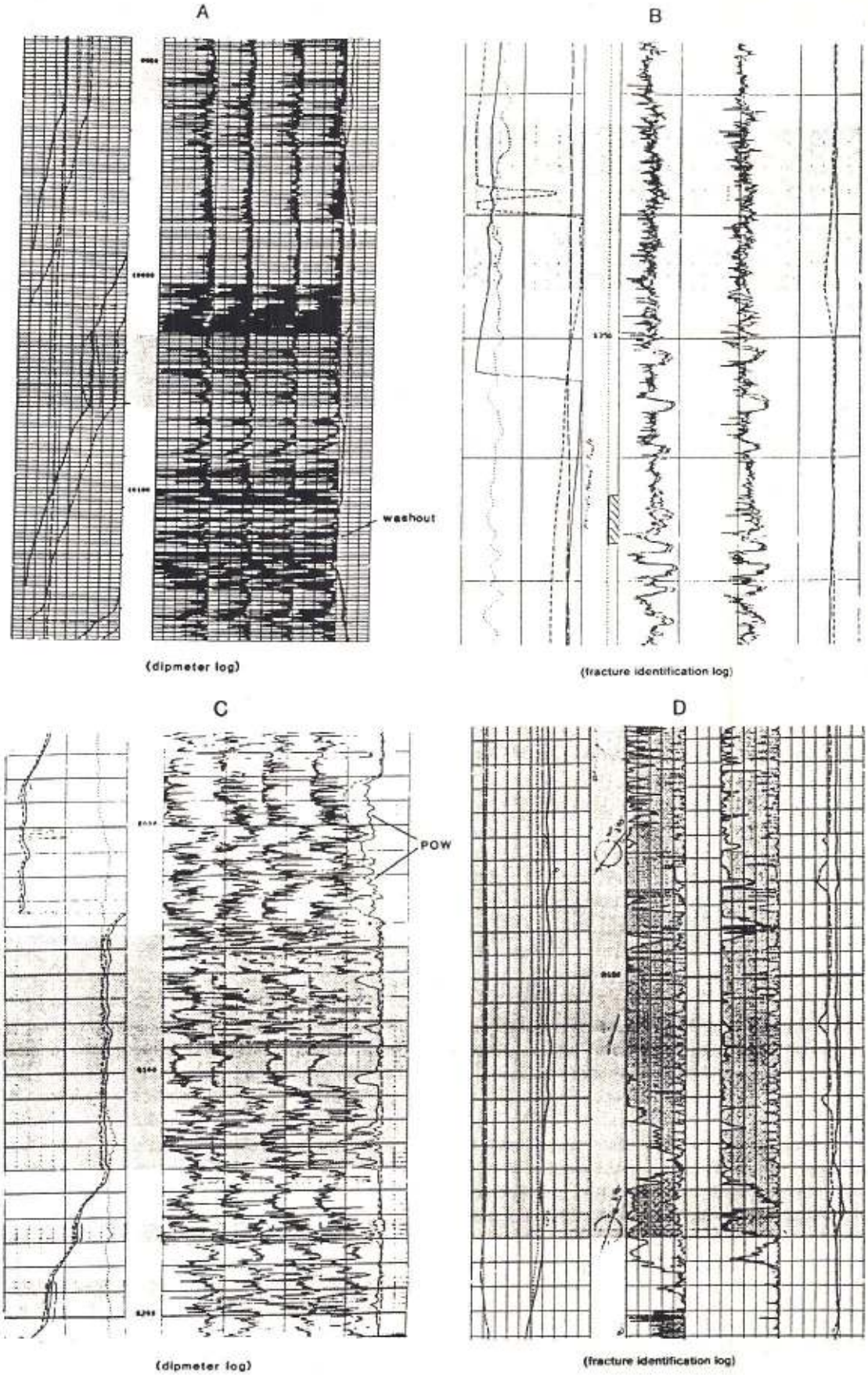
A
B
washout
(dipmeter log)
(fracture identification log)
C
D
POW
(dipmeter log)
(fracture identification log)

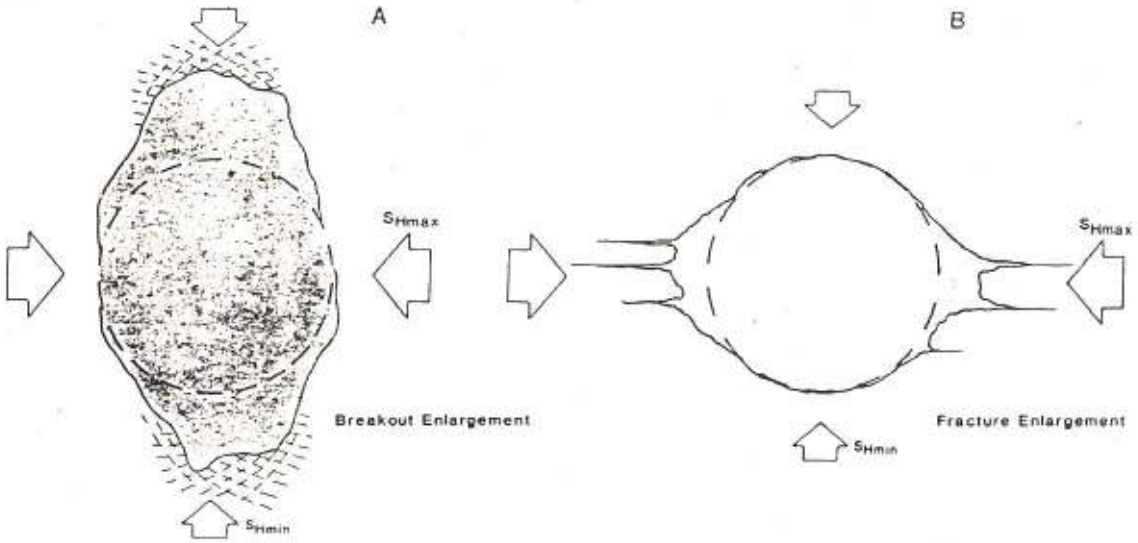

Figure 5: Cross-sectional schematics of wellbores with elliptical breakout and fracture-related enlargements associated with curvilinear shear failure (A) and extensional drilling-induced hydraulic fracturing or open preexisting vertical fractures (B).

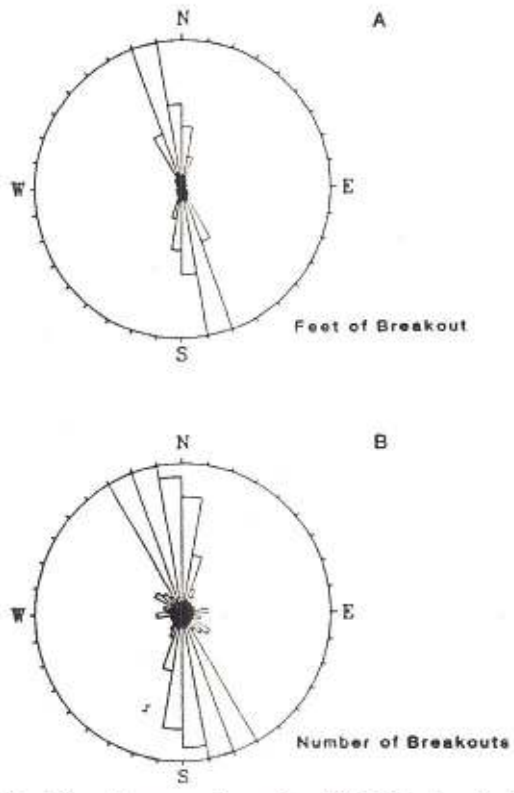

Figure 6: Rose diagrams of combined individual well-data sets for the Anadarko basin illustrating the distribution of wellbore enlargement orientations. Wellbore enlargement frequency of occurrence and azimuthal orientation are expressed as vector length and vector direction, respectively. Vector length (radial distance) is the sum of vertical feet of borehole elongation (A) or number of individual wellbore enlargements (B). Vector direction is wellbore enlargement orientation (azimuthal direction).

number of discrete enlargement intervals (number of breakouts) plus azimuthal orientation. Because there appear to be fewer physical factors governing the frequency of wellbore-enlargement occurrence, enlargement number seems to be a more reliable statistical measurement of the mean distribution of the data than enlargement length.

Statistical calculations include determinations of the mean orientation, the standard or angular deviation of the distribution, and the standard error of the mean (Batschelet, 1965). These statistical data are typically displayed as rose diagrams. Rose-diagram plots (Figures 6, 7) are proportional to pedal length (radial length), not pedal area; therefore, the reader is cautioned to avoid making biased interpretations of apparent data orientations. That is, some degree of areal distortion is inherent in this type of rose diagram display (Werner, 1976).

In compiling rose diagrams of wellbore enlargement azimuths and frequencies of data occurrence from wells located in the Bravo dome area of the Texas Panhandle, we found the data distribution to be both bimodal and the modes orthogonal (Figure 7). One trend of wellbore enlargements had a mean direction of N 50° E and the other N 40° W. Testing in the nearby Stone and Webster Holtzclaw #1 well located in the central Texas Panhandle yielded hydraulic fractures oriented between N 40° E and N 60° E (Borjeson and Lamb, 1987). These hydrofrac data suggest a N 50° E SH_{max} direction implying that the N 40°W trend of wellbore enlargements are probably "true" stress-induced breakouts. The N 50° E orthogonally oriented trend of wellbore enlargements may be either drilling-induced hydrofractures or preexisting natural fractures opened during drilling. It was not possible to conclusively differentiate between orthogonally ori-

computer analysis of digitized well logs. However, this technique probably works best only when orthogonally oriented wellbore enlargements occur in rock with very low porosities. That is, contrasts among conductivity values should be strongest when the influence of rock porosities on induced current flow is at a minimum.

COMPARISON OF STRESS DATA

In all areas studied (Figure 2), the stress orientations inferred from the analysis of wellbore enlargement data are consistent with the pattern of regional stresses inferred from other types of stress data (e.g., focal mechanisms, hydrofrac stress measurements, geologic data of recent slip on faults, and volcanic vent alignments). The inferred state of stress in the various study areas in summarized as follows:

1. Breakout stress orientations from the Denver basin are consistent with ENE extension (Figure 2) inferred from the Rocky Mountain Arsenal earthquakes and extensional tectonics associated with southern Great Plains basaltic volcanism (Evans, 1966; Healy et al., 1968; Zoback and Zoback, 1980).
2. An E–W orientation of SH_{max} (Figure 2) inferred from the breakout data for the southern Illinois basin is consistent with focal mechanisms, borehole-hydrofrac data (Dart, 1985), and other breakout stress data from the Appalachian region (Plumb and Cox, 1987) and with the general NE to E–W oriented regional SH_{max} found throughout the midcontinent stress province (Zoback and Zoback, 1980).
3. Along the Atlantic outer continental shelf, breakout data yielded SH_{max} orientations (Figure 2) that were broadly consistent with the NW to ENE compression observed throughout the Eastern United States and Canada (Zoback and Zoback, 1980; Podrouzek and Bell, 1985; Dart and Zoback, 1987; Ervine and Bell, 1987). However, within the three Atlantic-margin basin settings studied (Georges Bank basin, Baltimore canyon trough, and the Southeast Georgia embayment), the inferred directions of Sh_{min} are normal or nearly normal to the local trend of the continental slope, indicating local rotation of principal stress directions parallel and perpendicular to the shelf–slope break (Dart and Zoback, 1987). This apparent rotation may result from a superimposed margin-normal extensional stress along the continental shelf derived from flexure due to sediment loading on the margin (Dart and Zoback, 1987).
4. The ENE to NE SH_{max} orientation inferred from breakout data in the basins and uplifted areas of the southern midcontinent study region (Figure 2, Texas Panhandle to the Mississippi embayment) (Dart, in press) is consistent with the general state of stress throughout the rest of the midcontinent (Zoback and Zoback, 1980) and is supported by earthquake focal mechanism data from the Mississippi embayment (Herrman, 1979) and hydrofrac data from Oklahoma (von Schonfeldt et al., 1973) and the Texas Panhandle (Borjeson and Lamb, 1987). In central Oklahoma, the generally ENE SH_{max} orientation inferred from breakout data is consistent with the observed left-lateral oblique Holocene slip along the WNW-trending Meers fault (Luza et al., 1987; Ramelli et al., 1987; Madole, 1988). Extensional stress conditions (normal-faulting stress regime) exist within the Bravo dome area of the central Texas Panhandle (Figure 2), as evidenced by a vertical maximum principal stress magnitude calculated from hydrofrac stress-measurements made in the Stone and Webster Holtzclaw #1 well (Figure 7) (Borjeson and Lamb, 1987). The orthogonal trend of inferred fracture-related wellbore enlargements in the Bravo dome area bimodal data set may reflect this extensional stress regime (Dart, in press). That is, hydraulically induced borehole fracturing is more likely to occur in wells located in areas subjected to extensional stress conditions (Stock et al., 1985). Extensional stress conditions may possibly exist north of the Bravo dome area in the Hugoton embayment. The wellbore enlargement data set from the Hugoton embayment area was bimodal-orthogonal. A third bimodal-orthogonal wellbore enlargement data set from Marietta basin wells, located in south-central Oklahoma, may also be indicative of an extensional stress setting (Dart, in press). Stress conditions outside the Marietta basin appear to be compressional indicating that this inferred extensional stress regime within the basin may be a local stress anomaly (Dart, in press).

CONCLUSIONS

Types of observed wellbore enlargements include (1) reliable stress indicators (i.e., stress-induced breakouts, preferentially oriented washouts oriented subparallel and orthogonal to the trend of breakouts, stress-related drilling-induced hydraulic fracture enlargements, and preexisting natural fracture enlargements), and (2) nonindicators of stress (i.e., vertical deviation drilling-induced enlargements, shallow soft-sediment enlargements possibly associated with plastic deformation of the wellbore, and washouts).

Wellbore enlargements as reliable stress indicators are always elliptically shaped in cross section, whereas wellbore enlargements that are not reliable stress indicators may or may not be elliptical in cross section.

Differentiation among the various types of borehole enlargements is possible through a careful evaluation of dipmeter and fracture-identification well logs and by correlating enlargement orientation data with other borehole data (mud weights, fracture history, drilling conditions,

Earthquakes in the Denver Area, Colorado, J. H. Healy (ed.), U.S. Geological Survey Open-File Report, pp. 1–17.

Lowe, D. R. (1985), "Ouachita Trough—Part of a Cambrian Failed Rift System," *Geology*, v. 13, no. 11, pp. 790–793.

Luza, K. V., Madole, R. F., and Crone, A. J. (1987), "Investigation of the Meers Fault, Southwestern Oklahoma," Oklahoma Geological Survey Special Publication 87-1, 75 p.

Madole, R. F. (1988), "Stratigraphic Evidence of Holocene Faulting in the Mid-Continent; the Meers Fault, Southwestern Oklahoma," *Geological Society of American Bulletin*, v. 100, no. 3, pp. 392–401.

Mastin, R. L. (1984), "The Development of Borehole Breakouts in Sandstone," M.S. Thesis, Stanford University, Stanford, California, 101 p.

Plumb, R. A. and Cox, J. W. (1987), "Stress Distributions in Eastern North America Determined to 4.5 km from Borehole Elongation Measurements," *Journal of Geophysical Research*, v. 92, no. B6, pp. 4805–4816.

——— and Hickman, S. H. (1985), "Stress-Induced Borehole Elongation: A Comparison Between the Four-Arm Dipmeter and the Borehole Televiewer in the Auburn Geothermal Well: *Journal of Geophysical Research*, v. 90, no. B7, pp. 5513–5521.

Podrouzek, A. J. and Bell, J. S. (1985), "Stress Orientations from Well Bore Breakouts on the Scotian Shelf, Eastern Canada," Geological Survey of Canada, Paper 85-1B, pp. 59–62.

Ramelli, A. R., Slemmons, D. B., and Brocoum, S. J. (1987), "The Meers Fault—Tectonic Activity in Southwestern Oklahoma," U.S. Nuclear Regulatory Commission, NUREG/CR-4852, 51 p.

Scholle, P. A. (ed.) (1979), "Geological Studies of COST G5-1 Well, U.S. South Atlantic Outer Continental Shelf Area," U.S. Geological Survey Circular 800, 114 p.

——— (ed.) (1980), "Geological Studies on the COST No. B-2 Well, U.S. Mid-Atlantic Outer Continental Shelf Area," U.S. Geological Survey Circular 750, 71 p.

——— and Wenkam, C. R. (eds.) (1982), "Geological Studies of the COST Nos. G-1 and G-2 Wells, U.S. North Atlantic Outer Continental Shelf Area," U.S. Geological Survey Circular 861, 193 p.

Six, D. A. (1968), "Red Oak-Norris Gas Field, Brazil Anticline, Latimer and LeFlore Counties, Oklahoma," *in* Natural Gases of North America, American Association of Petroleum Geology Memoir 9, v. 2, pp. 1644–1657.

Stock, J. M., Healy, J. H., Hickman, S. H., and Zoback, M. D. (1985), "Hydraulic Fracturing Stress Measurements at Yucca Mountain, Nevada, and Relationship to the Regional Stress Field," *Journal of Geophysical Research*, v. 90, no. B10, pp. 8691–8706.

Teufel, L. W. (1985), "Insights into the Relationship Between Well Bore Breakouts, Natural Fractures, and In Situ Stress," *in* U.S. Symposium on Rock Mechanics, E. Ashworth (ed.), 26th Proceedings, Rapid City, South Dakota, 1985, v. 2, pp. 1199–1206.

von Schonfeldt, H. A., Kehle, R. O., and Gray, K. E. (1973), "Mapping of Stress Field in the Upper Earth's Crust of the U.S.," U.S. Geological Survey, Final Technical Report, Grant 14-08-0001-1222, Reston, Virginia, 78 p.

Werner, E. (1976), "Graphic Display of Orientation Data for Visual Analysis, *in* Proceedings of the Second International Conference on Basement Tectonics, M. H. Prodwysocki and J. L. Earle (eds.), pp. 521–527.

Zoback, M. D., Moss, D., Mastin, R. L., and Anderson, R. M. (1985), "Well Bore Breakouts and In Situ Stress," *Journal of Geophysical Research*, v. 90, no. B7, pp. 5523–5530.

Zoback, M. L., Nishenko, S. P., Richardson, R. M., Hasegawa, H. S., and Zoback, M. D. (1986), "Mid-Plate Stress, Deformation, and Seismicity," in *The Geology of North America*, Vol. M, *The Western North Atlantic Region*, P. R. Vogt and B. E. Tucholke (eds.), Geological Society of America, pp. 297–312.

Zoback, M. L. and Zoback, M. (1980), "State of Stress in the Conterminous United States," *Journal of Geophysical Research*, v. 85, no. B11, pp. 6113–6156.

——— and ——— (in press), "Tectonic Stress Field of the Continental United States," *in* Geophysical Framework of the Continental United States, L. Pakiser and W. Mooney (eds.), U.S. Geological Society of America Memoir.

Chapitre 12

INFORMATIONS SUR LA TECTONIQUE

(Déformation des roches)

12.1. INTRODUCTION

Après leur formation, les hydrocarbures sont expulsés de la roche-mère vers les réservoirs sous l'action essentiellement de la pression. C'est à ce mécanisme qu'on donne le nom de *migration primaire*. Dès qu'ils ont atteint un réservoir, les hydrocarbures continuent à s'y déplacer, sous l'action cette fois de la *poussée d'Archimède*, la densité des hydrocarbures étant inférieure à celle des eaux occupant l'espace poreux. C'est à ce deuxième mécanisme qu'on donne le nom de *migration secondaire*. Cette dernière peut être accentuée, ou freinée, sous l'action de gradients hydrodynamiques déplaçant les aquifères. Lors de ces déplacements les hydrocarbures peuvent rencontrer des barrières de perméabilité qui constituent des *pièges* (« traps »), en amont desquels ils vont s'accumuler et former des *gisements*.

On a l'habitude de classer les pièges en trois catégories (Fig. 12-1) :

- les pièges structuraux;
- les pièges stratigraphiques;
- les pièges mixtes ou divers.

Parmi ces trois types, les pièges structuraux jouent le rôle principal. Selon HALBOUTY (1976), 78 % des 306 champs majeurs des Etats Unis (plus de 14 Mt d'huile ou d'équivalent gaz), sont liés à l'existence de pièges structuraux. Si l'on considère maintenant les 266 champs géants du monde (plus de 70 Mt d'huile ou d'équivalent gaz) les pièges structuraux représentent 89 % de l'ensemble (PERRODON, 1980). Ces pièges sont liés à l'action de forces qui ont déformé les roches, *la fermeture* étant assurée par des roches *couvertures* à très faible perméabilité.

Les pièges stratigraphiques, qui représentent 10 % du nombre et des réserves des champs géants du monde (de plus de 70 Mt), correspondent à des barrières de perméabilité soit par variation latérale de faciès, soit par biseaux stratigraphiques ou sous discordance.

Enfin, les pièges mixtes ou divers sont liés à des phénomènes de diagenèse ou de pression différentielle (anomalies de pression).

Compte tenu de leur importance, puisqu'ils conditionnent l'existence de gisements, on va s'efforcer de déceler ces pièges à l'aide de prospection géologique de surface ou de géophysique (gravimétrie, sismique ...).

Ces méthodes permettent la reconnaissance a priori des déformations du sous-sol ou la détection de biseaux. Cette étape de l'étude d'un bassin sédimentaire conduit le plus souvent à l'implantation de puits d'exploration. Mais à ce stade l'image du sous-sol est en général simple, la résolution des techniques de surface utilisées et le maillage n'étant pas suffisants pour permettre de déceler des phénomènes de faible amplitude ou plus complexes.

L'enregistrement des pendagemétries dans les puits d'exploration et de développement et leur analyse, menée conjointement à l'établissement de corrélations, à l'étude des régimes de pression dans les réservoirs et éventuellement, quand c'est possible, à des compléments sismiques à plus haute résolution, permettent souvent de préciser l'image de la structure.

Ainsi, dans le cas de l'exemple de la Fig. 12-2, les corrélations entre les trois puits X, Y et Z conduisaient à la forme structurale représentée par la Fig. 12-2a. La prise en compte des données de pendagemétrie modifie sensiblement l'allure structurale finale, en particulier la position du point haut de l'anticlinal (Fig. 12-2b).

De même certaines structures de Mer du Nord, telles que celle de Piper (Fig. 12-3), interprétées à l'origine comme des anticlinaux ou des biseaux

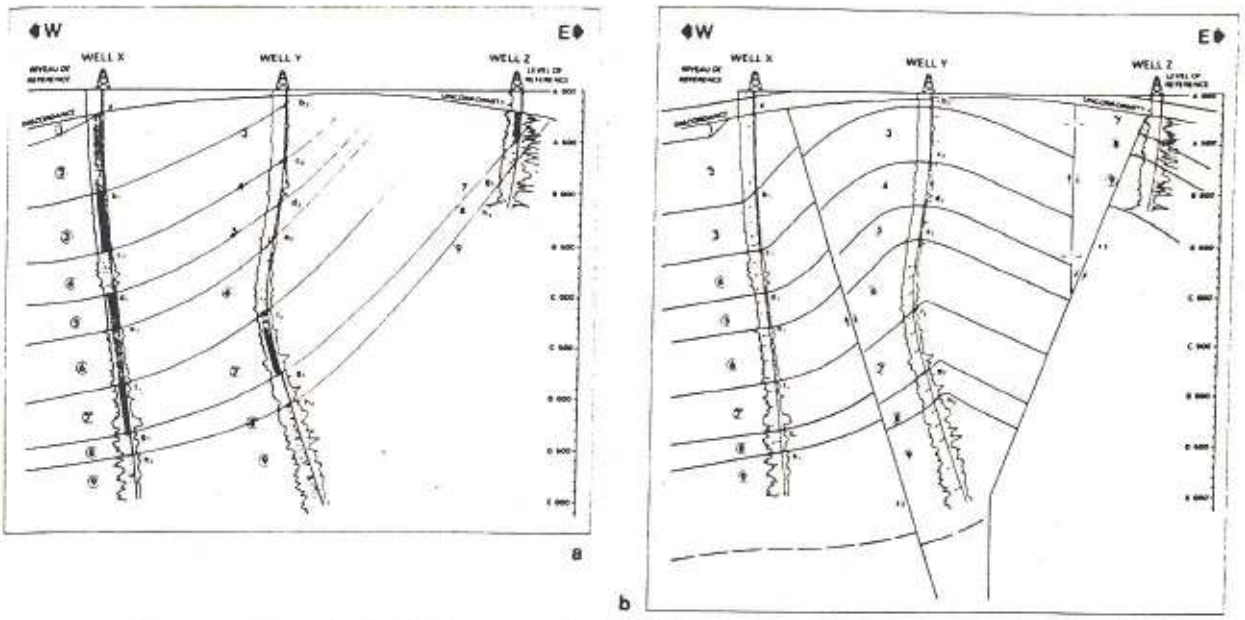

Fig. 12-2. - (a) Structure déduite des corrélations entre trois puits; (b) image structurale obtenue en introduisant les données de pendage (d'après Evaluation de formaciones en Venezuela, 1980)

sous discordance, sont apparues beaucoup plus complexes et constituées par une succession de panneaux faillés.

Mais il faut se convaincre que l'interprétation des données de pendagemétrie ne peut se faire dans l'absolu ou isolément, c'est-à-dire sans connaissance de la lithologie, du type d'environnement et du style tectonique du bassin dans lequel se trouve le forage. Par ailleurs, la connaissance de quelques notions essentielles sur les mécanismes entraînant les déformations, sur le comportement mécanique des roches et sur les relations entre les types de déformation et les bassins, nous semble indispensable. Ces notions permettent d'avoir une meilleure compréhension des problèmes auxquels on va être confronté.

C'est pourquoi il nous paraît utile de les rappeler avant d'aborder l'interprétation proprement dite des données de pendagemétrie.

12.2. RAPPEL DE NOTIONS GENERALES

12.2.1. Définitions

La *géologie structurale* est la branche de la géologie qui traite de la forme, de l'arrangement et de la structure interne des roches, et plus spécialement de la description, de la représentation et de l'analyse des structures à moyenne ou petite échelle.

La *tectonique* traite des mêmes objets mais à plus grande échelle. Elle s'attache de surcroît à l'étude de leurs relations mutuelles, de leur origine et de leur évolution historique.

Une *structure*, au sens tectonique du terme, est la forme, tel un pli ou une faille, produite par

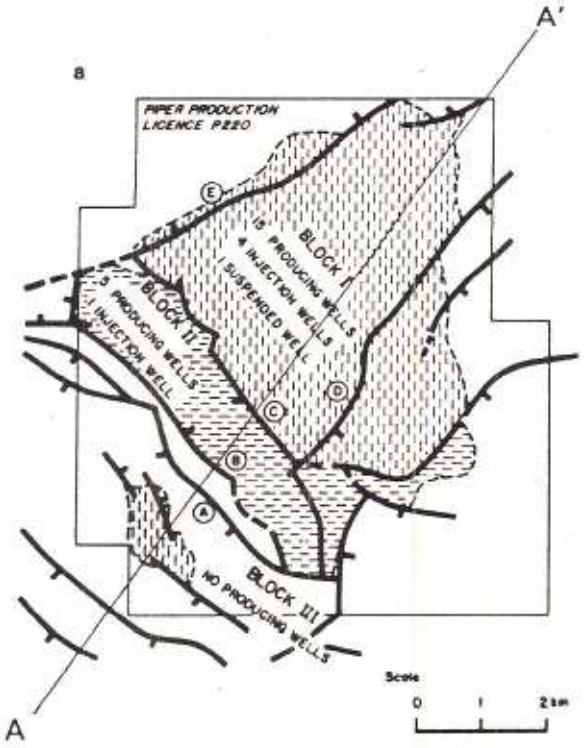

Fig. 12-3. - a) Plan de position de la coupe à travers le champ de Piper.

en grandeur et direction suivant l'orientation de la surface sur laquelle elle s'applique. La pression s'exerçant en A sur l'ensemble des plans passant par A, s'appelle la contrainte . Physiquement on peut l'appeler la cohésion, existant en A, entre les éléments de roche. Si on intègre à l'ensemble lithologique on a un *champ de contrainte*. On démontre qu'on peut calculer l'ensemble des contraintes en un point d'un corps si l'on connaît celles qui s'appliquent en ce point sur trois plans perpendiculaires entre eux (Fig. 12-6). On démontre aussi qu'en chaque point A, il existe 3 plans orthogonaux entre eux pour lesquels $\tau = 0$, et donc pour lesquels la contrainte leur est perpendiculaire.

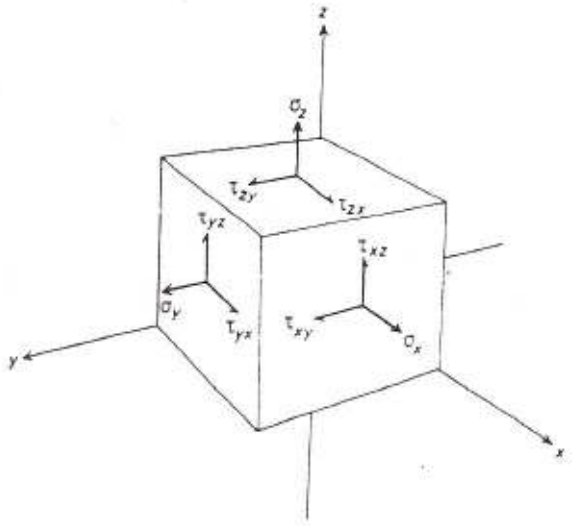

Fig. 12-6. - Décomposition des contraintes agissant sur les surfaces d'un cube (d'après RAMSAY, 1967).

Les trois vecteurs normaux à ces plans s'appellent les contraintes principales. Ce sont :
- la contrainte principale majeure, σ_1;
- la contrainte principale intermédiaire, σ_2;
- la contrainte principale mineure σ_3;

avec naturellement : $\sigma_1 > \sigma_2 > \sigma_3$.

Il existe également deux plans formant entre eux un angle inférieur à 90°, dont le plan (σ_1, σ_2) est bissecteur et pour lesquels τ est maximum. Ce sont les plans de cisaillement. C'est le long de ces plans que se produiront les ruptures et les glissements (Figs. 12-6 et 12-7).

12.2.3. Comportement mécanique des roches

Tout champ de contrainte impose un champ de déformation. Mais la déformation résultante dépend de la nature et du comportement mécanique du milieu déformé.

Il existe trois types de comportement mécanique :
- Le *comportement élastique* :

il se caractérise par un retour possible à l'état

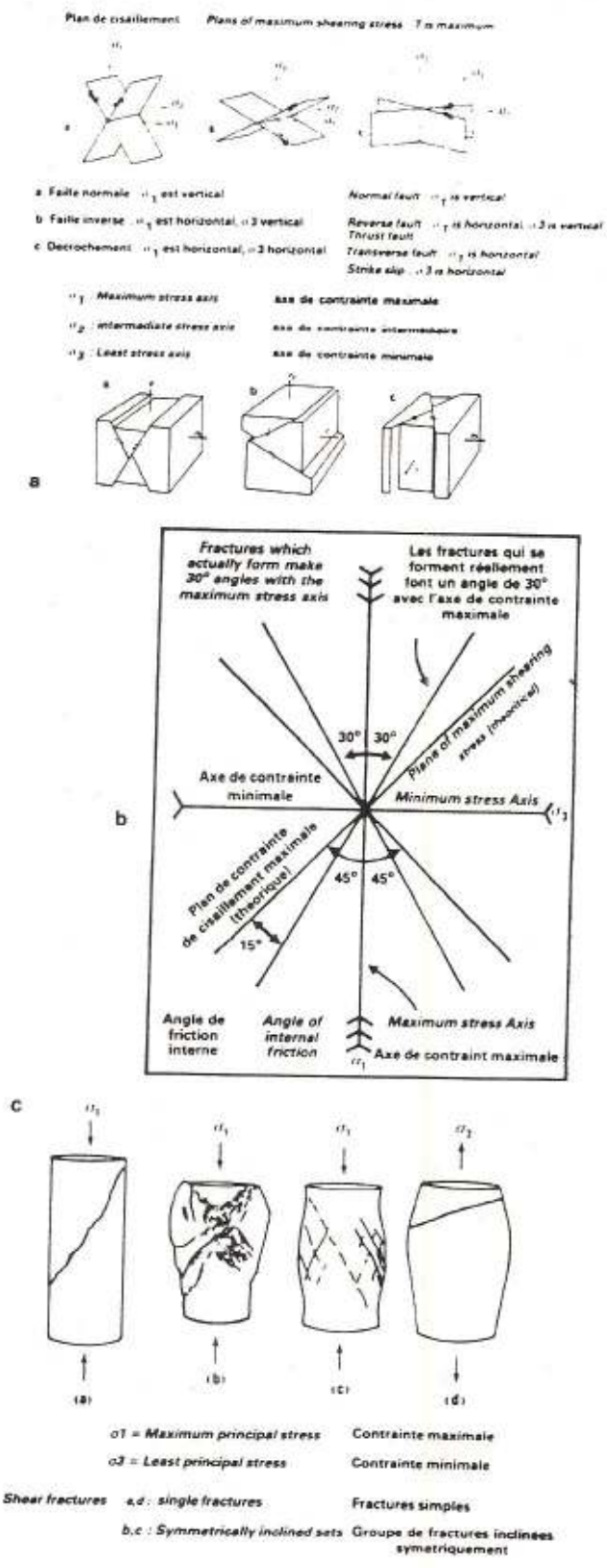

Fig. 12-7. - (a) Types de déformation suivant la direction des contraintes maximale et minimale; (b) relations entre les directions des plans de fractures et les directions de contraintes; (c) déformation d'une roche suivant les directions de contraintes.

- Dominante élastique :

Le cristal de quartz a un comportement élastique parfait. Les roches à comportement élastique sont :

. les roches cristallines;

. les roches sédimentaires compactes sans porosité (anhydrite ...).

- Dominante plastique :

Ce sont essentiellement les roches poreuses (grès, craie).

- Dominante visqueuse :

Certaines roches peuvent avoir un comportement visqueux à des températures et pressions faibles à moyennes : argiles sous-compactées ou « boues », (halo- ou argilo-cinèse).

12.2.5. Influence du temps

Le temps joue un rôle très important dans le comportement des roches. Ces dernières peuvent avoir un comportement élastique en réponse à des contraintes de très courtes durées, ou un comportement plastique si ces contraintes sont appliquées sur une longue période. Cette influence est mise en évidence dans les expériences de fluage où une charge faible appliquée suffisamment longtemps produit une déformation pouvant aller jusqu'à la rupture, alors qu'au cours d'un essai instantané cette même contrainte n'aurait provoquée aucune déformation mesurable. Aussi, à l'échelle des temps géologiques, les roches peuvent-elles être considérées comme des corps plus ou moins visqueux.

12.2.6. Influence de la pression et de la température

Le comportement des roches varie beaucoup avec la pression et la température, donc avec la profondeur. En fonction de ces facteurs on peut donc définir différents domaines de déformation :

- un *domaine supérieur* où les roches ont un comportement élasto-plastique;

- un *domaine intermédiaire* ou moyen, où elles ont un comportement plastique à visqueux;

- un *domaine profond* où elles vont avoir un comportement visqueux. C'est celui qui se caractérise par l'apparition de la schistosité puis de la foliation. Il correspond à l'anchimétamorphisme et au métamorphisme. Il n'interesse donc pas la recherche pétrolière, la porosité et la perméabilité des roches ayant alors disparu.

12.2.7. Types de contraintes

Il existe trois types de contraintes :

- la *tension* ou *traction* : c'est une contrainte qui étire le matériau et peut en augmenter le volume;

- la *compression* : c'est une contrainte qui diminue le volume du matériau;

- la *contrainte de cisaillement* : elle produit un changement de forme mais non de volume (Fig. 12-14).

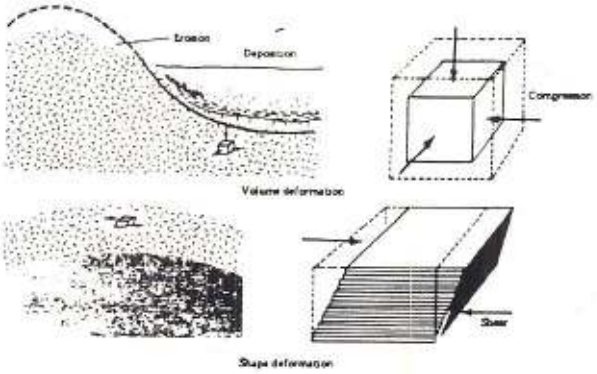

Fig. 12-14. - Déformation sans changement de volume sous l'effet d'une contrainte de cisaillement (d'après LEET et al., 1978).

12.2.8. Résistance des roches

Les roches résistent plus ou moins aux contraintes. La *résistance* d'une roche correspond à la contrainte à partir de laquelle elle commence à être déformée de façon permanente.

Les roches présentent plusieurs types de résistance, du fait qu'elles répondent différemment aux différentes contraintes. On a ainsi pour chaque roche une résistance à la compression, à la traction et au cisaillement.

Tableau 12-I

Résistance moyenne des roches à la compression, la traction et la torsion (d'après BILLINGS, 1942).

En kg par cm²

Roche	*Compression*	*Tension*	*Cisaillement*
Grès	500 à 1 500	10 à 30	50 à 150
Calcaire	400 à 1 400	30 à 60	100 à 200
Granite	1 000 à 2 800	30 à 50	150 à 300
Diorite	1 000 à 2 500	.....	.....
Gabbro	1 000 à 1 900	.....	.....
Basalte	2 000 à 3 500	.....	.....
Felsite	2 000 à 2 900	.....	.....
Marbre	800 à 1 500	30 à 90	100 à 300
Ardoise	700	250	150 à 250

Quand la différence entre les résistances à la compression et à la traction est très grande on dit que la roche est *cassante* (« brittle »).

Si Δl est un incrément infiniment petit, alors on peut écrire :

$$\varepsilon = \int_{l_0}^{l_1} \frac{\Delta l}{l} = \log_e \frac{l_1}{l_0} = \log_e(1 + e) \quad (12 - 4)$$

- *l'angle de cisaillement*, ψ, et la *déformation de cisaillement*, γ, qui traduisent les variations d'angle :

$$\gamma = \tan\psi \quad (12 - 5)$$

Dans une déformation dans trois dimensions (Fig. 12-17), on considère les variations de coordonnées d'un point avant (x, y, z) et après déformation (x_1, y_1, z_1).

On a l'habitude de classer les déformations en deux types, en fonction des critères géométriques suivants :

- *les déformations homogènes* (Fig. 12-16b)

Elles se caractérisent par les propriétés suivantes :

. les lignes droites restent droites après déformation;

. les lignes parallèles restent parallèles après déformation;

. toutes les lignes dans la même direction présentent des valeurs constantes de e, et ψ.

- *les déformations non homogènes* (Fig. 12-16c)

Dans ce cas on observe que :

. les lignes droites deviennent courbes après déformation;

. les lignes parallèles perdent leur parallélisme;

. Pour n'importe quelle direction donnée dans le corps déformé, les valeurs e et ψ sont variables.

Il existe deux grandes catégories de déformation.

12.2.11. Les déformations continues : les plis

Un pli est une déformation souple de matériaux soumis à des contraintes tant en compression qu'en distension.

. En *distension* :

une faille normale dans le socle peut se traduire dans la couverture par une flexure des couches sus-jacentes (Fig. 12-18a). De même dans le cas d'une compaction différentielle (Fig. 12-18b), ou de mouvements verticaux : montées diapiriques (argilo- ou halo-cinèse), intrusions magmatiques.

. En *compression* :

on peut avoir tous les types possibles de plis suivant le mécanisme mis en oeuvre (flexure par compression ou action d'un couple, plissement par cisaillement), le comportement mécanique des roches et leur *compétence*. Cette dernière est une propriété relative qui traduit la capacité d'une roche de supporter une compression sans écoulement et donc sans variation d'épaisseur. Une roche compétente va transmettre une force de compression plus loin qu'une roche incompétente. Ainsi, sous l'effet d'une compression, les couches

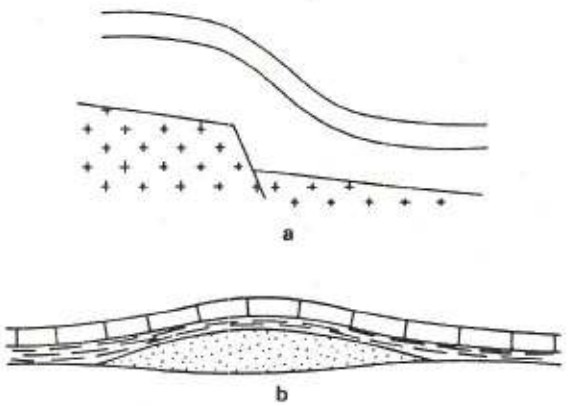

Fig. 12-18. - Exemples de plis en distension.

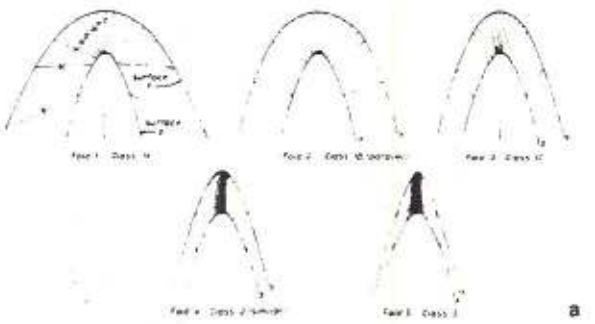

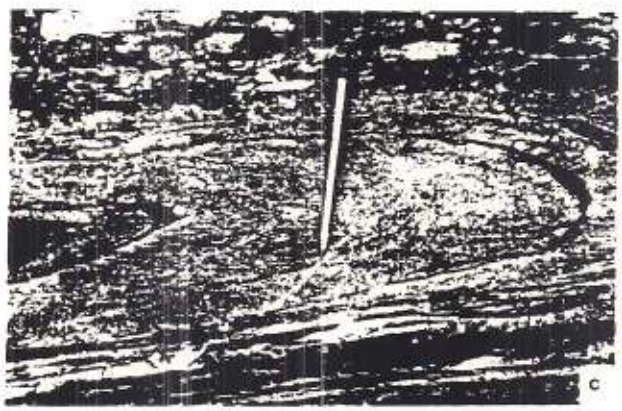

Fig. 12-19. - Types fondamentaux de classes de plis : a) plis théoriques; b) plis isopaches; c) plis semblables (d'après RAMSAY, 1967).

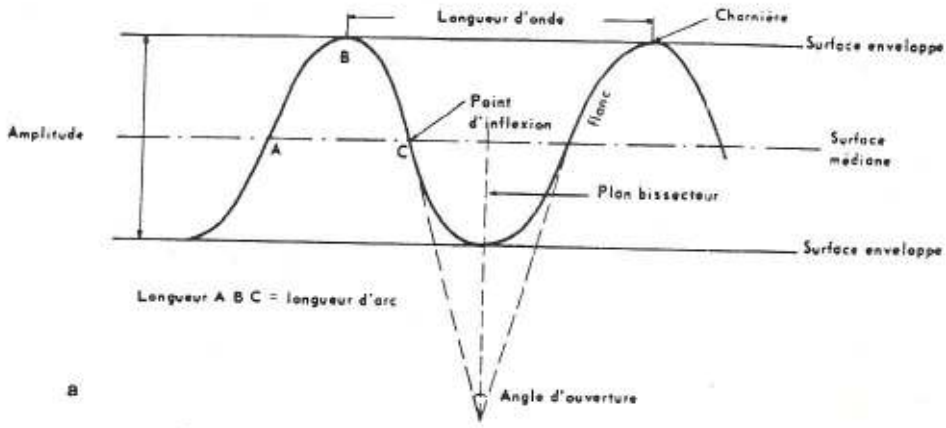

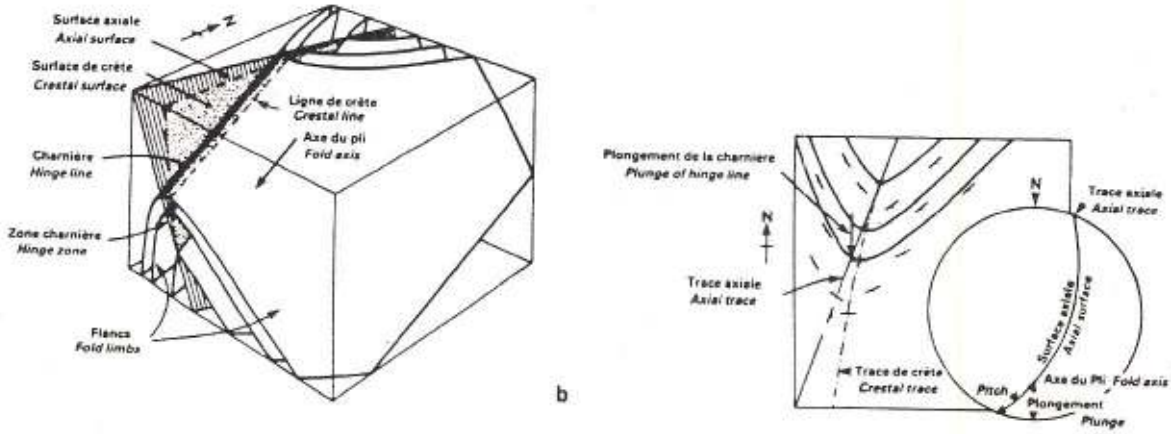

Fig 12-22. - Les éléments descriptifs d'un pli (d'après RAMSAY, 1967).

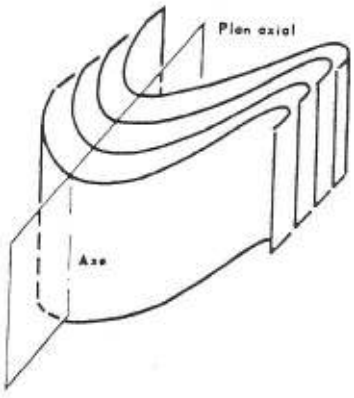

Fig 12-23. - Pli à axe vertical.

Fig. 12-24. - Les différentes formes de plis.

forme du pli ne varie pas avec la profondeur (Fig. 12-19c). Ces plis sont formés à grande profondeur et dans la zone à schistosité.

12.2.11.4. *Nomenclature des plis*

Outre les classements ci-dessus par courbure et par type, les plis sont classés en fonction de leur forme géométrique telle qu'elle peut être révélée par une section transversale. La Fig. 12-25 rassemble les principaux d'entre eux avec leur nomenclature et la représentation théorique des pendages dans un plan perpendiculaire à l'axe.

verticale sensu stricto ou « dip slip fault »); *horizontale* : on parle alors de *décrochement* (« strike slip fault »); ou mixte (« diagonal slip fault »).

Dans un mouvement de rotation, certaines lignes droites dans chaque compartiment, qui étaient parallèles avant la dislocation, ne le restent plus après. Le pendage des couches dans chaque compartiment est différent de part et d'autre du plan de faille (Fig. 12-28).

D'une certaine façon la plupart des failles avec mouvement de translation présentent un certain pourcentage le rotation. Les déplacements le long du plan de faille ne sont en effet pas constants par suite des différences de résistance des matériaux en chaque point. Toutefois, si la rotation n' est pas trop importante, on peut considérer le mouvement comme étant seulement de translation.

Fig. 12-28. - Failles avec déplacement par rotation.

12.2.12.2. *Eléments descriptifs d'une faille* (Fig. 12-29)

Une faille est complètement décrite quand on a défini les éléments suivants :

- *Son orientation* ou sa *direction* (« strike ») c'est-à-dire la direction, par rapport au nord, de la ligne d'intersection du « plan » de faille avec l'horizontale.

- *Son rejet* (« net slip ») qui définit l'ampleur du déplacement. Il se décompose lui-même en :

. *glissement oblique, bc,* (« dip slip »), qui est la longueur mesurée parallèlement au pendage du plan de faille, qui se décompose à son tour en :

. *rejet vertical, ae,* (« throw ») qui correspond au déplacement mesuré suivant une verticale,

. *rejet transversal, ed,* (« heave »), qui est égal au déplacement mesuré sur une horizontale perpendiculairement à la direction de la faille;

. *décrochement,* ou encore *rejet horizontal longitudinal, ac,* (« strike slip ») qui correspond au déplacement horizontal mesuré parallèlement à la direction de la faille.

- *Sa rotation* qui est l'angle formé par les deux parties d'une même couche après séparation, et mesuré dans un plan perpendiculaire à l'axe de rotation.

D'autres éléments sont parfois utilisés pour décrire une faille. Ainsi le « pitch » est l'angle qu'une ligne, dans un plan, fait avec une ligne horizontale du plan. Dans la Fig. 12-29 l'angle bac, mesuré dans le plan de faille, est le « pitch » du rejet.

La charnière (« hinge line ») est la ligne, dans le plan de faille, qui sépare les parties déplacées vers le haut de celles déplacées vers le bas.

D'autres termes sont également utilisés pour décrire une faille. Les deux parties séparées par le plan de faille sont les *compartiments*. Le compartiment haut est le *toit* (« hanging wall »), le compartiment bas est le *mur* (« footwall »). Les surfaces engendrées par le plan de faille sur chaque compartiment sont appelées les *lèvres*. Une de ces dernières est parfois dégagée par l'érosion, et polie ou striée suivant la direction du déplacement. On parle alors de *miroir de faille* (« slickenside »). Le *regard* (« upthrow side ») de la faille est le côté vers lequel est tournée la lèvre du compartiment soulevé.

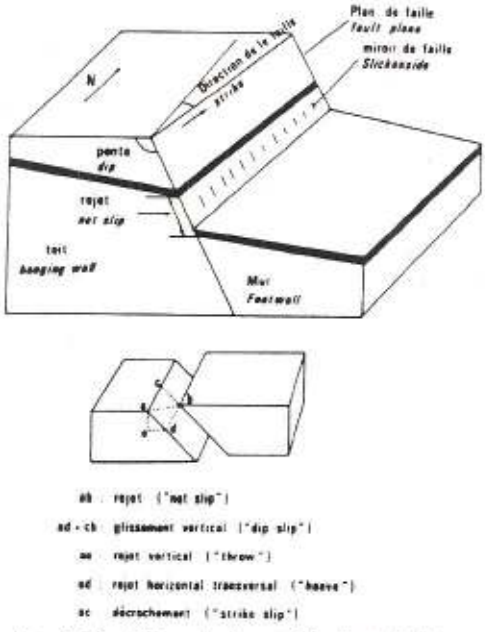

Fig. 12-29. - Eléments descriptifs d'une faille.

12.2.12.3. *Classification des failles*

Différents critères sont habituellement retenus. C'est ainsi que l'on peut classer les failles suivant la *position relative des couches* (Fig. 12-30). On parle ainsi, suivant le rejet, de :

- faille *normale,* (« gravity fault » ou « normal fault »), encore appelée faille *directe,* dans laquelle le rejet horizontal transversal correspond à une distension. Elle conduit à une suppression de couches sur une verticale donnée;

- faille *inverse,* (« thrust fault » ou « reverse fault »), dans laquelle le rejet horizontal transversal correspond à un racourcissement par suite d'une compression. On observe alors un chevauchement du compartiment situé au-dessus du plan de faille

12.4. METHODES DES ANALYSES STRUCTURALES A PARTIR DES PENDAGEMETRIES*

Afin d'entreprendre efficacement l'interprétation d'une pendagemétrie, il faut rassembler un certain nombre de documents et de données, utiles, sinon indispensables pour une analyse sérieuse et complète.

- Le « tracé-flèches » dont l'en-tête précise le type de traitement (MARK IV, CLUSTER, GEODIP, LOCDIP) et les paramètres utilisés pour le traitement (intervalle de corrélations, angle de recherche, recouvrement; nombre d'échantillons pour le calcul de la dérivée). A ce stade il convient de s'assurer de la qualité du traitement, et donc du bon choix des paramètres, par un examen du log-terrain.

- Le « listing », ou tableau de résultats, donnant les valeurs d'azimut et de pendage ainsi qu'une idée sur la qualité du résultat.

- Le « log-terrain », comportant les courbes de résistivité, les diamétreurs, la déviation, l'azimut du patin 1, le balourd; il permet de vérifier la vitesse de rotation de l'outil et de contrôler le bon contact des patins avec la paroi du trou; par ailleurs il donne également une idée sur l'importance des contrastes lithologiques à travers ceux observés sur les résistivités.

- Le « log-composite », rassemblant l'ensemble des autres diagraphies enregistrées permettant de se faire une idée de la lithologie.

- La coupe lithologique détaillée de l'intervalle à analyser, établie à partir de l'analyse des déblais de forage ou à partir d'une interprétation des diagraphies par un programme du type LITHO.

- La bande magnétique avec les résultats en vue d'un traitement automatique par ordinateur.

Remarque : Toutes ces informations ne sont malheureusement pas toujours disponibles (cas des puits d'échange).

Une des caractéristiques de la pendagemétrie est de fournir généralement une grande quantité de mesures de pendages. De ce fait il est nécessaire d'utiliser des méthodes analytiques susceptibles de formaliser l'organisation de ces pendages et d'aboutir à des présentations plus synthétiques des géométries qu'ils décrivent.

Il existe deux méthodes : l'une que l'on peut qualifier de rapide (« Quick-look ») qui utilise les groupements de pendages, l'autre plus élaborée qui fait appel aux projections stéréographiques. Cette dernière, quoique plus longue, permet une analyse plus détaillée des données de pendagemétrie, conduisant à une reconstitution plus complète et précise des structures traversées.

* Ce chapitre a été rédigé avec le concours de J. HENRY, SNEA(P), Pau.

12.4.1. Méthode des groupements de pendage

Quand on examine le tracé-flèches (« arrow-plot »), où sont présentés les résultats du calcul des pendages (Fig. 12-32), on constate souvent que les « flèches », ou pendages, s'ordonnent, de bas en haut d'un intervalle, suivant trois types de groupement (« pattern »), auxquels GILREATH et al. (1964) ont donnée des codes de couleur :

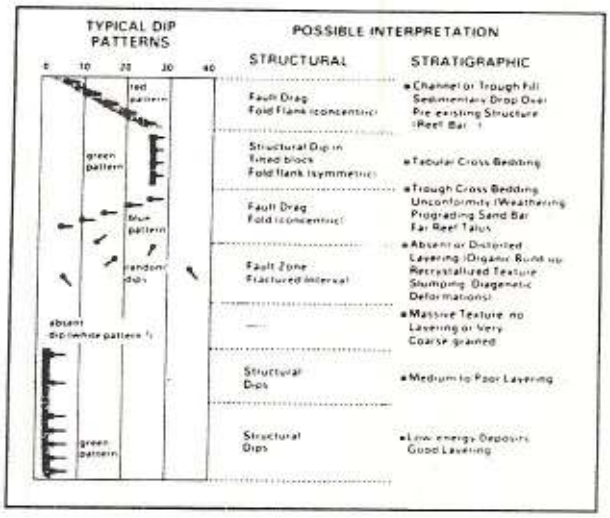

Fig. 12-32. - Groupements typiques de pendages

- *groupement vert* (« green pattern ») : il correspond à une succession de pendages présentant sensiblement le même angle et le même azimut;

- *groupement bleu* (« blue pattern ») : il correspond à une augmentation de l'angle du pendage vers le haut, sans grande modification de l'azimut;

- *groupement rouge* (« red pattern ») : c'est l'inverse du cas précédent : l'angle du pendage diminue vers le haut, l'azimut restant à peu près constant.

Le premier groupement, quand il s'observe dans des séries de basse énergie, correspond généralement au pendage structural (monoclinal ou flanc d'un pli semblable, Fig. 12-33, zone 4860-4940).

Les deux autres groupements, s'ils s'observent aussi dans des séries de basse énergie, révèlent des déformations structurales des couches pouvant être reliées à des plis, à des failles avec phénomènes associés : basculement (« rollover »), étirement ou crochon (« drag »); ou à des discordances (« unconformity »).

Les schémas de la Fig. 12-34 rassemblent les réponses théoriques dans les différents cas.

L'analyse rapide d'une pendagemétrie débute en général par la détermination du *pendage structural* sur le *tracé-flèches*. Il s'agit de définir le pendage de couches présumées avoir été déposées horizontalement et parallèlement. L'extrapo-

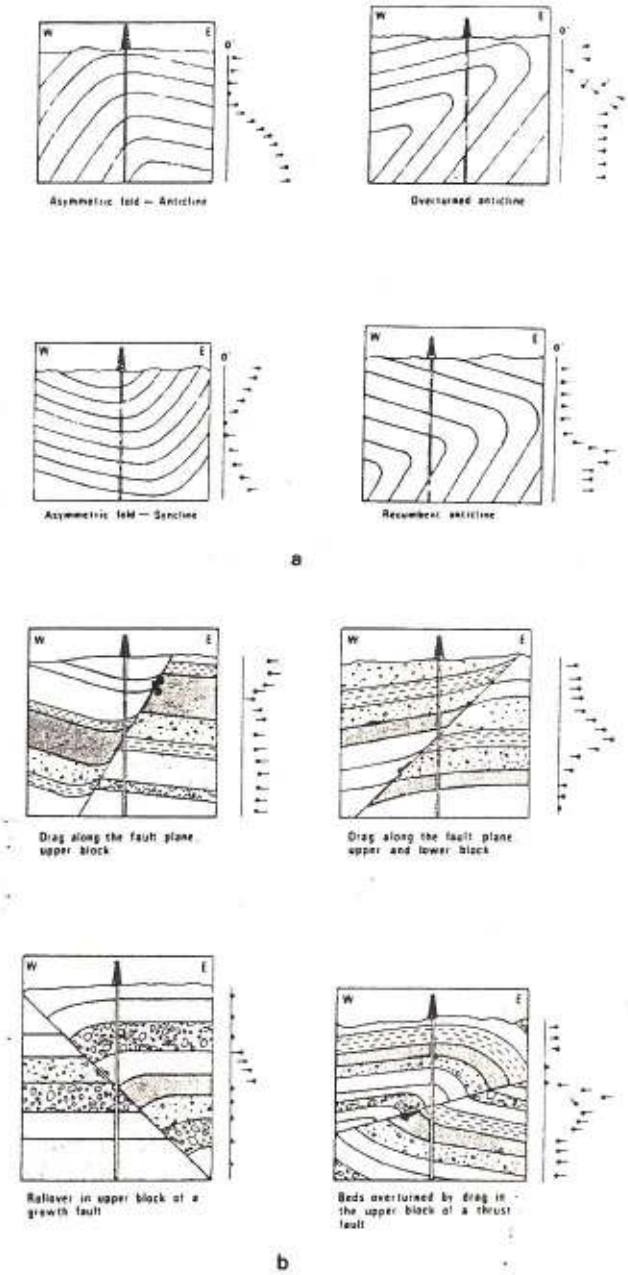

Fig. 12-34. - Tracés-flèches théoriques (a) : dans le cas de plis; (b) : dans le cas de failles (documents Schlumberger).

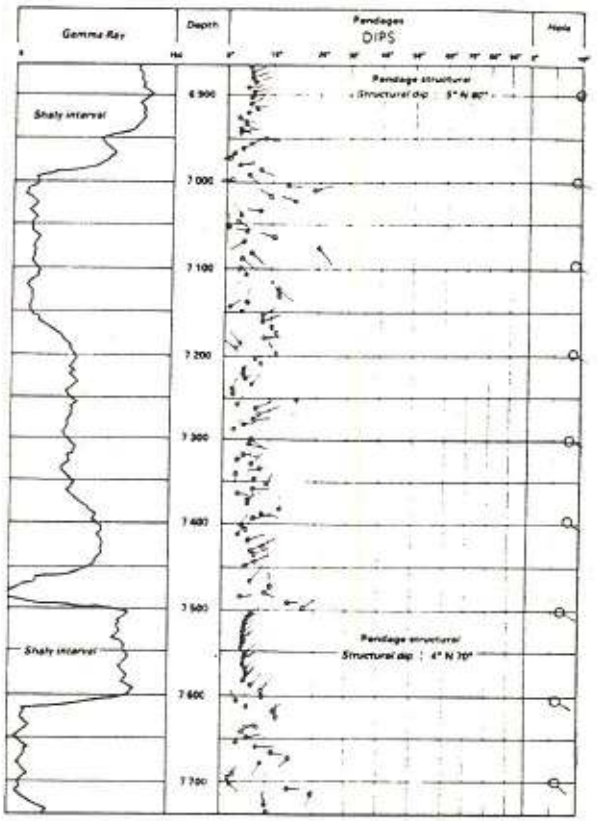

Fig. 12-35. - Exemple d'un tracé-flèches et de son interprétation pour la détermination du pendage structural par sélection des groupements « verts ».

contours d'horizons donnés qui sont orthogonaux aux azimuts déterminés.

La seconde étape de l'analyse d'une pendagemétrie est la *mise en évidence* de *déformations des couches* sous l'effet des contraintes tectoniques. Parmi ces déformations, les *failles* sont en général celles que l'on cherche, en premier, à *identifier* et à *localiser en profondeur*. Il faut se souvenir qu'une faille ne peut être détectée que si sa formation s'est accompagnée de phénomènes associés (basculement, étirement, rotation, bréchification ....).

C'est fort heureusement souvent le cas et ceci se traduit alors fréquemment sur le tracé-flèches par l'apparition de groupements rouges ou bleus. On va donc rechercher ces figures, en se souvenant toutefois que tout groupement (rouge ou bleu) n'est pas nécessairement associé à une faille. Il peut en effet correspondre à des figures sédimentaires (« foreset », stratification entrecroisée, ...), ou à un pli, un drapé ou encore à une discordance. Le rattachement de ces groupements à l'un ou l'autre des ces phénomènes se fera en considérant d'une part la lithologie, le faciès et l'environnement de dépôt dans lequel il s'observe, d'autre part le groupement lui-même et sa position dans la série stratigraphique. Ainsi, un groupement rouge superposé à une formation sableuse ou carbonatée et s'arrêtant à son toit, correspond plus vraisemblablement à un drapé sur la forme convexe définie par le banc de sable ou le récif qu'à une faille.

Dans le cas de la forme convexe, on peut définir d'une part la direction de l'*allongement de la forme* : perpendiculaire à la direction des azimuts des couches qui la surmontent; d'autre part sa *crête* : elle est dans la direction opposée à celle du pendage (cf. Fig. 4-38 et 4-39 chapitre 4).

Un groupement sans variation significative

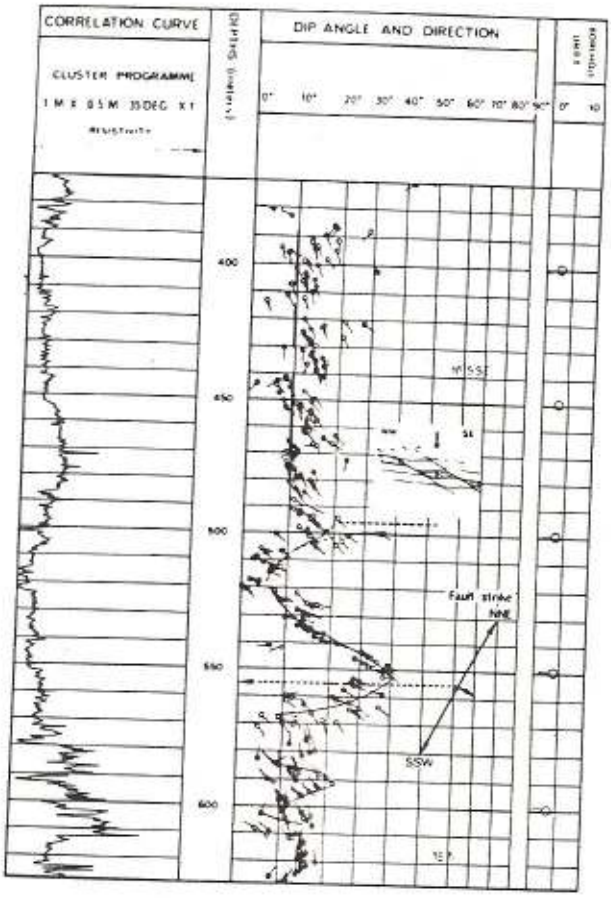

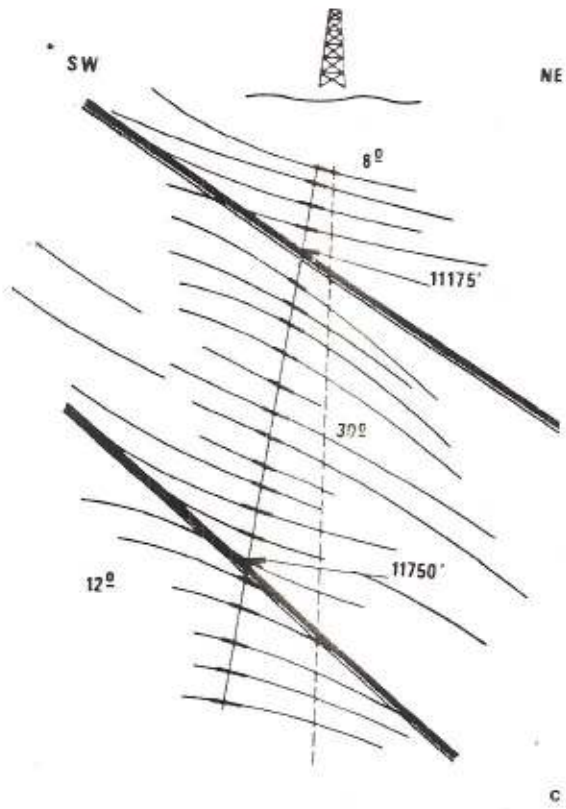

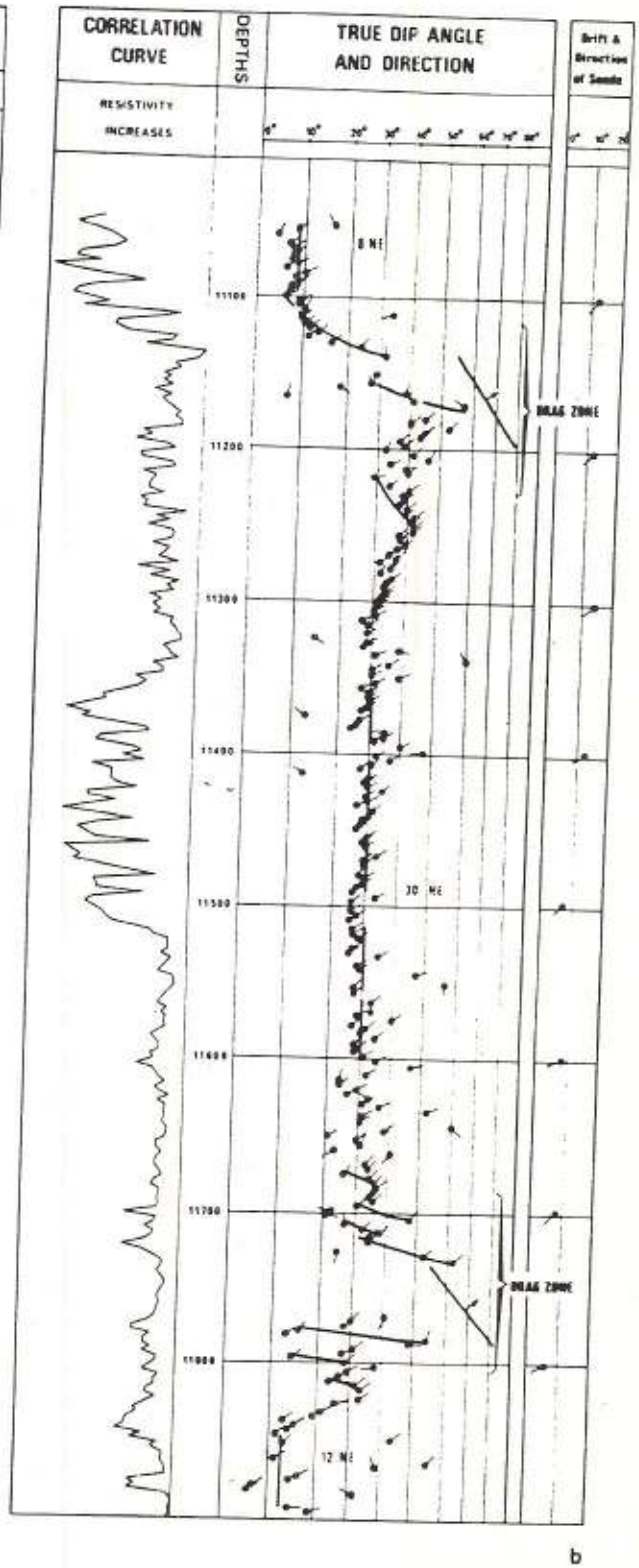

Fig. 12-36 - Exemples de zones faillées telles que vues sur un tracé-flèches. (a) : extrait de la WEC Algeria, 1979. (b) : extrait de la WEC Iran, 1976. (c) : interprétation du dernier exemple

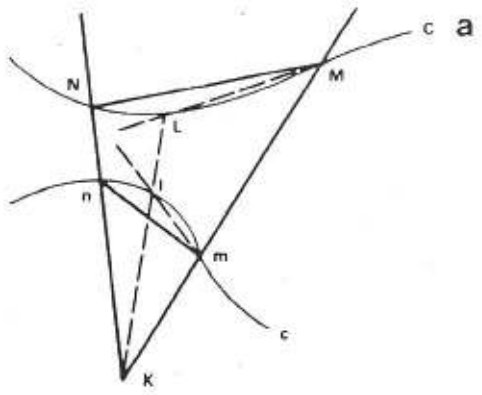

KM.km = KL. KI = KN. kn = constant

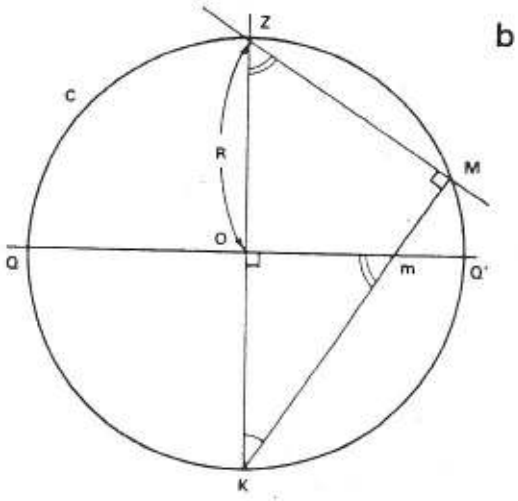

KM.km = KZ.KO = 2 R²

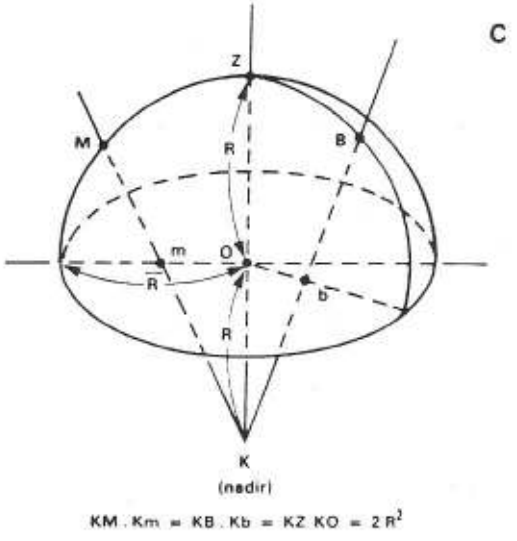

KM . Km = KB . Kb = KZ.KO = 2 R²

Fig. 12-39. - La projection stéréographique est un cas particulier d'inversion.

12.4.2.2. *Construction du stéréogramme ou canevas isogone de WULFF*

Le stéréogramme de WULFF représente la projection stéréographique des *parallèles* et des *méridiens* de la demi-sphère de référence sur le plan horizontal contenant l'axe nord-sud, avec comme pôle de la projection le pôle inférieur ou *nadir*.

Les schémas de la Fig. 12-40 expliquent comment les méridiens sont représentés par des arcs de grands cercles, dénommés sur la projection des *grands cercles*, et les parallèles par des arcs de petits cercles, désignés comme des *petits cercles*.

La Fig. 12-41 représente le canevas isogone de WULFF pour des méridiens inclinés de 2° en 2° et des parallèles recoupant le méridien nord-sud, de 2° en 2°.

Le cercle extérieur du canevas est dénommé le *cercle fondamental* ou la *primitive*. Cette projection conserve les angles : les grands cercles et les petits cercles sont orthogonaux entre eux. Les aires délimitées par deux parallèles et deux méridiens successifs varient suivant leur position.

Cette projection est couramment utilisée. Elle sert en effet à déterminer le pendage vrai à partir de pendages apparents (voir Annexe 3, Tome 1), à déterminer l'angle entre deux plans, le plan bissecteur entre deux plans, l'intersection de couches et d'une faille ... .

Par contre, elle présente l'inconvénient de ne pas conserver les surfaces puisqu'il s'agit d'une inversion. On ne peut donc pas établir facilement des diagrammes de densité de points à partir de ce stéréogramme. Pour établir ces diagrammes on doit utiliser le stéréogramme *isoaire* de SCHMIDT.

12.4.2.3. *Construction du stéréogramme ou canevas isoaire de SCHMIDT*

Le canevas isoaire de SCHMIDT correspond à une projection LAMBERT, par rapport au centre de la sphère, des parallèles et des méridiens qui sont alors représentés par des arcs d'ellipse. Les surfaces limitées par deux parallèles et deux méridiens sont égales quelle que soit leur position sur la projection (Fig. 12-42).

Ce canevas se prête aux même types de constructions et manipulations effectuées sur le stéréogramme de WULFF. Il présente l'avantage d'étaler plus les pôles des plans à pendage faible et est de ce fait préférable quand il s'agit d'analyser des structures faiblement plissées. Il conserve les angles avec une bonne approximation mais surtout il se prête aux études statistiques. Comme l'explique J. HENRY (ouvrage cité) : quand on a énormément de mesures on peut étudier « la répartition des attitudes d'éléments structuraux sous un angle statistique et traiter des populations d'éléments structuraux. En d'autres termes il est possible de considérer comme négligeables des variations d'attitude liées soit à des phénomènes accessoires et complexes, soit à des erreurs de

mesures, et de rechercher dans un ensemble de mesures des moyennes statistiques sur lesquelles porteront les analyses et les interprétations ».

12.4.2.4. *Représentation stéréographique des éléments structuraux*

Les éléments structuraux qu'on va avoir à représenter sont des droites, des plans ou des plis.

On va utiliser pour cela une planchette ou un carton sur lequel est représenté le stéréogramme (WULFF ou SCHMIDT). Puis, on superpose au canevas un papier calque, fixé sur le support par une épingle piquée au centre du stéréogramme (Fig. 12-43). On trace sur le calque le cercle fondamental; on marque le centre par une croix; enfin, on repère les quatre points cardinaux.

- *Représentation stéréographique d'une droite*

Soit la droite N 160° — 40° NW à représenter.

Tourner le calque dans le sens inverse des aiguilles d'une montre pour mettre en coïncidence le N du stéréogramme (calque) sur la division 160° du canevas support (Fig. 12-44). Comptons 40° sur le diamètre principal nord-sud en partant du cercle fondamental, du nord vers le sud. Le point ainsi déterminé représente l'attitude de la droite (on a l'habitude de rajouter une petite queue au point, dirigée vers le centre, pour distinguer une droite des représentations polaires d'un plan).

- *Représentation stéréographique d'un plan*

Soit à représenter le plan d'azimut N 25° avec un pendage de 60° (Fig. 12-45). Ainsi que nous l'avons vu, il y a deux façons de le représenter.

. Représentation polaire d'un plan

Tournons le calque dans le sens inverse des aiguilles d'une montre pour mettre en coïncidence

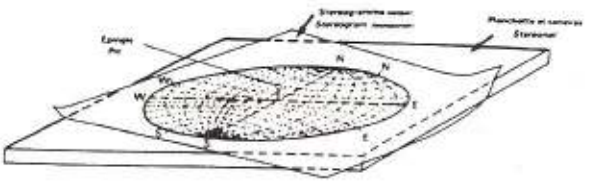

Fig. 12-43. - Planchette pour le report stéréographique des données de pendagemetrie.

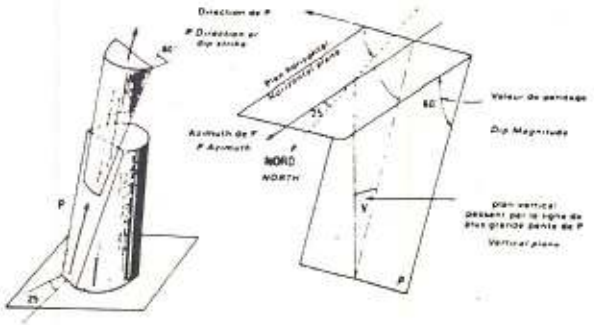

Fig. 12-45. - Eléments descriptifs d'un plan d'azimut N 25° avec un pendage de 60°.

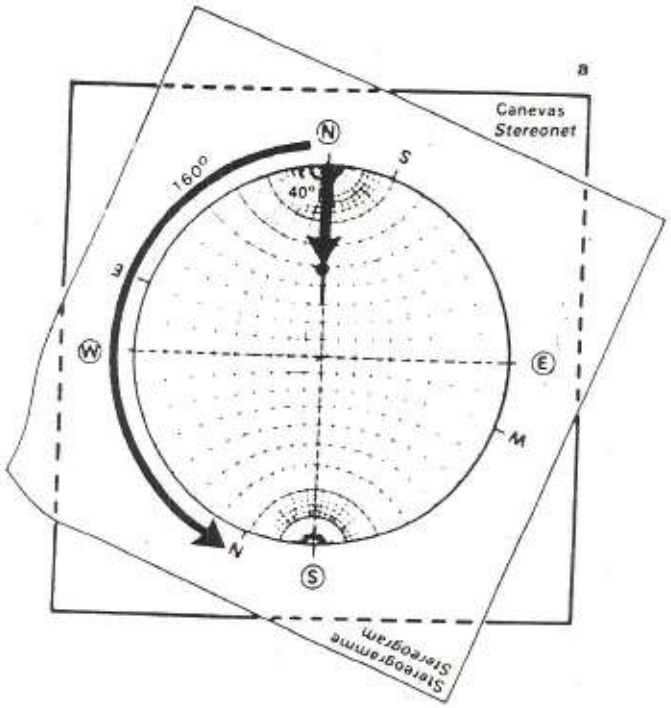

Fig. 12-44. - (a) Représentation d'une droite N 160° - 40° N-W; (b) Stéréogramme de cette droite; et (c) sa représentation dans l'espace.

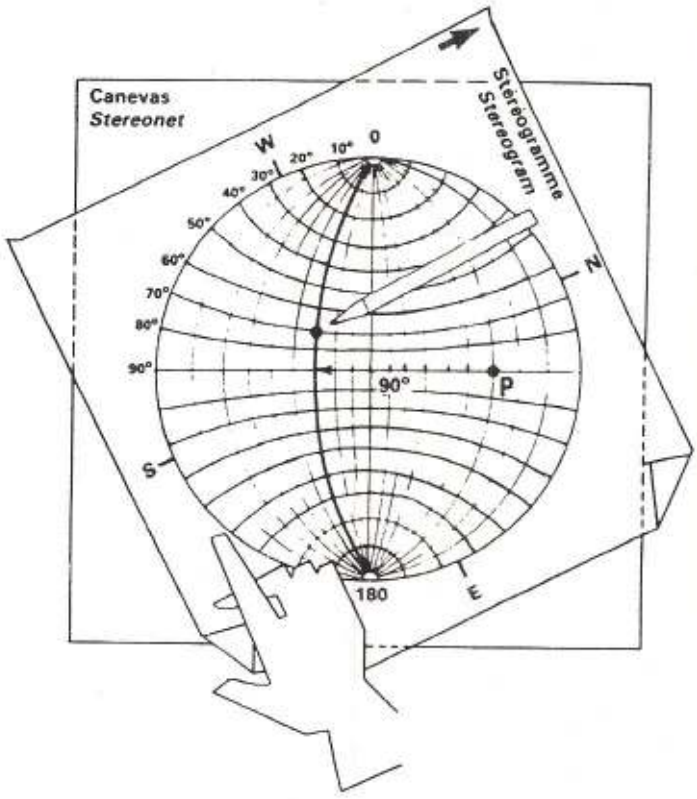

Fig. 12-48. - Représentation cyclographique du plan de la Fig. 12-46.

On dessine la trace cyclographique en décalquant le grand cercle correspondant du canevas.

- *Représentation stéréographique d'une droite portée par un plan*

C'est un cas qui se présente souvent en géologie structurale, en particulier dans le cas de reports de pendages apparents dans un plan de coupe. Pour résoudre le problème il faut d'une part connaître la direction et le pendage du plan porteur, d'autre part l'azimut et le plongement (« pitch ») de la droite.

Soit par exemple un plan de direction N 60° incliné de 50° vers le N-W portant la droite dont le « pitch » est de 50° vers l'ouest. On construit la trace cyclographique du plan porteur suivant la méthode décrite par la Fig. 12-47. On compte sur cette trace les 50° du « pitch » en partant du bord de l'arc N-E en suivant le grand cercle (Fig. 12-49). Par rotation du calque on amène la trace de la droite sur le diamètre principal N-S et on lit son azimut et son plongement.

- *Représentation stéréographique des plis*

Ainsi que nous l'avons vu précédemment, les plis sont des surfaces courbes à symétrie générale, soit cylindrique, soit conique. L'axe du pli peut être horizontal ou incliné et sa surface axiale verticale ou inclinée, plane ou gauche (« warped »).

On a vu que la projection stéréographique imposait la translation des éléments géométriques parallèlement à eux-mêmes jusqu'à l'hémisphère de référence. Comme il est plus simple de translater des plans que des surfaces courbes, on va substituer à ces surfaces une infinité de plans qui leur sont tangents. Ceci correspond d'ailleurs à la

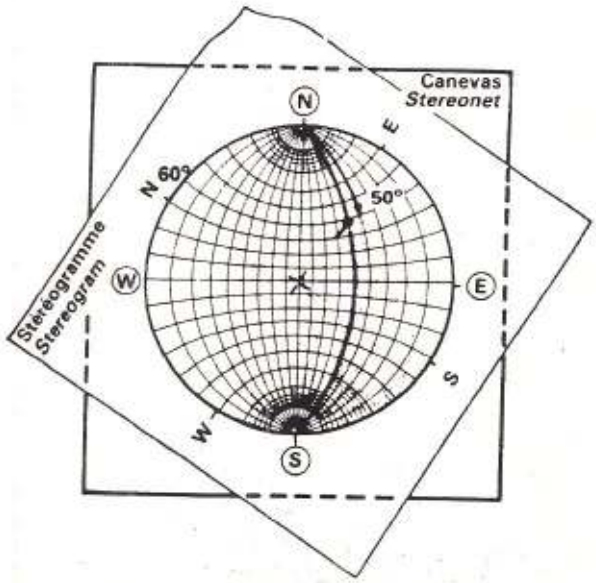

Fig. 12-49. - Représentation stéréographique d'une droite avec un « pitch » de 50° vers l'ouest, portée par un plan N 60 - 50° N-W (d'après HENRY, 1976).

Si on connaît l'axe, on reporte son point représentatif; de ce point, ramené par rotation sur le diamètre W-E, on dessine le grand cercle distant de 90°.

. Représentation stéréographique d'un cylindre à axe vertical (Fig. 12-52)

Dans ce cas les pôles des plans tangents se mettent en zone sur le cercle fondamental. L'axe du pli est au centre du stéréogramme.

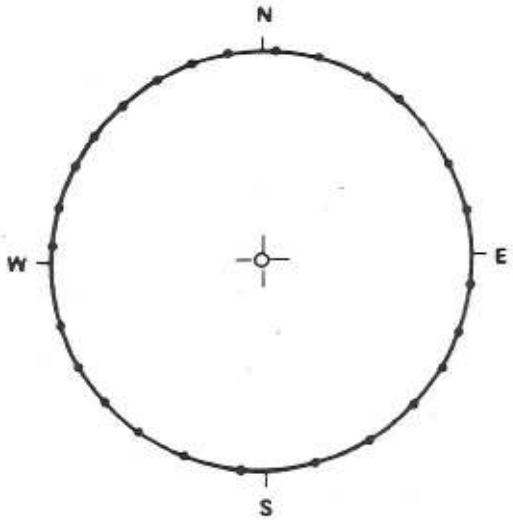

Fig. 12-52. - Stéréogramme d'un cylindre à axe vertical (d'après HENRY, 1976).

. Représentation stéréographique d'un pli cylindrique à plan axial incliné

Un cylindre ayant une symétrie de révolution autour d'un axe n'a pas de plan axial défini. Mais si l'on tient compte du fait que, dans la nature, un pli ne représente qu'une partie d'un cylindre, celle définie par l'angle d'ouverture (angle dièdre formé par les plans tangents aux flancs), on peut définir un plan axial qui peut alors être incliné, l'axe du pli pouvant être horizontal (Fig. 12-53) ou plongeant (Fig. 12-54). Si on est sûr que le stéréogramme comporte les valeurs des pendages aux points d'inflexion A et B des deux flancs du pli (a et b sur les stéréogrammes) l'angle d'ouverture du pli est défini comme le supplément de l'écart entre les deux couches extrêmes. Le plan axial est matérialisé par le grand cercle passant par l'axe du pli et le point bissecteur ou équidistant des deux couches extrêmes, en supposant que le plan axial et le plan bissecteur sont peu différents (cas de plis isopaches ou semblables). Le pôle du plan axial se construit facilement en ramenant le plan axial sur un grand cercle et en comptant sur le diamètre E-W une distance angulaire de 90° à partir de ce grand cercle. L'inclinaison du plan axial par rapport à la verticale se détermine en comptant la distance angulaire entre le centre du stéréogramme et le grand cercle qui matérialise ce plan axial. Son azimut se définit en faisant pivoter le

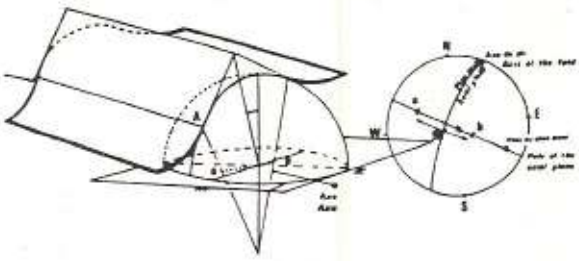

Fig. 12-53. - Représentation d'un pli cylindrique à plan axial incliné mais à axe horizontal.

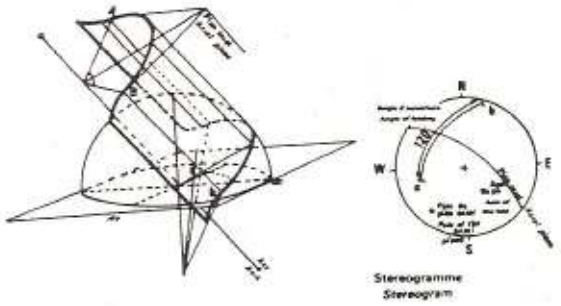

Fig. 12-54. - Représentation d'un pli cylindrique à plan axial et axe inclinés.

calque pour amener le pôle sur la branche N du diamètre N-S et en comptant sur le cercle fondamental, dans le sens inverse des aiguilles d'une montre le nombre de divisions séparant le N du canevas et celui du stéréogramme.

Les schémas de la Fig. 12-55 représentent la coupe, le tracé-flèches et la représentation stéréographique de plis pour différentes inclinaisons du plan axial et différents plongements de l'axe.

. Représentation stéréographique d'un cône à axe horizontal (Fig. 12-56)

Dans l'exemple illustré on a supposé un cône de révolution dont l'axe horizontal est orienté à N 150° et dont l'angle apical est de 60°. La projection stéréographique de ce cône par translation sur la sphère de référence de tous les plans tangents donne une figure symétrique : les plans sont en effet tangents à deux petits cercles de la demi-sphère et leurs pôles se mettent en zone sur deux petits cercles du stéréogramme. L'axe, horizontal, est situé sur le cercle fondamental sur un diamètre perpendiculaire aux petits cercles.

La position des petits cercles est fonction de l'angle apical qui peut être déterminé en comptant la distance angulaire entre le centre et l'un des petits cercles (ici 30°) et en multipliant par deux, ou encore directement la distance angulaire entre les deux petits cercles. L'un des petits cercles correspond au pli synforme, l'autre au pli antiforme. La direction de la pointe du cône du pli est celle de la concavité du petit cercle où s'alignent les pôles.

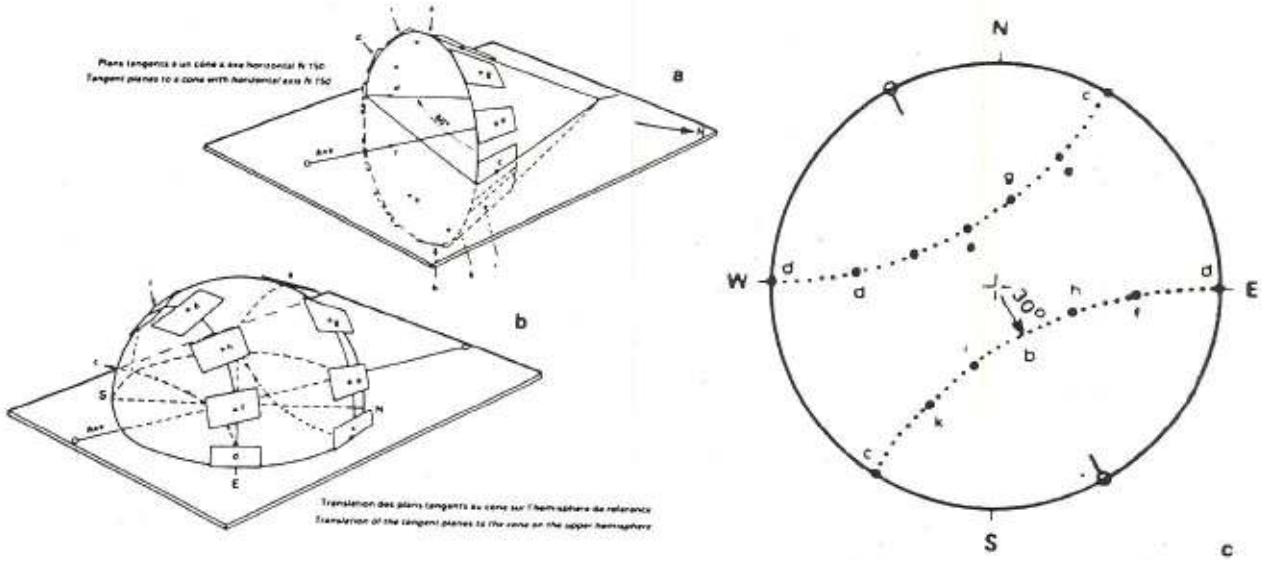

Fig. 12-56. - Représentation stéréographique d'un cône à axe horizontal (a) : plans tangents à un cône; (b) : translation des plans tangents sur l'hémisphère supérieur; (c) : stéréogramme du cône (d'après HENRY, 1976)

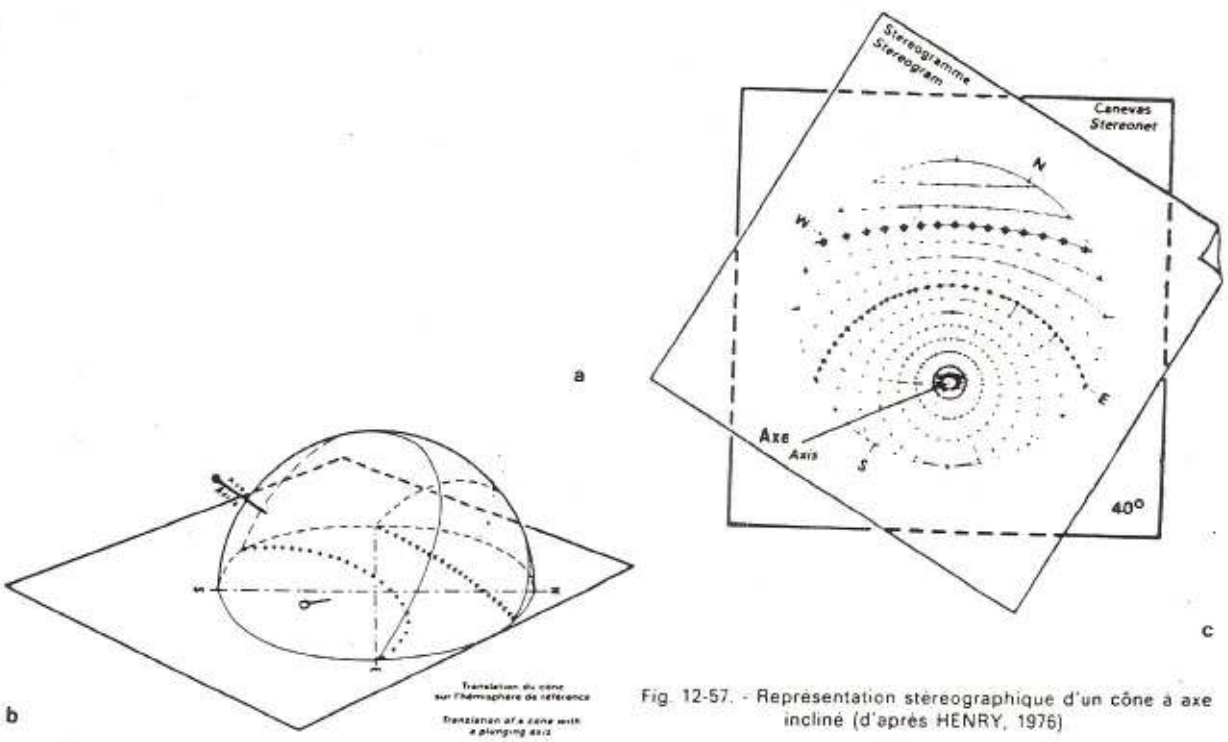

Fig. 12-57. - Représentation stéréographique d'un cône à axe incliné (d'après HENRY, 1976)

. Représentation stéréographique d'un cône à axe vertical (Fig. 12-58).

Dans ce cas les pôles des plans tangents se mettent en zone sur un cercle dont le centre coïncide avec celui du canevas. Le demi-angle apical est défini par la distance angulaire entre ce cercle et le cercle fondamental. L'axe du cône est au centre du canevas.

12.4.2.5. ***Reports des données de pendagemétrie***

Ainsi qu'on l'a vu, chaque donnée (pendage et

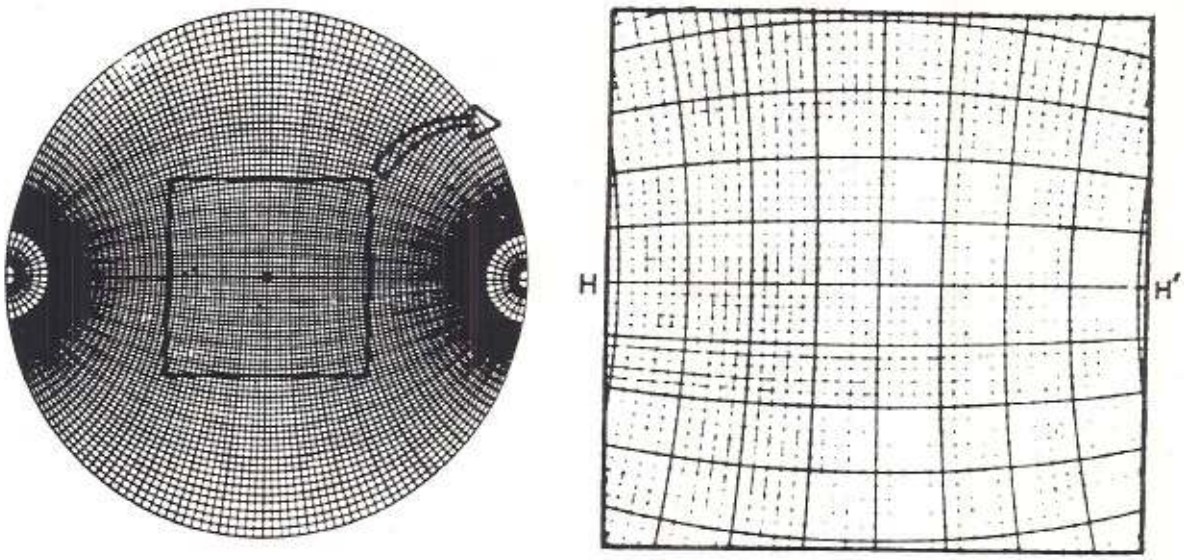

Fig. 12-59 - Agrandissement de la partie centrale du canevas de WULFF.

privilégie les pendages structuraux, tous les événements, sur les courbes de résistivité, correspondant à des bancs ou laminations dont les surfaces sont planes et parallèles, donc, a priori, peu déformées par l'action de courants, se mettant en phase pour un même déplacement, créant ainsi un maximum dans le corrélogramme.

Si l'on utilise un tracé-flèches provenant d'un traitement par GEODIP ou LOCDIP, on sélectionnera les intervalles au droit de couches correspondant à des dépôts de basse énergie et présentant une succession de pendages ayant sensiblement le même azimut et le même angle.

La seconde étape consiste à réaliser un stéréogramme pour chaque intervalle cohérent défini à l'étape précédente, en reportant, soit manuellement en suivant la technique décrite précédemment, soit par traitement informatique, les différentes valeurs de pendage.

12.4.3. Exploitation des stéréogrammes

Il s'agit, à ce stade de l'analyse, de réduire l'information géométrique contenue dans chaque stéréogramme par intervalle, en une donnée plus synthétique.

Plusieurs cas peuvent se présenter.

a) Le cas le plus simple est celui d'un intervalle à pendages et azimuts à peu près constants. Dans ce cas la projection stereographique permet de définir deux données synthétiques : le pendage moyen de l'intervalle et la valeur angulaire de la dispersion autour de cette moyenne. Pour ce faire on recherche un cercle qui englobe la majorité des pendages et dont le centre coïncide avec la plus grande concentration de points. On peut aussi utiliser les canevas-compteurs (voir paragraphe 12.6.5.). Le chiffre indiquant la valeur de la dispersion est intéressant à plusieurs titres. Associé au pourcentage de bonnes valeurs dans l'intervalle, il permet d'estimer la fiabilité du pendage moyen. Il est, d'autre part, d'observation courante que la valeur de la dispersion soit caractéristique de certaines formations, puisqu'elle traduit le réglage plus ou moins parfait de la stratification.

b) L'intervalle étudié correspond sur le tracé-flèches à une variation régulière d'attitude, en pendage et/ou en azimut, des plans successifs. Une telle organisation se traduit généralement sur le stéréogramme par un nuage allongé dans lequel la définition d'un pendage moyen devient impossible. La projection stéréographique va cependant fournir une information synthétique importante. Elle est en effet la traduction d'une géométrie précise, qui peut se schématiser comme une succession de segments de cylindres, ou de cônes, emboîtés l'un dans l'autre. Chaque pendage correspond ainsi aux tangentes à des cylindres ou cônes successifs.

Si les pendages se *mettent en zone suivant un diamètre*, on peut en conclure que l'axe du pli est horizontal.

Si les pendages se *mettent en zone sur un grand cercle*, ils appartiennent alors au même pli cylindrique à axe plongeant. La détermination de l'azimut et du plongement de l'axe se fait de la façon suivante :

Dessiner le grand cercle passant par les pôles des plans. Compter 90° à partir de ce grand cercle sur le diamètre E-W en direction du centre. Le point ainsi défini est l'axe du pli cylindrique. Son plongement est défini en comptant la distance angulaire de la périphérie à ce point. Son azimut l'est en faisant pivoter le calque pour amener l'axe sur la branche N du diamètre N-S et en lisant la

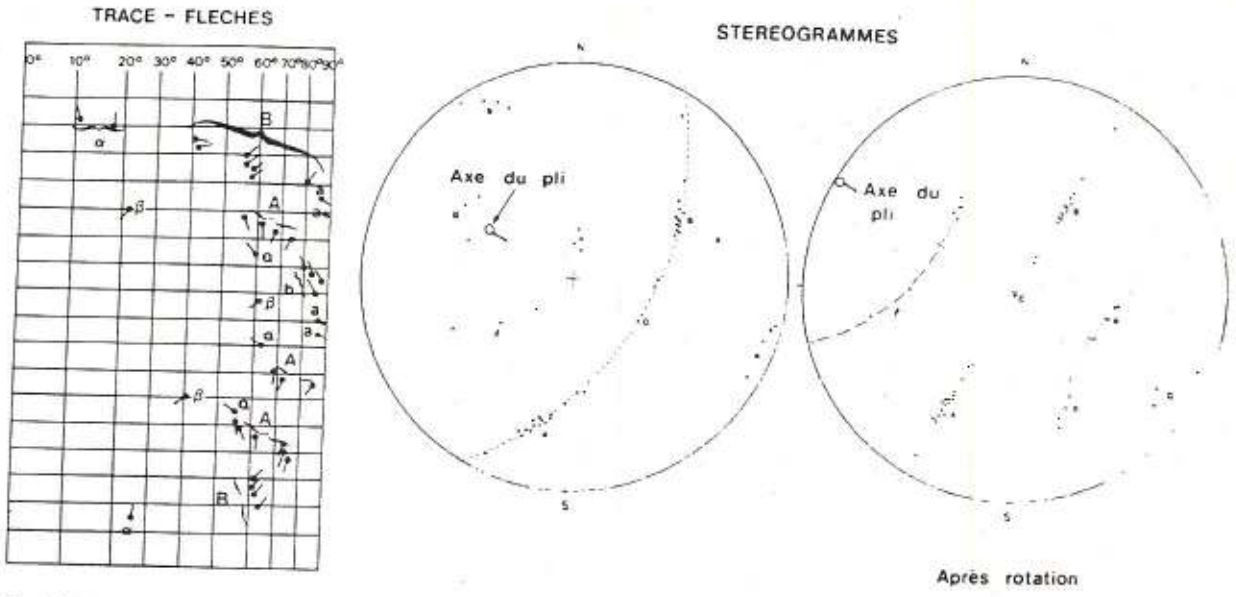

Fig. 12-61. - Exemple de tracé-flèches en apparence anarchique. Le report stéréographique montre un groupement cohérent le long d'un grand cercle de certains points représentatifs de plans de stratification (A et B). Les autres points (a et b, α et β) s'ordonnent parfaitement sur le stéréogramme de droite obtenu après rotation ramenant l'axe du pli à l'horizontal. Ils correspondent à des joints orthogonaux.

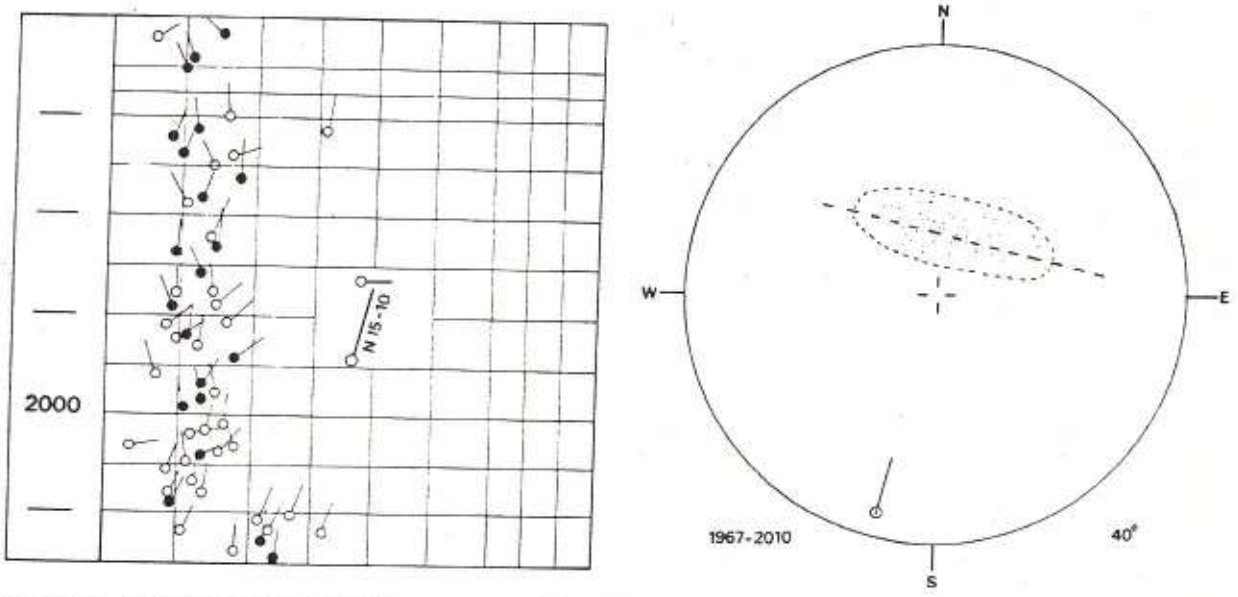

Fig. 12-62. - Autre exemple de tracé-flèches un peu anarchique correspondant à un groupement dispersé le long d'un grand cercle (contribution J. HENRY).

semble de la structure. Là encore la projection stéréographique va intervenir sous la forme d'un stéréogramme récapitulatif. Sur celui-ci sont reportés en premier lieu tous les points moyens issus des stéréogrammes par intervalle. Si le puits a traversé une structure monoclinale le centre du nuage de points fournira le pendage régional moyen. Dans le cas de la Fig. 12-65, les points s'organisent en un nuage allongé qui permet de définir l'axe général de la structure. En outre certains intervalles fournissent des évolutions des points moyens qui permettent de construire des axes majeurs caractérisant la géométrie de la structure sur des intervalles de plusieurs centaines de mètres. Ces axes peuvent eux-mêmes varier d'orientation avec la profondeur et l'analyse de cette évolution peut être révélatrice de la géométrie globale. Enfin, tous les axes construits sur les intervalles de l'analyse (axes mineurs) sont reportés sur le stéréogramme récapitulatif. Une autre

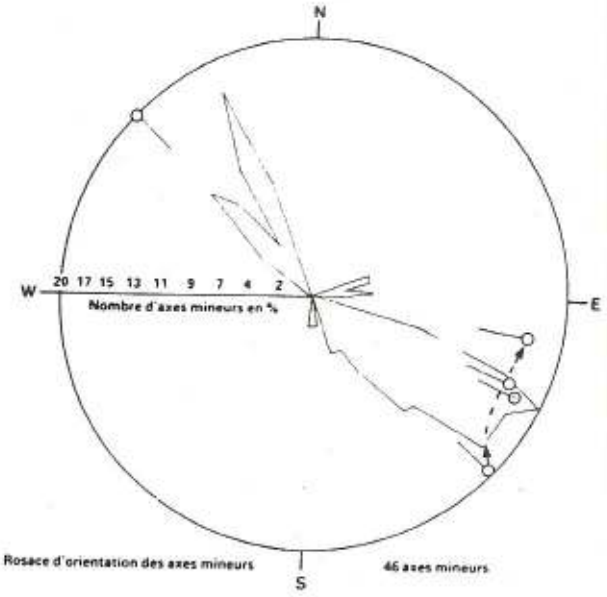

Fig. 12-66. - Rosace d'orientation des axes mineurs (contribution J. HENRY)

des principales formations ou étages recoupés par le sondage. Il est aussi possible de numéroter les points moyens successifs pour mieux mettre en évidence les différentes évolutions de pendages rencontrées par le puits.

La fiche d'analyse de pendagemétrie (Fig.12-67) présente sous une forme synthétique la même information, en conservant les positions relatives en profondeur des éléments de la structure. Certaines colonnes méritent quelques commentaires. Dans la rubrique « aspect » sont figurées en blanc les zones de pendage régulier, en hachuré les intervalles dans lesquels des évolutions de pendage organisées permettent de construire des axes, et en noir des zones présentant une succession de pendages trop dispersés pour fournir un pendage moyen ou un axe. La colonne « pendage moyen » indique les valeurs issues des stéréogrammes par intervalle. La colonne « direction axiale » répertorie tous les axes mineurs construits lors de l'analyse des stéréogrammes par intervalle. Sous le titre « % de bonnes mesures » figure le rapport entre les mesures de qualité A, B et C du listing sur la totalité des mesures figurant sur le tracé-flèches. Dans la colonne « facteur de dispersion en degrés » sont reportées les valeurs angulaires du cercle contenant le nuage de points. Enfin, une dernière colonne indique les numéros des intervalles qui ont été utilisés pour la construction des stéréogrammes analytiques. Ces fiches analytiques serviront à leur tour de document de base pour l'analyse géométrique des différents sondages effectués sur une même structure.

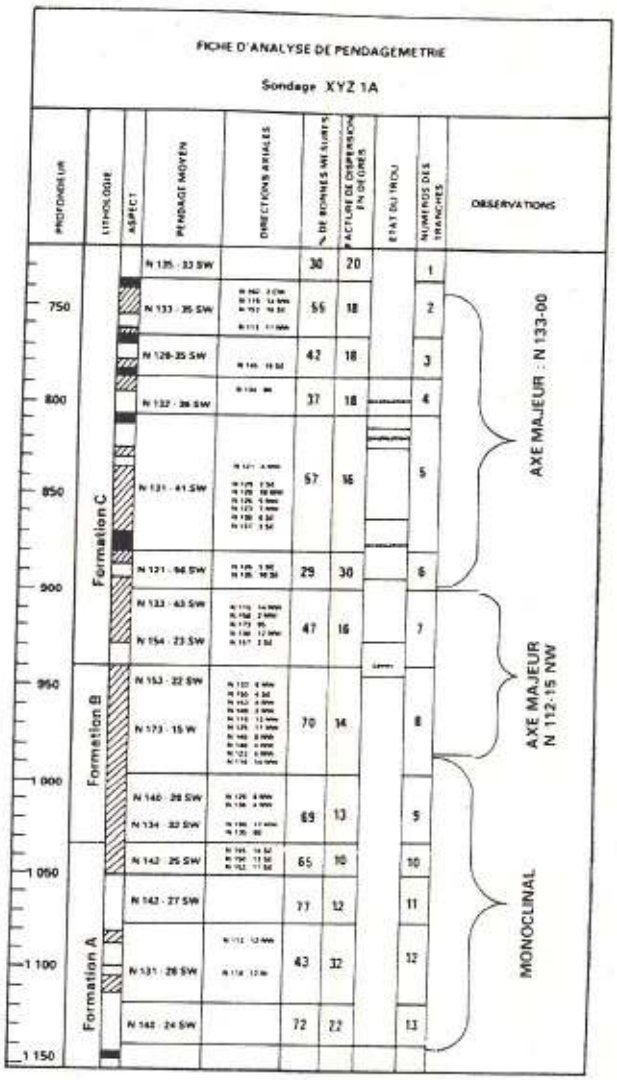

Fig. 12-67. - Exemple de fiche d'analyse de pendagemétrie (contribution J. HENRY)

12.5. INTERPRETATION*

Les méthodes d'analyse proposées ci-dessus fournissent des données précises et chiffrées sur la géométrie des couches traversées par le sondage.

L'interprétation, elle, a pour but une description géologique de cette géométrie. Malheureusement, une organisation géométrique n'est pas, à elle seule, révélatrice et se prête, le plus souvent, à plusieurs interprétations géologiques. L'apport d'autres sources d'information (stratigraphie, sédimentologie, corrélations diagraphiques, géophysique, géologie régionale) est toujours indispensable pour lever cette ambiguïté. Ceci est illustré par l'exemple suivant.

* Ce chapitre a été rédigé avec le concours de J. HENRY, SNEA(P), Pau.

12.6. AUTRES APPLICATIONS DU STEREOGRAMME

Le stéréogramme est l'outil de base pour la détermination de certaines relations angulaires dans l'espace. Ces applications sont rappelées ci-après.

12.6.1. Trouver la ligne d'intersection de deux plans

La ligne d'intersection de deux plans, du fait qu'elle appartient aux deux plans, sera représentée sur le stéréogramme par le point d'intersection des deux représentations cyclographiques des plans. Il suffit donc de tracer les deux grands cercles, représentations cyclographiques des deux plans (Fig. 12-70). Le point d'intersection P est la projection de cette ligne. On détermine son pendage et son azimut en ramenant P sur la branche N du diamètre N-S, par rotation du calque, d'une part en lisant de la périphérie au point P la distance angulaire qui correspond au pendage, d'autre part en comptant, dans le sens contraire aux aiguilles d'une montre, le nombre de degrés séparant le N du canevas de celui du stéréogramme.

12.6.2. Déterminer l'angle entre deux plans

L'intersection de deux plans définit quatre angles dièdres égaux deux à deux par le sommet, et dont la somme fait 360°.

L'un des angles sera mesuré dans le plan perpendiculaire à la ligne d'intersection et contenant les pôles des plans, donc sur le grand cercle passant par ces pôles en comptant, le long de ce grand cercle, la distance angulaire entre les pôles P_1 et P_2.

L'angle dièdre supplémentaire (pour contrôle) se détermine en mesurant la distance angulaire entre les traces cyclographiques, toujours le long de ce grand cercle (Fig. 12-70).

12.6.3. Déterminer le pendage vrai d'une couche à partir du pendage apparent mesuré dans deux plans verticaux

Le plan matérialisant la couche recoupe les plans verticaux suivant deux lignes qui définissent le pendage apparent. Il contient donc ces deux lignes qui sont matérialisées sur le stéréogramme par deux points.

Le plan recherché est représenté par le grand cercle passant par ces deux points (Fig. 12-71). La méthode consiste à tracer la représentation cyclographique des plans dont on connaît l'orientation (ici plans verticaux orientés dans l'exemple de la Fig. 12-71 à N 30° et N 295°). Dans le cas présent, les plans sont représentés par des diamètres sur lesquels on reporte les angles apparents (« pitches ») en partant du S du calque puisqu'ils sont orientés vers le N. Le plan recherché est le grand cercle passant par ces deux points. La construction de ce grand cercle et de son pôle permet de déterminer son azimut et son pendage : N 350° — 30° dans ce cas.

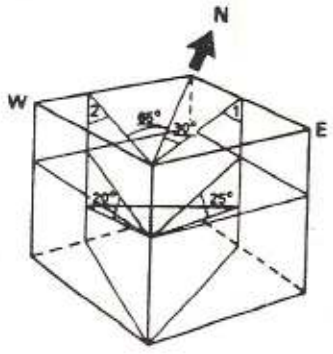

vue perspective
Perspective View

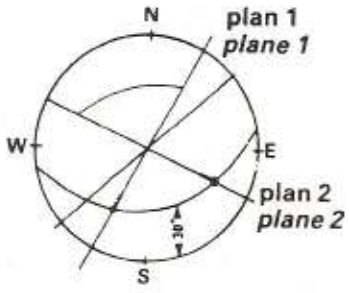

stéréogramme
Stereogram

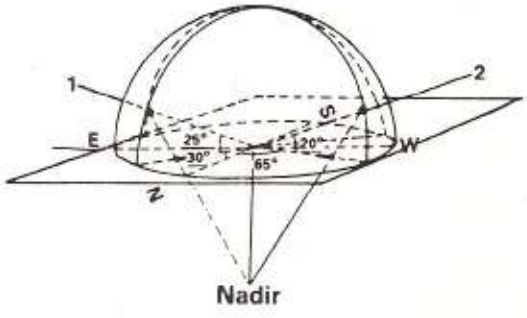

signification du stéréogramme
Meaning of the Stereogram

Fig. 12-71. - Détermination du pendage vrai d'une couche à partir du pendage apparent mesuré dans deux plans verticaux.

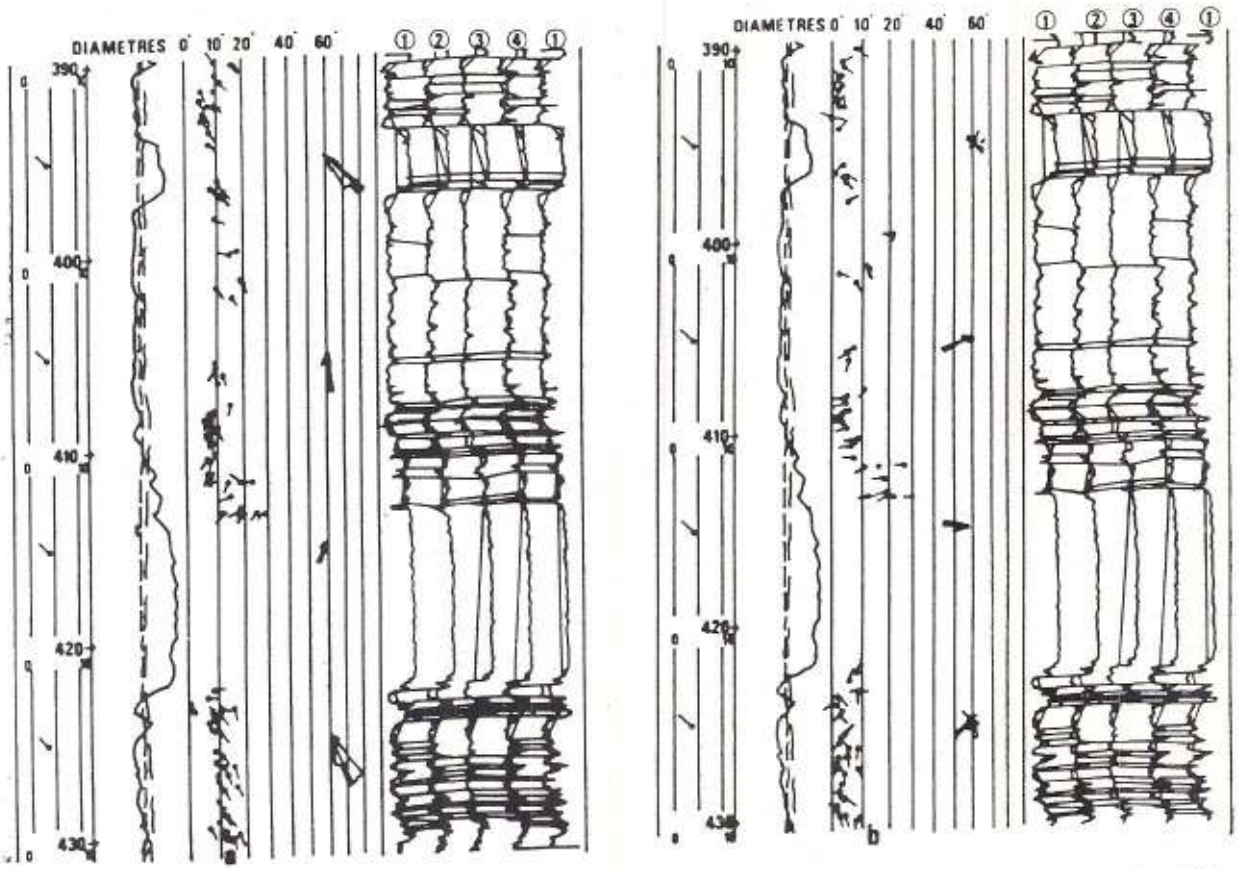

Fig. 12-73. - Exemple d'un drapé sur une barre sableuse apparaissant clairement après soustraction du pendage structural (b)

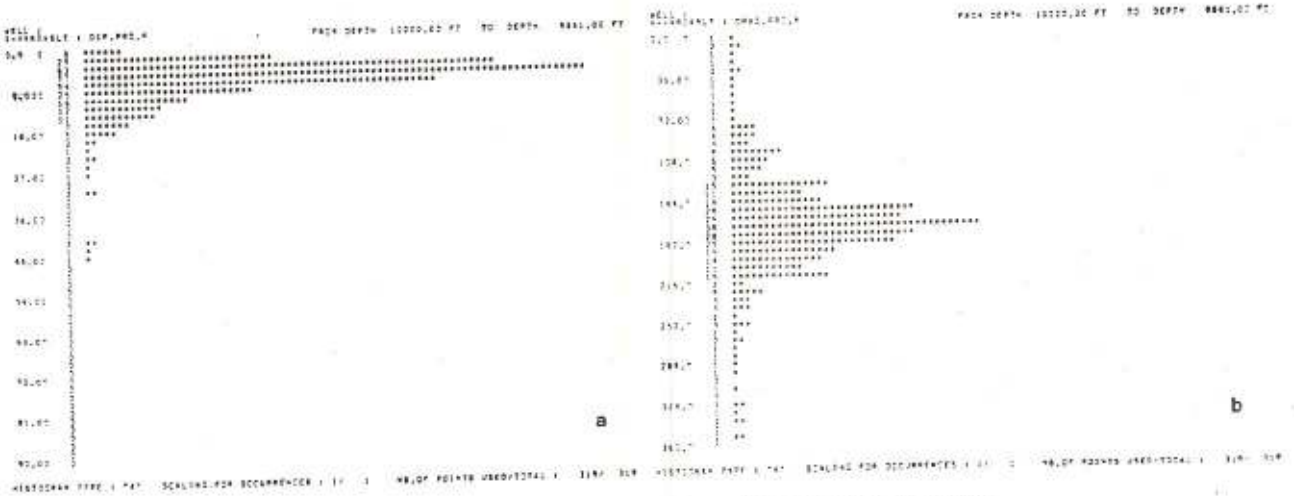

Fig. 12-74. - Exemple d'histogramme de pendages (a) et d'azimut (b)

Ce report (qui n'est pas une projection) est connu sous le nom de « polar plot » (Fig. 12-77).

12.7.3. Diagrammes en rosace ou de fréquence d'azimut (« azimuth frequency plot »)

On utilise le canevas du « polar plot ». Les azimuts de pendage sont reportés sur un cercle, et regroupés en tranches de 5° ou 10° par exemple. Les longueurs des rayons du secteur indiquant leur azimut (Fig. 12-78) sont proportionnelles aux fréquences. Diagramme polaire et diagramme en rosace sont souvent regroupés sur un même document connu sous le nom de « polar frequency plot » (Fig. 12-79).

Histogrammes, diagrammes polaires et en rosace sont réalisés automatiquement par zone.

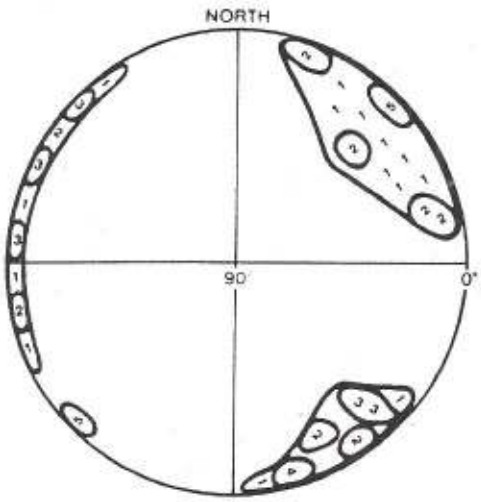

Fig. 12-80. - Exemple d'interprétation d'un canevas de SCHMIDT (document Schlumberger).

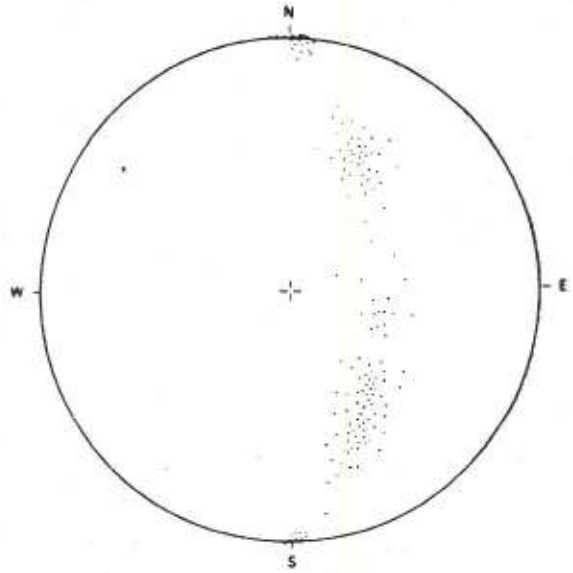

Fig. 12-81. - Stéréographie de 150 pôles de couches sur un canevas de SCHMIDT (d'après J. HENRY, 1976).

tectoniques, soit à des figures sédimentaires.

Quand le diagramme présente une distribution plus concentrée, telle que celle de la Fig. 12-77, les secteurs à haute densité et valeurs de pendage faibles définissent vraisemblablement le pendage structural auquel se surajoutent soit des figures sédimentaires, soit des plis.

12.7.5. **Stéréogrammes de densité**

Durant l'examen des diagrammes précédents ou des stéréogrammes (Fig. 12-81), l'œil peut apprécier facilement les zones où les points sont plus ou moins rapprochés. Dans certains cas de mesures très dispersées (Fig. 12-82) il n'est plus capable de trouver des groupements ou les tendances. Le stéréogramme de densité a pour objectif de transformer l'appréciation qualitative en une représentation quantitative plus facilement interprétable.

Le principe consiste à dénombrer les points à l'intérieur d'une unité de surface fixe répartie selon une grille homogène sur le diagramme de points. Pour cela on utilise des canevas-compteurs : Pronin pour une projection conforme (canevas de WULFF), Dimitrijevic (Fig. 12-83) pour une projection isoaire (canevas de SCHMIDT).

Construction du stéréogramme de densité

On utilise généralement le canevas de SCHMIDT (isoaire). On va donc utiliser le canevas-compteur de Dimitrijevic.

On compte le nombre de points dans chaque petite ellipse du compteur. On inscrit ce nombre (ou sa correspondance en pourcentage) sur le calque au centre de chaque ellipse.

On trace les contours d'isodensité (ou d'isopourcentage). Sur la ou les zones de densité maximale (ou pourcentage maximum) on définit l'azimut et la valeur de pendage moyen à l'aide du canevas de base (Fig. 12-84 et 12-82).

12.8. **COUPES INTERPRETATIVES**

Elles vont permettre de visualiser l'agencement et la géométrie des structures, déduite de l'interprétation de la pendagemétrie, sur l'ensemble ou une partie du sondage.

La position du plan de coupe doit être choisie de façon judicieuse afin de ne pas trop altérer l'image de la structure. Les pendages représentés seront les pendages apparents dans le plan choisi (le plus généralement vertical).

On peut partir des résultats d'un « stick plot », pour lequel on aura au préalable défini la direction du plan de coupe. Il peut être perpendiculaire au plan vertical passant par l'axe du sondage. Mais si cet axe est incliné, cette coupe va altérer l'image géométrique, exagérer par exemple le rayon de courbure. Dans ce cas il vaut mieux avoir une coupe pentée orthogonale à l'axe. La position du plan de coupe peut varier le long d'un même sondage suivant l'orientation des structures traversées.

Le dessin des couches se fera en respectant la règle des plis isopaches, ces derniers étant les plus courants, surtout pour les couches compactes, cassantes. On pourra admettre des variations d'épaisseur dans des couches plastiques (argiles, sables, halite ...) au niveau des charnières ou des points d'inflection.

Dans le dessin des structures, il faut, tout en tenant compte des valeurs mesurées, s'inspirer de

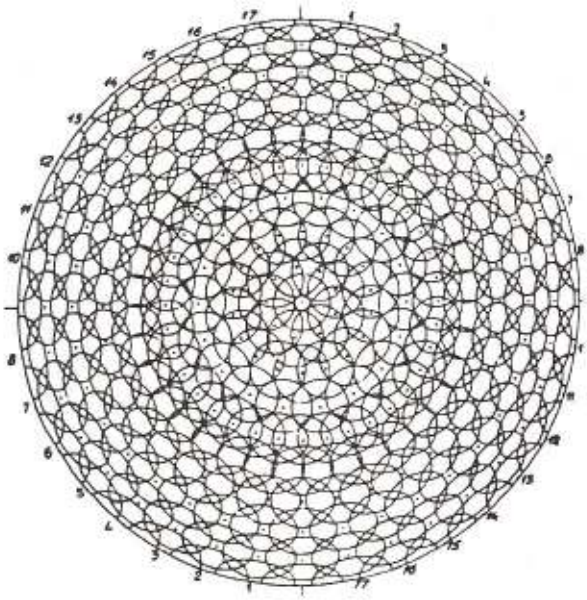

Fig. 12-83. - Compteur de DIMITRIJEVIC.

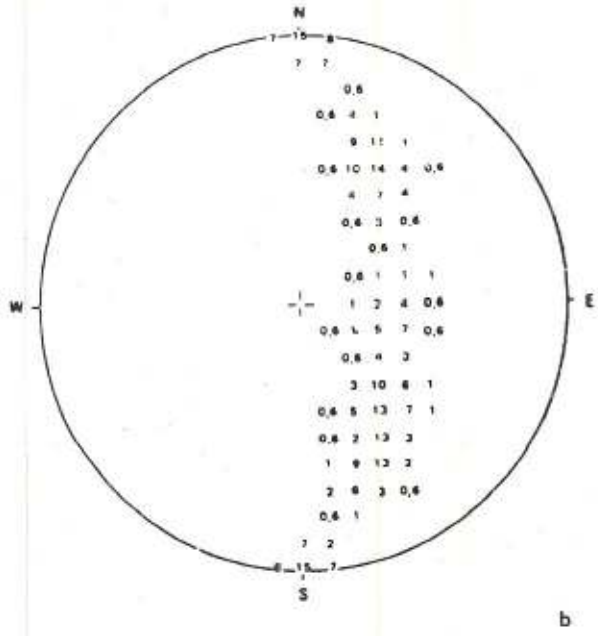

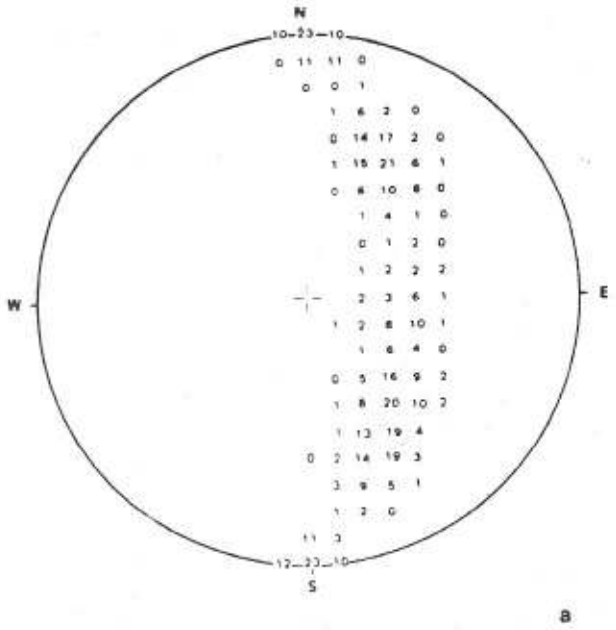

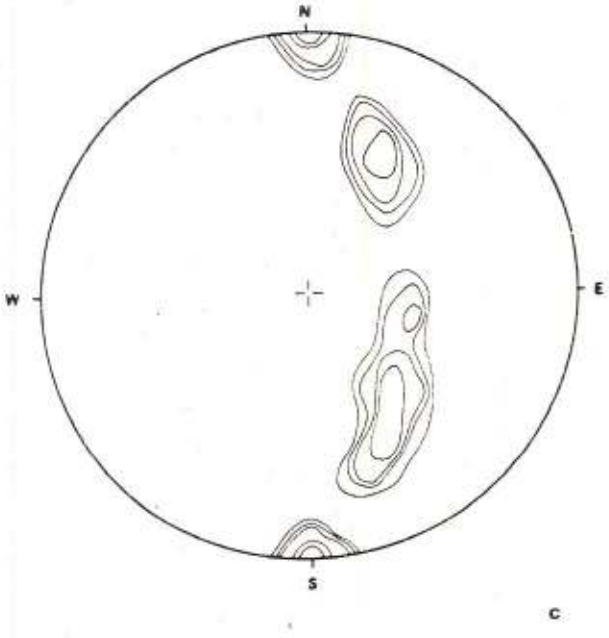

Fig. 12-84. - Construction du stéréogramme de densité. (a) : Comptage des points du stéréogramme de la Fig. 12-81; (b) : Pourcentages correspondants. (c) : Courbes d'isodensités du stéréogramme de la Fig. 12-81 (d'après J. HENRY, 1976).

l'allure tectonique de la région. La Fig. 12-37b donne un exemple d'une coupe basée sur l'interprétation du tracé-flèches de la Fig. 12-37a.

La Fig. 12-85 donne un exemple d'une interprétation faite dans le cas de plis complexes.

Enfin, pour la représentation de structures complexes, on peut utiliser la technique des blocs-diagrammes en s'aidant au besoin de « Fast plot ». Mais leur réalisation est longue et nécessite une certaine expérience du dessin en perspective.

GARY, M., McAFEE, R.Jr. & WOLF, C.L. (1972). -Glossary of Geology. *Amer. Geol. Institute, Washington, D.C.*

GILREATH, J.A. & MARICELLI, J.J. (1964) - Detailed Stratigraphic control through Dip computations. *Bull. amer. Assoc. Petroleum Geol.*, **48**, *12, p. 1902-1910.*

GOGUEL, J. (1952). - Traité de Tectonique. *Masson & Cie, Paris.*

HALBOUTY, M.T. & al. (1970). - World's Giant oil and gas fields, Geological factors affecting their formation, and basin classification. *Amer. Assoc. Petroleum Geol. Mem.*, **14.**

HENRY, J. (1976). - Voir : *Chambre syndicale...*

HEPP, V. & DUMESTRE, A.C. (1975). - CLUSTER -A method for selecting the most probable dip results from dipmeter survey. *SPE of AIME, 50th Ann. Fall Mtg., Dallas, Paper SPE 5543.*

HOBBS, B.E., MEANS, W.D. & WILLIAMS, P.F. (1976). - An outline of Structural Geology. *John Wiley & Sons, New York.*

HOBSON, G.D. & TIRATSOO, E.N. (1975). - Introduction to Petroleum Geology. *Scientific Press Ltd, Beaconsfield, England.*

LANDES, K.K. (1951). - Petroleum Geology. *John Wiley & Sons, New York.*

LEET, L.Don, JUDSON, S. & KAUFFMAN, M.E. (1978). - Physical Geology. 5th ed. *Prentice-Hall Inc., Englewood Cliffs, New Jersey.*

LINK, P.K. (1982). - Basic Petroleum Geology. *OGCI Publications, Tulsa.*

PERRODON, A. (1980). - Géodynamique pétrolière. Genèse et répartition des gisements d'hydrocarbures. *Masson et Elf Aquitaine, Pau et Paris.*

PIRSON, S.J. (1977). - Geologic Well Log Analysis. 2nd ed. *Gulf Publishing Co., Houston.*

PRESS, F. & SIEVER, R. (1978). - Earth. 2nd ed. *W.H. Freeman, San Francisco.*

RAGAN, D.M. (1973). - Structural Geology. *John Wiley & Sons, New York.*

RAMSAY, J.G. (1967). - Folding and Fracturing of Rocks. *McGraw-Hill Book Co. Inc., New York.*

RUSSELL, W.L. (1951). - Principles of Petroleum Geology. *McGraw-Hill Book Co. Inc., New York.*

SCHLUMBERGER Ltd :

1970 - Fundamental of Dipmeter interpretation.

1981 - Dipmeter interpretation - Vol. 1 -Fundamentals.

1974 - Well Evaluation Conference - North Sea.

1974 - Well Evaluation Conference - Nigeria.

1975 - Well Evaluation Conference - Arabia.

1976 - Well Evaluation Conference - Iran.

1979 - Well Evaluation Conference - Algeria.

1980 - Evaluacion de formaciones en Venezuela.

1981 - Well Evaluation Conference - South East Asia.

1981 - Well Evaluation Conference - Emirates/Qatar.

1983 - Well Evaluation Conference - India.

VINCENT, P., GARTNER, J. & ATTALI, G. (1979). -GEODIP - An approach to detailed dip determination using correlation by pattern recognition. *J. Petroleum Technol., Feb. 1979, p. 232-240.*

WILLIS, B. & WILLIS, R. (1934). - Geologic Structures. *McGraw-Hill, New York.*